NASA CR-72142

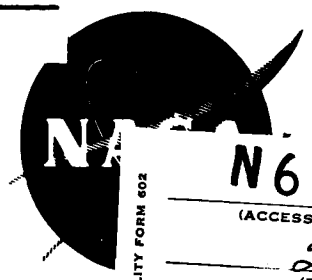

INVESTIGATION OF THE EFFECT OF MATERIAL PROPERTIES ON COMPOSITE ABLATIVE MATERIAL BEHAVIOR

by

P. B. Cline and F. E. Schultz

prepared for

NATIONAL AERONAUTICS AND SPACE ADMINISTRATION

CONTRACT NAS 3-6291

GENERAL ELECTRIC

RE-ENTRY SYSTEMS DEPARTMENT
A Department Of The Missile and Space Division
P. O. Box 8555 • Philadelphia, Penna. 19101

NASA CR-72142

FINAL REPORT

INVESTIGATION OF THE EFFECT OF MATERIAL PROPERTIES ON COMPOSITE ABLATIVE MATERIAL BEHAVIOR

by

P. B. Cline and F. E. Schultz

prepared for

NATIONAL AERONAUTICS AND SPACE ADMINISTRATION

April 17, 1967

CONTRACT NAS 3-6291

Technical Management
NASA Lewis Research Center
Cleveland, Ohio
Liquid Rocket Technology Branch
Erwin A. Edelman

GENERAL ELECTRIC

RE-ENTRY SYSTEMS DEPARTMENT
A Department Of The Missile and Space Division
P. O. Box 8555 • Philadelphia, Penna. 19101

TABLE OF CONTENTS

LIST OF TABLES

LIST OF ILLUSTRATIONS

LIST OF ILLUSTRATIONS (Continued)

LIST OF ILLUSTRATIONS (Continued)

LIST OF ILLUSTRATIONS (Continued)

LIST OF ILLUSTRATIONS (Continued)

LIST OF ILLUSTRATIONS (Continued)

LIST OF ILLUSTRATIONS (Continued)

INVESTIGATION OF THE EFFECT OF MATERIAL PROPERTIES ON COMPOSITE ABLATIVE MATERIAL BEHAVIOR

by

P. B. Cline and F. E. Schultz

ABSTRACT

The influence of material properties on the ablative performance of the silica phenolic, graphite phenolic and graphite epoxy materials was analytically investigated. Those properties which have the greatest effect on the surface recession were established. The reasons for the property variation within a given material are stated along with the measured range of their values.

INTRODUCTION

Prior to the development of analytical reaction kinetics ablation models, such as those developed under NASA contract NAS3-2566, the evaluation of ablative materials for use as rocket nozzle materials has been solely an empirical process. New or modified materials were made up and these materials were then test fired to determine whether they would perform better than previous materials. Although this approach does assess the gross ablative performance of a material in a given environment, it does not provide a detailed understanding as to what particular parameters or properties of that material caused it to perform better or worse than some other materials. Recognizing these limitations of the empirical approach of evaluating rocket nozzle heat protection materials, several analytical methods have been derived for the theoretical prediction of the thermal performance of ablation materials. One of these programs was the Reaction Kinetics Ablation Program (REKAP) which was developed by General Electric for NASA Lewis under contract NAS3-2566. This program is described in complete detail in Reference 20.

The analytical approach of evaluating materials allows one to readily investigate the influence of the various material properties and environments on the thermal performance of the material. It was, therefore, the purpose of this contract, using the developed REKAP computer program, to establish the order of importance that the material and environment parameters have on the ablation performance (surface recession) of three materials. The materials considered within this study were silica phenolic, graphite phenolic and graphite epoxy. The steady state surface recession rates were calculated and the results are presented as a function of the various parameters within this report. The first four material properties which had the greatest effect on the surface recession were then studied in detail. The property variations caused by processing, fabrication and design were investigated to establish a reasonable range for a comprehensive thermal investigation where the interplay of these four properties on the surface recession of each material was studied.

SUMMARY

A three task analytical investigation was made to determine the influence of material property variations on the ablative performance of silica cloth/phenolic resin, graphite cloth/phenolic resin and graphite cloth/epoxy resin materials as used for the thermal protection system of rocket nozzles. The thermal environment for which these materials were to be evaluated was that produced by the two propellant combinations, N_2O_4/Aerozine 50 and OF_2/B_2H_6, fired at a chamber pressure of 100 psia and operating at the combustion temperature corresponding to a 98% C* efficiency. The calculated surface recession at the nozzle throat was the ablative performance parameter of interest. The initial throat diameters were 1.5 inches and 7.82 inches. Only the environment resulting from N_2O_4/Aerozine 50 was considered for the 7.82-inch throat nozzle.

The thermal response of the materials, including the surface recession, was calculated using a Reaction Kinetics Ablation Computer Program. This program calculates the material temperature response including the thermochemical decomposition of the resin and the melting or oxidation of the reinforcing fibers or cloth. The ablation performance of a material depends on a number of material and environment properties. These properties are:

Material Properties

1. Char Density
2. Virgin Material Density
3. Char Thermal Conductivity
4. Virgin Material Thermal Conductivity
5. Char Specific Heat
6. Virgin Material Specific Heat
7. Heat of Gasification
8. Collision Frequency
9. Activation Energy
10. Heat of Melting or Heat of Reaction of Reinforcing Fibers
11. Wall Emissivity
12. Specific Heat of Ablation Gases
13. Melting Temperature of Reinforcing Fibers

Environment Properties

1. Heat Transfer Coefficient

2. Recovery Temperature

3. Nozzle Geometry

The first phase of the study was to determine the amount of influence that each of the above properties had on the surface recession of the three materials. The material properties presented in descending order of their relative effect on the ablative performance of each material are tabulated below:

	Silica Cloth/ Phenolic Resin		Graphite Cloth/ Phenolic Resin		Graphite Cloth/ Epoxy Resin	
1.	Melting Temperature	.0288	Surface Reaction Rate Constants	.0064	Surface Reaction Rate Constants	.0082
2.	Virgin Plastic Density	.007	Char Density	.002	Char Density	.0028
3.	Specific Heat (Char and Virgin Mat'l)	.005	Thermal Conductivity (Char and Virgin Material)	.0017	Thermal Conductivity (Char and Virgin Material)	.0018
4.	Activation Energy	.003	Virgin Plastic Density	.00085	Virgin Plastic Density	.0011
5.	Char Density	.002	Collision Frequency	.00065	Activation Energy	.0006
6.	Collision Frequency	.001	Specific Heat (Char and Virgin Material)	.0004	Specific Heat (Char and Virgin Material)	.0004
7.	Heat of Gasification	.0009	Activation Energy	.0002	Specific Heat of Ablation Gases	.0004
8.	Heat of Melting of Reinforcing Fibers	.0008	Specific Heat of Ablation Gases	.0002	Collision Frequency	.0001
9.	Specific Heat of Ablation Gases	.0008	Wall Emissivity	.0001	Wall Emissivity	.0001
10.	Thermal Conductivity (Char and Virgin Mat'l)	.0008	Heat of Gasification	.0001	Heat of Gasification	.0001
11.	Wall Emissivity	.0005				

The number alongside each property is the total variation in the surface recession rate (inches per second) over the range of interest of each parameter.

Selecting the first four properties for each material, a detailed investigation of their variation, the reason for the variation, and the thermal response of the materials allowing each property to vary over its range, was made during Tasks II and III of the program. The conclusions of the materials property determination task (Task II) were that the material conductivities are more dependent on the lamination angle than on the resin or fiber content or the material density. The parameters found to have the major effect on the surface recession rate, such as the melting temperature of the silica fibers and the surface reaction rate constants of the carbonaceous char of the graphite cloth/phenolic resin or the graphite cloth/epoxy resin materials, are independent of the char or virgin plastic density, thermal conductivity, or activation energy. The activation energy is only a function of the resin material and not dependent on any of the other first three parameters. Therefore, it was concluded that each of the first four material properties which most affect the surface recession rate of these rocket nozzle materials are essentially independent of each other. Thus, during Task III the thermal performance (surface recession) of the three materials were analytically evaluated allowing each property to vary over its entire range regardless of the values of the other properties.

The surface recession of the silica cloth/phenolic resin material was most influenced by the melting temperature of the silica fiber. The melting temperature range for the silica fiber extended from 3000°R to 4000°R. Increasing the melting temperature from 3000°R to 4000°R decreased the recession rate by a factor of three. The virgin plastic density, specific heat and activation energy are the next most important material properties affecting the surface recession of the silica cloth/phenolic resin material. The combination of these properties in going from the minimum (88 lb/ft^3) to the maximum (118 lb/ft^3) value of virgin plastic density, from the maximum (75600 BTU/lb) to the minimum (21600 BTU/lb) value of activation energy and from the minimum (.26 BTU/lb°R @ 530°R) to the maximum (.36 BTU/lb°R @ 530°R) value of specific heat increases the surface recession rate by 91 percent. Therefore, it is the melting temperature of the silica fiber which has the greatest effect on the surface recession of the silica phenolic material.

The surface reaction constants most influence the surface recession of both the graphite cloth/phenolic resin and the graphite cloth/epoxy resin materials. The surface reaction constants are defined by the following equation:

$$\dot{m}_o = \frac{\dot{q}_c}{K_1 + K_2 (h_r - h_w)}$$

where $\dot{m}o$ is the mass loss from the surface of the material, $\dot{q}_c$ is the convective heat flux received at the wall, K_1 and K_2 are the reaction constants, h_r is the recovery enthalpy; and h_w is the enthalpy of the boundary layer gases evaluated at the wall temperature. The actual values of K_1 and K_2 depend on chemical species in the boundary layer in addition to the chemical composition of the surface of the material. The values of K_1 and K_2 can be determined either empirically, through the correlation of experimental data obtained from the

exposure of the material to the exhaust products of a rocket engine or, theoretically, through the use of a chemically reacting boundary layer program. Since the operating pressures of most rocket engines are relatively high (> 10 atm) and the temperature of the exhaust products is less than $8000^{o}R$, the graphite ablation is controlled by species diffusion within the boundary layer. Therefore, the surface mass loss may be calculated using a multicomponent chemical model as developed by Scala and Gilbert (Reference 1). The results of these calculations are then correlated, yielding K_1 and K_2. For graphitic materials exposed to a turbulent air boundary layer, the constants K_1 and K_2 are 4240 and 5.77 respectively. For the extremes of the chemical composition of the propellents considered in this study, the range of values for the constants were 1,000 to 12,000 for K_1 and 2 to 10 for K_2. The surface recession rate of the graphite cloth/phenolic resin material increases from approximately 0.003 inches per second to approximately 0.024 to 0.027 inches per second in going from the maximum values of the surface reaction constants to their minimum value. Similarly for the graphite cloth/epoxy resin material, the surface recession rate increased from approximately 0.003 inches per second to 0.030 inches per second. The other three properties, char density, thermal conductivity and virgin plastic density, which most influence the surface recession rate, have a considerably lesser effect on the surface recession. The combination of these properties in going from the maximum (82 lb/ft^3) to the minimum (70 lb/ft^3) value of char density, from the minimum (1.3×10^{-4} BTU/ft-sec^{o}R @ 530 ^{o}R) to the maximum (11.3×10^{-4} BTU/ft-sec^{o}R @ 530^{o}R) value of thermal conductivity and from the maximum (95 lb/ft^3) to the minimum (85 lb/ft^3) value of virgin plastic density causes the surface recession rate of the graphite cloth/phenolic resin material to increase only 44 per cent. Similarly the surface recession rate for graphite cloth/epoxy resin material increases only 39 per cent in allowing the char density to decrease from 76 to 64 lb/ft^3, the thermal conductivity to increase from its minimum to its maximum value (1.2×10^{-4} to 11.4×10^{-4} BTU/ft-sec^{o}R @ 530^{o}R) and the virgin plastic density to decrease from 95 lb/ft^3 to 85 lb/ft^3. Therefore, to minimize the surface recession of graphitic materials, additives or methods of protecting the nozzle walls from the reactive chemical species in the boundary are desirable.

DISCUSSION

The analytical investigation of the influence of the material properties and the external environment on the ablative performance of silica phenolic, graphite phenolic and graphite epoxy was divided into three phases or tasks. The first task was a screening investigation to determine the relative importance of each parameter in the ablation or surface recession process. The second task was to determine the range of variation of the four most important material properties affecting the surface recession. The third task was a detailed study of the ablation performance as these four parameters were allowed to change. The analytical evaluation of the material performance was accomplished by using the Reaction Kinetics Ablation Program (REKAP) developed on NASA Lewis Contract NAS3-2566. A mathematical description of the program is given in Appendix A.

The screening investigation involved evaluating the steady surface recession rate of the three materials for each of several variables. The variables included material properties and environments. The variables considered were:

Material Properties

1. Char Density
2. Virgin Plastic Density
3. Char Thermal Conductivity
4. Virgin Material Thermal Conductivity
5. Char Specific Heat
6. Virgin Material Specific Heat
7. Heat of Gasification
8. Collision Frequency
9. Activation Energy
10. Heat of Melting or Heat of Reaction of Reinforcing Fibers
11. Wall Emissivity
12. Specific Heat of Ablation Gases
13. Melting Temperature of Reinforcing Fibers

Environment Parameters

1. Heat Transfer Coefficient

2. Recovery Temperature

3. Nozzle Geometry

The ranges of the material properties used for the screening process are tabulated in Table 1. The nominal material property values are those which are commonly accepted as being the average properties for these classes of materials. The range of each variable is based on numerous ground test results and the judgement of material manufacturers of what future modification in the material formulation would do to the material properties. The environment parameters were those calculated for the nozzle throat, assuming the propellant combinations to be either N_2O_4/Aerozine 50 or OF_2/B_2H_6, throat diameters of 1.2 and 7.82 inches, a chamber pressure of 100 psia and a combustion temperature (or recovery temperature) corresponding to a C* efficiency of 96 per cent. Maximum environment parameters for the graphite phenolic and graphite epoxy materials resulted from the OF_2/B_2H_6 propellant combination but are limited to the 1.2 inch diameter throat. The range of environments for the silica phenolic material results from considering both the 1.2 and 7.82 inch diameter throat nozzle using the N_2O_4/Aerozine 50 propellant combination only. The procedure followed during the screening effort was to vary each of the parameters given in Table 1 individually while holding the rest of the parameters at their nominal values. Tabulated in Table 2 in descending order are the parameters and their relative importance in effecting the surface recession of the three materials. The relative importance parameter is the change in surface recession rate as the parameter is varied over its range. The actual surface recessions as functions of the various parameters, are presented in Figures 6 through 44. The thermal conductivities and specific heats are presented as ratios (the value under investigation divided by the nominal value) rather than the absolute value, since in this way the temperature variation was eliminated.

The environment parameters (film coefficient and recovery temperature) appeared among the first four parameters which most affect the surface recession rate of all materials. Since these parameters were independent of material, they were not investigated any further. The nominal environment conditions corresponding to the propellants and nozzle sizes were used during phase three of the investigation. The four material properties selected for the detailed investigation were:

Silica Cloth/ Phenolic Resin	Graphite Cloth/ Phenolic Resin	Graphite Cloth/ Epoxy Resin
Melting Temperature of Reinforcing Fibers	Surface Reaction Constants K_1 and K_2	Surface Reaction Constants K_1 and K_2
Virgin Plastic Density	Char Density	Char Density
Specific Heat (Solid)	Thermal Conductivity	Thermal Conductivity
Activation Energy	Virgin Plastic Density	Virgin Plastic Density

The surface reaction constants K_1 and K_2 are dependent on the composition of the boundary layer gases and on the chemical composition of the ablative material. Since these constants describe a single surface reaction rate, they were grouped together and were considered to be a single value during Phase III.

Tabulated in Table 3 in descending order are the material properties which most affect the steady-state mass loss rates. The "Relative Importance Parameter" columns within this table give the mass loss rate differences between that occuring at the maximum and minimum values of each of the properties. Mass loss rates are shown in Figures 45 through 80.

Tabulated in Table 4 is the amount of internal degradation, or increase in char thickness, occurring during the nozzle cool-down period. The nominal degradation during nozzle cool-down of the Silica Cloth/Phenolic Resin material is approximately 1/6 that of the other two materials. This is due to the fact that less thermal energy is stored in the char material. Similarly, it can be seen that when the thermal or structural properties are such that very little char is formed (for example, the low melting temperature of the reinforcing fiber condition), the internal degradation during cool-down is minimal.

The Phase II portion was a study to characterize the variation in thermal properties resulting from processing and fabrication techniques for silica-phenolic, graphite-phenolic, and graphite-epoxy materials. This effort was primarily accomplished by conducting an extensive literature search of existing data generated by both government and industry sponsored efforts. Certain prominent trends and peculiarities were discernible in the variations in thermal conductivity and specific heat coefficients due to change in lamination angle, resin content, density, and lot-to-lot variation.

Table 5 identifies the graphite-phenolic thermal conductivity data plotted in Figure 82 with respect to lamination angle, resin content, density, and source of information. Figure 82 illustrates, in general, that an increase in the resin content of the graphite-phenolic laminates, keeping lamination angle constant, decreases the thermal conductivity. For example, an increase in resin from 30 percent to 50 percent decreases both the across lamina and with lamina direction (Figure 81) thermal conductivity coefficients for a particular resin-cloth composite by approximately 43 percent (Figure 82, curves 13 and 16) and 25 percent (Figure 82, curves 1 and 6) respectively (See Reference 13). Also, a decrease in thermal conductivity with decreasing density was observed for the across lamina specimens. This trend is anticipated since an increase in resin content would be expected to result in a graphite-phenolic composite of decreased density and lower interlamina thermal conductance. This dependence of thermal conductivity upon changes in resin content and/or density may well explain the variation between lots of graphite-phenolic.

It was observed that the width of the scatter bands for the thermal conductivity data of the across lamina and with lamina specimens was comparable. However, the values of thermal conductivity for the with lamina specimens are considerably higher than those for the across lamina. This is true because a more direct path for heat flow exists in the warp or fill direction compared to the across lamina path with its discontinuous resin-cloth layered configuration. Also, for the "with lamina direction" one observes higher thermal

conductivity coefficients for the warp direction whose fibers are more direct and usually more numerous than for the woven fill direction which normally contains less fibers per unit length. For example, a 23 percent difference in thermal conductivity coefficients between the warp and fill directions was observed for two graphite-phenolic specimens of identical composition (See Figure 82). This points out the hazard in simply defining a single thermal conductivity function for this type of material.

Figure 84 shows a slight variation in specific heat for the graphite-phenolic materials. This is due to the fact that specific heat does not appear to be as strong a function as thermal conductivity of resin content, density, or lot-to-lot variation. It can also be seen that, as expected, lamination angle has no effect upon specific heat.

Based upon the data listed in Tables 5 and 6 and plotted in Figures 82 and 83, nominal curves for the thermal conductivity and specific heat coefficients of graphite-phenolic are shown with a tolerance band in Figures 84 and 85, respectively. Due to the scarcity of char data, the tolerances placed on the virgin material thermal conductivity and specific heat nominal curves were extended to the char portion of the curves. The tolerance bands for graphite-phenolic composites, as well as the other subject materials, are wider than those which appeared in the preliminary release as a result of the evaluation of additional data.

The previous trends observed for graphite-phenolic are not discernible for silica-phenolic. In fact, the trend is reversed for one composite grouping where a lower density is recorded in both the across and with lamina directions for the lower resin content composites (See Tables 7 and 8). This suggests that the creation of voids may have been associated with the reduction in resin content. The presence of high void content would be expected to yield lower thermal conductivity coefficients.

Referring to Figure 86, it can be seen that the with lamina materials exhibit higher thermal conductivity coefficients than the across lamina materials. Also, the spread in thermal conductivity data for the with lamina composites is less than that for the across lamina composites.

A slight variation in the specific heat of the silica-phenolic composites can be seen in Figure 87. The specific heat coefficients of these composites are lower than those of graphite-phenolic and graphite-epoxy. Since the silica cloth has a lower specific heat than graphite cloth, it is not surprising that this trend is retained when each system is introduced as a woven cloth in a resin binder. It should also be noted that the specific heat of the phenolic resin is significantly higher than that of the reinforcements of silica and graphite resulting in composite specific heat coefficients lying between those of the resin and the reinforcement.

Nominal curves for the thermal conductivity and specific heat coefficients of silica-phenolic are shown with a tolerance band in Figures 88 and 89, and are based on the data presented in Figures 86 and 87. It should be noted that the tolerances placed on the virgin material thermal conductivity and specific heat curves were extended to the char portion of the curve because of the lack of char data. In fact, the thermal conductivity and specific heat coefficients of fused amorphous silica at elevated temperatures served as the basis for the high temperature trend (See Figures 86 and 87).

For the graphite-epoxy system, experimental thermal properties data is very limited. Therefore, the nominal curves of thermal conductivity and specific heat coefficients of graphite-epoxy presented (in Figures 90 and 85, respectively) are based on the trends established for graphite-phenolic because of the similarity that exists between the thermal conductivity and specific heat coefficients of the phenolic and epoxy resin systems, with one exception (Reference 10). This exception occurs in the region of resin decomposition. In this region the thermal conductivity of graphite-epoxy is shown with a steeper slope than that of graphite-phenolic. This arises because epoxy resins lose approximately 80 percent of their initial weight in this region of decomposition, whereas the phenolic resins lose about 47 percent of their initial weight in this region which extends over a wider temperature range. In addition it should be noted that the epoxy systems have poor thermal stability at high temperatures, and therefore, are not desirable for rocket nozzle design.

A fiber reinforced plastic, such as discussed in the context of this report, is normally fabricated from prepreg materials. This prepreg is a web material such as carbon cloth, refrasil cloth, etc., impregnated with a resin. The resin is advanced to a dry stage by partial curing. This operation is continuous, and is accomplished by passing the web through a pan of resin, then metering through squeeze rolls, followed by resin advancement into temperature controlled ovens or towers. From these prepreg materials, various shapes are laid up in layer form utilizing predesigned patterns. These materials are then fully cured in molds under heat and pressure to attain the desired configuration. In most cases, additional machining techniques are required to complete the fabrication procedure.

The pressure employed in molding is dependent upon the resin system employed. Cure of epoxy type resins is by addition; i.e. no volatile products are produced or evolved in the cure mechanism. Thus relatively low pressures are required in laminating. The phenolic resins cure by condensation; i.e., water is a by-product of the cure mechanism. Thus to maintain the desired high density of the molded part, high pressure, in excess of 1000 psi, is required in molding these materials.

The curing temperature is dependent upon the resin system. Temperatures normally applied are in the 300°F range. Normal practice is to step-wise attain the maximum temperature and to hold sufficiently long enough to insure thorough resin cure. This time factor also is dependent upon the resin system employed.

Depending on several factors such as shape, size, materials, etc., the part may be fabricated between platens, by hydraulic press or in a hydroclave. (a hydroclave is a pressure container filled with water; the sealed, immersed laminate is cured by the hot water under hydraulic pressure).

The amount of resin, the degree of resin advancement, and the volatile content of the prepreg material is carefully controlled prior to laminating. A resin advanced too far will not flow and knit in the laminating operation. A resin with excess flow will squeeze out, and result in a resin starved laminate. With phenolic resins, a critical level of volatile is essential to plasticize the resin, and obtain the desired resin flow. Excessive volatiles distort particular laminate properties - dielectric, ablation, etc.

When a load is applied to a fiber reinforced plastic material, a complex stress pattern is produced within the material depending upon the orientation and proportion of the fiber-matrix as well as strength and adhesive properties of the resinous component. In these composite plastic structures, the resin supports the reinforcement under hydrostatic pressure, and the reinforcement continues to function as a load-carrying member up to the point at which this pressure decreases as the resin yields, following which the composite fails. A common mode of tensile failure is a delamination between plies and across plies.

The limiting strength of current unreinforced resin systems appears to be about 15,000 psi in tension and 25,000 psi in compression. Thus, to attain improved physical properties, reinforcement materials are employed with the resinous adhesives. The choice of these materials are usually selected by trade-off studies, and are strictly dependent upon the demands imposed by the end application.

From a consideration of the variables involved in making reinforced shapes, it is apparent that a process history and web orientation be established before acceptable physical properties can be determined in a uniform and realistic manner. Some variation is to be expected when comparing properties provided by several techniques and on parts prepared using non-uniform processing.

The manufacture of sophisticated items such as an ablative rocket nozzle requires the utlization of all of the art and science at the disposal of the laminating industry. Due to the non-homogeneity of the product, the resulting properties are directionally dependent and subject to variations caused by the processing techniques. A specific resin fiber system is seldom processed in the same manner by individual vendors which in turn potentially introduces further property variations within the laminates. The variations in vendor processing are, most often, due to capability of fabricating equipment and manufacturing philosophy. In general, the methods employed are company proprietary and are not for general publication.

The properties of laminates will vary with different levels of resin content. Of course, many additional factors come into play. The variation in resin content, or density of the laminate, however, is a very important processing factor and much effort is extended to control the ratios of reinforcement to resin within the laminate. In addition to the proportions of these two ingredients, there are other considerations such as the relative location of the resin on and in the web, as well as the degree of resin advancement prior to molding. Additional factors which influence final properties at this point of fabrication include age of material prior to laminating, residual volatiles, etc.

The mechanism of impregnating and wetting the fibers in the reinforcing bundle is to utilize a solvent solution of the resin. The solvents employed with the systems discussed herein are normally low boiling materials such as alcohol, toluene, etc. The solution may contain additional proprietary ingredients such as wetting agents, surface activating agents, fillers, catalysts, etc.

The surfaces of filamentary and fibrous materials are not always receptive to chemical bonding to matrices, so that untreated fiber surfaces are rarely used in the preparation of reinforced composites. A specific example may be found in the use of finishes of various types of surfaces of glass fibers. Silane or chrome finishes with appropriate organic groups in the molecule are widely used to form a "bridge" between the glass surface and the resin; the silane portion of the bridging agent reacts with the 0-Si-0 molecules in the glass, and the organic portion is free to react with the resinous binder. In some instances, this bridging agent is incorporated in the impregnating solution and in others, it is applied by a separate operation to the glass surface prior to resin impregnation. The use of this agent is not reflected in the density or resin content of the final laminate; it does, however, display its absence by changes in mechanical properties upon aging.

In some instances, such as with carbon, improved fiber wetting by the phenolic resin is realized with traces of proprietary wetting agents added to the resin solution. This item promotes greater uniformity in resin distribution and thus enhances the uniformity of the laminated product.

A factor in considering carbon webs initially was the wide variation of the active surface area within a given batch of carbon cloth. This variation resulted in poor impregnation and excessive localized deposits of resin on the web surface. This condition very likely distorted physical properties. The vendors of carbon cloth today appear to have this problem under satisfactory control.

Test data developed in the evaluation of carbon phenolic composites in rocket engines indicated the need of a carbon filler in addition to the carbon web within the fabricated parts. These data indicated improved ablation resistance, thus, the same materials are durrently employed in carbon base heat shields. Studies are under way to establish the need of these fillers. The presence of these carbon fillers within the resin solution reduces or retards resin impregnation into the fiber bundle, deposits the particles onto the web surface and results in a general lowering of the potential available interply adhesive bond strength, which thus results in lower flexural strength of the finished laminates.

Of the systems considered in this evaluation, only the epoxy formulations incorporate a catalyst component. The phenolic resins cure by condensation reactions under heat and high pressure; the epoxy resins cure by addition in the presence of a catalytic agent under heat and relatively moderate pressures. In general, epoxy systems may have a greater density spread due to the lower fabricating pressures.

The observed density variations of 35 phenolic carbon and 48 phenolic refrasil items recently purchased to a given density specification of 92.5 lb/ft^3 for phenolic carbon and 105 lb/ft^3 for phenolic refrasil are as follows:

Density of Laminates (lb/ft^3)

	Phenolic Carbon	Phenolic Refrasil
Min.	90.5	99.5
Max.	93	110
Average	92.5	105
Range	-2, + 1/2	± 5

The refrasil fibers have a density of 131 lb/ft^3 and the carbon 106 lb/ft^3. Data on the graphite phenolic was not available, but it is expected that its density variation would be similar to that of the carbon base laminates. Data on epoxy composite formulations was not obtained.

The narrow spread in density range for the carbon phenolic system is indicative of the excellent control of the processing variables. The spread in density range for phenolic refrasil, though broader, is reasonable.

The relationship of density of a laminate to some physical properties has been established. Graphic representation of these relationships, assuming proper fiber treatment, displays optimum or maximum values over a relatively narrow spread in resin content. Resin content by itself, however, is not indicative of the material performance. The distribution of the resin within the prepreg and the production and fabrication procedures of the laminate combined, impart the final system properties.

With a given resin system, differences exist in the impregnating characteristic of various webs. Thus the ability of the resin to wet through and impregnate the center of the fiber bundle contributes to the variability of the product density, etc.

For example, the fibrous bundles, be they carbon, refrasil, asbestos, etc., in each case require a certain amount of resin to restrain their relative motion by filling in the natural voids within the bundle. In turn, the voids between bundles, and likewise, the voids between plies, etc., each require a specific resin content which, commensurate with optimum fabrication procedures, reflect maximum or ultimate performance. Thus a specific resin content in a given laminate may yield a maximum compressive strength, whereas a different level of resin content may be required to realize the ultimate in interlaminar bond strength. Obviously, in these instances, a trade-off is essential to comply with the overall desired end properties of the laminate.

Thus in rocket engines, the mechanical ablative performance is determined by the selection of raw materials, and each succeeding step in combining these materials and processing them into finished hardware. Control of the potential variables in overall processing of the materials is essential to realize ultimate quality parts.

Based on the results of the material property investigation (Phase II), the variations in the thermal conductivities were more dependent on lamination angles than on the resin or fiber content. The parameters which were shown to have a major effect on the surface recession rate, such as melting temperature of the silica fibers and the surface reaction constants of the carbonaceous char, were independent of the char or virgin plastic densities, thermal conductivity, or activation energy. The activation energy was a function only of the resin material and not dependent on the other three parameters. Therefore, it was concluded that each of the properties is independent of the others. The material performance during the detailed investigation of Phase III was calculated allowing each of the properties to vary over their entire range.

The ablative performance during Phase III was calculated using the information given in Tables 9, 10, 11 and 12 and in Figures 84, 85, 88, 89 and 90. The surface recession rates for silica cloth/phenolic resin are plotted in Figures 6 through 23 for the range of material and environment properties given in Table 1. Figures 91 through 99 show the recession rates obtained for the conditions existing within the 1.2 inch throat diameter nozzle, while Figures 100 through 108 give the recession rates for a 7.82 inch throat diameter nozzle. Figures 91 through 108 indicate the following descending order of property influence on the recession rate of silica cloth/phenolic resin A, for the property variations given in Table 1: silica fiber melting temperature, virgin plastic density, specific heat, activation energy. The specific heat is presented as the ratio of the value used to the nominal value. The recession rates for the 1.2 inch throat diameter nozzle were slightly higher than those for the 7.82 inch throat diameter nozzle, which is expected since the convective heat transfer coefficient is higher for the smaller throat diameter (0.294 BTU/ft.^{2} sec ^oF as compared to 0.223 BTU/ft.^{2} sec ^oF for the larger throat diameter).

The surface recession rates for the graphite cloth/phenolic resin and for the graphite cloth/epoxy resin materials are shown in Figures 109 through 117 and in Figures 118 through 126 respectively. For both of these materials, the property which has the strongest influence on surface recession rate is the reaction rate (constants K_1 and K_2), followed (in descending order) by char density, thermal conductivity and virgin plastic density. The thermal conductivity is divided by the nominal value in order to eliminate the effect of the variation of conductivity with temperature (Figures 115-117 and 124-126).

TABLE 1. PROPERTY VARIATION FOR SCREENING INVESTIGATION

PROPERTY	SILICA CLOTH/PHENOLIC RESIN			GRAPHITE CLOTH/PHENOLIC RESIN			GRAPHITE CLOTH/EPOXY RESIN		
	Min	Nominal	Max	Min	Nominal	Max	Min	Nominal	Max
Material Properties									
1. Char Density (lb/ft^3)	78	92	106	64	76	88	58	70	82
2. Virgin Plastic Density (lb/ft^3)	94	110	126	76	87	101	23	87	101
3. Char Thermal Conductivity (Btu/ft-sec^oR)		Figure 1			Figure 2			Figure 3	
4. Virgin Material Thermal Conductivity (Btu/ft-sec^oR)		Figure 1			Figure 2			Figure 3	
5. Char Specific Heat (Btu/lb^oR)		Figure 4			Figure 5			Figure 5	
6. Virgin Material Specific Heat (Btu/lb^oR)		Figure 4			Figure 5			Figure 5	
7. Heat of Gasification (Btu/lb)	100	550	1000	100	550	1000	100	550	1000
8. Collision Frequency (1/sec)	130	3×10^4	7.5×10^7	130	3×10^4	7.5×10^7	300	3×10^4	3×10^7
9. Activation Energy (Btu/lb)	21600	48600	75600	21600	48600	75600	20000	37500	55000
10. Heat of Melting or Heat of Reaction of Reinforcing Fibers (Btu/lb)	30	71	111	Surface Reaction			Surface Reaction		
11. Wall Emissivity	0.4	0.65	0.9	0.7	0.8	0.9	0.7	0.8	0.9
12. Specific Heat of Ablation Gases (Btu/lb^oR)	0.3	0.75	1.2	0.3	0.75	1.2	0.3	0.75	1.2
13. Melting Temperature Temperature of Reinforcing Fibers (^oR)	3000	3600	4200	Surface Reaction			Surface Reaction		
				$K_1 = 1000$	4240	12000	$K_1 = 1000$	4240	12000
				$K_2 = 2$	5.77	10	$K_2 = 2$	5.77	10

TABLE 1. PROPERTY VARIATION FOR SCREENING INVESTIGATION (CONT)

PROPERTY	SILICA CLOTH/PHENOLIC RESIN			GRAPHITE CLOTH/PHENOLIC RESIN			GRAPHITE CLOTH/EPOXY RESIN		
	Min	Nominal	Max	Min	Nominal	Max	Min	Nominal	Max
Environment Parameters									
1. Heat Transfer Coefficient (Btu/ft^2-sec^oR)	0.118	0.294	0.47	0.10	0.425	0.7	0.10	0.425	0.75
2. Recovery Temperature (^oR)	3500	4565	5630	3500	4990	8160	3500	4990	8160
3. Nozzle Geometry (Throat Diameter in Inches)	1.5	7.82	∞	1.5	7.82	∞	1.5	7.82	∞

TABLE 2. SURFACE RECESSION RATE RESULTS OF SCREENING STUDY

SILICA CLOTH/PHENOLIC RESIN		GRAPHITE CLOTH/PHENOLIC RESIN		GRAPHITE CLOTH/EPOXY RESIN	
Properties in Decreasing Effect	Relative Importance Parameter (in/sec)	Properties in Decreasing Effect	Relative Importance Parameter (in/sec)	Properties in Decreasing Effect	Relative Importance Parameter (in/sec)
Melting Temperature of Reinforcing Fibers	0.0288	Recovery Temperature	0.0085	Recovery Temperature	0.0083
Recovery Temperature	0.0255	Surface Reaction Constant (K_1)	0.0064	Surface Reaction Constant (K_1)	0.0082
Film Coefficient	0.0238	Film Coefficient	0.0042	Film Coefficient	0.0053
Virgin Plastic Density	0.007	Surface Reaction Constant (K_2)	0.0031	Surface Reaction Constant (K_2)	0.0041
Specific Heat (Solid)	0.005	Char Density	0.002	Char Density	0.0028
Activation Energy	0.003	Thermal Conductivity	0.0017	Thermal Conductivity	0.0018
Char Density	0.002	Virgin Plastic Density	0.00085	Virgin Plastic Density	0.0011
Collision Frequency	0.001	Collision Frequency	0.00065	Activation Energy	0.0006
Heat of Gasification	0.0009	Specific Heat (Solid)	0.0004	Specific Heat (Solid)	0.0004
Heat of Vaporization of Reinforcing Fibers	0.0008	Activation Energy	0.0002	Specific Heat (Gases)	0.0004
Specific Heat (Gases)	0.0008	Specific Heat (Gases)	0.0002	Collision Frequency	0.0001
Thermal Conductivity	0.0008	Wall Emissivity	0.0001	Wall Emissivity	0.0001
Wall Emissivity	0.0005	Heat of Gasification	0.0001	Heat of Gasification	0.0001

TABLE 4. ABLATIVE MATERIAL DEGRADATION DURING NOZZLE COOL-DOWN

SILICA CLOTH/PHENOLIC RESIN			GRAPHITE CLOTH/PHENOLIC RESIN			GRAPHITE CLOTH/EPOXY RESIN		
Properties	Property Value	Degradation (In.)	Properties	Property Value	Degradation (In.)	Properties	Prop. Value	Degradation (In.)
Activation Energy (Btu/lb)	21600 48600 75600	0.079 0.009 ≈ 0	Recovery Temperature (^{o}R)	3500 4990 8160	0.018 0.055 0.101	Activation Energy (Btu/lb)	20000 37500 55000	0.130 0.075 0.034
Melting Temperature of Reinforcing Fibers (^{o}R)	3000 3600 4200	≈ 0 0.009 0.027	Activation Energy (Btu/lb)	21600 48600 75600	0.063 0.055 0.015	Recovery Temperature (^{o}R)	3500 4990 8160	0.056 0.075 0.123
Recovery Temperature (^{o}R)	3500 4565 5630	0.025 0.009 ≈ 0	Film Coefficient (Btu/ft^2-sec ^{o}R)	0.10 0.425 0.7	0.042 0.055 0.077	Heat of Gasification (Btu/lb)	100 550 1000	0.102 0.075 0.042
Film Coefficient (Btu/ft^2-sec ^{o}R)	0.118 0.294 0.24	0.015 0.009 ≈ 0	Chemical Reaction (K_1)	1000 4240 12000	0.042 0.055 0.058	Chemical Reaction (K_1)	1000 4240 12000	0.063 0.075 0.095
Thermal Conductivity Ratio (K/K_{mean})	0.52 1.0 1.64	0.007 0.009 0.011	Virgin Plastic Density (lb/ft^3)	76 87 101	0.063 0.055 0.049	Film Coefficient (Btu/ft^2-sec ^{o}R)	0.10 0.425 0.7	0.067 0.075 0.098
Virgin Plastic Density (lb/ft^3)	94 110 126	0.008 0.009 0.010	Chemical Reaction (K_2)	2 577 10	0.048 0.055 0.057	Char Density (lb/ft^3)	58 70 82	0.055 0.075 0.082
Specific Heat Ratio (Cp/Cp_{mean})	0.8 1.0 1.2	0.008 0.009 0.010	Thermal Conductivity Ratio (K/K_{mean})	0.30 1.0 1.7	0.051 0.055 0.058	Virgin Plastic Density (lb/ft^3)	73 87 101	0.087 0.075 0.063

TABLE 3. STEADY-STATE MASS LOSS RATE OR INTERNAL DEGRADATION RATE RESULTS

SILICA CLOTH/PHENOLIC RESIN		GRAPHITE CLOTH/PHENOLIC RESIN		GRAPHITE CLOTH/EPOXY RESIN	
Properties in Decreasing Order of Effect	Relative Importance Parameter (lb/ft^2 sec)	Properties in Decreasing Order of Effect	Relative Importance Parameter (lb/ft^2 sec)	Properties in Decreasing Order of Effect	Relative Importance Parameter (lb/ft^2 sec)
Char Density	0.041	Char Density	0.028	Char Density	0.036
Melting Temperature of Reinforcing Fibers	0.031	Virgin Plastic Density	0.027	Virgin Plastic Density	0.035
Activation Energy	0.029	Recovery Temperature	0.015	Recovery Temperature	0.022
Virgin Plastic Density	0.028	Activation Energy	0.011	Thermal Conductivity	0.014
Recovery Temperature	0.023	Thermal Conductivity	0.008	Activation Energy	0.013
Film Coefficient	0.018	Film Coefficient	0.010	Film Coefficient	0.0057
Thermal Conductivity	0.010	Surface Reaction Constant (K_1)	0.005	Surface Reaction Constant (K_1)	0.010
Specific Heat (Solid)	0.008	Surface Reaction Constant (K_2)	0.003	Surface Reaction Constant (K_2)	0.006
Wall Emissivity	0.0012	Specific Heat (Solid)	0.002	Specific Heat (Solid)	0.003
Heat of Gasification	0.0006	Specific Heat (Gases)	0.0004	Specific Heat (Gases)	0.001
Heat of Vaporization of Reinforcing Fibers	0.0006	Heat of Gasification	0.0004	Heat of Gasification	0.001
Specific Heat (Gases)	0.0004	Wall Emissivity	≈ 0	Wall Emissivity	≈ 0

TABLE 4. ABLATIVE MATERIAL DEGRADATION DURING NOZZLE COOL-DOWN (Continued)

SILICA CLOTH/PHENOLIC RESIN			GRAPHITE CLOTH/PHENOLIC RESIN			GRAPHITE CLOTH/EPOXY RESIN		
Properties	Property Value	Degra-dation	Properties	Property Value	Degra-dation	Properties	Prop. Value	Degra-dation
Heat of Gasification (Btu/lb)	100 550 1000	0.009 0.009 0.009	Specific Heat Ratio (Cp/Cp_{mean})	0.8 1.0 1.2	0.054 0.055 0.057	Thermal Conductivity Ratio (K/K_{mean})	0.32 1.0 1.69	0.059 0.075 0.083
Heat of Vaporization of Reinforcing Fibers (Btu/lb)	30 71 111	0.009 0.009 0.009	Char Density (lb/ft^3)	64 76 88	0.054 0.055 0.056	Chemical Reaction (K_2)	2 5.77 10	0.064 0.075 0.084
Wall Emissivity	0.4 0.65 0.9	0.009 0.009 0.009	Heat of Gasification (Btu/lb)	100 550 0.000	0.055 0.055 0.053	Specific Heat Ratio (Cp/Cp_{mean})	0.79 1.0 1.19	0.073 0.075 0.078
Specific Heat of Ablation Gases (Btu/lb ^oR)	0.3 0.75 1.2	0.009 0.009 0.009	Specific Heat of Ablation Gases (Btu/lb ^oR)	0.3 0.75 1.2	0.055 0.055 0.055	Wall Emissivity	0.7 0.8 0.9	0.076 0.075 0.075
Char Density (lb/ft^3)	78 92 106	0.009 0.009 0.009	Wall Emissivity	0.7 0.8 0.9	0.055 0.055 0.055	Specific Heat of Ablation Gases Btu/lb ^oR)	0.3 0.75 1.2	0.075 0.075 0.075

TABLE 5. GRAPHITE CLOTH/PHENOLIC RESIN - THERMAL CONDUCTIVITY

FIGURE NO.	CURVE NO.	DIRECTION OF MEASUREMENT	RESIN CONTENT (%)	DENSITY (LB/FT^3)	LITERATURE SOURCE REF. NO. (SEE REFERENCES)
83	1	With Lamina	30	---	13
	2	With Lamina	29 ± 2.5	93.5	2
	3	With Lamina	30	---	13
	4	With Lamina (Warp)	36	92	2
	5	With Lamina (Fill)	36	92	2
	6	With Lamina	50	---	13
	7	Across Lamina	29 ± 2.5	93.5	2
	8	Across Lamina	29 ± 2.5	93.5	2
	9	Across Lamina	50	---	13
	10	Across Lamina	29 ± 2.5	93.5	2
	11	Across Lamina	30	90	11
	12	Across Lamina	36	92	2
	13	Across Lamina	30,30	90,90	11,13
	14	Across Lamina	40	89	11
	15	Across Lamina	40	85	11
	16	Across Lamina	50	---	13
	17	10^{o} Lamination	--	70	16
	18	20^{o} Lamination	--	76	3

Here, $\dot{W}_i$ is the net amount of specie i produced per unit volume per unit time. Note that $\dot{W}_i$ includes the formation of the species from the unreacted solid as well as any further gas phase or gas-solid phase reactions that might occur.

The surface integral involved in (13) can be transformed into a volume integral by means of the Divergence Theorem*:

$$\int_A \rho_i \left(\vec{V} + \vec{V}_{d_i} \right) \cdot \vec{\eta} \, dA = \int_V \nabla \cdot \rho_i \left(\vec{V} + \vec{V}_{d_i} \right) dV$$

The order of integration and differentiation can be interchanged* so that:

$$\frac{d}{dt} \int_V \rho_i \, dV = \int_V \frac{\partial \rho_i}{\partial t} \, dV$$

Substituting these relations into (13) yields:

$$\int_V \left[\frac{\partial \rho_i}{\partial t} + \nabla \cdot \rho_i \left(\vec{V} + \vec{V}_{d_i} \right) - \dot{W}_i \right] dV = 0$$

Since the volume is arbitrary the integrand must be identically zero. Thus, the species continuity equation is:

$$\frac{\partial \rho_i}{\partial t} + \nabla \cdot \rho_i \left(\vec{V} + \vec{V}_{d_i} \right) = \dot{W}_i \tag{14}$$

Summing this equation over all gaseous species and noting that

$$\sum_i \rho_i \vec{V}_{d_i} = 0 : \sum_i \rho_i = \rho_g : \sum_i \dot{W}_i = \dot{W}_g$$

results in the continuity equation for the gas:

$$\frac{\partial \rho_g}{\partial t} + \nabla \cdot \rho_g \vec{V} = \dot{W}_g \tag{15}$$

*It is assumed that all functions are continuous and continuously differentiable and that the region is simply connected (Reference 6).

Now, gas phase reactions do not change the total mass of gas present; rather, they redistribute the species. Therefore, $\dot{W}_g = \sum_i W_i$ is the total rate at which gas is being produced by the decomposition of the unreacted material and by gas-solid phase reactions.

The continuity equations for the solid species are:

$$\frac{\partial \rho_p}{\partial t} = \dot{W}_p \tag{16}$$

$$\frac{\partial \rho_c}{\partial t} = \dot{W}_c \tag{17}$$

$\dot{W}_p$ is the rate of depletion of the unreacted material due to decomposition. For charring ablation materials, the decomposition is irreversible and the rate at which it proceeds is generally limited by chemical kinetics. $\dot{W}_p$ is deduced from TGA (thermogravimetric analysis) experiments and is often expressed analytically as a single nth order reaction with an Arrhenius "rate constant".

$$\dot{W}_p = - A (\rho_p)^n$$

$$A = A_o \exp \left(- \frac{E}{RT} \right)$$

$\dot{W}_c$ is the rate at which char is formed from the decomposition of the unreacted material (generally a known fraction of W_p) plus gas-solid phase reactions. There is no overall production of mass so that:

$$\dot{W}_p + \dot{W}_c + \dot{W}_g = 0 \tag{18}$$

It is useful to separate out the mass production rates due to the decomposition, the gas phase reactions, and the gas-solid phase reactions. This can be done by introducing some new quantities.

$$\dot{W}_c = - f_c \dot{W}_p + \dot{W}_c'' \tag{19}$$

$$\dot{W}_g = - (1 - f_c) \dot{W}_p + \dot{W}_g'' \tag{20}$$

Here f_c denotes the fraction of unreacted material which forms char (not necessarily constant) and the superscript double prime denotes gas-solid phase reactions only. The first part of these equations state that char and gas are produced from the decomposition of the unreacted material, while the second part accounts for additional formation due to gas-solid phase reactions. Note that

$$\dot{W}_g'' = -\dot{W}_c'' \tag{21}$$

which follows from (18).

Finally, the species continuity equation can be expressed in terms of gas phase reactions only. Using $\rho_i = K_i \rho_g$ and the chain rule on (14) yields:

$$K_i \left[\frac{\partial \rho_g}{\partial t} + \nabla \cdot \rho_g \nabla\right] + \rho_g \left[\frac{\partial K_i}{\partial t} + V \cdot \nabla K_i\right] + \nabla \cdot \left(\rho_g \vec{V}_{d_i} K_i\right) = \dot{W}_i$$

The first term in brackets equals $\dot{W}_g$ by virtue of (15) and so:

$$\rho_g \left[\frac{\partial K_i}{\partial t} + V \cdot \nabla K_i\right] + \nabla \cdot \left(\rho_g K_i \vec{V}_{d_i}\right) = \dot{W}_i' \tag{22}$$

Where:

$$\dot{W}_i' = \dot{W}_i - K_i \dot{W}_g \tag{23}$$

$\dot{W}_i'$ is the net rate of production of the ith species minus the amount of the ith species formed by the decomposition of the unreacted material plus gas-solid phase reactions. Consequently, $\dot{W}_i'$ is the net rate of production due to gas phase reactions only. Note that:

$$\sum_i \dot{W}_i' = 0$$

In general, the $\dot{W}_i'$ are functions of temperature, pressure and composition and are determined from a knowledge of the exact chemical reactions (and these rates) which occur. For very slow reactions in the gas phase (i.e., "frozen-flow"), the $\dot{W}_i' = 0$. For very fast reactions, the flow will be in local thermochemical equilibrium and the $\dot{W}_i'$ are determined by imposing constraints on the composition (i.e., equilibrium "constants").

Energy Equation

The energy equation is derived by applying the First Law of Thermodynamics to a stationary control volume within the material. This means that the time rate of change of the total energy within the volume equals the rate at which energy is transported into the volume

minus the rate at which energy is being convected out plus the rate at which work is being done on the volume. The mathematical expression is

$$\frac{d}{dt}\int_V \left[\rho_p e_p + \rho_c e_c + \sum_i \rho_i \left(e_i + \frac{\vec{V}\cdot\vec{V}}{2}\right)\right] dV = -\int_A \vec{Q}\cdot\vec{n}\, dA$$

$$-\int_A \left[\sum_{i'} \rho_i \vec{V}\left(e_i + \frac{\vec{V}\cdot\vec{V}}{2}\right)\cdot\vec{n}\right] dA + \int_A \vec{P}\cdot\vec{V}\, dA \qquad (24)$$

The energy flux vector Q may be expressed in terms of contributions due to heat conduction, thermal radiation and diffusion (References 2-4):

$$\vec{Q} = \vec{q}_c + \vec{q}_R + \sum_i \rho_i \vec{V}_{d_i} h_i$$

It now remains to relate the heat flux vectors and the surface force per unit area to the variables of the problem. Since the solid and the gas are in intimate contact, it is assumed that the temperature of the gas equals that of the solid. The conduction heat flux vector is approximately linearly dependent upon the temperature gradients. For an isotropic material* this implies

$$\vec{q}_c = -K \nabla T$$

which is Fourier's Law.

For an isotropic material, the heat flux depends upon temperature gradients through a second order conductivity tensor. In rectangular cartesion coordinates, this is (p. 38, Reference 7):

$$\vec{q}_c = K_{i_j} \frac{\partial T}{\partial X_j} \vec{e}_i \qquad (25)$$

For example, the ablation material may be somewhat anisotropic due to fiber-type fillers in the solid material or because of the changes in composition.**

*Isotropic material - medium whose structure and properties in the neighborhood of any point are the same relative to all directions through the point (p. 6, Ref. 7)

**An excellent example of an anisotropic material of current interest is pyrolytic graphite but since it does not decompose in depth it is not pertinent to the present problem.

For the purposes of the present analysis, the material will be considered isotropic although it is noted that it would be easy to include (25) in the analysis should sufficient data be available to justify it. Thus, the conduction heat flux vector is related to the temperature by:

$$\vec{q}_c = - K \nabla T \tag{26}$$

Note that the conductivity will be a weighed average of the conductivities of all species that are present, both solid and gas.

In general, the radiation heat flux vector accounts for the net effect of emission, absorption and scattering of thermal radiation of all wavelengths within the material. It is usually assumed that scattering is negligible, the material is isotropic and that the optical properties do not depend on the wavelength. Even with these drastic assumptions, the calculation of $\vec{q}_R$ is quite complex. Thus, for practical calculations, $\vec{q}_R$ is usually neglected and the transport of thermal radiation is approximately accounted for by an increase in thermal conductivity with temperature.

The surface force per unit area can be related to the stresses by considering the forces acting on a small tetrahedron (p. 101, Reference 8).

$$\vec{P} = \vec{n} \cdot \underset{\sim}{T}$$

$\vec{n}$ is an outward unit normal and $\underset{\sim}{T}$ is a second order stress tensor whose components are σ_{ij}.

Note that this is a dot product of a vector with a tensor and the result is a vector which is different than $\vec{n}$, both in magnitude and direction. Using indicial notation, the surface force would be expressed as:

$$\vec{P} = \sigma_{ij} n_i \vec{e}_j$$

The required work term is:

$$\vec{P} \cdot \vec{V} = (\vec{V} \cdot \underset{\sim}{T}) \cdot \vec{n}$$

The stress tensor may be separated into a hydrostatic pressure component (a scalar) and a viscous stress tensor.

$$\underset{\sim}{T} = - P + \underset{\sim}{\tau}$$

For a linear isotropic fluid, the viscous stresses are linearly related to the velocity gradients. For the purposes of this analysis, the viscous stresses will be retained in the general form of $\underset{\sim}{\tau}$. The final form of the work term is then:

$$\vec{P} \cdot \vec{V} = - (p \vec{V}) \cdot \vec{n} + (\vec{V} \cdot \underset{\sim}{\tau}) \cdot \vec{n}$$

Substituting (26) and (27) into (24) and following exactly the same procedure as with the species continuity equation results in the differential energy equation:

$$\frac{\partial}{\partial t}\left[\rho_p e_p + \rho_c p_c + \sum_i \rho_i \left(e_i + \frac{\vec{V}\cdot\vec{V}}{2}\right)\right] + \nabla\cdot\left[\sum_i \rho_i \vec{V}\left(e_i + \frac{\vec{V}\cdot\vec{V}}{2}\right)\right]$$
$$+ \nabla\cdot\left[\sum_i \rho_i \vec{V}_{d_i} h_i\right] = \nabla\cdot K\nabla T - \nabla\cdot\vec{q}_R - \nabla\cdot p\vec{V} + \nabla\cdot(\vec{V}\cdot\underset{\sim}{\tau}) \tag{28}$$

The various terms of the energy equation can be expanded and rearranged to a more co convenient form. Adding the term $\frac{\partial p}{\partial t} + \nabla\cdot p\vec{V}$ to both sides of (28) and using Dalton's Law gives:

$$\frac{\partial}{\partial t}\left[\rho_p e_p + \rho_c e_c + \sum_i \rho_i \left(e_i + \frac{p_i}{\rho_i} + \frac{\vec{V}\cdot\vec{V}}{2}\right)\right]$$
$$+ \nabla\cdot\left[\sum_i \rho_i \vec{V}\left(e_i + \frac{p_i}{\rho_i} + \frac{\vec{V}\cdot\vec{V}}{2}\right)\right] + \nabla\cdot\left[\sum_i \rho_i \vec{V}_{d_i} h_i\right] \tag{29}$$
$$= \nabla\cdot K\nabla T - \nabla\cdot\vec{q}_R + \frac{\partial p}{\partial t} + \nabla\cdot(\vec{V}\cdot\underset{\sim}{\tau})$$

Noting that

$$h_i = e_i + \frac{p_i}{\rho_i} \quad ; \quad \rho_g = \sum_i \rho_i$$

and using the chain rule, (29) can be expanded to:

$$\left[\rho_p \frac{\partial e_p}{\partial t} + e_{v_p}\frac{\partial \rho_p}{\partial t} + \rho_c \frac{\partial e_c}{\partial t} + e_c \frac{\partial \rho_c}{\partial t} + \sum_i\left(\rho_i \frac{\partial h_i}{\partial t} + h_i \frac{\partial \rho_i}{\partial t}\right)\right.$$
$$\left. + \frac{\partial}{\partial t}\left(\rho_g \frac{V\cdot V}{2}\right)\right] + \left[\sum_i\left(\rho_i\left(\vec{V} + \vec{V}_{d_i}\right)\cdot\nabla h_i + h_i \nabla\cdot\rho_i\left(\vec{V} + \vec{V}_{d_i}\right)\right)\right. \tag{30}$$
$$\left. + \nabla\cdot\rho_g\vec{V}\frac{\vec{V}\cdot\vec{V}}{2}\right] = \nabla\cdot K\nabla T - \nabla\cdot\vec{q}_R + \frac{\partial p}{\partial t} + \nabla\cdot(\vec{V}\cdot\underset{\sim}{\tau})$$

Combining these relations, the final form of the second term of (31) is:

$$[\cdot\ \cdot\ \cdot] = -\dot{W}_p \left[(1 - f_c)\, h_g + f_c\, e_c - e_{vp}\right] + \sum_i \dot{W}_i'\, h_i - \dot{W}_c''\, (h_g - e_v) \qquad (32)$$

The eighth term of (31) can be expanded to:

$$[\cdot\ \cdot\ \cdot] = \frac{\vec{V} \cdot \vec{V}}{2} \left[\frac{\partial \rho_g}{\partial t} + \nabla \cdot \rho_g \vec{V}\right] + \rho_g \left[\frac{\partial}{\partial t}\left(\frac{\vec{V} \cdot \vec{V}}{2}\right) + \vec{V} \cdot \nabla \left(\frac{\vec{V} \cdot \vec{V}}{2}\right)\right]$$

Using (15), the final form of the eighth term is:

$$[\cdot\ \cdot\ \cdot] = \frac{\vec{V} \cdot \vec{V}}{2}\, \dot{W}_g + \rho_g \left[\frac{\partial}{\partial t}\left(\frac{\vec{V} \cdot \vec{V}}{2}\right) + V \cdot \nabla \left(\frac{\vec{V} \cdot \vec{V}}{2}\right)\right] \qquad (33)$$

Substituting (32) and (33) into (31) yields a final form of the energy equation.

Storage

$$\left(\rho_p C_{v_p} + \rho_c C_{v_p} + \rho_g \bar{C}_{p_g}\right) \frac{\partial T}{\partial t}$$

I

Decomposition — Cracking — Gas-solid phase reaction

$$-\dot{W}_p \left[(1 - f_c)\, h_g + f_c\, e_c - e_p\right] + \sum \dot{W}_i h_i - \dot{W}_c''\, (h_g - e_c)$$

II — III — IV

Convection — Diffusion

$$+ \rho_g \bar{C}_{p_g}\, \vec{V} \cdot \nabla T + \sum_i \rho_i C_{p_i} \vec{V}_{d_i} \cdot \nabla T$$

V — VI

Heat Conduction — Thermal Radiation — Pressure — Kinetic Energy

$$= \nabla \cdot K \nabla T - \nabla \cdot \vec{q}_R + \frac{\partial P}{\partial t} + \frac{\vec{V} \cdot \vec{V}}{2}\, \dot{W}_g$$

VII — VIII — IX — X

Noting that the temperature of the gas equals that of the solid, differentiating the caloric equations of state, (1), (2) and (5) yields:

$$\frac{\partial e_p}{\partial t} = C_{v_p} \frac{\partial T}{\partial t} \qquad \frac{\partial h_i}{\partial t} = C_{p_i} \frac{\partial T}{\partial t}$$

$$\frac{\partial e_c}{\partial t} = C_{v_c} \frac{\partial T}{\partial t} \qquad \nabla h_i = C_{p_i} \nabla T$$

Substituting these relations into (30) and rearranging terms gives

$$\left[\rho_p C_{v_p} + \rho_c C_{v_c} + \sum_i \rho_i C_{p_i}\right] \frac{\partial T}{\partial t} + \left[e_p \frac{\partial \rho_p}{\partial t} + e_c \frac{\partial \rho_c}{\partial t} + \sum_i h_i \left(\frac{\partial \rho_i}{\partial t} + \nabla \cdot \rho_i \left(\vec{V} + \vec{V}_{d_i}\right)\right)\right] + \left[\sum_i \rho_i C_{p_i} \left(\vec{V} + \vec{V}_{d_i}\right)\right] \cdot \nabla T = \nabla \cdot K \nabla T - \nabla \cdot \vec{q}_R \quad (31)$$

$$+ \frac{\partial \rho}{\partial t} + \nabla \cdot (\vec{V} \cdot \tau) - \left[\frac{\partial}{\partial t}\left(\rho_g \frac{\vec{V} \cdot \vec{V}}{2}\right) + \nabla \cdot \left(\rho_g \vec{V} \frac{\vec{V} \cdot \vec{V}}{2}\right)\right]$$

The second and eighth terms can be simplified by use of the continuity equations. Using (14), (16) and (17), the second term becomes

$$[\cdot\ \cdot\ \cdot] = e_p \dot{W}_p + e_c \dot{W}_c + \sum_i h_i \dot{W}_i$$

Using (23), this last term is:

$$\sum_i \dot{W}_i h_i = \sum_i \dot{W}_i' h_i + \dot{W}_g h_g$$

From (19), (20), and (21) we have:

$$\dot{W}_c = -f_c \dot{W}_p + \dot{W}_c''$$

$$\dot{W}_g = -(1 - f_c) \dot{W}_p + \dot{W}_g''$$

$$\dot{W}_g'' = -\dot{W}_c''$$

Viscous Stresses

$$+\left[\nabla\cdot(\vec{V}\cdot\underset{\sim}{\tau})-\rho_g\left\{\frac{\partial}{\partial t}\left(\frac{\vec{V}\cdot\vec{V}}{2}\right)+\vec{V}\cdot\nabla\left(\frac{\vec{V}\cdot\vec{V}}{2}\right)\right\}\right] \tag{34}$$

XI

Summary of Equations

Energy Equation

$$\left(\rho_p C_{v_p}+\rho_c C_{v_c}+\rho_g \overline{C}_{p_g}\right)\frac{\partial T}{\partial t}-\dot{W}_p\left[(1-f_c)h_g+f_c e_c-e_p\right]$$

$$+\sum_i \dot{W}_i'\,h_i-\dot{W}_c''\,(h_g-e_c)+\rho_g C_{p_g}\vec{V}\cdot\nabla T+\sum_i \rho_i\,\vec{V}_{d_i}\,h_i\cdot\nabla T \tag{35}$$

$$=\nabla\cdot K\nabla T-\nabla\cdot\vec{q}_R+\frac{\partial P}{\partial t}+\frac{\vec{V}\cdot\vec{V}}{2}\dot{W}_g+\nabla\cdot(\vec{V}\cdot\underset{\sim}{\tau})$$

$$-\rho_g\left\{\frac{\partial}{\partial t}\left(\frac{\vec{V}\cdot\vec{V}}{2}\right)+\vec{V}\cdot\nabla\left(\frac{\vec{V}\cdot\vec{V}}{2}\right)\right\}$$

Species Continuity

$$\rho_g\left(\frac{\partial K_i}{\partial t}+\vec{V}\cdot\nabla K_i\right)+\nabla\cdot\left(\rho_i\,\vec{V}_{d_i}\right)=\dot{W}_i' \tag{36}$$

Continuity

$$\frac{\partial\rho_g}{\partial t}+\nabla\cdot\rho_g\vec{V}=-(1-f_c)\dot{W}_p-\dot{W}_c'' \tag{37}$$

$$\frac{\partial\rho_p}{\partial t}=\dot{W}_p \tag{38}$$

$$\frac{\partial \rho_c}{\partial t} = - f_c \dot{W}_p + \dot{W}_c'' \tag{39}$$

The various terms of this equation are identified as:

I energy storage

II energy absorbed due to the decomposition of the solid

III energy absorbed due to gas phase reactions (i.e. cracking)

IV energy absorbed due to gas-solid phase reactions

V energy transfer due to convection

VI energy transfer due to diffusion

VII energy transfer due to heat conduction

VIII energy transfer due to thermal radiation

IX rate of work associated with the pressure

X kinetic energy associated with gas formation

XI rate of work associated with the viscous stresses and kinetic energy

The "heat of decomposition" appears in term II.

$$h_{gf} = (1 - f_c) h_g + f_c e_c - e_{v_p}$$

If the usual momentum equation could be used to simplify term XI, it would reduce to the familiar work of pressure forces plus the work of viscous forces (i.e. $V \cdot \nabla_p + \Phi$ where Φ is the dissipation function).

State

$$P = \rho_g \frac{R}{M_g} T \tag{40}$$

Momentum

$$\vec{V} = - \frac{k}{\mu} \nabla P \tag{41}$$

Diffusion (binary mixture approximation)

$$\rho_i \vec{V}_{d_i} = - \rho_g D_{12} \nabla K_i \tag{42}$$

Neglecting $\underset{\sim}{\tau}$ and q_r, there are 6 + 2 (N-1) equations for the following physical variables (N is the total number of gaseous species):

$$T, \rho_p, \rho_c, \rho_g, P, \vec{V}, \vec{V}_{d_i}, K_i$$

These equations require that the following material properties (10 + 4N in all) be known functions of the variables.

$$C_{v_p}, e_p, \dot{W}_p$$

$$C_{v_c}, e_c, f_c, \dot{W}_c''$$

$$C_{p_i}, h_i, \dot{W}_i', M_i$$

$$K, \frac{k}{\mu}, D_{12}$$

Discussion

The equations developed so far represent a quite general physical model of charring ablation. They account for the simultaneous transfer of energy and mass within a solid material of variable porosity which is decomposing. The ablation gases may be flowing, diffusing, reacting with themselves or reacting with the char and they are not necessarily in local thermochemical equilibrium.

It is generally desirable to invoke further physical assumptions in order to simplify the mathematical analysis and to reduce the number of required material properties, which are often not known. Several of these assumptions will now be discussed.

Two approaches will be described for the simplification of the general equations derived above. One approach to the problem is to simplify the gas chemistry while retaining the gas dynamical features. The ultimate end in this approach is to assume that the gas contains only a single specie. Note that this assumption does not exclude gas-solid phase reactions. Thus, we have $\vec{V}_{d_i} = 0$, $\dot{W}_i' = 0$ and the species continuity equation is superfluous.

Neglecting the radiant flux and using the definitions of $\dot{W}_c$ (19) and $\dot{W}_g$ (20), equations (35) - (39) simplify to:

Energy

$$\left(\rho_p C_{vp} + e_c C_{vc} + \rho_g \bar{C}_{p_g}\right)\frac{\partial T}{\partial t} + \left(\dot{W}_p e_p + \dot{W}_c e_c + \dot{W}_h h_g\right) + (\rho_g C_{p_g} \vec{V}) \cdot \nabla T \tag{43}$$

$$= \nabla \cdot K \nabla T + \frac{\partial P}{\partial t} + \frac{\vec{V} \cdot \vec{V}}{2}\dot{W}_g + \nabla \cdot (\vec{V} \cdot \underset{\sim}{\tau}) - e_g\left[\frac{\partial}{\partial t}\left(\frac{\vec{V} \cdot \vec{V}}{2}\right) + \vec{V} \cdot \nabla\left(\frac{\vec{V} \cdot \vec{V}}{2}\right)\right]$$

Continuity

$$\frac{\partial \rho_g}{\partial t} + \nabla \cdot e_g \vec{V} = \dot{W}_g \tag{44}$$

$$\frac{\partial \rho_p}{\partial t} = \dot{W}_p \tag{45}$$

$$\frac{\partial \rho_c}{\partial t} = \dot{W}_c \tag{46}$$

$$\dot{W}_p + \dot{W}_c + \dot{W}_g = 0 \tag{47}$$

State

$$P = \rho \frac{R}{M} T \tag{48}$$

Momentum

$$\vec{V} = - \nabla \frac{k}{\mu} P \tag{49}$$

The gas density used in the derivation of the equations described here is the weight of the gas in a given solid-gas volume divided by that volume. The gas density referred to within the REKAP program is the above density divided by the porosity of the material. Porosity is defined as:

$$\epsilon = \frac{\text{Actual Gas Volume}}{\text{Total Volume}} = \frac{\text{Void Volume}}{\text{Total Volume}}$$

The porosity is calculated at each time step by:

$$\epsilon = 1 - \tilde{\rho}_c \left(\frac{1}{\tilde{\rho}_c} - \frac{1}{\tilde{\rho}_{vp}} \right) - \frac{\rho_s}{\tilde{\rho}_{vp}}$$

The thermal conductivity of the gas (k_g) and thermal conductivity of the solid (K_S) are each based on their respective areas.

$\tilde{\rho}_c$ is the final density of the char based on the volume of the char (i.e. if the char is carbon then $\tilde{\rho}_c$ is equal to the density of carbon) and $\tilde{\rho}_{vp}$ is the initial density of the virgin plastic before heating or any charring has taken place.

Now simplifying the equations it will be assumed that the gas is in local thermochemical equilibrium and that diffusion is negligible. This means that the gas composition is a known function of temperature and pressure. Finally, it is assumed that radiation can be accounted for as an increase in effective conductivity and that the mechanical work terms are negligible compared to the thermal terms in the energy equation. All of these are reasonably plausible engineering assumptions.

In the absence of diffusion, the species continuity equation (22) is:

$$\rho_g \left[\frac{\partial K_i}{\partial t} + \vec{V} \cdot \nabla K_i \right] = \dot{W}_i'$$

Since the composition is a known function of temperature and pressure, this implies:

$$\dot{W}_i' = \rho_g \left(\frac{\partial K_i}{\partial T} \right) \left[\frac{\partial T}{\partial t} + \vec{V} \cdot \nabla T \right] + \rho_g \left(\frac{\partial K_i}{\partial P} \right) \left[\frac{\partial P}{\partial t} + \vec{V} \cdot \nabla P \right]$$

Substituting this into the energy equation (34) and neglecting diffusion, radiation, and mechanical work terms we get:

$$\left(\rho_P C_{v_p} + \rho_c C_{v_c} + \rho_g \overline{C}_{p_g}\right)\frac{\partial T}{\partial t} - \dot{W}_p\left[(1-f_c)\,h_g + f_c\,e_c - e_p\right]$$

$$+\rho_g\left(\sum_i h_i \frac{\partial K_i}{\partial T}\right)\left[\frac{\partial T}{\partial t} + \vec{V}\cdot\nabla T\right] + \rho_g\left(\sum_i h_i \frac{\partial K_i}{\partial P}\right)\left[\frac{\partial P}{\partial t} + \vec{V}\cdot\nabla P\right] \quad (50)$$

$$-\dot{W}_c''\,(h_g - e_c) + \left(\rho_g \overline{C}_{p_g}\vec{V}\right)\cdot\nabla T = \nabla\cdot K\nabla T$$

The continuity equations (34) - (39), thermal equation of state (40) and the momentum equation (41) remain unchanged.

It is possible to simplify (50) even further by neglecting the gas density in comparison with the solid density, while retaining the mass flow rate term. This implies that as $\rho_g \to 0$, $\rho_g V$ remains finite so that $\vec{V} \to \infty$, i.e., the "residence time" is negligible. This means that the equation of state and the momentum equation are superfluous. The pressure is assumed to be uniform at its ambient value, which is not necessarily steady. The continuity equations remain unchanged except the time derivative of the gas density in (37) is dropped. The energy equation (50) becomes:

$$\left(\rho_p C_{v_p} + \rho_c C_{v_c}\right)\frac{\partial T}{\partial t} + \rho_g \vec{V}\left(\overline{C}_{p_g} + \sum_i h_i \frac{\partial K_i}{\partial T}\right)\cdot\nabla T = \nabla\cdot K\nabla T$$

$$+\dot{W}_p\left[(1-f_c)\,h_g + f_c\,e_c - e_p\right] + \dot{W}_c''\,(h_g - e_i) \quad (51)$$

This equation in one dimension is the equation solved in the REKAP program. Without the pressure option, and neglecting the gas-solid phase reactions and by combining equations (37) - (39) and (51), the following equations result:

Derivation	REKAP Program
$h_g + \frac{f_c}{1 - f_c} e_c - \frac{1}{1 - f_c} e_p$	H_{gf}
$(1 - f_c) \dot{W}_p$	$\rho_{vp}\left(\frac{\rho - \rho_c}{\rho_{vp}}\right)^{n_1} Z e^{-E/RT}$

Summary of the Equations

REKAP Equations:

Energy:

$$\rho C_p \frac{\partial T}{\partial t} = \frac{\partial}{\partial X}\left(K \frac{\partial T}{\partial t}\right) + M_g\left(\overline{C}_{p_g} + H_{c_g}\right)\frac{\partial T}{\partial X} + H_{gf} \frac{\partial \rho}{\partial t}$$

Continuity:

$$\dot{M}_g = - \int_x^{\text{backface}} \frac{\partial \rho}{\partial t} \, dX$$

Density:

$$\frac{\partial \rho}{\rho t} = - \rho_{vp}\left(\frac{\rho - \rho_c}{\rho_{vp}}\right)^n Z e^{-E/RT}$$

These are the equations that are solved in the non-pressure option of the program.

Energy:

$$\left(\rho_p C_{v_p} + \rho_c C_{v_c}\right) \frac{\partial T}{\partial t} + \rho_g V \left(\overline{C_{p_g}} + \sum_i h_i \frac{\partial K_i}{\partial T}\right) \frac{\partial T}{\partial X}$$

$$= \frac{\partial}{\partial X}\left(K \frac{\partial T}{\partial X}\right) + \left[\frac{\partial}{\partial t}\left(\rho_P + \rho_c\right)\right] \cdot \left[h_g + \frac{f_c}{1 - f_c} e_c - \frac{1}{1 - f_c} e_p\right]$$

Continuity:

$$\rho_g V = - \int_{\text{backface}}^{X} \frac{\partial}{\partial t} (\rho_p + \rho_c) \, dX$$

Density:

$$\frac{\partial}{\partial t} (\rho_p + \rho_c) = - (1 - f_c) \dot{W}_p$$

Derivation	REKAP Program
$\rho_p + \rho_c$	ρ
$\dfrac{\rho_p C_{v_p} + \rho_c C_{v_c}}{\rho_p + \rho_c}$	C_p
$\rho_g V$	$\dot{M}_g$
$\sum_i h_i \dfrac{\partial K_i}{\partial T}$	H_{cg}

Pressure Option Equations:

Energy (Gas):

$$\rho_g C_p \frac{\partial T_g}{\partial t} = - \rho_g C_p V \frac{\partial T}{\partial X} + \frac{\partial P}{\partial t} + \frac{\partial}{\partial X}\left(\epsilon K_g \frac{\partial T}{\partial X}\right) + \dot{Q}_{\text{transferred from gas}}$$

$$+ \dot{W}_g h_g + \frac{\partial}{\partial X}\left(\epsilon \tau_{i_j} - V\right) - \rho_g V \frac{\partial V}{\partial t} - \rho_g V^2 \frac{\partial V}{\partial X} - \frac{\dot{W}_g V^2}{2}$$

Energy (Solid):

$$(1 - \epsilon)\left(\rho_p C_{r_{vp}} + \rho_c C_{v_c}\right) \frac{\partial T_s}{\partial t} + \frac{\partial}{\partial X}\left[(1 - \epsilon) K_s \frac{\partial T_s}{\partial X}\right]$$

$$- \left(e_c \dot{W}_c + e_{vp} \dot{W}_{vp}\right) - \dot{Q}_{\text{transferred from gas}}$$

If the temperature of the gas and the temperature of the adjacent solid material are the same, the above two equations may be added together.

$$\left[\rho_g C_p + (1 - \epsilon)\left(\rho_p C_{v_{vp}} + \rho_v C_{v_c}\right)\right] \frac{\partial T}{\partial t} = \frac{\partial T}{\partial t}\left\{\left[\epsilon K_g + (1 - \epsilon) K_s\right] \frac{\partial T}{\partial X}\right\}$$

$$+ \frac{\partial P}{\partial t} + h_g \dot{W}_g - (\rho_c \dot{W}_c + \rho_p \dot{W}_p) - \rho_g C_p V_g \frac{\partial T}{\partial X} + \frac{\partial}{\partial X}\left(\epsilon \tau_{i_j} V\right)$$

$$- \rho_g V \frac{\partial V}{\partial X} - \rho_g V^2 \frac{\partial V}{\partial X} - \frac{V^2 \dot{W}_g}{2}$$

Continuity:

$$\frac{\partial \rho_g}{\partial t} + \frac{\partial (\rho_g V)}{\partial X} = \dot{W}_g$$

$$\frac{\partial \rho_g}{\partial t} = \dot{W}_g = -\dot{W}_s = \beta \rho_{vp} \left(\frac{\rho_s - \rho_c}{\rho_{vp}} \right)^n e^{-E/RT}$$

$$\frac{\partial \rho_{vp}}{\partial t} = \dot{W}_{vp}$$

$$\frac{\partial \rho_c}{\partial t} = \dot{W}_c$$

$$\dot{W}_s = \dot{W}_c + \dot{W}_{vp}$$

Momentum:

$$\overline{V} = \frac{\partial}{\partial X} \left(\frac{g \bar{R} T}{\mu} \frac{R}{\epsilon} \rho_g \right)$$

which was obtained by substituting the Equation of State in the momentum equation (12).

Boundary Conditions:

The boundary conditions that are of concern here are those describing the material heat input or removal from the front and back face and the surface recession at the heated face. The heating of the material can be described by three methods: front face temperature (T_w), front face heat flux ($\dot{q}_c$ and/or $\dot{q}_{hgr}$), and front face convective film coefficient ($\dot{q}_c/\Delta h$ or $\dot{q}_c/\Delta T$).

Each of these quantities can be a function of time. The convective film coefficient option is the one most commonly used for the analysis of rocket engines, however, for some propellant combinations, it is necessary to account for the radiation ($\dot{q}_{hgr}$) from the exhaust gases. The program includes the capability of combining the radiative flux and the convective heat transfer by taking a thermal balance at the front face. The thermal balance is described by:

$$\dot{q}_{net} = \dot{q}_c + \dot{q}_{hgr} - \dot{q}_{rr} - \dot{q}_b = K_w \frac{\partial T}{\partial X}$$

The convective heat flux ($\dot{q}_c$) is determined either from program input which is a function of time or it is calculated from:

$$\dot{q}_c = \frac{\dot{q}_c}{\Delta h} (h_r - h_{ff}) \qquad h_{ff} = C_{p_{bl}} T_w$$

or

$$\dot{q}_c = \frac{\dot{q}_c}{\Delta T} (T_r - T_w)$$

where h_r is the recovery enthalpy and T_r is the recovery temperature.

If the convective film coefficient is in terms of temperature rather than enthalpy, the specific heat ($C_{p_{bl}}$) of the boundary layer gases must be set equal to 1.0 for all values of gas temperature. The convective film coefficient is an input to the program and is considered to be a function of time.

The fourth term in the heat balance equation is the rate of energy loss from the front face due to thermal radiation. It is expressed by:

$$\dot{q}_{rr} = \epsilon \sigma T_w^4$$

where σ is the Stefan-Boltzmann constant which equals 0.476×10^{-12} BTU/sec Ft^2 $^oR^4$ and ϵ is the product of the surface emissivity and the configuration factor (F_a) between the point radiating and the cold (relative to the hot wall) external environment.

The fifth term is the decrease in the convective heat flux due to the injection of ablation gases into the boundary layer. This is commonly referred to as the "blocking action effect." The expressions describing the blocking action were derived from the correlation of

experimental data (References 14 to 34). The expressions for the blockage of the convective energy are:

Laminar:

$$\dot{q}_b = \dot{q}_c \left[.69 \left(\frac{M_2}{M_1} \right)^{1/3} \frac{\varphi_o}{P_r^{1/3}} \right]$$

Turbulent:

$$q_b = q_c \left[1 - e^{.38\, C_T \varphi} \right]$$

$$\varphi = \dot{M}_w \frac{1}{\dot{q}_c/\Delta h}$$

where:

M_1 is the molecular weight of the injection gases

M_2 is the molecular weight of the boundary gases

C_T is the ratio of the specific heat of the injection gases to the specific heat of the boundary layer gases. C_{p_1}/C_{p_2}

P_r is the Prandtl number of the boundary layer gases.

$\dot{M}_w$ is the mass injection rate at the front face. $\sim$ lb/sec ft^2

The quantities (M_2/M_1), C_T and P_r are input constants while $(\dot{q}_c/\Delta h)$ is the value of the convective film coefficient. If the blocking action is expected to be significant (however, for most materials exposed to a rocket engine environment, the blockage effects amount to only a few per-cent of the convestive heat flux) it is necessary to use the film coefficient defined in terms of the enthalpy difference since that is how the above blocking action equations are correlated. Included for completeness is the laminar blocking action equation although for most rocket nozzle applications, the boundary layer is assumed to be turbulent.

The last term in the front face heat balance equation is the rate of thermal energy which is transferred by conduction into the material.

The heat transfer from the back face of the material is controlled by specifying the back face temperature (T_{BF}) or heat transfer rate ($\dot{q}_{BF}$) as a function of time. If radiation from the back face is desired, included is a routine to allow for an air-gap or a non-solid layer in the nozzle wall. Therefore, to account for radiation from the back face of a nozzle, the third layer from the last in the program is the actual nozzle backside, the second from last is the air-gap and the final layer is the nozzle surroundings for which the back face temperature is specified. Using the air-gap routine not only can radiation from the back face be accounted for but also natural convection and forced convection by the proper adjustment of constants. For the details of the mathematical equations, see Appendix B and E.

Front Face Recession

The front face recession is presently controlled by five methods: no melting, or recession. specified char length, graphite oxidation and sublimation, refrasil option and fixed melting temperature. The first method is normally used for the purpose of evaluating the temperature distribution within material which is known not to have a dimensional change. The options most commonly used are the specifiec char length, graphite sublimation and the fixed melting temperature. The fourth option which is referred to as the refrasil option is based on the work done by Munson and Spindler (Reference 12). For this option, the heat balance equation at the front face is:

$$- K \frac{dT}{dX} = \dot{q}_c + \dot{q}_{hgr} - \dot{q}_{rr} - q_b - (\rho L) \dot{S}$$

where the surface recession rate is given by:

$$\dot{S} = \beta_1 \, T_w^{\beta_2} \, e^{-\beta_3/T_w}$$

The constants β_1, β_2 and β_3 are determined from experimental data. In their paper, Munson and Spindler listed the values of β_1, β_2 and β_3 for silica phenolic as 0.00917 ft/sec $^oR^2$, 2.0 and 1×10^5 ^oR.

The quantity ($\rho_c L$), the surface or final char density and the latent heat of fusion or vaporization depending upon whether the material melts or is vaporized. Empirical and analytical (Reference 35) work done on the analysis of glassy materials within rocket nozzles has shown that the major portion of the surface loss to be by melting and not by vaporization. Therefore, the value of L for a phenolic refrasil material should be the heat of fusion for the char material which is primarily refrasil. The refrasil option has the disadvantage of being relatively slow (requires several times as much computation time as the fixed melting temperature option) since it must iterate on the rate of melt for each time step.

The fixed melting temperature option usually satisfies the rate of melt criterion after the first iteration. The net heat balance for the fixed melting temperature option is the same as for the refrasil option. However, the rate of melt (S_m) is given by:

$$\dot{S}_m = \frac{K \frac{dT}{dX} + \dot{q}_{net}}{\Gamma \rho_c L}$$

where ρ_c is the density of the char and L is the latent heat of vaporization or melting depending on whether the material vaporizes or melts. The gasification factor Γ is the ratio of the char material which is either vaporized or melted to the total char that is lost. Some of the char may be lost by char popoff or some other mechanical means. The value of Γ must be determined experimentally. The front face is not allowed to recede until the front face temperature reaches the specified melting temperature.

The specified char thickness option is as the name inplies, the char layer is allowed to grow until it reaches the specified value. Then the outer boundary moves at the same ratio as the reaction zone. The maximum allowable char thickness is determined by the material and the environment to which it is exposed. The thickness values are determined from experimental data.

The graphite oxidation and sublimation option for the control of front face recession also accounts for the oxidation of most graphite materials including pyrolytic graphite and on an oxidation process, which is rate-controlled at low (1500°R) surface temperatures, but rapidly become diffusion-controlled as the surface temperature rises (see Figure A2 and A3). For the range of surface temperatures, approx. between 2500°R and 5000°R the rate of the overall mass loss is dominated by the slowest step, which is the counterdiffusion process in the multicomponent boundary layer. When the surface temperature is in this range, the oxidation rate levels off and becomes insensitive to the magnitude of surface temperature, simply because the mass loss is controlled by the diffusion of oxygen-bearing species to the surface rather than the specific reactivity of graphite. At even higher surface temperature (T_w 500°R) the mass loss due to vaporization exceeds the diffusion controlled oxidation mass loss rate. This region is normally referred to as the sublimation regine. The results shown in Figure A3 were correlated (Refs. 36 and 37) and the resulting equations were:

$$\dot{M}_t = \dot{M}_o \left[r + 2.64 \times 10^{9} P_e^{-.67} e^{-\frac{11.05 \times 10^{-4}}{T_w}} \right]$$

where the $\dot{M}_o$ is the mass loss within the diffusion controlled regime

$$\dot{M}_o = \frac{\dot{q}_c}{Q^*} = \frac{\dot{q}_c}{K_1 + K_2 (h_r - C_{p_{bl}} T_w)}$$

The quantities K_1 and K_2 are input constants and for turbulent flow, their values for an air boundary layer are 4240 and 5.77 respectively. The rate of front face recession is given by:

$$\dot{S}_m = \frac{\dot{M}_t}{\rho_{surface}}$$

The heat balance at the front face is given by:

$$-K \frac{dT}{dX} = \dot{q}_c' + \dot{q}_{hgr} - \dot{q}_{rr} - \dot{q}_b$$

where

$$\dot{q}_c' = \dot{q}_c \left[1 - S^* (3.96 \times 10^8) P_e^{-.67} e^{-\frac{11.05 \times 10^4}{T_w}} \right]$$

The local edge pressure P_e is an input quantity which is a function of time and S* is a table lookup which is a function of the recovery enthalpy.

NOMENCLATURE

A	surface area	ft^2
C_v	specific heat at constant volume	BTU/lbm ^oR
C_p	specific heat at constant pressure	BTU/lbm ^oR
$\overline{C_{p_g}}$	$\sum_i K_i C_{pi}$ = average specific heat	BTU/lbm ^oR
$C_{p_{bl}}$	specific heat of the boundary layer gases	BTU/lb
C_t	ratio of the specific heat of the injection gases to the specific heat of the boundary layer gases	--------
D_{i_j}	multicomponent diffusion coefficient	ft^2/sec
D_{12}	binary diffusion coefficient	ft^2/sec
e	specific internal energy	BTU/lbm
e_F	energy of formation	BTU/lbm
$\vec{e}$	unit base vector	--------
f_c	fraction of unreacted material that forms char	--------
h_r	recovery enthalpy	BTU/lb
h_{ff}	boundary layer gas enthalpy at wall temperature	BTU/lb
k	permeability	ft^2
K	thermal conductivity	BTU/ft-sec ^oR
K_i	$\frac{\rho_i}{\rho}$ = mass concentration	--------
K_{i_j}	conductivity tensor	BTU/ft-sec ^oR
K_1 & K_2	constants in mass loss equation	--------
M	molecular weight	lbm/mole

M_g	$\frac{1}{\sum \frac{K_i}{M_i}}$ = average molecular weight	lbm/mole
M_1	molecular weight of the injection gases	--------
M_2	molecular weight of the boundary layer gases	lb/lb mole
$\dot{M}_w$	mass injection rate at the front face	lb/sec-ft^2
n	total number of moles per unit volume; degradation reaction order	moles/ft^3
p	pressure	lbf/ft^2
$\vec{P}$	surface force per unit area	lbf/ft^2
P_e	boundary layer edge pressure	lb/ft^2
Pr	Prandtl number of the boundary layer gases	--------
ϵ	porosity	--------
$\tilde{\rho}_c$	final density of the char based on the volume of the char	lbf/ft^3
$\tilde{\rho}_{vp}$ or ρ_{vp}	initial density of the virgin plastic	lbf/ft^3
$\dot{q}_c$	convective heat flux	BTU/ft^2-sec
$\dot{q}_{hgr}$	heat flux due to hot gas radiation	BTU/ft^2-sec
$\dot{q}_{rr}$	reradiative heat flux	BTU/ft^2-sec
$\dot{q}_b$	convective heat flux blocked due to mass injection	BTU/ft^2-sec
$\dot{q}_{bf}$	heat flux to the backface	BTU/ft^2-sec
$\vec{qc}$ or $\vec{q}_c$	conduction heat flux vector	BTU/ft^2-sec
$\vec{qR}$ or $\vec{q}_R$	radiant heat flux vector	BTU/ft^2-sec
R	universal gas constant	lbf ft/lbm mole ^oR

T	temperature	^{o}R
T_r	recovery temperature	^{o}R
T_w	wall temperature	^{o}R
T_{bf}	temperature of backface	^{o}R
$\underset{\sim}{T}$	stress tensor	lbf/ft^2
V	volume	ft^3
$\vec{V}_i$	absolute velocity of ith species	ft/sec
$\vec{V}_{d_i}$	diffusion velocity of ith species	ft/sec
$\vec{V}$	mass averaged velocity	ft/sec
$\dot{W}_i$ or ω_i	net rate of production of the ith gaseous species due to all chemical reactions	lbm/ft^3
$\dot{W}_i'$ or $\dot{\omega}_i'$	net rate of production of ith species due to gas phase reactions	lbm/ft^3
$\dot{W}_g''$ or $\dot{\omega}_g''$	rate of production of gas due to gas-solid phase reactions	lbm/ft^3
X	mole fraction	--------
$\vec{\eta}$	outward unit normal	--------
ρ	density	lbm/ft^3
σ_{i_j}	component of the stress tensor	lbf/ft^2
$\underset{\sim}{\tau}$	viscous stress tensor	lbf/ft^2
μ	gas viscosity	$lbf\text{-}sec/ft^2$
σ	Stefan-Boltzmann constant (0.476×10^{-12} $Btu/sec\text{-}ft^2\,{}^{o}R^4$)	--------
Γ	gasification ratio	--------

APPENDIX A

REFERENCES

1. Von Karman, T., "Fundamental Equations in Aerothermochemistry" Proc. 2nd AGARD Combustion Collog., Liege, Belgium, Dec. 1955.

2. Scala, S. M., "The Equations of Motion in a Multicomponent Chemically Reacting Gas," General Electric Co. Missile and Ordnance Systems Dept., Doc. No. R58SD205, Dec. 1957.

3. Hirschfelder, J.D., Curtiss, C.F. and Bird, R.B., Molecular Theory of Gases and Liquids, John Wiley and Sons, 1954.

4. Bird, R.B., Stewart, W.E., and Lightfoot, E.N., Transport Phenomena, John Wiley and Sons, 1960.

5. Hayday, A.A., "Governing Equations of Multicomponent Fluid Continua with Chemical Reactions," University of Illinois, Technical Report No. ILL-6-P (Project SQUID), April 1962.

6. Sokolnikoff, I.S. and Redheffer, R.M., Mathematics of Physics and Modern Engineering, McGraw Hill, 1958.

7. Carslaw, H.S. and Jaeger, J.C., Conduction of Heat in Solids, Oxford Press 1959.

8. Aris, R.A., Vectors, Tensors and The Basic Equations of Fluid Mechanics Prentice Hall, 1962.

9. Muskat, M., The Flow of Homogeneous Fluids Through Porous Media, J.W. Edwards Inc., 1946.

10. Kratsch, K.M., Hearne, L.F. and McChesney, H.R., "Thermal Performance of Heat Shield Composites During Planetary Entry," paper presented at the AIAA-NASA National Meeting, Palo Alto, Calif., Oct. 1963.

11. Lafazan, S., and Welsh, W.E., Jr., "The Charring Ablator Concept: Application to Lifting Orbital and Superorbital Entry," paper presented at the Symposium on Dynamics of Manned, Lifting Planetary Entry, Philadelphia, Pa., 1963.

12. Munson, T.R. and Spindler, R.J., "Transient Thermal Behavior of Decomposing Materials, Part I: General Theory and Application to Convective Heating," paper presented at IAS 30th Annual Meeting, New York, N.Y. Jan. 1962.

13. Wells, P.B., "A Method for Predicting the Thermal Response of Charring Ablation Materials," The Boeing Co., Aero Space Div., Doc. No. D2-23256, June, 1964.

14. Pappas, C.C. and Okuno, A.F., "Measurements of Skin Friction of the Compressible Turbulent Boundary Layer on a Cone with Foreign Gas Injection", Journal of the Aerospace Sciences, May 1960.

15. Tewfik, O.E., Jurewicz, L.S., and Eckert, E.R.G., "Measurements of Heat Transfer from a Cylinder with Air Injection into a Turbulent Boundary Layer," ASME Paper No. 63-HT-45, August 1963.

16. Bartle, E.R. and Leadon, B.M., "The Effectiveness as a Universal Measure of Mass Transfer Cooling for a Turbulent Boundary Layer," Proceedings of the 1962 Heat Transfer and Fluid Mechanics Institute, Stanford Univ. Press, June, 1962.

17. Leadon, B.M. and Scott, C.J., "Measurement of Recovery Factors and Heat Transfer Coefficients with Transpiration Cooling in a Turbulent Boundary Layer at M = 3 Using Air and Helium as Coolants," Rosemount Aero. Lab. Research Report Number 126, February 1956.

18. Gross, Hartnett, Masson, and Gazley: "A Review of Binary Laminar Boundary Layer Characteristics" - International Journal of Heat and Mass Transfer, 3,3, pages 198 to 221, October 1961.

19. Baron: "The Binary Boundary Layer Associated with Mass Transfer Cooling at High Speed" - MIT Naval Supersonic Lab Report 160 (1956).

20. Eckert, Schenider, Hayday and Larson: "Mass Transfer Cooling of a Laminar Boundary Layer by Injection of a Light Weight Gas" - Rand Symposium on Mass Transfer Cooling for Hypersonic Flight.

21. Sziklas and Banas: "Mass Transfer Cooling in Compressible Laminar Flow" - Rand Symposium on Mass Transfer Cooling for Hypersonic Flight.

22. Hartnett and Eckert: "Mass Transfer Cooling in a Laminar Boundary Layer with Constant Fluid Properties: - Trans. ASME, 79, 247 (1957).

23. Eckert: "Engineering Relations for Heat Transfer and Skin Friction in High Velocity Laminar and Turbulent Boundary Layer Flow over Surfaces with Constant Pressure and Temperature" - Trans. ASME 78, 1273 (1956).

24. Gross: "The Laminar Binary Boundary Layer" - RM-1915 - The Rand Corporation, September 1956.

25. Spalding: "Mass Transfer through Laminar Boundary Layers - 1. The Velocity Boundary Layer" Int. J. Ht. Mass Transfer, 3, Nos. 1 and 2, Pg. 15, March 1961.

26. Faulders: "Heat Transfer in the Laminar Boundary Layer with Ablation of Vapor of Arbitrary Molecular Weight" - J. Aero. Sci 29, 1, 76, Jan. 1962.

27. Eckert, Hayday and Minkowycz: "Heat Transfer, Temperature Recovery, and Skin Friction on a Flat Plate with Hydrogen Release into a Laminar Boundary Layer" - Int. J. Ht. Mass Trans. 4, Page 17, Dec. 1961.

28. Emmons and Leigh: "Tabulation of the Blasius Function with Blowing and Sunction" Harvard Report: Combustion Aero Lab Int. Tech. Rpt. #9 (1953).

29. Lew and Fanucci: "The Laminar Compressible Boundary Layers Over a Flat Plate with Sunction or Injection" - J. Aeron. Sci. 22, 9, pg. 589-597, September 1955.

30. Brown: "Tables of Exact Laminar Boundary Layer Solutions when the Wall is Porous and Fluid Properties are Variable" - NACA TN 2479 - September 1951.

31. Eschenroeder: "The Compressible Laminar Boundary Layer with Constant Injected Mass Flux at the Surface" - Jour. Aero - Space Sceinces, 26, 11, Pg. 762 (1959).

32. Mickley, Ross, Squyers, & Stewart: "Heat, Mass and Momentum Transfer for Flow Over a Flat Plate with Blowing and Sunction" - NACA TN 3208 (1954).

33. Stewart: "Transpiration Cooling: An Engineering Approach" - General Electric Missile and Space Vehicle Department Report R59SD338 - May 1, 1959.

34. Schlichting: "Boundary Layer Theory", Pergamon Press (1955).

35. Nestler, D.E., "The Effects of Liquid Layers on Ablation Performance" - General Electric Co., RSD, Thermodynamics Fund. Memo No. 022, TFM-8151-022, December, 1963.

36. Scala, S.M., "The Ablation of Graphite in Dissociated Air, Part I - Theory", IAS Paper No. 62-154, Thirtieth National Summer Meeting, June 1962; also G.E. Co., MSD, TIS R62SD72, September 1962.

37. Scala, S.M., and Gilbert, L.M., "Aerothermochemical Behavior of Graphite at Elevated Temperatures," G.E. Co., MSD, TIS R63SD89, November, 1963.

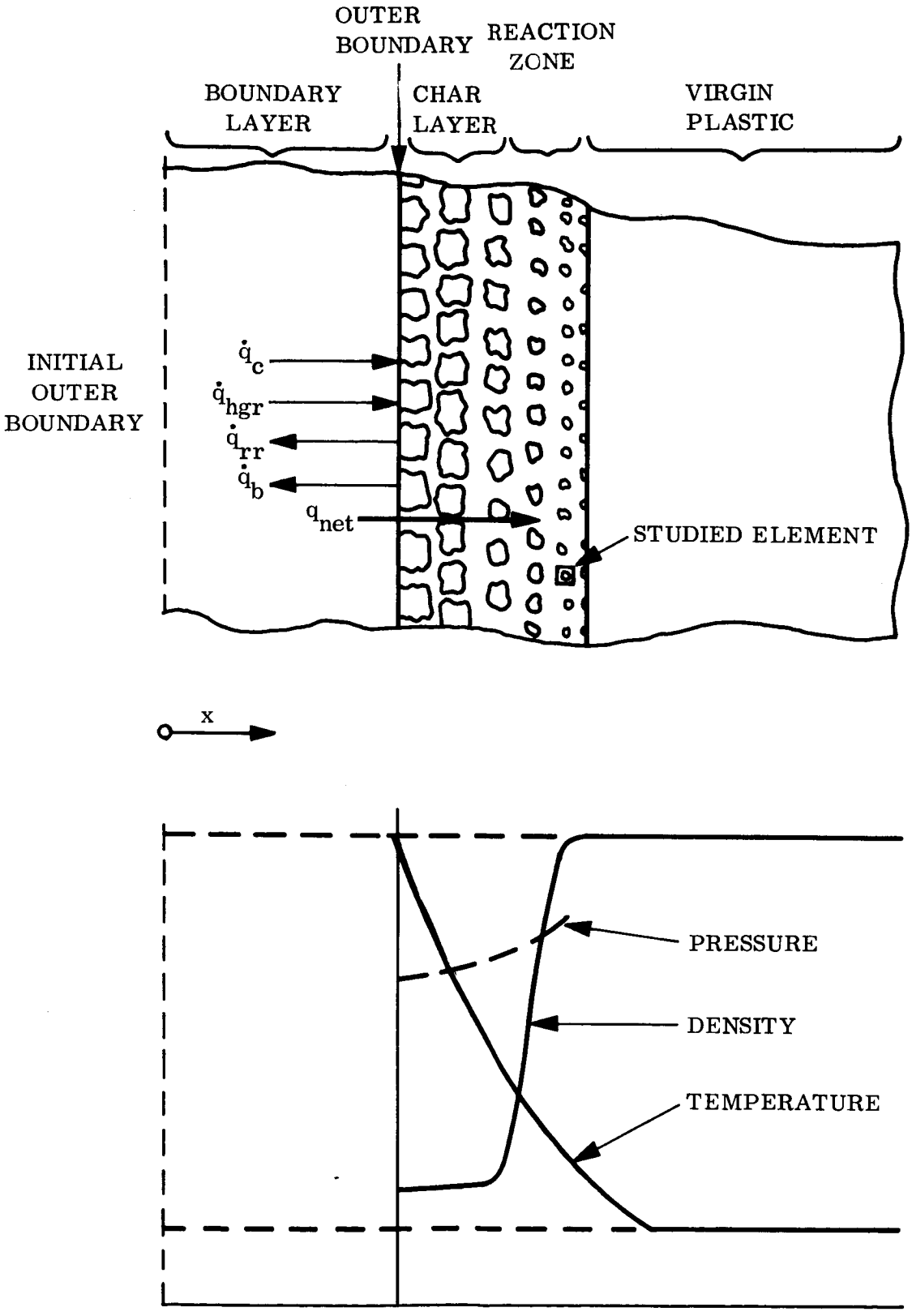

Figure A1. Schematic of a Degrading Plastic and Corresponding Profiles

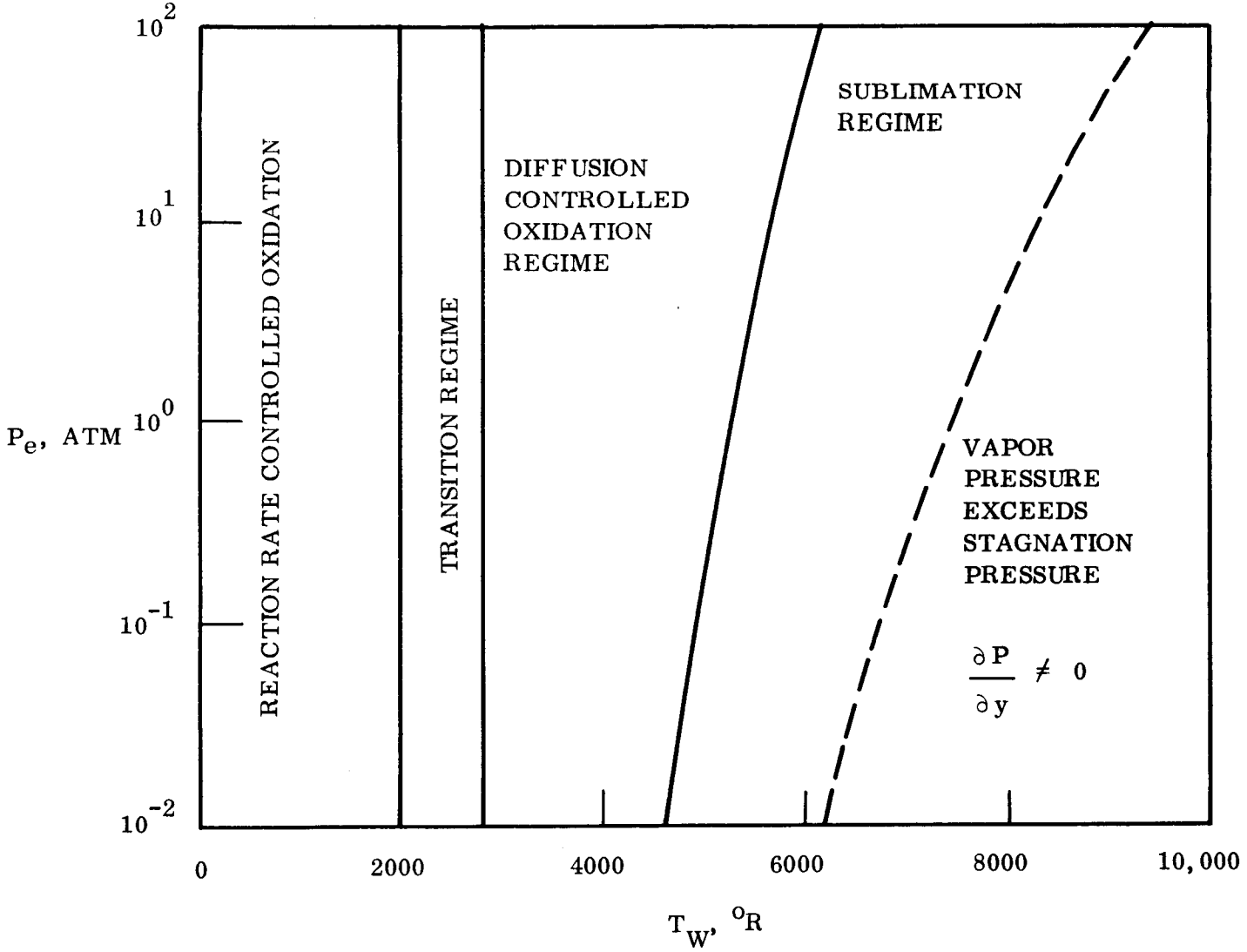

Figure A2. Mass Transfer Regimes for Ablating Graphite

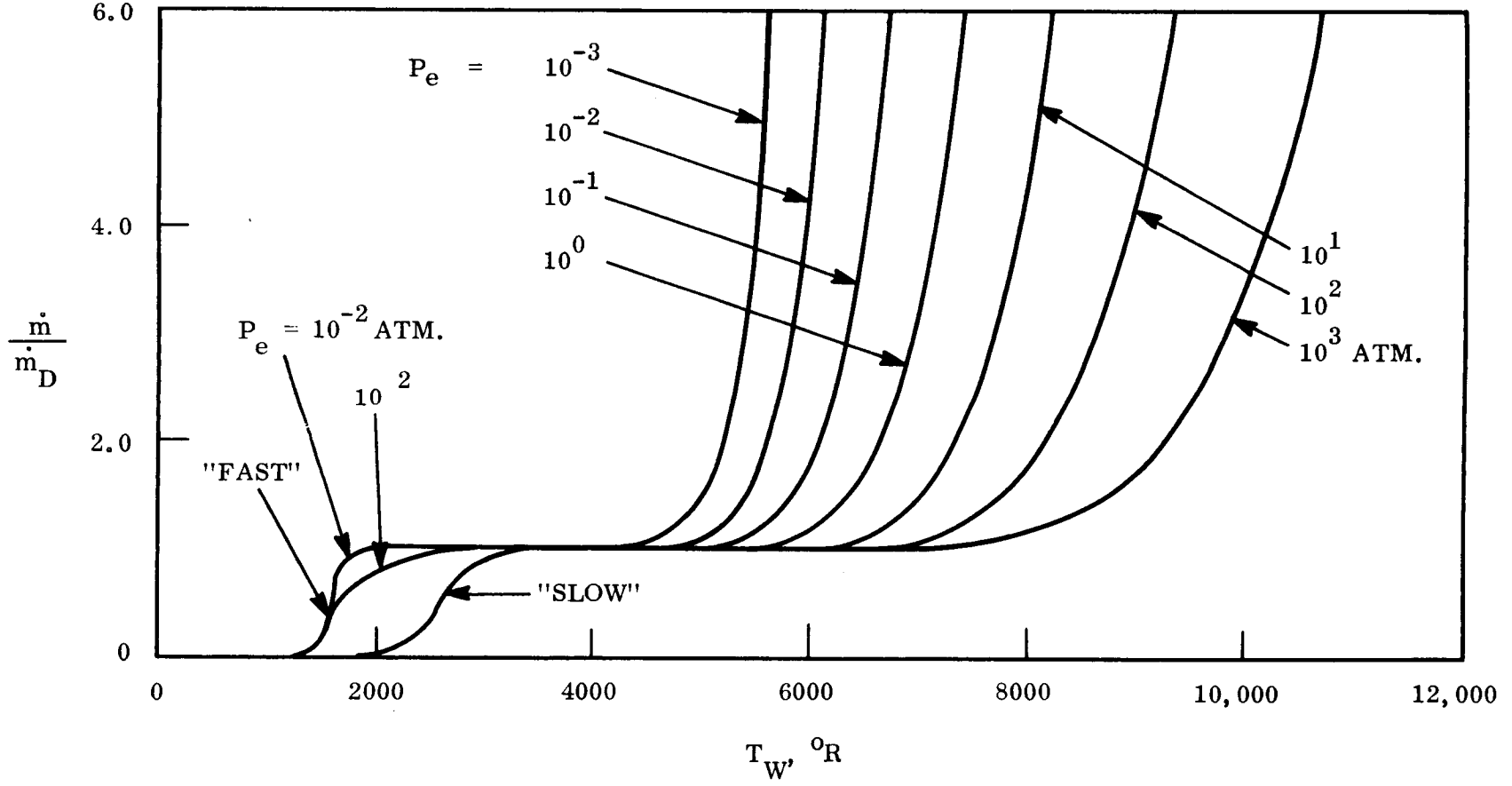

Figure A3. Normalized Ablation Rate of Graphite Over the Entire Range of Surface Temperature

TABLE 6. GRAPHITE CLOTH/PHENOLIC RESIN - SPECIFIC HEAT

FIGURE NO.	CURVE NO.	DIRECTION OF MEASUREMENT	RESIN CONTENT (%)	DENSITY (LB/FT^3)	LITERATURE SOURCE REF. NO. (SEE REFERENCES)
84	1	Does not affect specific heat	50	87	11
	2		50	86	11
	3		30	90	11
	4		36	92	2
	5		40	89	11
	6		--	--	18
	7		--	87	4
	8		--	76	3

TABLE 7. SILICA CLOTH/PHENOLIC RESIN - THERMAL CONDUCTIVITY

FIGURE NO.	CURVE NO.	DIRECTION OF MEASUREMENT	RESIN CONTENT (%)	DENSITY (LB/FT^3)	LITERATURE SOURCE REF. NO. (SEE REFERENCES)
84	1	With Lamina	30	106	11
	2	With Lamina	20	88	11
	3	With Lamina	30	112	11
	4	With Lamina	30	108	11
	5	With Lamina	20	88	11
	6	Across Lamina	30	106	11
	7	Across Lamina	30	110	2
	8	Across Lamina	30	112	11
	9	Across Lamina	31	109	2
	10	Across Lamina	30	108	11
	11	Across Lamina	20	88	11
	12	Across Lamina	20	88	11
	13	(Fused Amorphous Silica)	--	--	12

TABLE 8. SILICA CLOTH/PHENOLIC RESIN - SPECIFIC HEAT

FIGURE NO.	CURVE NO.	DIRECTION OF MEASUREMENT	RESIN CONTENT (%)	DENSITY (LB/FT^3)	LITERATURE SOURCE REF. NO. (SEE REFERENCES)
82	1	Does Not Affect Specific Heat	30	112	11
	2		--	104	19
	3		30	106	11
	4		31	109	2
	5		30	110	2
	6		20	88	11
	7		--	--	6, 12

TABLE 9. PROPERTY VARIATION FOR SIGNIFICANT PROPERTIES FOR SILICA CLOTH/PHENOLIC RESIN

PROPERTY	RANGE		
	MINIMUM	NOMINAL	MAXIMUM
Melting Temperature of Reinforcing Fibers (^{o}R)	3000	3500	4000
Virgin Plastic Density (lb/ft^3)	88	103	118
(Corresponding Char Density)	85	92	99
Specific Heat (Solid) ($Btu/lb^{o}F$)		See Figure 89	
Activation Energy (Btu/lb)	21600	48600	75600

TABLE 10. PROPERTY VARIATION FOR SIGNIFICANT PROPERTIES FOR GRAPHITE CLOTH/PHENOLIC RESIN

PROPERTY	RANGE		
	MINIMUM	NOMINAL	MAXIMUM
Thermal Conductivity (Btu/ft Fsec)		See Figure 84	
Surface Reaction Constants K_1 and K_2	$K_1 = 1000$ $K_2 = 2$	$K_1 = 4240$ $K_2 = 5.77$	$K_1 = 12000$ $K_2 = 10$
Char Density (lb/ft^3)	70	76	82
Virgin Plastic Density (lb/ft^3)	85	90	95

TABLE 12. NOMINAL PROPERTY VALUES FOR REKAP ANALYSIS

	SILICA CLOTH/ PHENOLIC RESIN	GRAPHITE CLOTH/ PHENOLIC RESIN	GRAPHITE CLOTH/ EPOXY RESIN
1. Heat of Gasification (Btu/lb)	550	550	550
2. Collision Frequency (1/sec)	3×10^4	3×10^4	3×10^4
3. Activation Energy (Btu/lb)	Table 9	Table 10	Table 11
4. Melting Temperature of Fibers (^oR)	Table 9	Table 10	Table 11
5. Heat of Vapor of Reinforced Fibers (Btu/lb)	71	Table 10	Table 11
6. Wall Emissivity	0.65	0.8	0.8
7. Recovery Temperature (^oR)			
a) N_2O_4/Aerozine 50	4565	----	----
b) OF_2/B_2H_6	----	6480	6480
8. Film Coefficient ($Btu/ft^2 sec^oR$)			
a) 1.2 in. dia. Throat	0.294	0.425	0.425
b) 7.82 in. dia. Throat	0.223	----	----
9. Specific Heat of Ablation Gases (Btu/lb^oR)	0.75	0.75	0.75
10. Molecular Weight of Ablation Gases	30	30	30
11. Virgin Plastic Density (lb/ft^3)	Table 9	Table 10	Table 11
12. Char Density (lb/ft^3)	Table 9	Table 10	Table 11
13. Thermal Conductivity (Btu/ft. sec^{o}F)	Figure 4 (Nom. Curve)	Table 10	Table 11
14. Specific Heat (Btu/lb)	Table 9	Figure 85 (Nom. Curve)	Figure 85 (Nom. Curve)
15. Order of Reaction	2	2	2

TABLE 11. PROPERTY VARIATION FOR SIGNIFICANT PROPERTIES FOR GRAPHITE CLOTH/EPOXY RESIN

PROPERTY	RANGE		
	MINIMUM	NOMINAL	MAXIMUM
Surface Reaction Constants K_1 and K_2	$K_1 = 1000$ $K_2 = 2$	$K_1 = 4240$ $K_2 = 5.77$	$K_1 = 12000$ $K_2 = 10$
Char Density (lb/ft^3)	64	70	76
Thermal Conductivity ($Btu/ft\ sec\ ^oF$)		See Figure 90	
Virgin Plastic Density (lb/ft^3)	85	90	95

CONCLUSIONS AND RECOMMENDATIONS

The surface recession of the silica phenolic material is most affected by the melting temperature of reinforcing fibers. The recession rate was decreased by a factor of three by increasing the melting temperature from 3000°F to 4000°R. Increasing the virgin plastic density from its minimum to its maximum value, increasing the activation energy from its minimum to its maximum value and increasing the specific heat from its minimum to its maximum value causes only a 91 per cent change in the surface recession rate of silica phenolic. Therefore, the greatest improvement in this material would be produced by increasing the fiber melting temperature.

The surface recession rates of the graphite phenolic and graphite epoxy are most affected by the surface reaction constants (measure of reactivity of the surface material with the boundary layer gases). The surface recession rate of the graphite phenolic material is increased by a factor of 8 in going from the minimum to the maximum values of the surface reaction constants. For graphite epoxy, changing the surface reaction constants from their minimum to maximum values increases the recession rate by a factor of ten. Allowing the three material properties (char density, thermal conductivity, virgin material density) which have the next strongest influence on the surface recession rate to go to their extreme values causes only a 44 per cent change in the recession rate of graphite epoxy. Therefore, to minimize the surface recession of the graphite materials, additives or methods of protecting the nozzle walls from the reactive chemical species in the boundary layer are required.

REFERENCES

1. Gilbert, L. M., Scala, S. M., "Combustion and Sublimation of Cones, Spheres, and Wedges at Hypersonic Speeds," AIAA Journal, Vol. 3, Number 11, Nov. 1965.

2. Pears, C. D., Engelke, W. J., Thornburgh, J. D., "The Thermal and Mechanical Properties of Five Ablative Reinforced Plastics From Room Temperature to 750°F," Southern Research Institute Technical Report No. AFML-TR-65-133, April 1965.

3. Alley, R. C., Neuenschwander, W. E., "Thermal Conductivity and Specific Heat of Charred Plastic (2nd series), "Thermatest Laboratories Report No. 52-0076a, August 1964.

4. Begany, A., Tanzilli, R., "Thermal Conductivity and Specific Heat of Typical Graphite and Carbon Phenolic Compounds," PIR 8155-R1-244, November 1963.

5. Begany, A., Tanzilli, R., "Orientation Study of Graphite and Carbon Phenolic Compounds," PIR 8155-R1-269, December 1963.

6. Tavakoli, M., "A Method of Solving Transient Heat Transfer in Diathermanous Materials," General Electric Company Aerophysics Engineering Technical Memorandum No. 188, February 1961.

7. Bleiler, K., "Thermogravimetric Analysis of PT-0181," PIR 8155-776, March 1965.

8. Melnick, A., Schneider, J., "DTA and TGA's of Phenolic Nylon, Phenolic Refrasil, and Phenolic Graphite," PIR 8155-362, March 1964.

9. Bleiler, K., "Vacuum T.G.A. on P.D.-142 Epoxy Resin," PIR 8155-694, January 1964.

10. Personal communication with R. Tanzilli.

11. Pears, C. D., Engelke, W. J., Thornburgh, J. D., "The Thermophysical Properties of Plastic Materials From -50°F to over 700°F," Southern Research Institute Technical Documentary Report No. AFML-TDR-64-87, August 1964.

12. Moeller, C. E., Wilson, D. R., "Thermal Conductivities of Several Metals and Non-Metals From 200° to 1300°C by the Radial Heat-Flow Technique," Midwest Research Institute, Proceedings of the Third Conference on Thermal Conductivity - Vol. 1, October 1963.

13. Pears, C. D., Pyron, C. M., Jr., "The Thermal Conductivity of Ablative Materials by the 'Boxing' Analysis," Southern Research Institute, Proceedings of the Fifth Conference on Thermal Conductivity, October 1965.

14. Wilson, C., "Density Variation of Phenolic Laminates," PIR 8158-1453, January 1966.

15. Tanzilli, R., "Thermal Properties of Carbon-Phenolic (CP109), " PIR 8155-661, December 1964.

16. Brazel, J., "Final Report on Thermal Conductivity of Refractory Reinforced Chars," General Electric Co. Re-Entry Systems Dept. TIS report 65SD251 (Conf.), April 1965.

17. Dubin, P., "Preliminary Material Behavior Study of Silica-Phenolic, Graphite-Phenolic, and Graphite-Epoxy," PIR 8155-891, August 1965.

18. Thermal Behavior Lab - unpublished data.

19. Begany, A., Tanzilli, R., "Thermal Property Data Release," PIR 8155-351, March 1964.

20. Swalin, R. A., "Relation Between Thermodynamic and Physical Properties," Thermodynamics of Solids, John Wiley and Sons, 1962.

21. Final Report, "Analytical Comparisons of Ablative Nozzle Materials," NASA Lewis Contract NAS 3-2566, NASA Report No.NASA CR-54257, July 1, 1965.

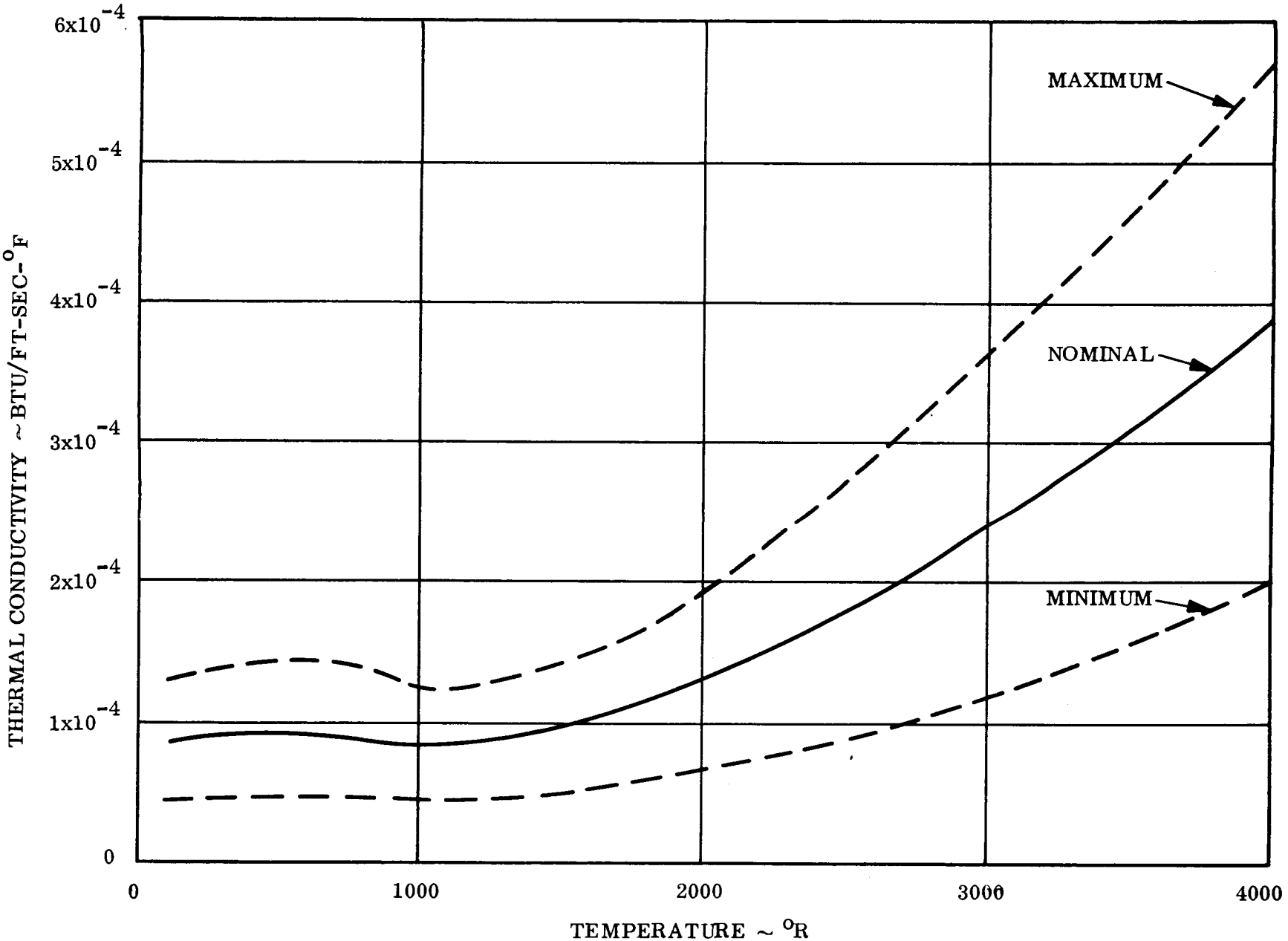

Figure 1. Preliminary Thermal Conductivity of Silica Cloth/Phenolic Resin for Virgin and Charred Condition

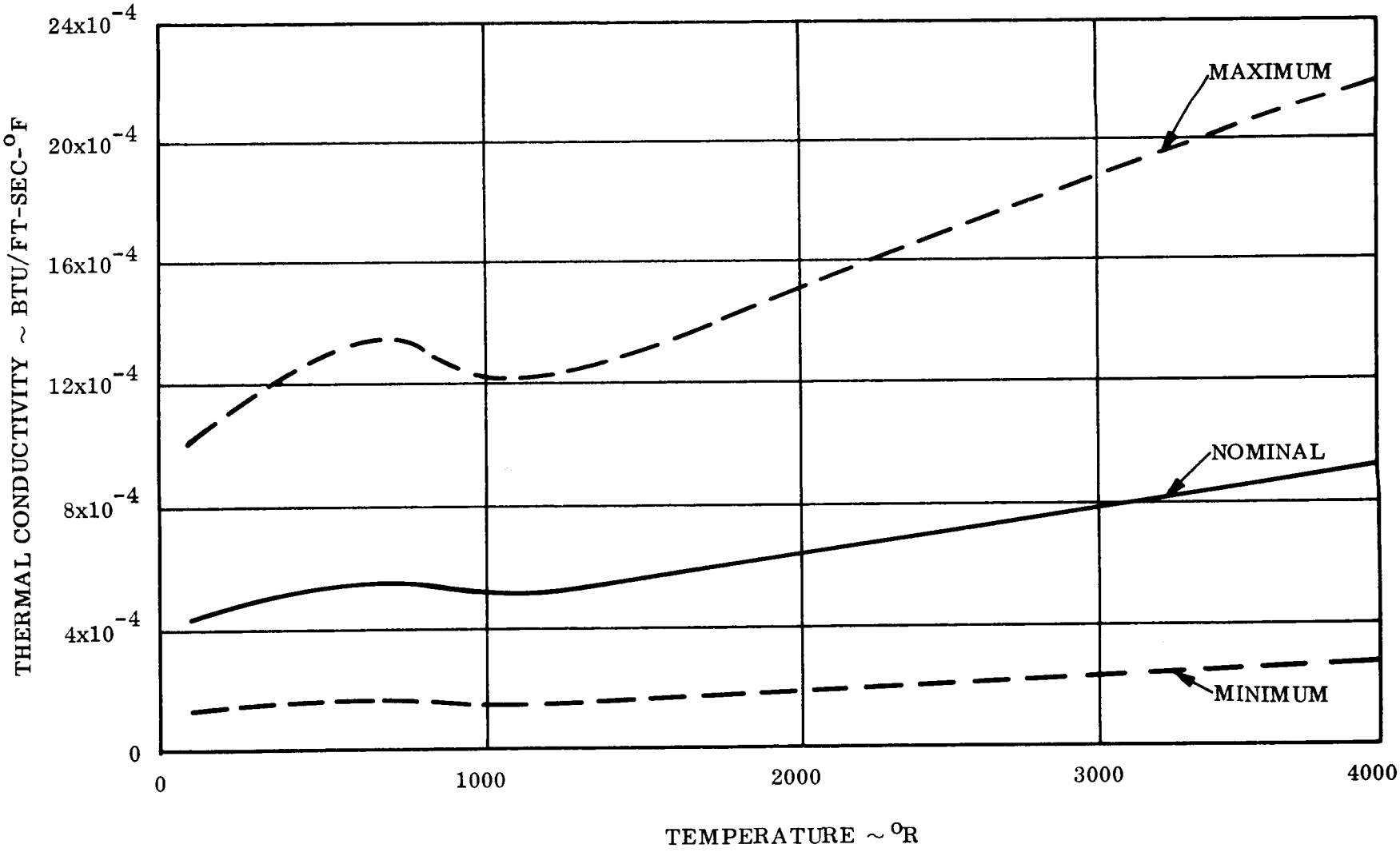

Figure 2. Preliminary Thermal Conductivity of Graphite Cloth/Phenolic Resin for Virgin and Charred Condition

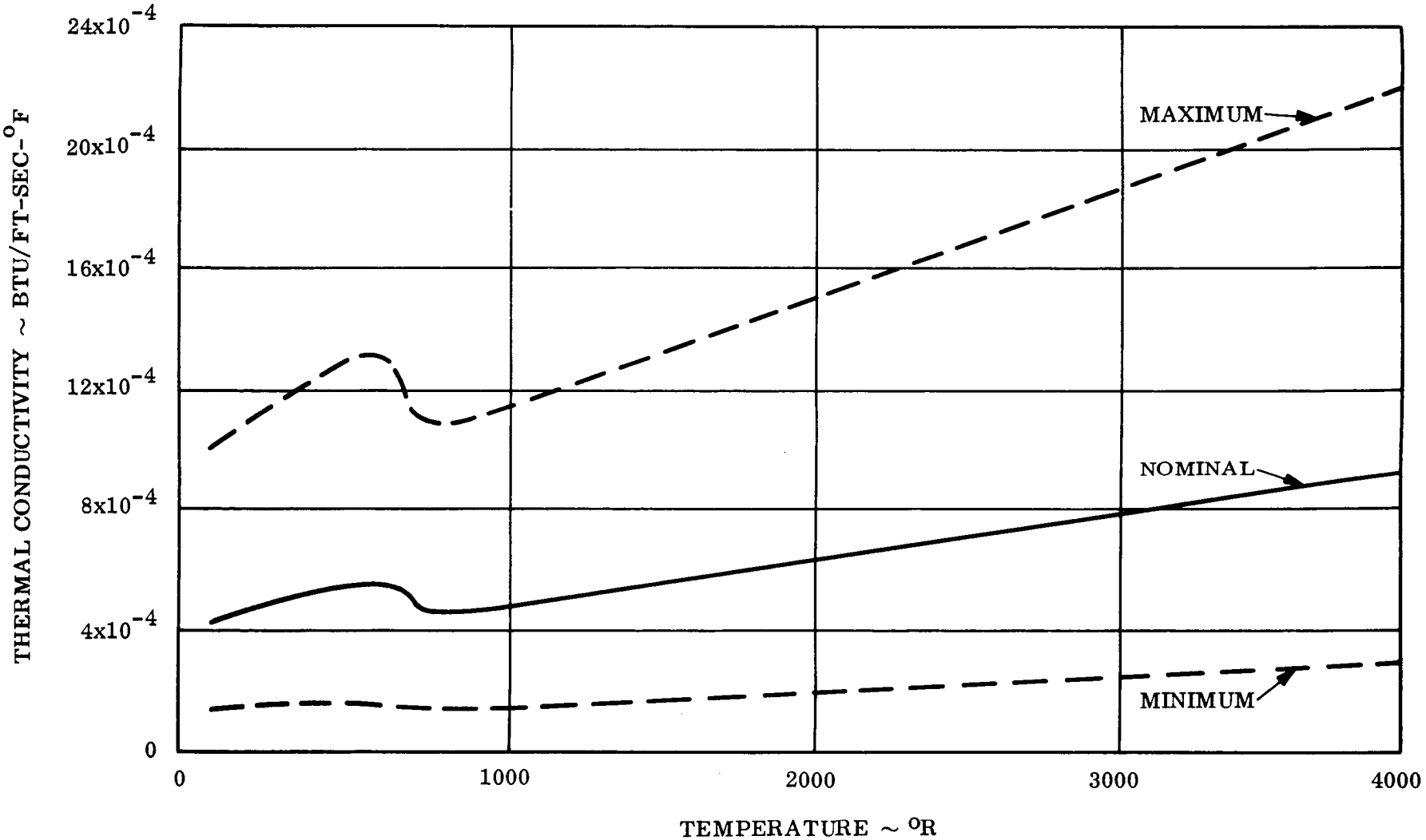

Figure 3. Preliminary Thermal Conductivity of Graphite Cloth/Epoxy Resin for Virgin and Charred Condition

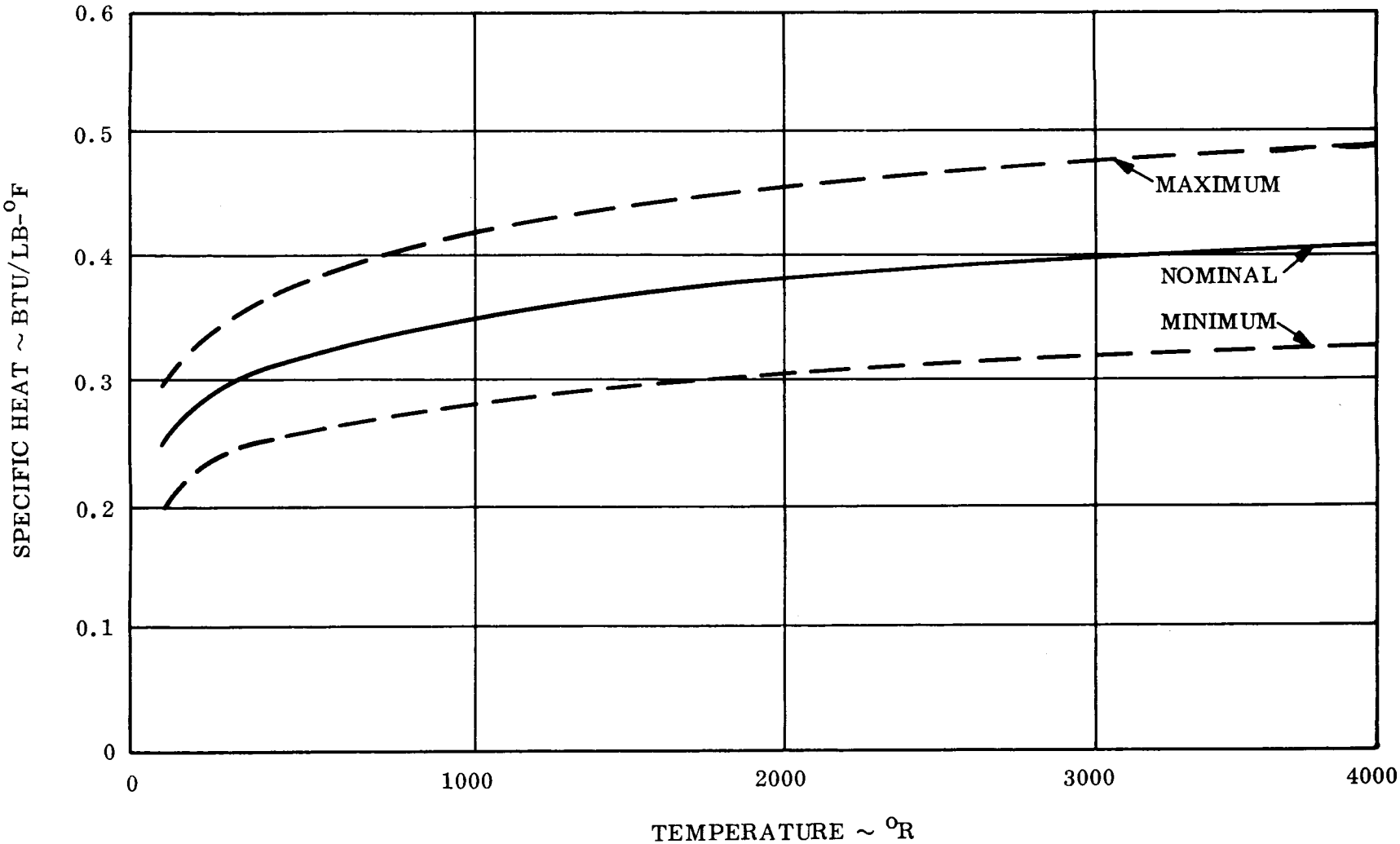

Figure 4. Preliminary Specific Heat of Silica Cloth/Phenolic Resin for Virgin and Charred Condition

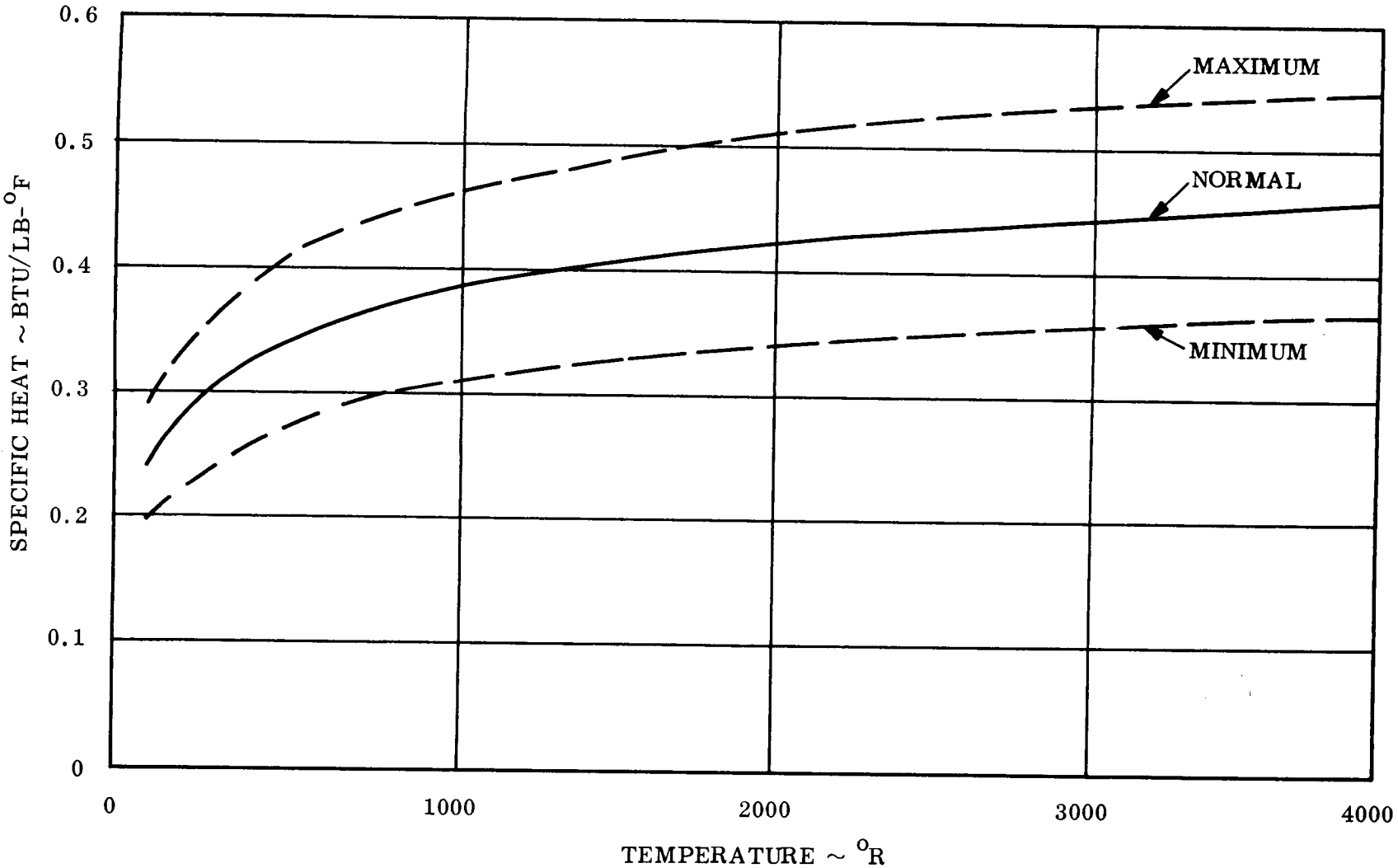

Figure 5. Preliminary Specific Heat of Graphite Cloth/Phenolic Resin and Graphite Cloth/Epoxy Resin for Virgin and Charred Condition

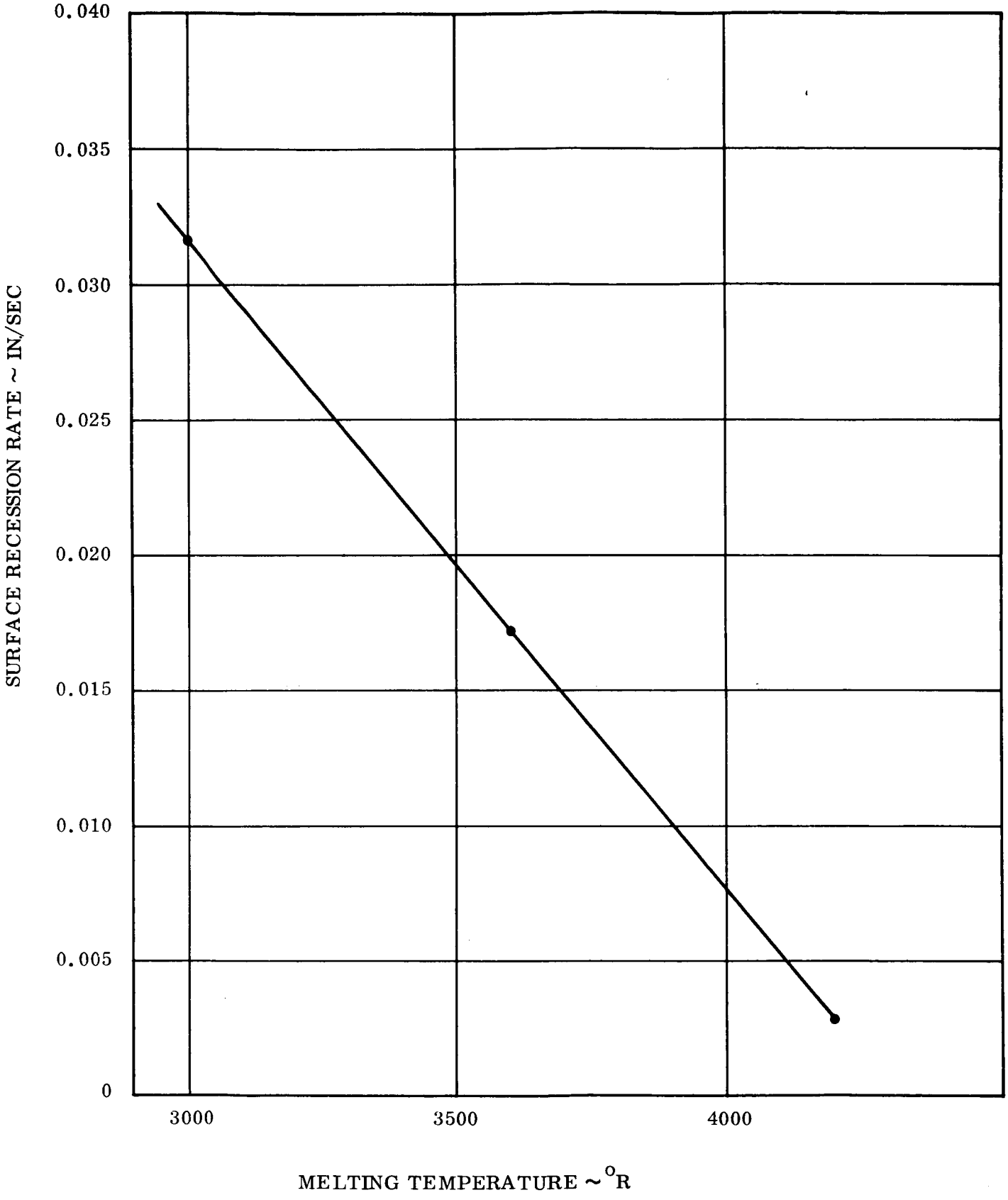

Figure 6. Surface Recession Rate Versus Melting Temperature of Reinforcing Fibers Silica Cloth/Phenolic Resin

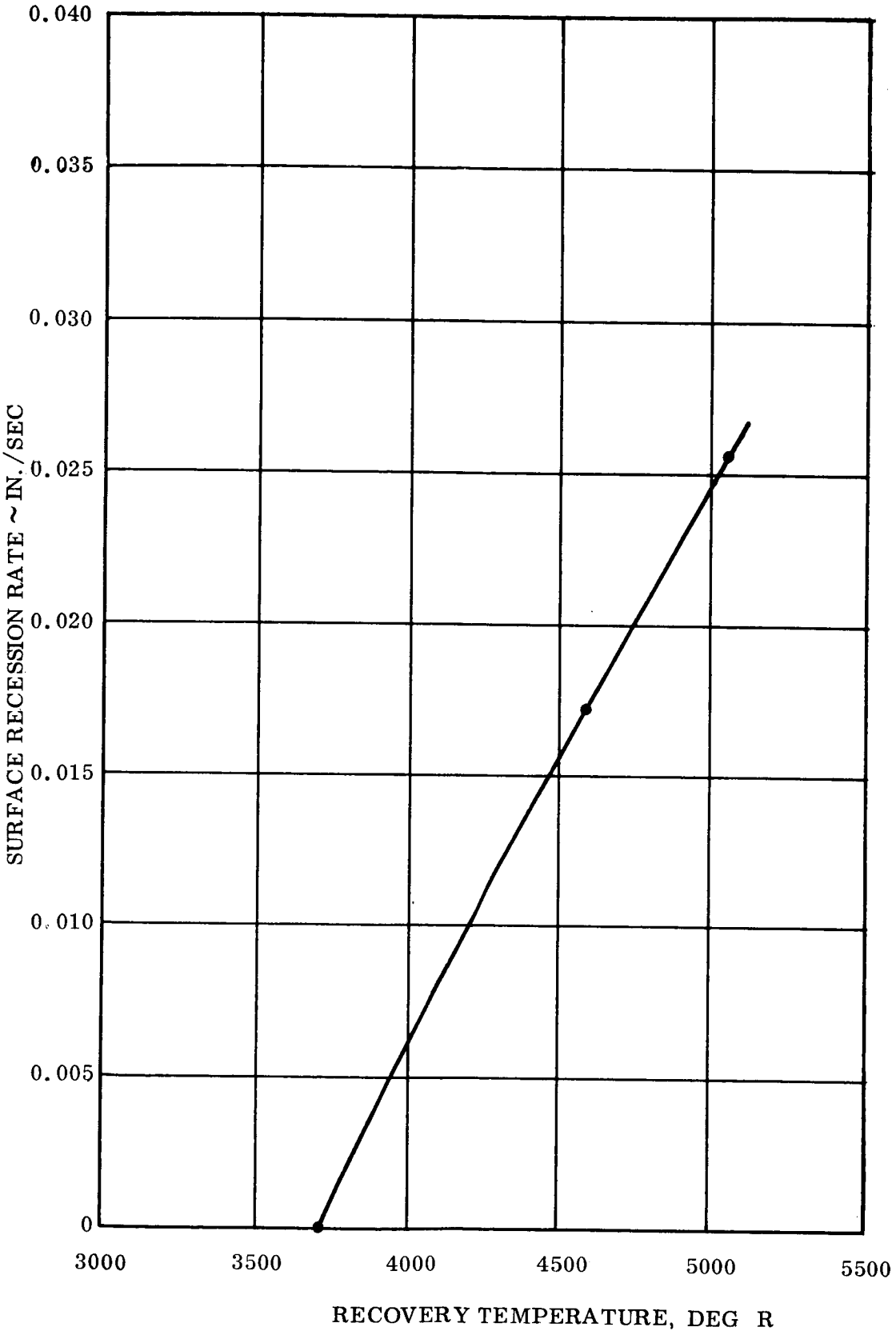

Figure 7. Surface Recession Rate Versus Recovery Temperature
Silica Cloth/Phenolic Resin

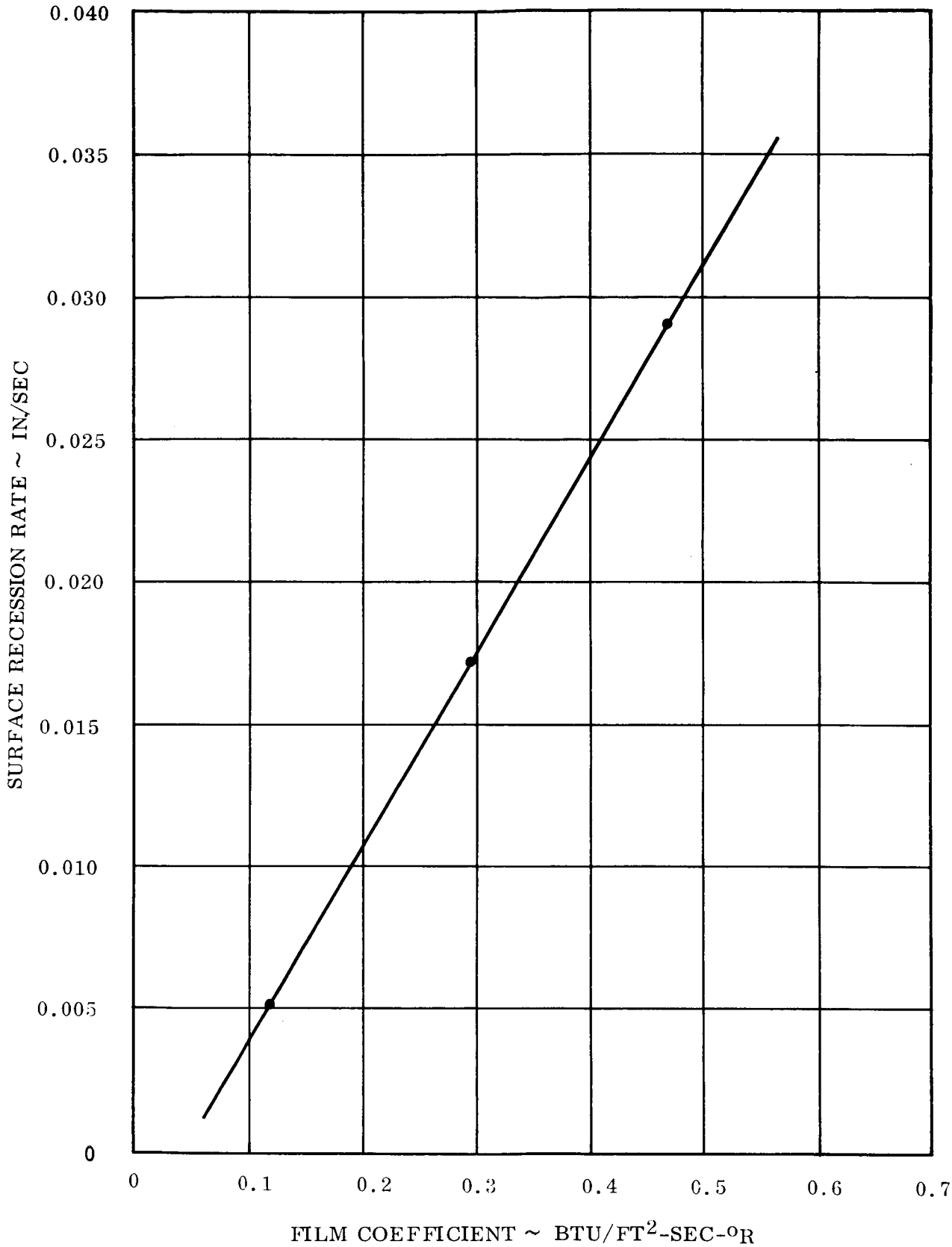

Figure 8. Surface Recession Rate Versus Film Coefficient Silica Cloth/Phenolic Resin

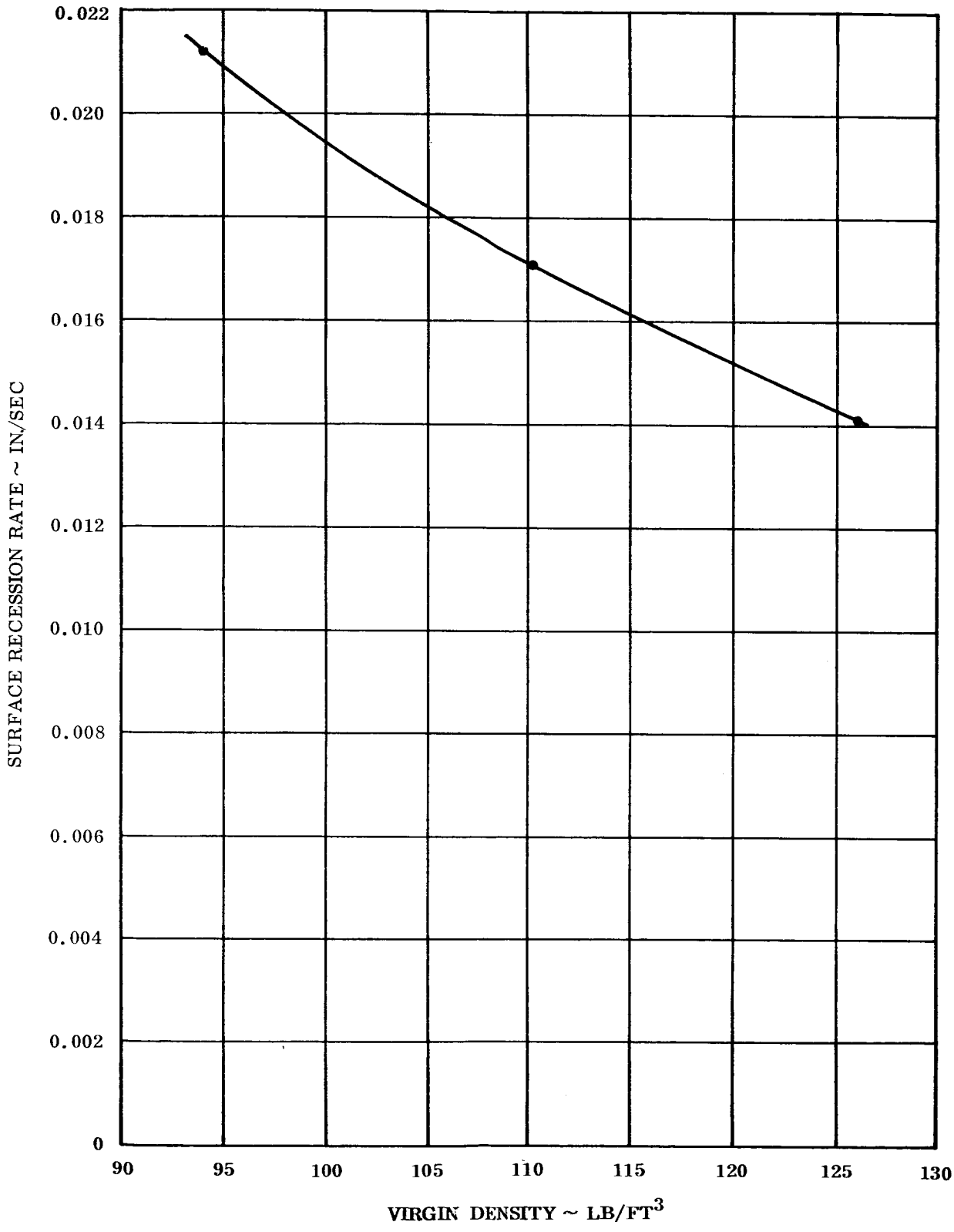

Figure 9. Surface Recession Rate Versus Virgin Density Silica Cloth/Phenolic Resin

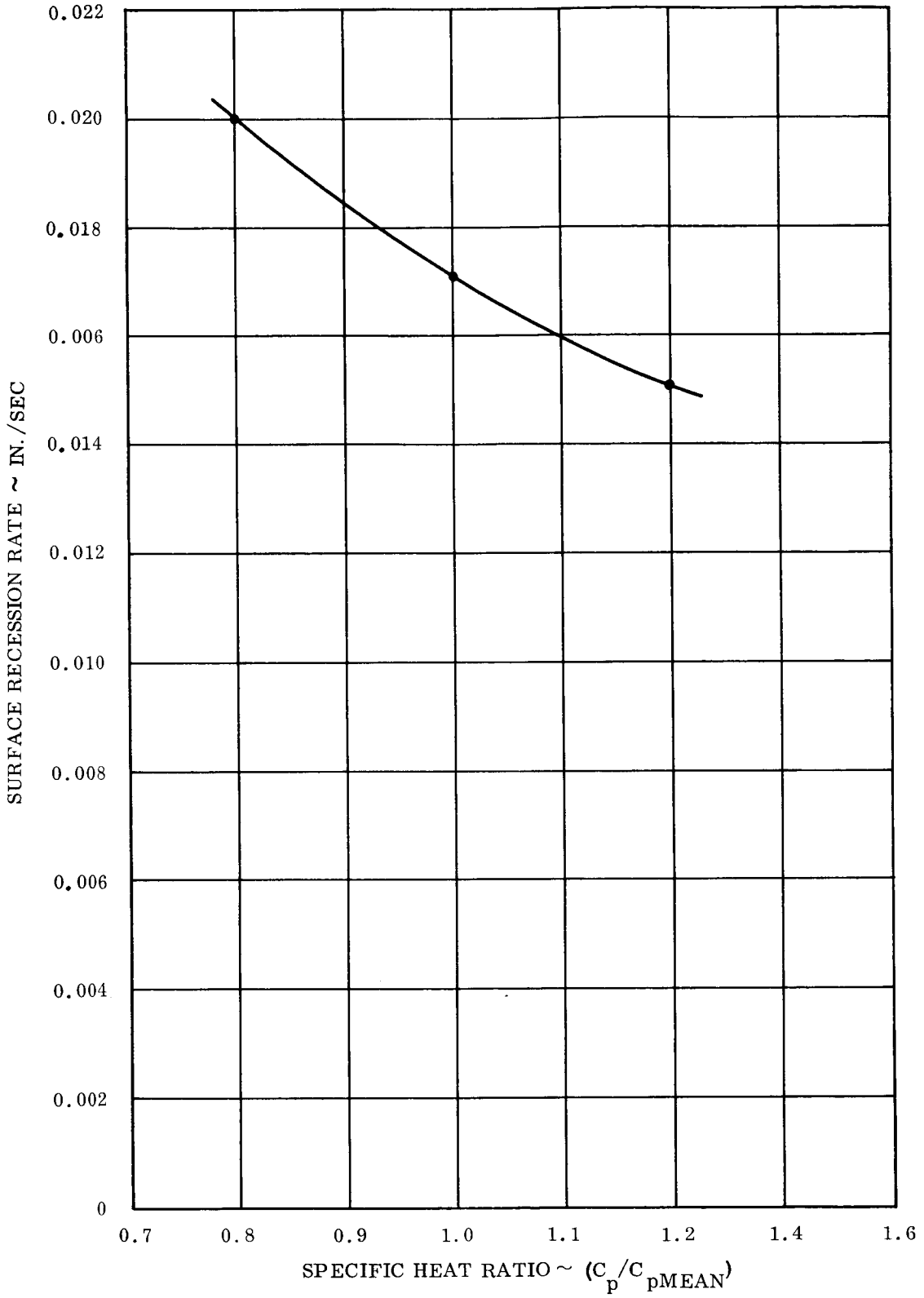

Figure 10. Surface Recession Rate Versus Specific Heat Ratio Silica Cloth/Phenolic Resin

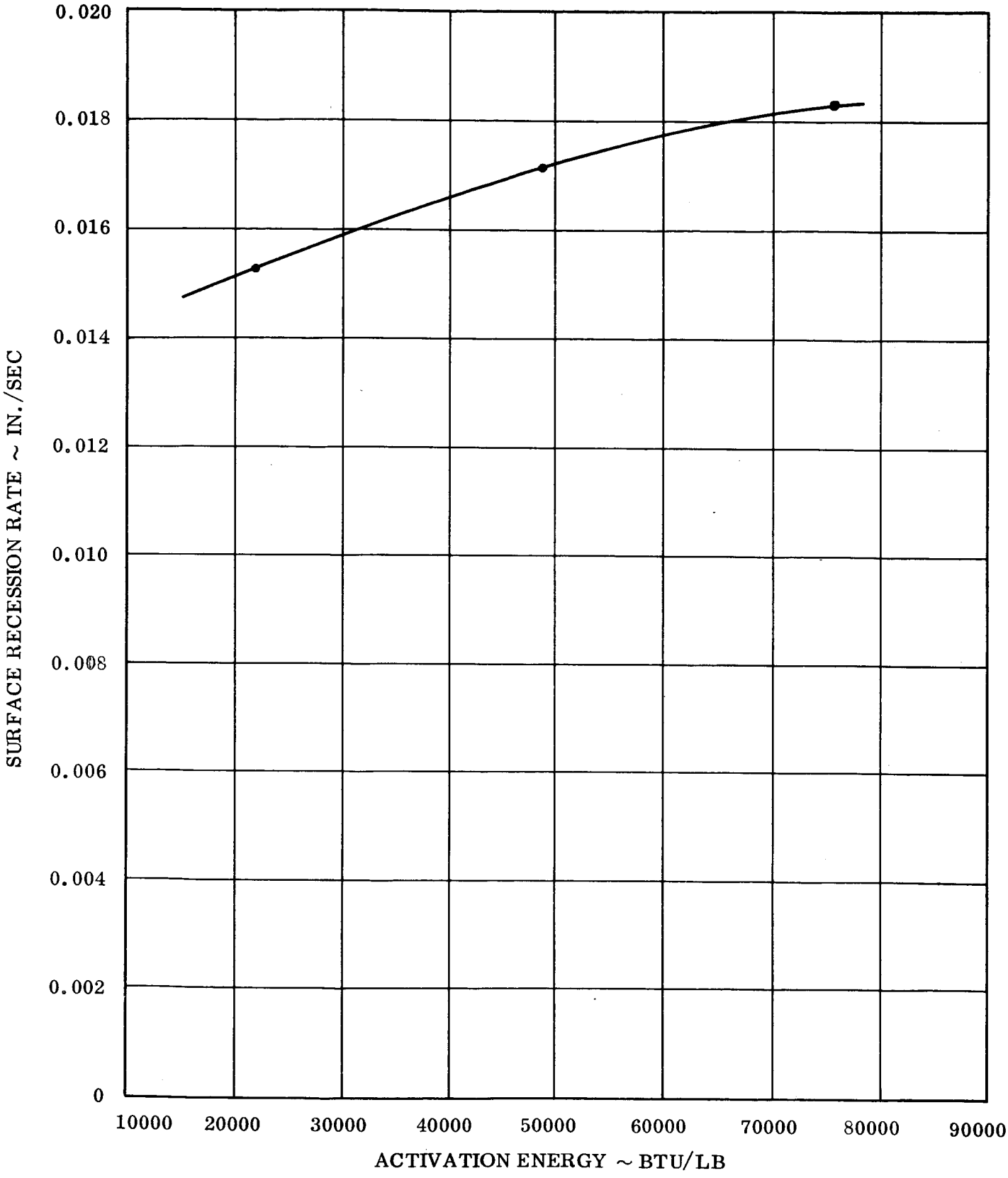

Figure 11. Surface Recession Rate Versus Activation Energy Silica Cloth/Phenolic Resin

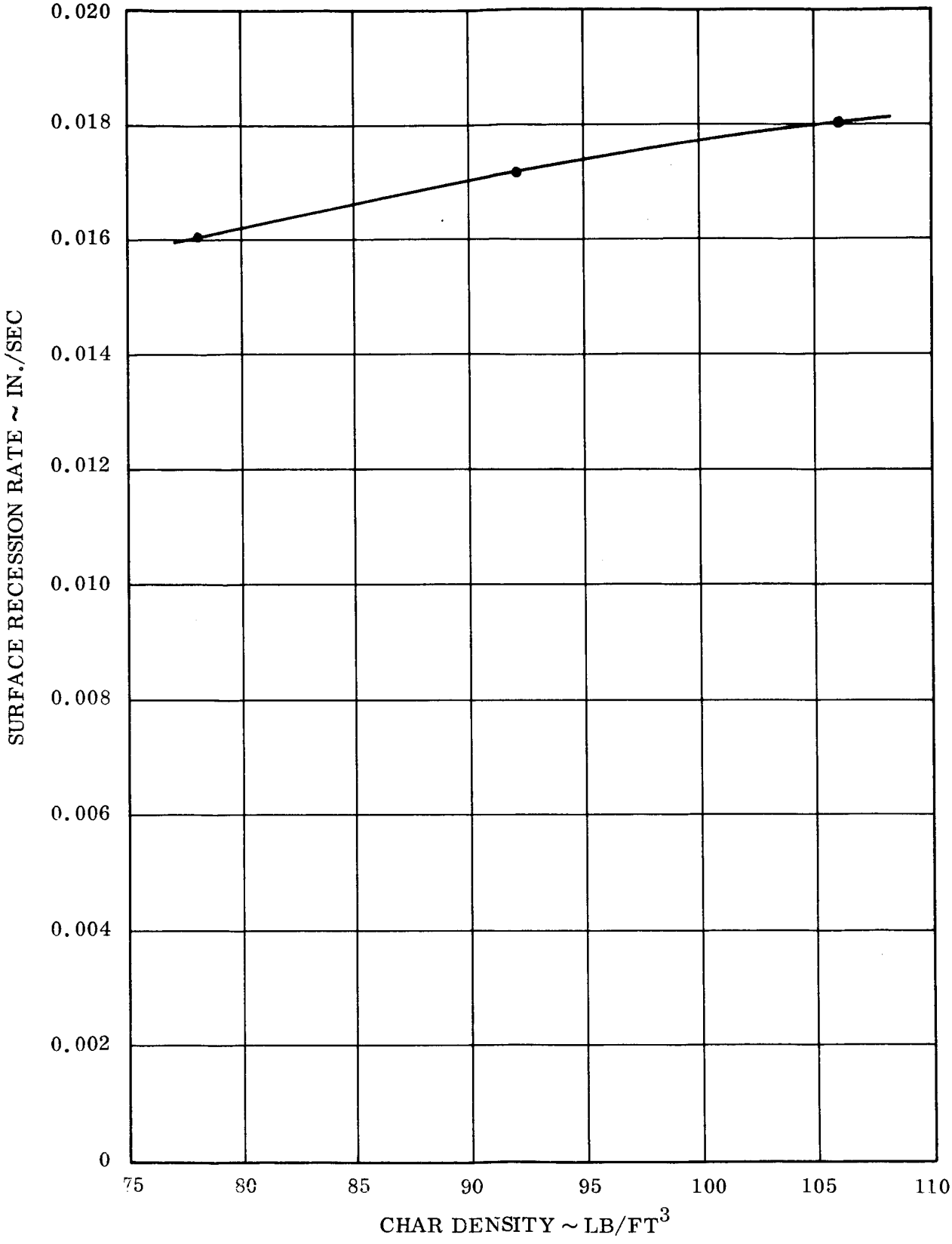

Figure 12. Surface Recession Rate Versus Char Density Silica Cloth/Phenolic Resin

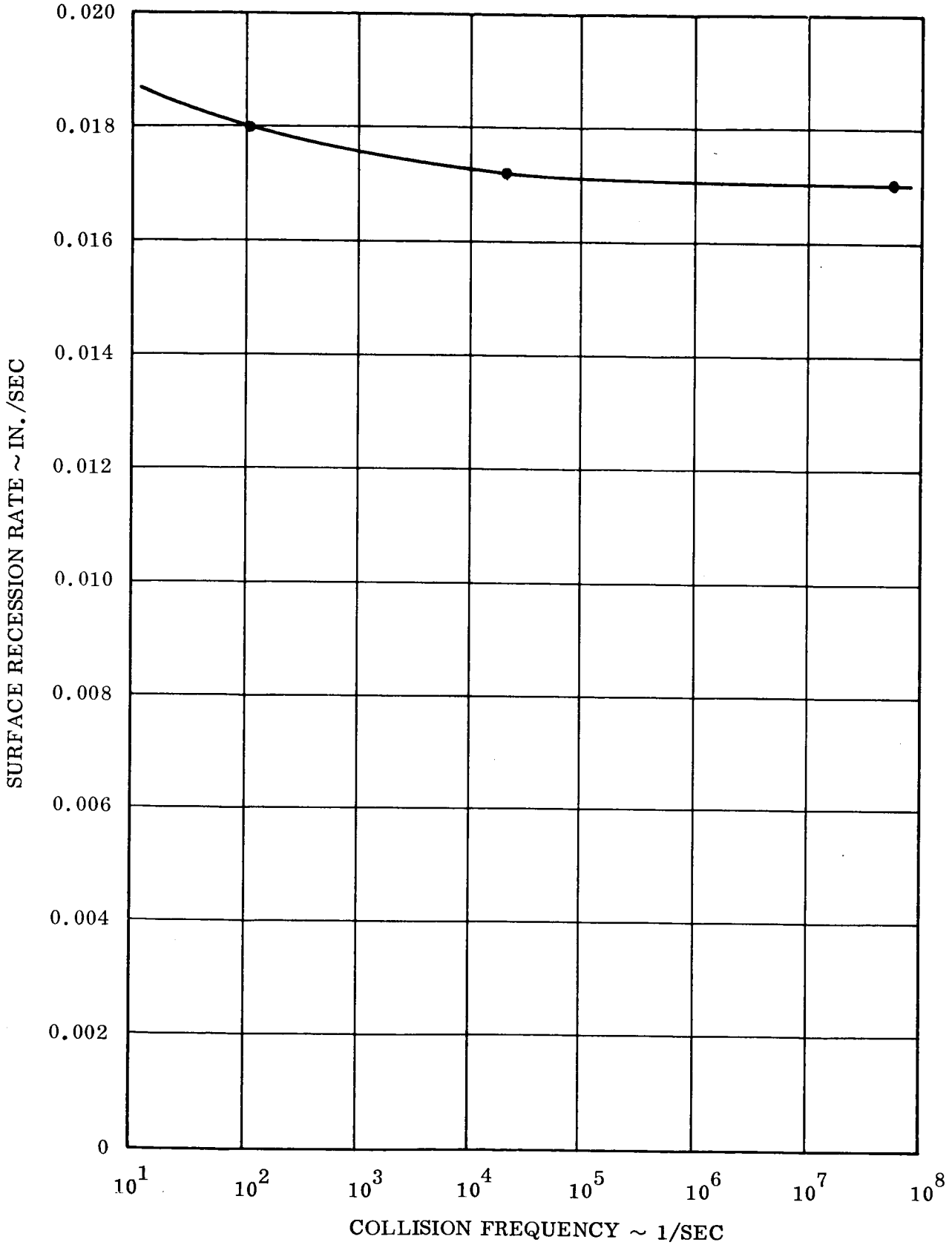

Figure 13. Surface Recession Rate Versus Collision Frequency Silica Cloth/Phenolic Resin

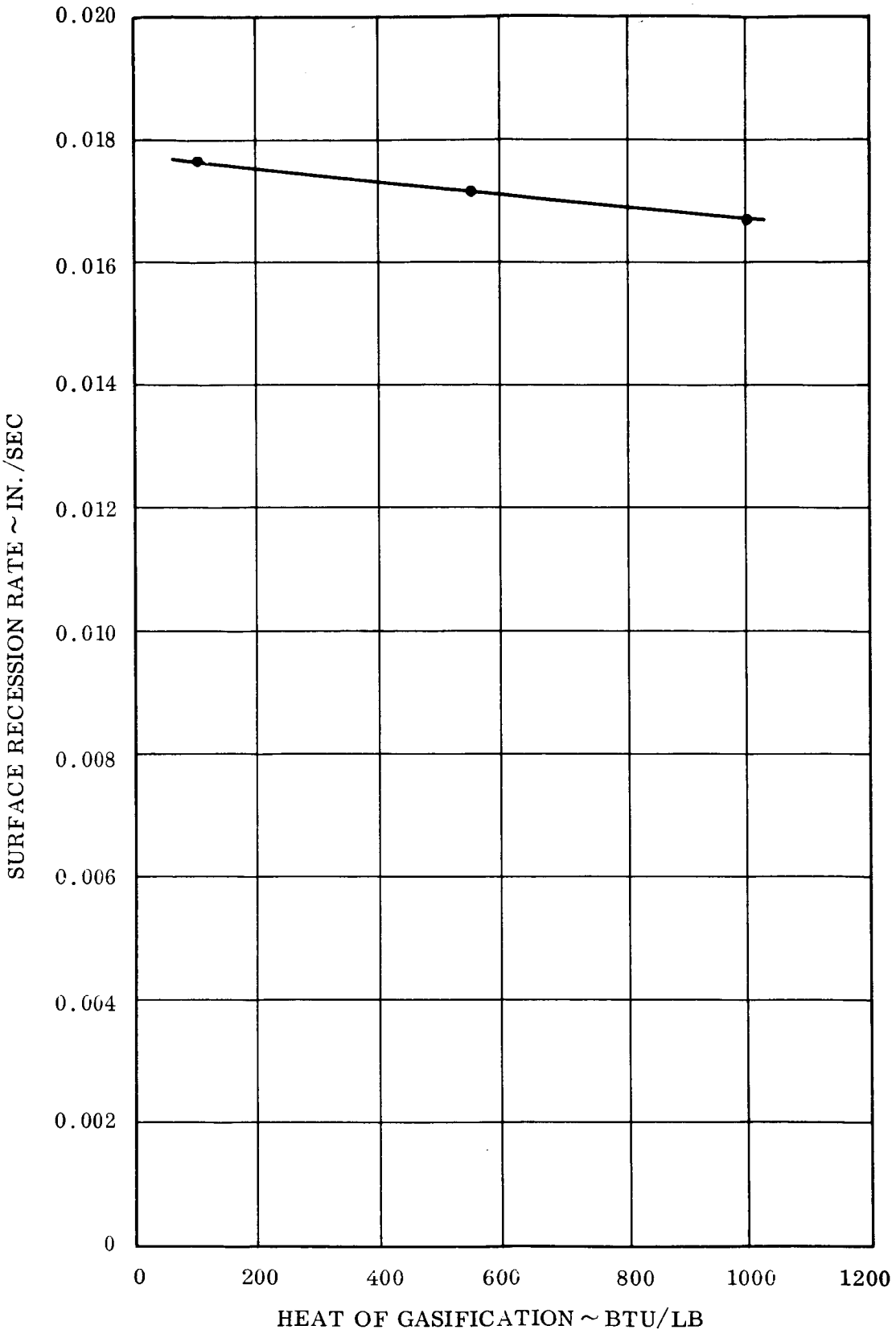

Figure 14. Surface Recession Rate Versus Heat of Gasification
Silica Cloth/Phenolic Resin

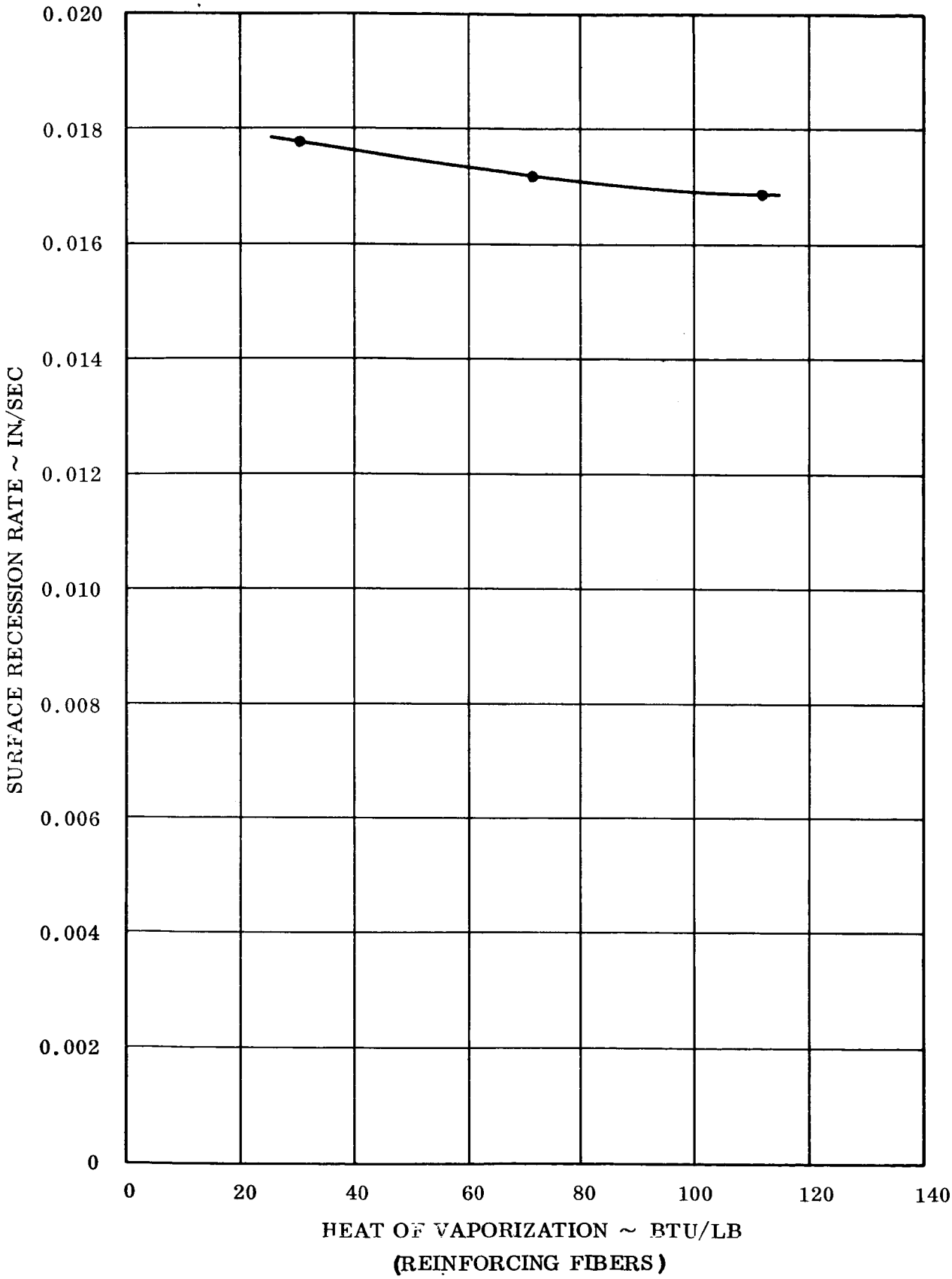

Figure 15. Surface Recession Rate Versus Heat of Vaporization of Reinforcing Fibers Silica Cloth/Phenolic Resin

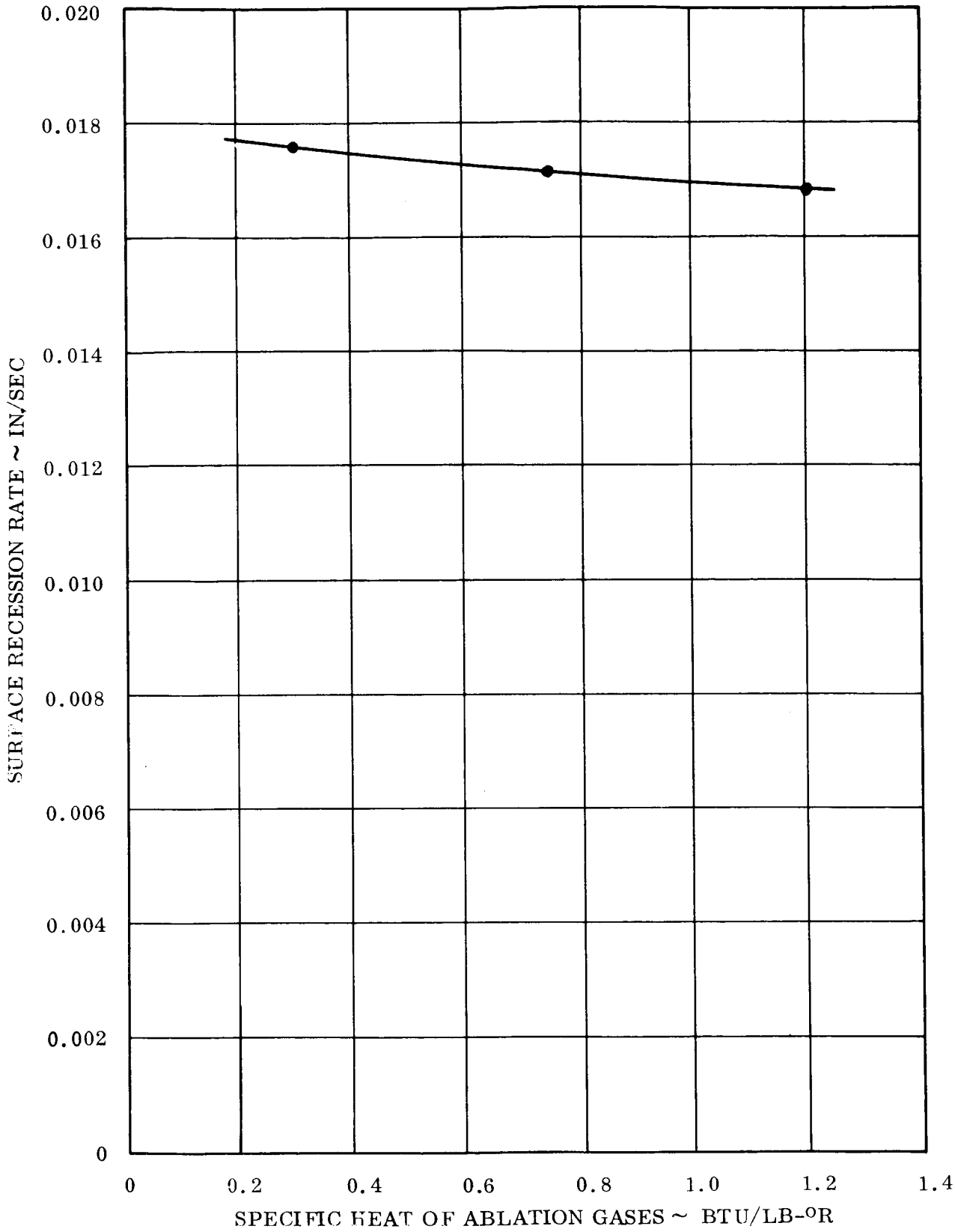

Figure 16. Surface Recession Rate Versus Specific Heat of Ablation Gases Silica Cloth/Phenolic Resin

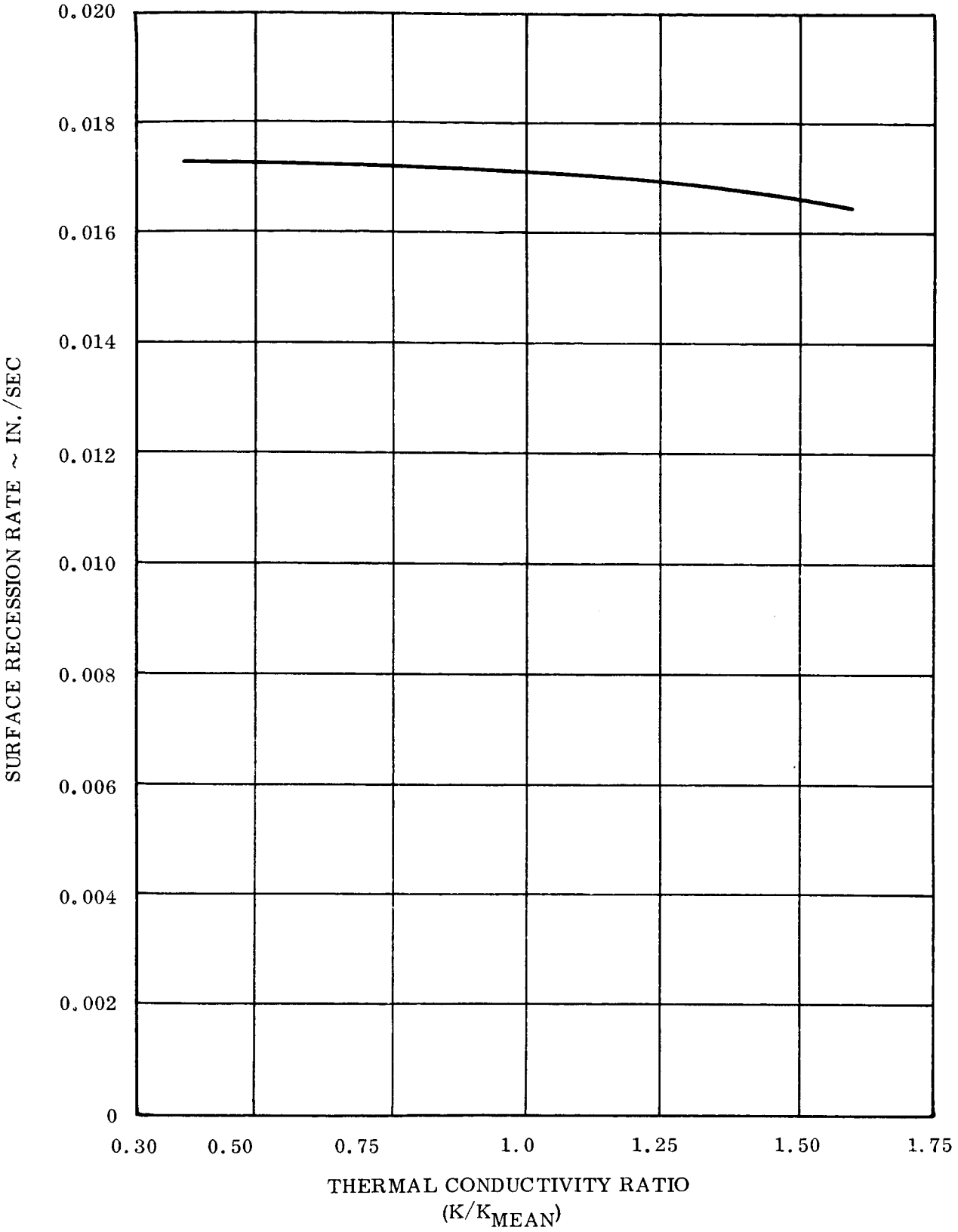

Figure 17. Surface Recession Rate Versus Thermal Conductivity Ratio Silica Cloth/Phenolic Resin

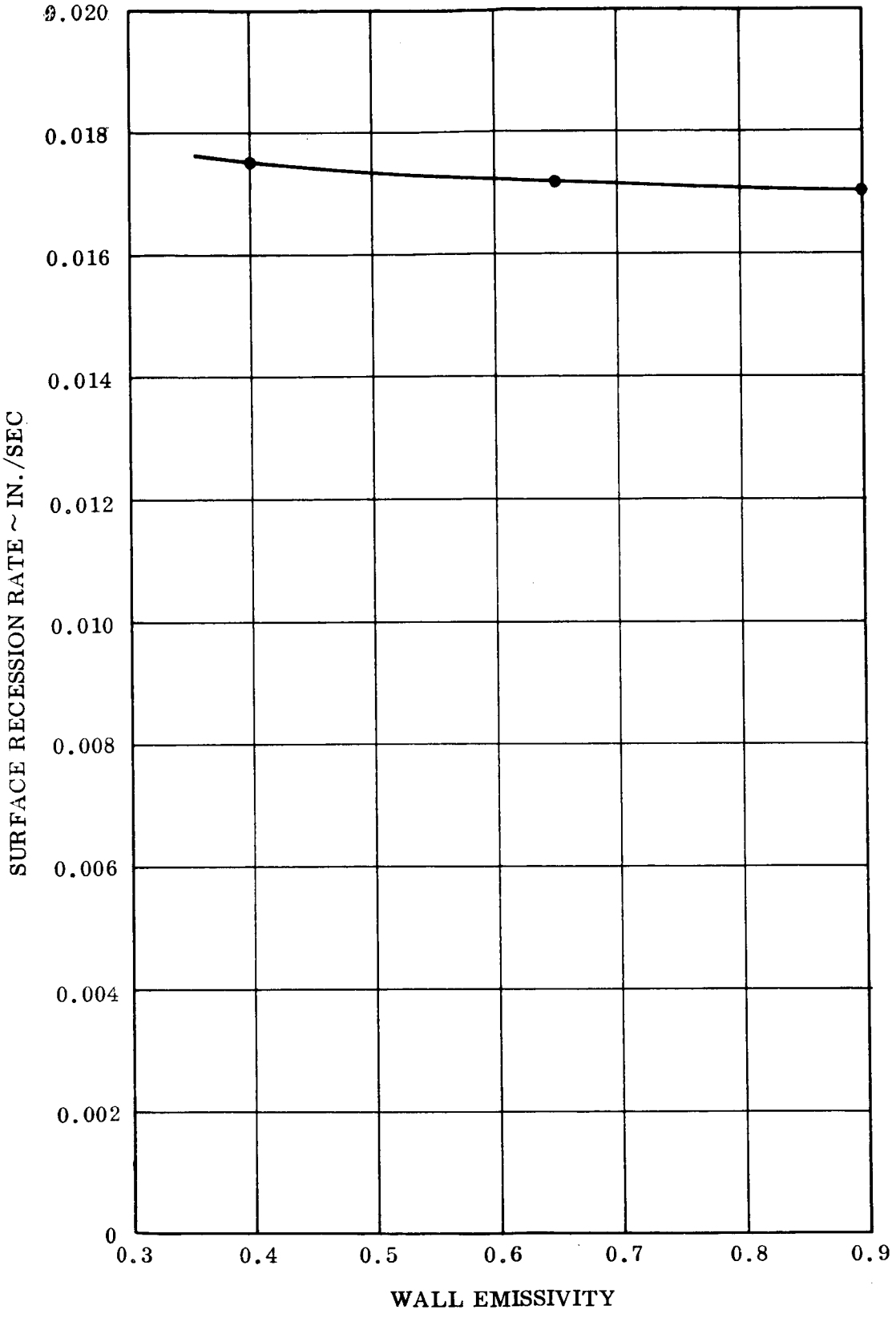

Figure 18. Surface Recession Rate Versus Wall Emissivity
Silica Cloth/Phenolic Resin

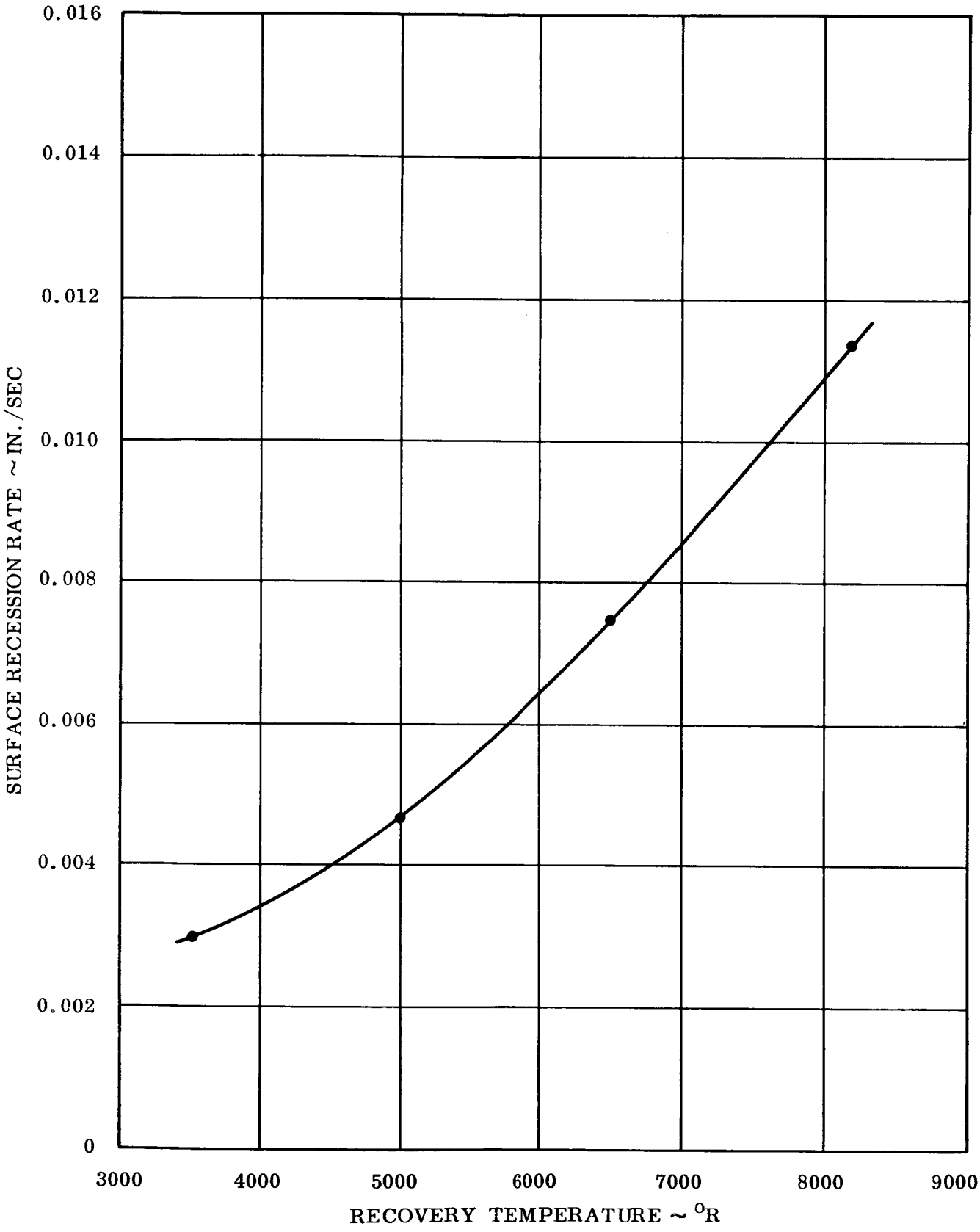

Figure 19. Surface Recession Rate Versus Recovery Temperature
Graphite Cloth/Phenolic Resin

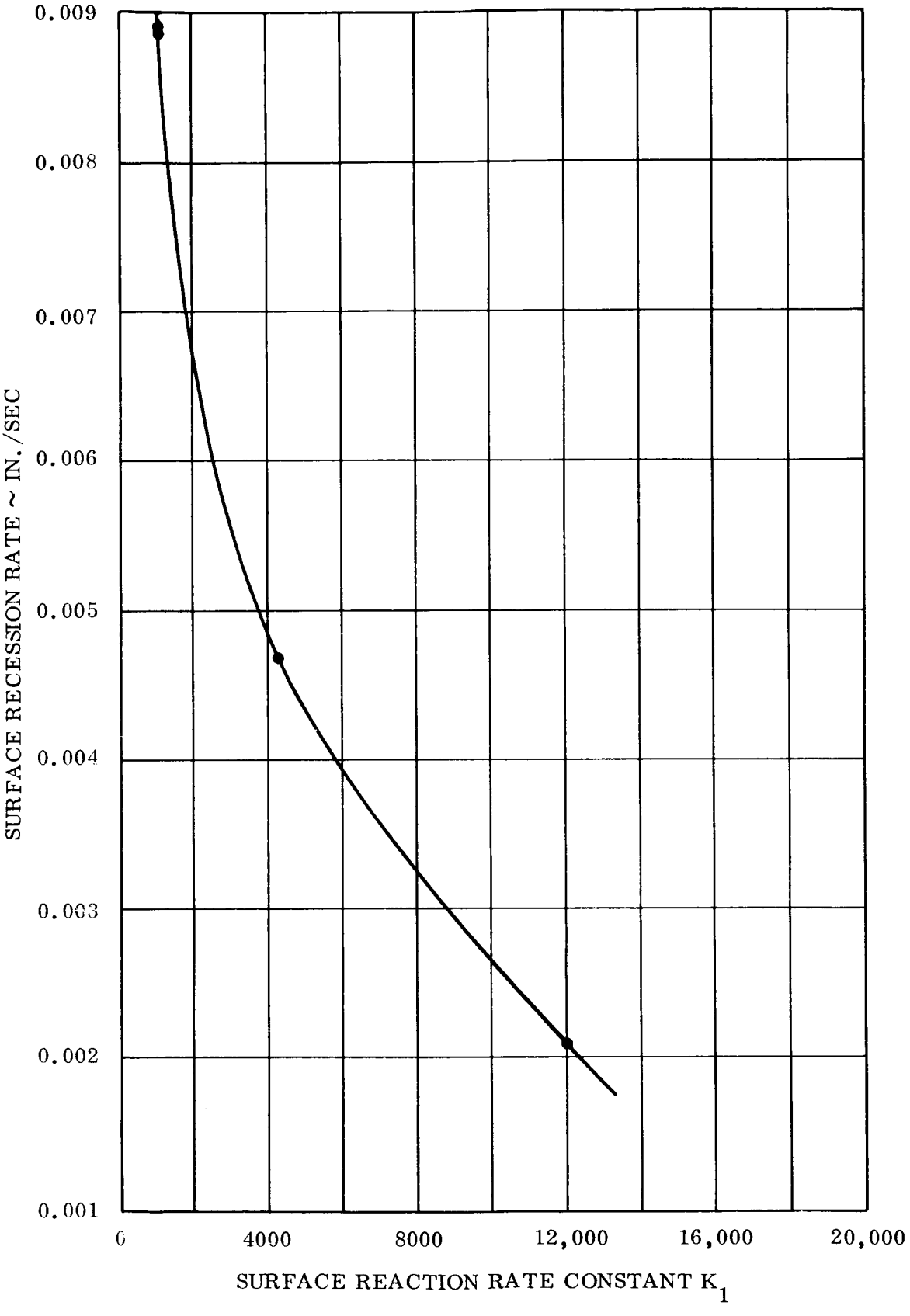

Figure 20. Surface Recession Rate Versus Surface Reaction Rate Constant K_1 Graphite Cloth/Phenolic Resin

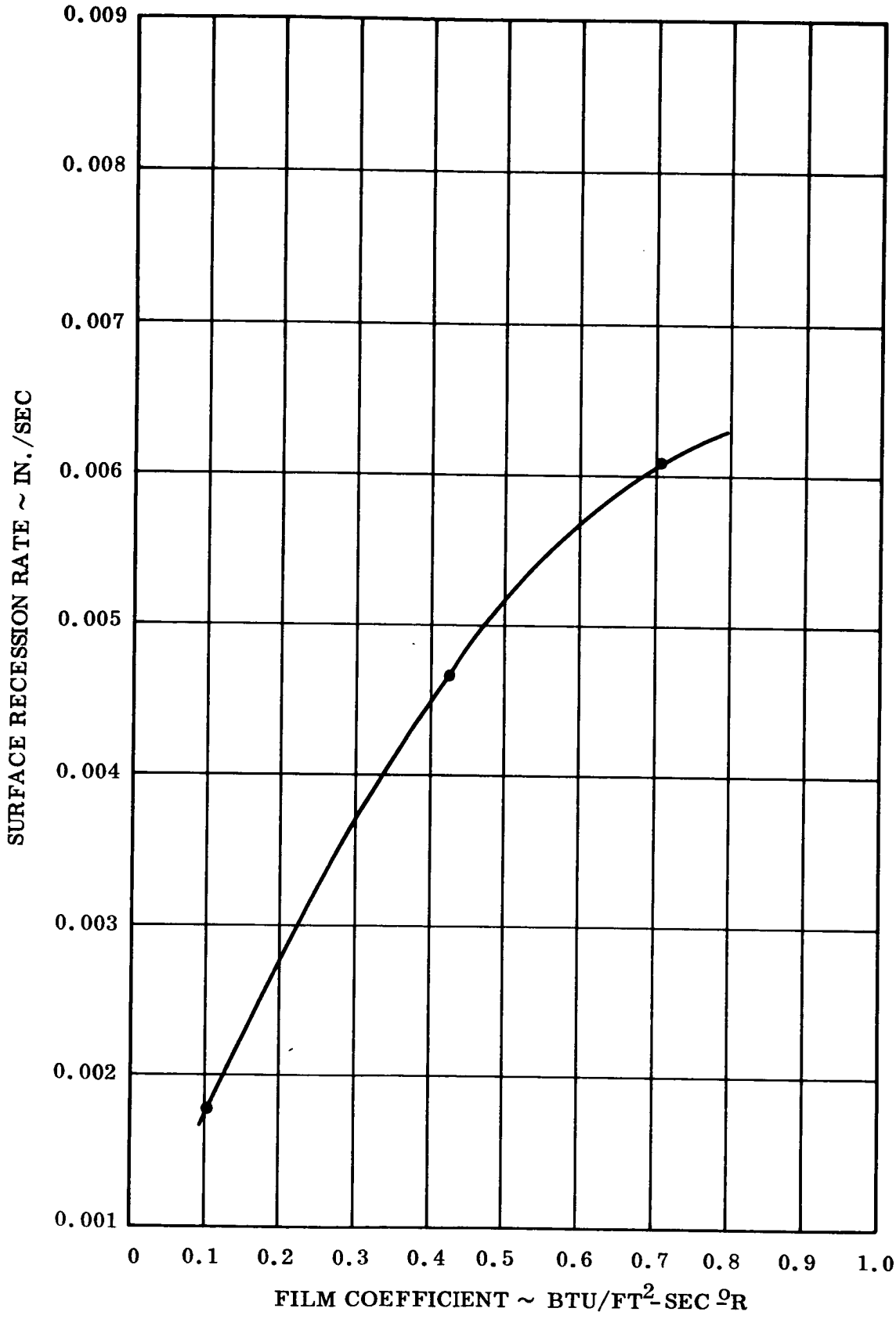

Figure 21. Surface Recession Rate Versus Film Coefficient Graphite Cloth/Phenolic Resin

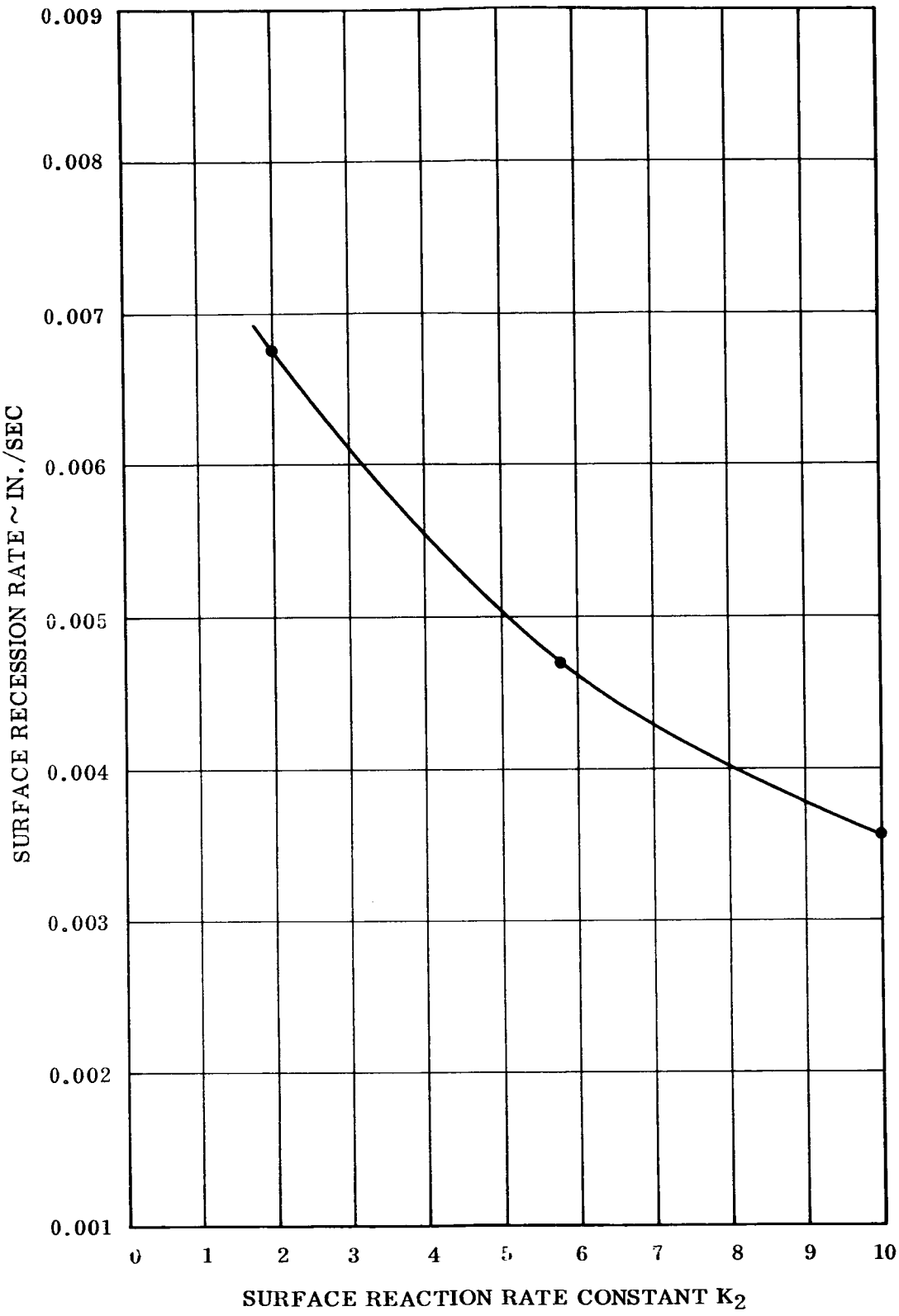

Figure 22. Surface Recession Rate Versus Surface Reaction Rate Constant K_2 Graphite Cloth/Phenolic Resin

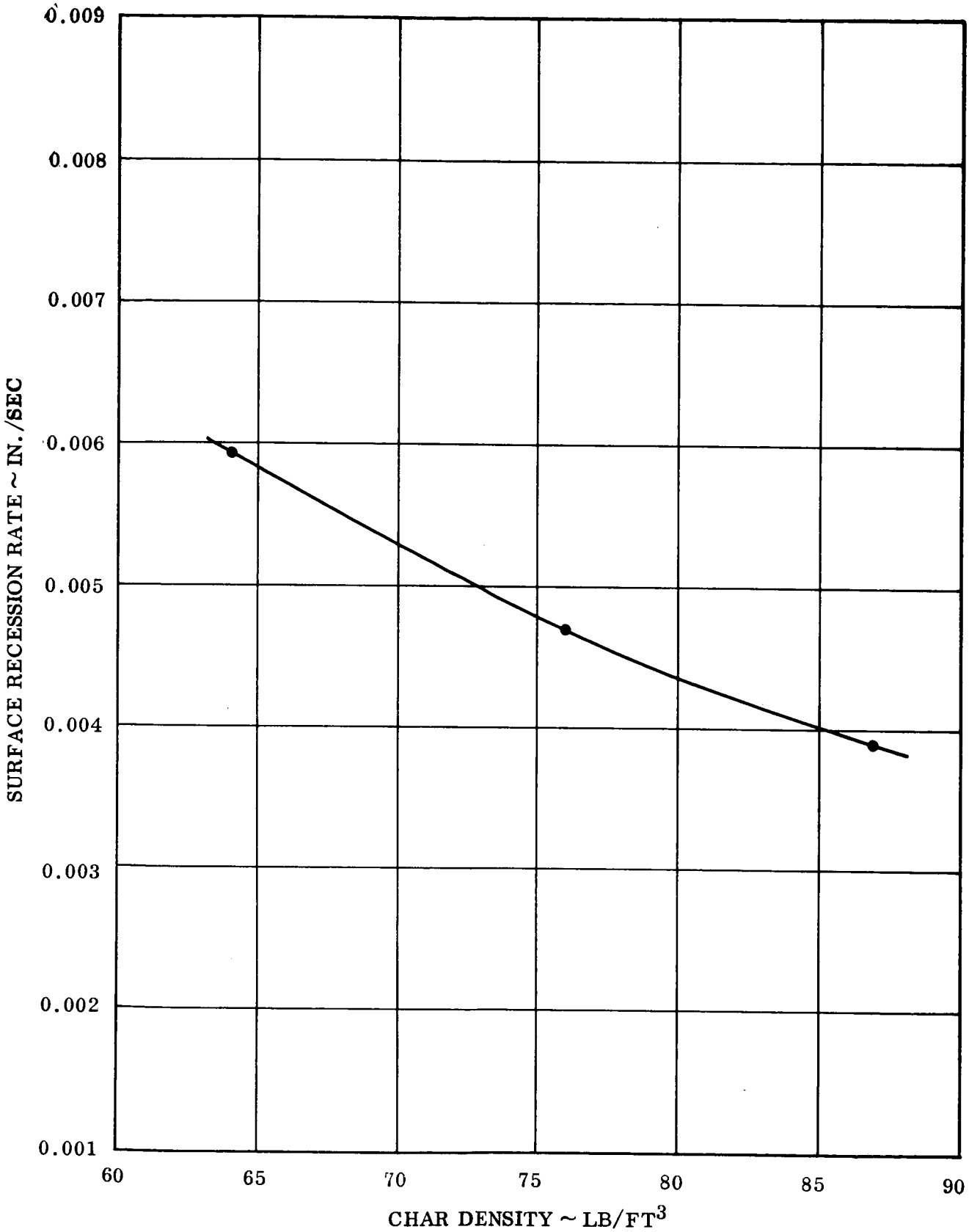

Figure 23. Surface Recession Rate Versus Char Density
Graphite Cloth/Phenolic Resin

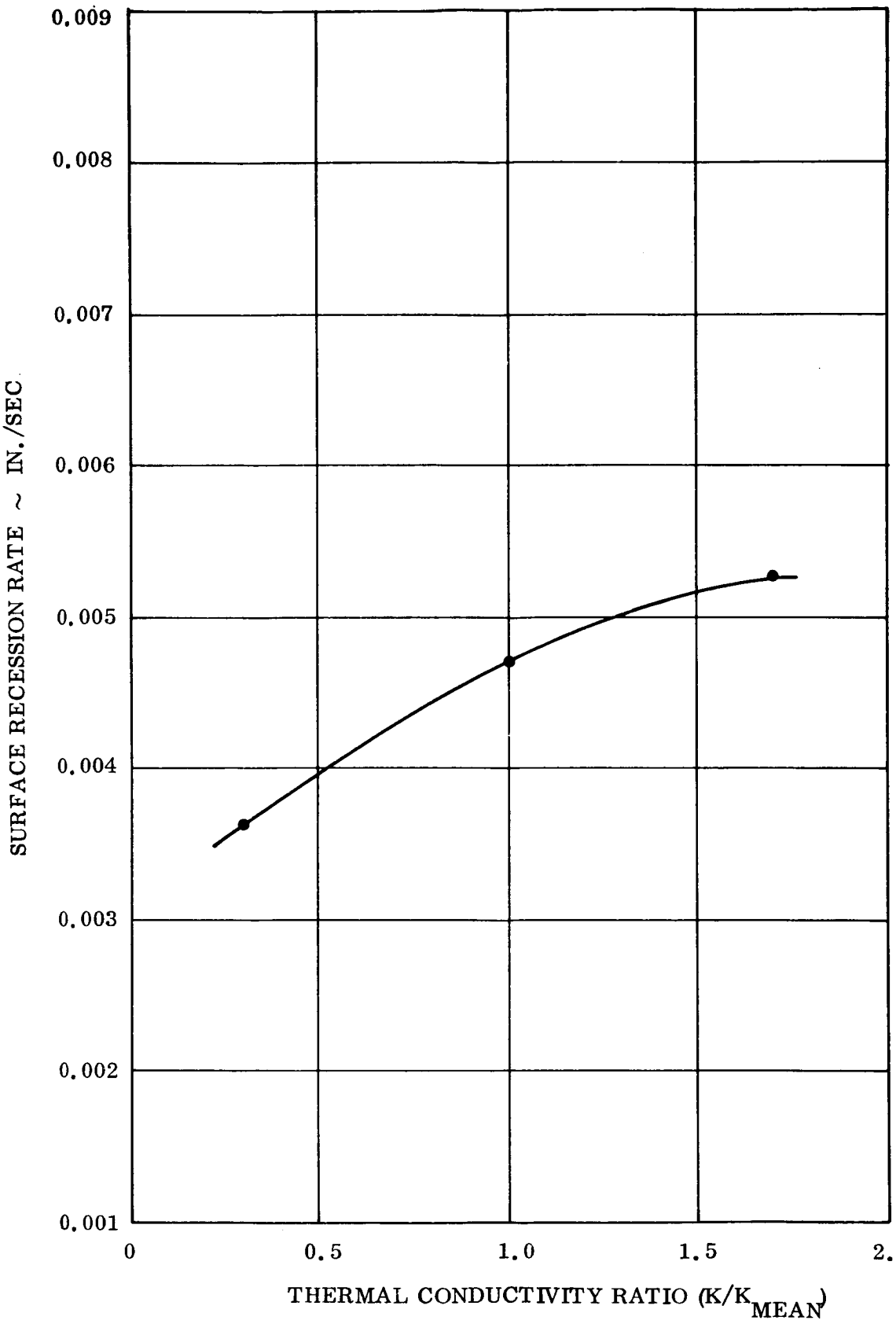

Figure 24. Surface Recession Rate Versus Thermal Conductivity Ratio Graphite Cloth/Phenolic Resin

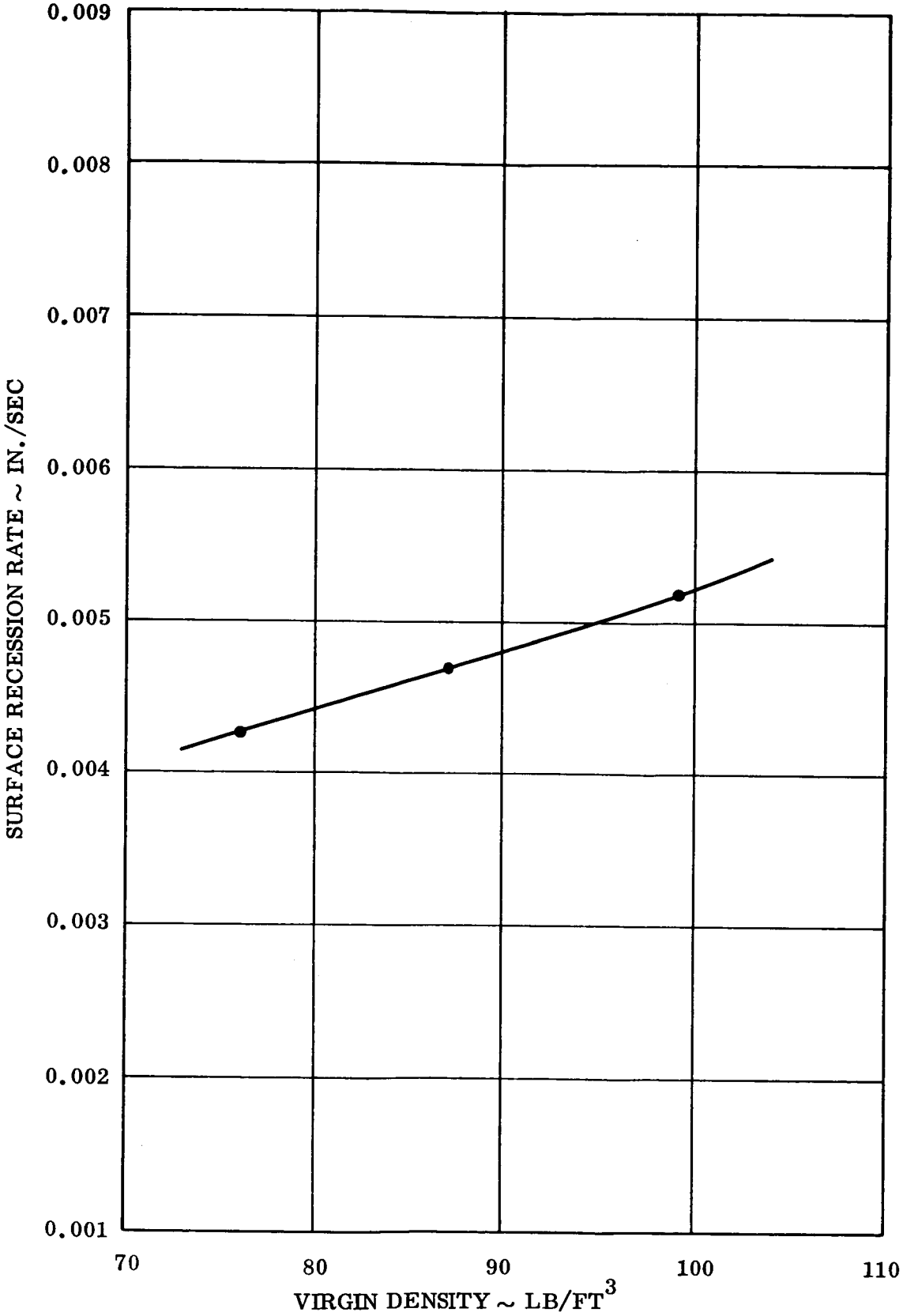

Figure 25. Surface Recession Rate Versus Virgin Density
Graphite Cloth/Phenolic Resin

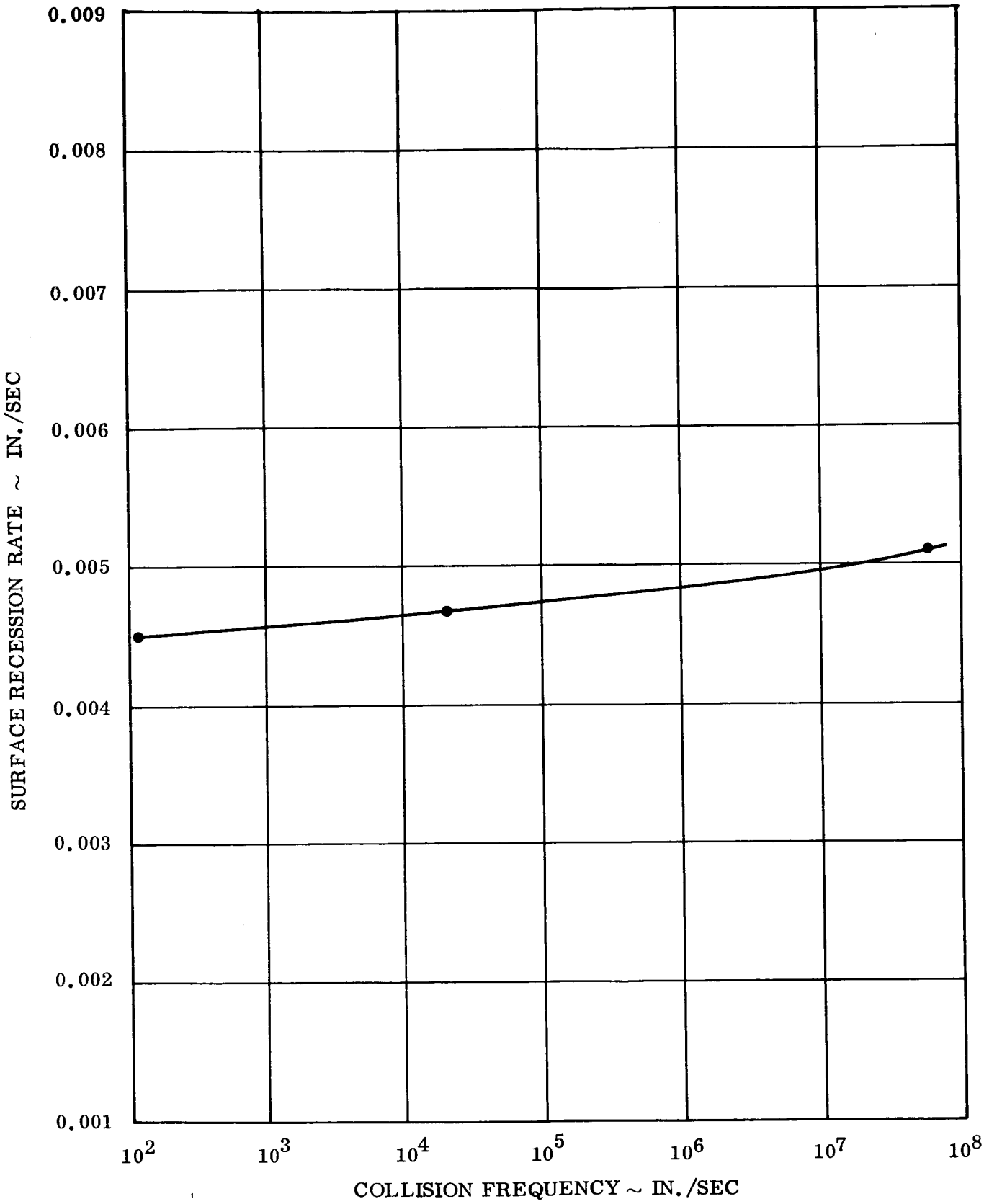

Figure 26. Surface Recession Rate Versus Collision Frequency Graphite Cloth/Phenolic Resin

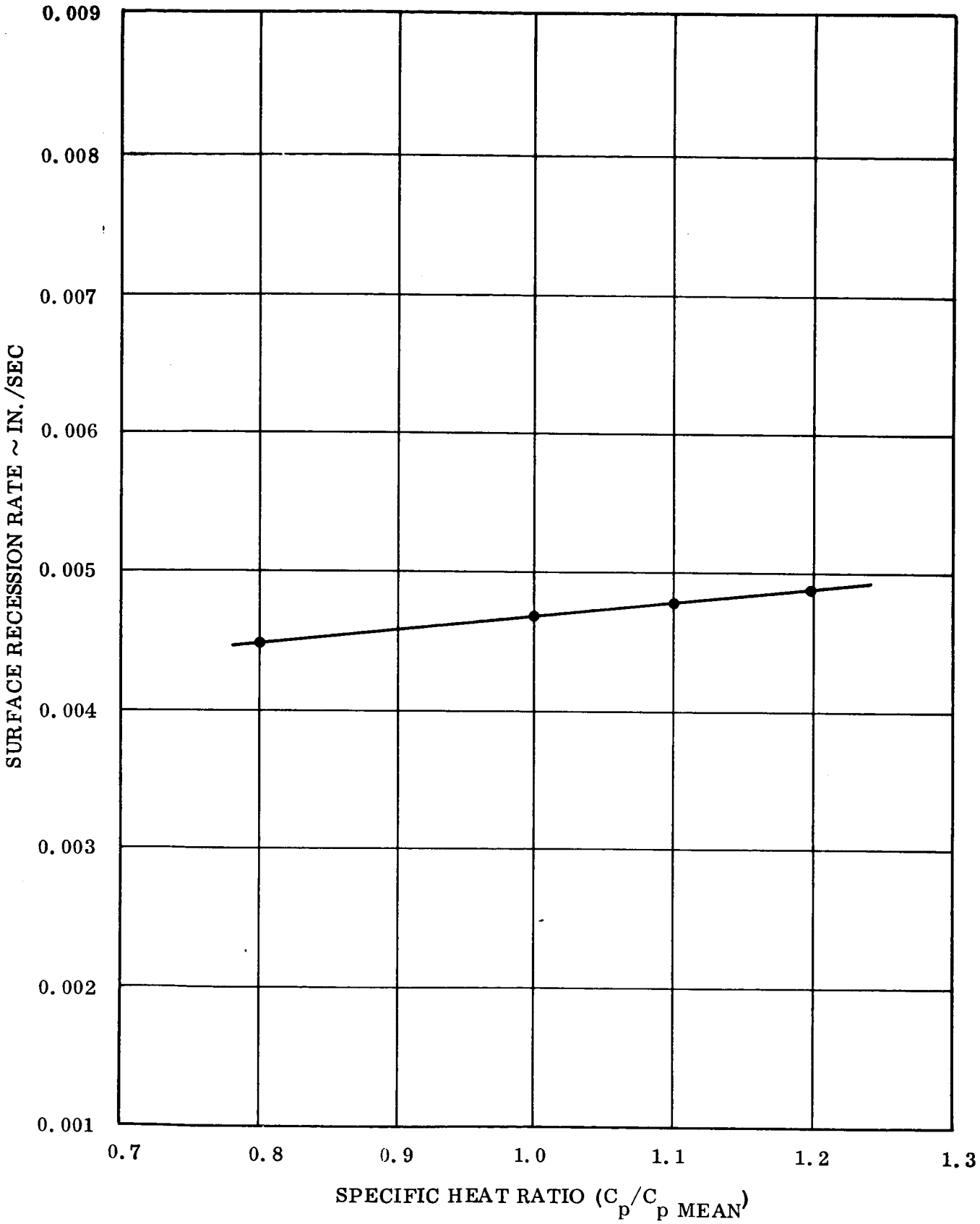

Figure 27. Surface Recession Rate Versus Specific Heat Ratio Graphite Cloth/Phenolic Resin

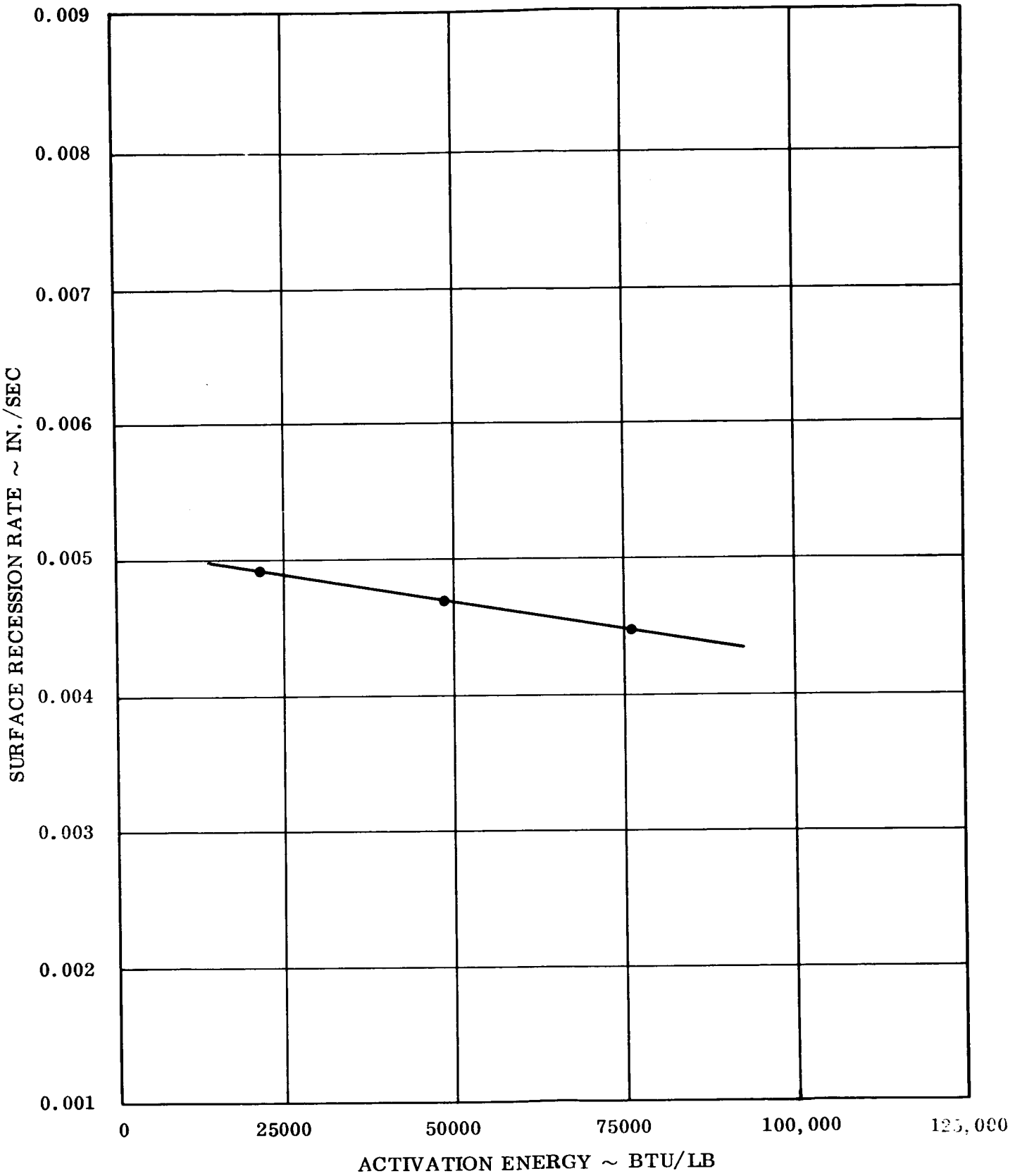

Figure 28. Surface Recession Rate Versus Activation Energy
Graphite Cloth/Phenolic Resin

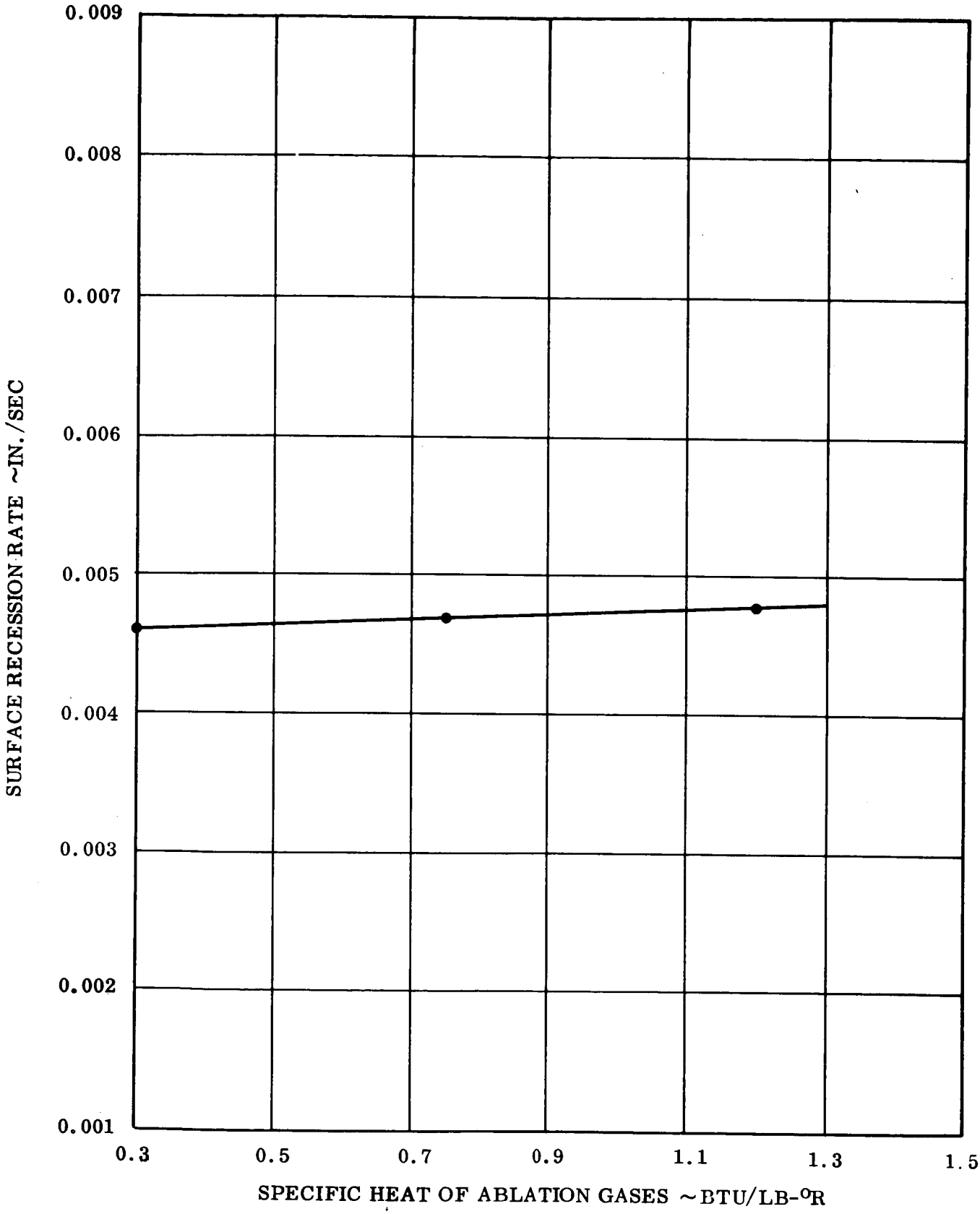

Figure 29. Surface Recession Rate Versus Specific Heat of Ablation Gases Graphite Cloth/Phenolic Resin

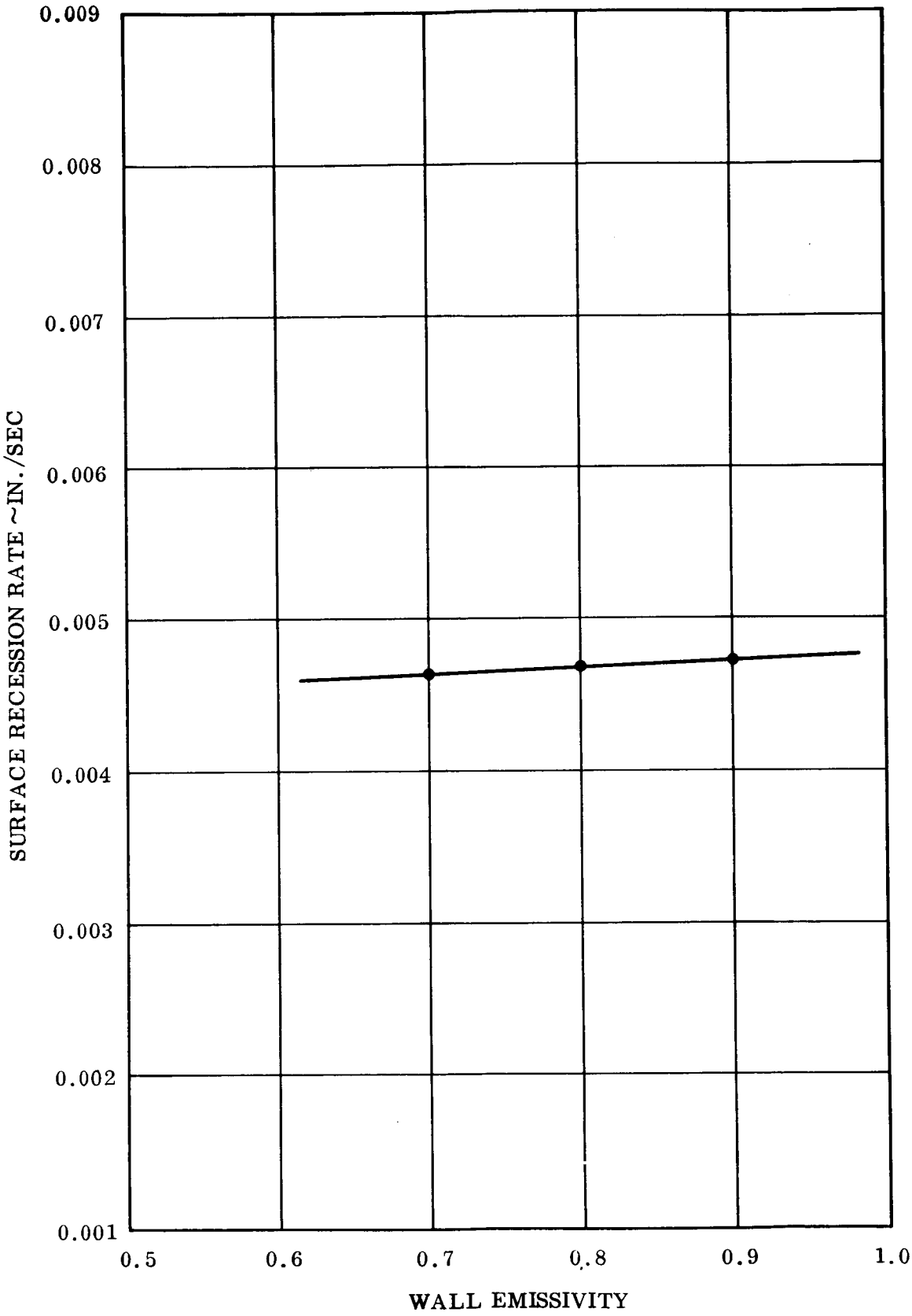

Figure 30. Surface Recession Rate Versus Wall Emissivity
Graphite Cloth/Phenolic Resin

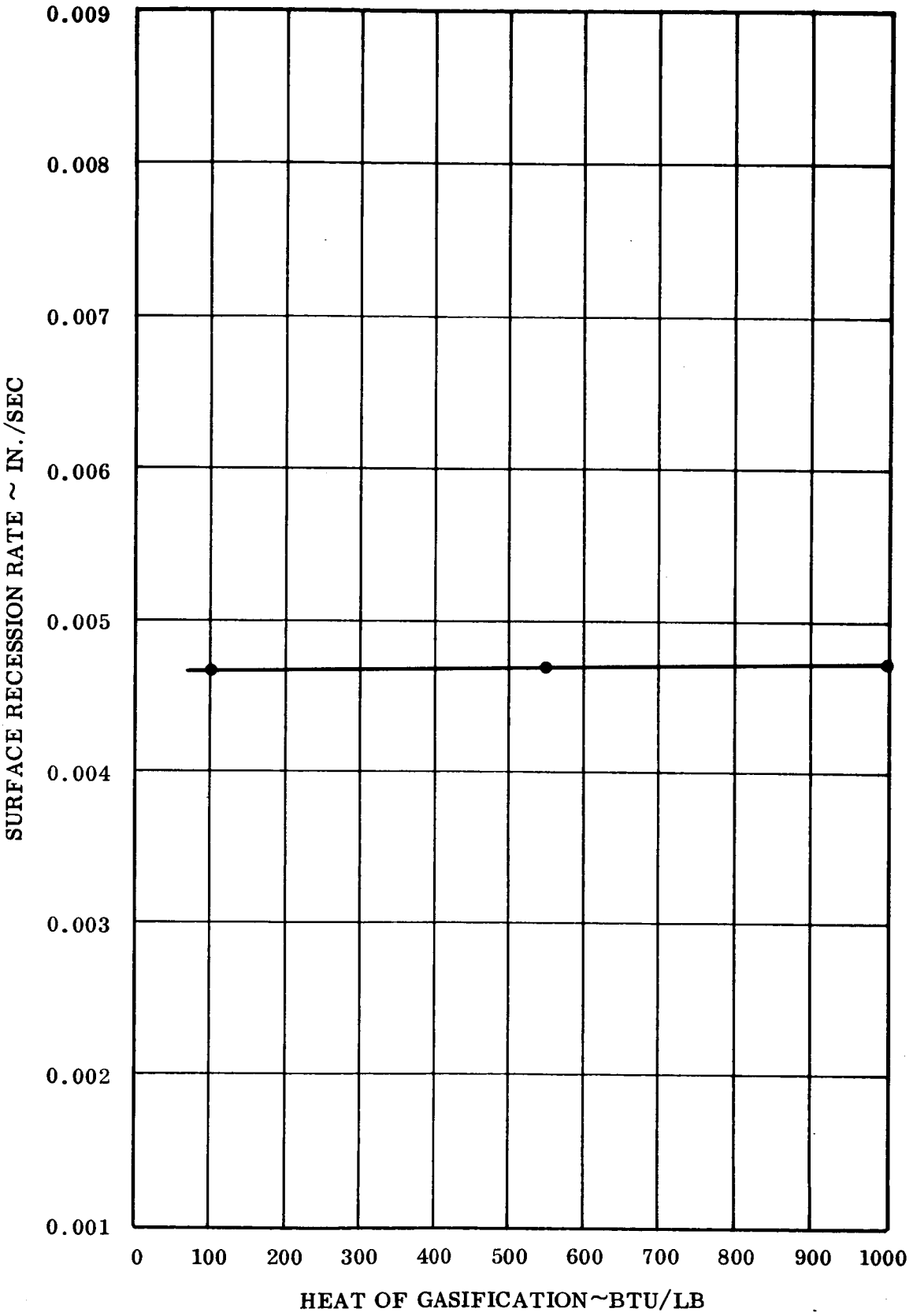

Figure 31. Surface Recession Rate Versus Heat of Gasification
Graphite Cloth/Phenolic Resin

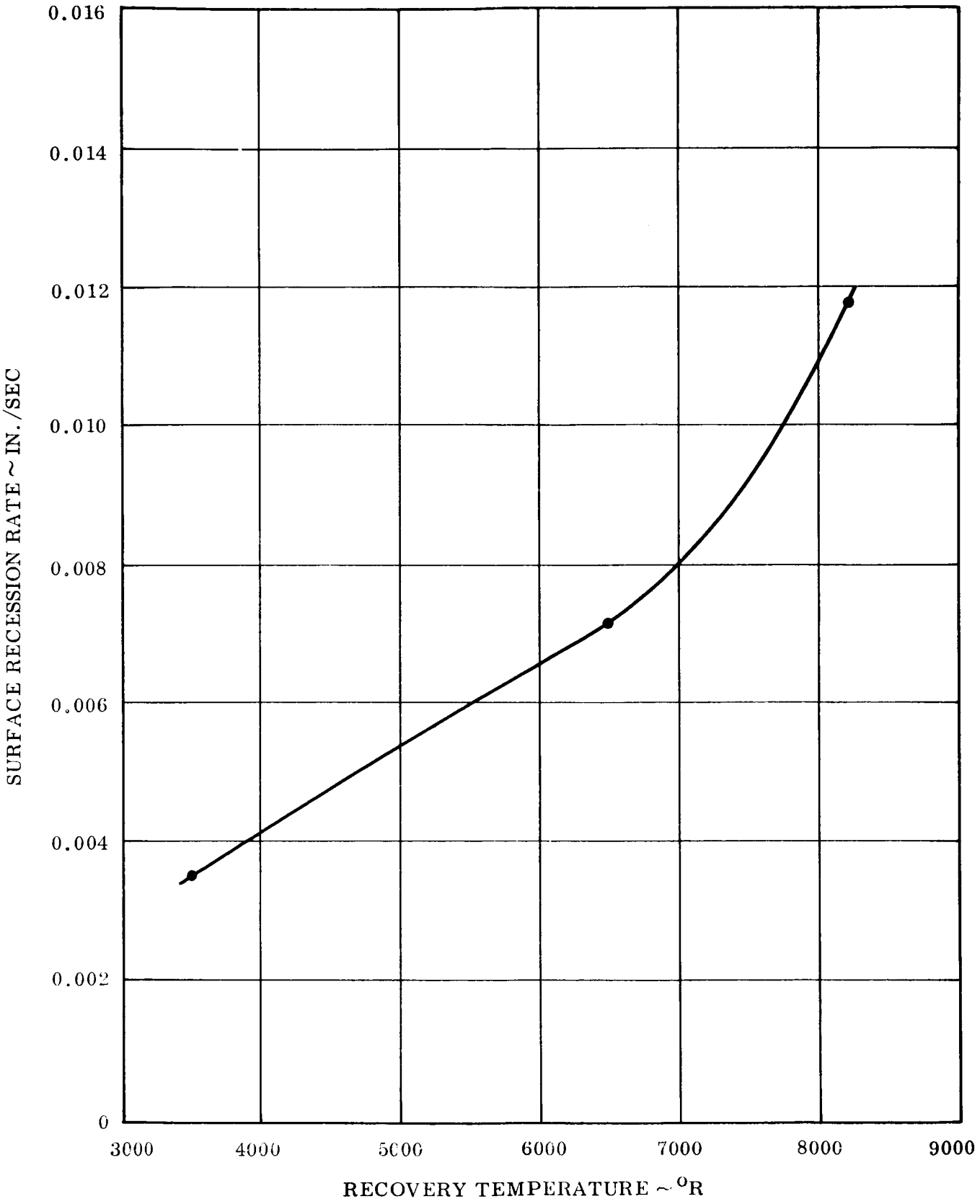

Figure 32. Surface Recession Rate Versus Recovery Temperature
Graphite Cloth/Epoxy Resin

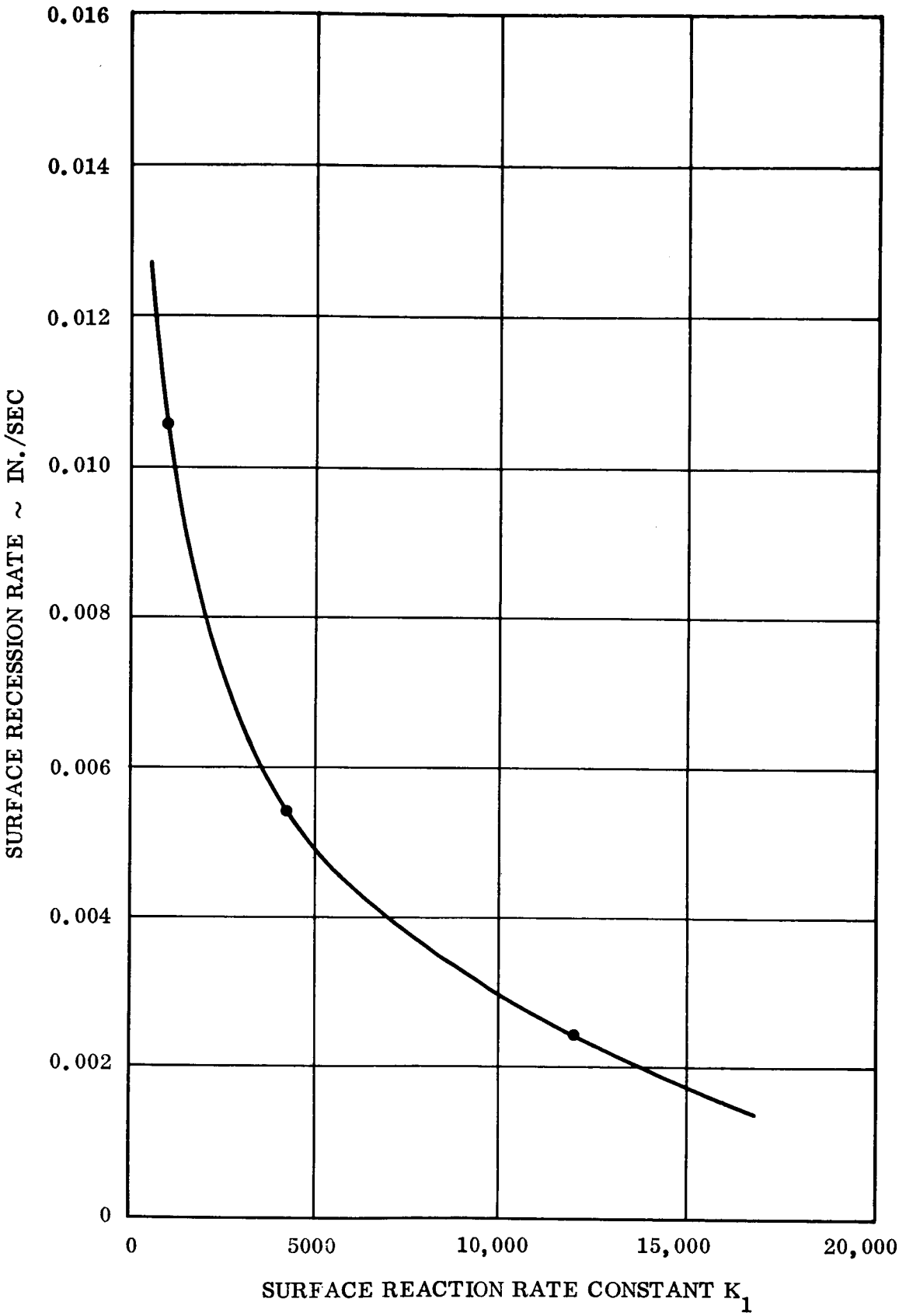

Figure 33. Surface Recession Rate Versus Surface Reaction Rate Constant K_1 Graphite Cloth/Epoxy Resin

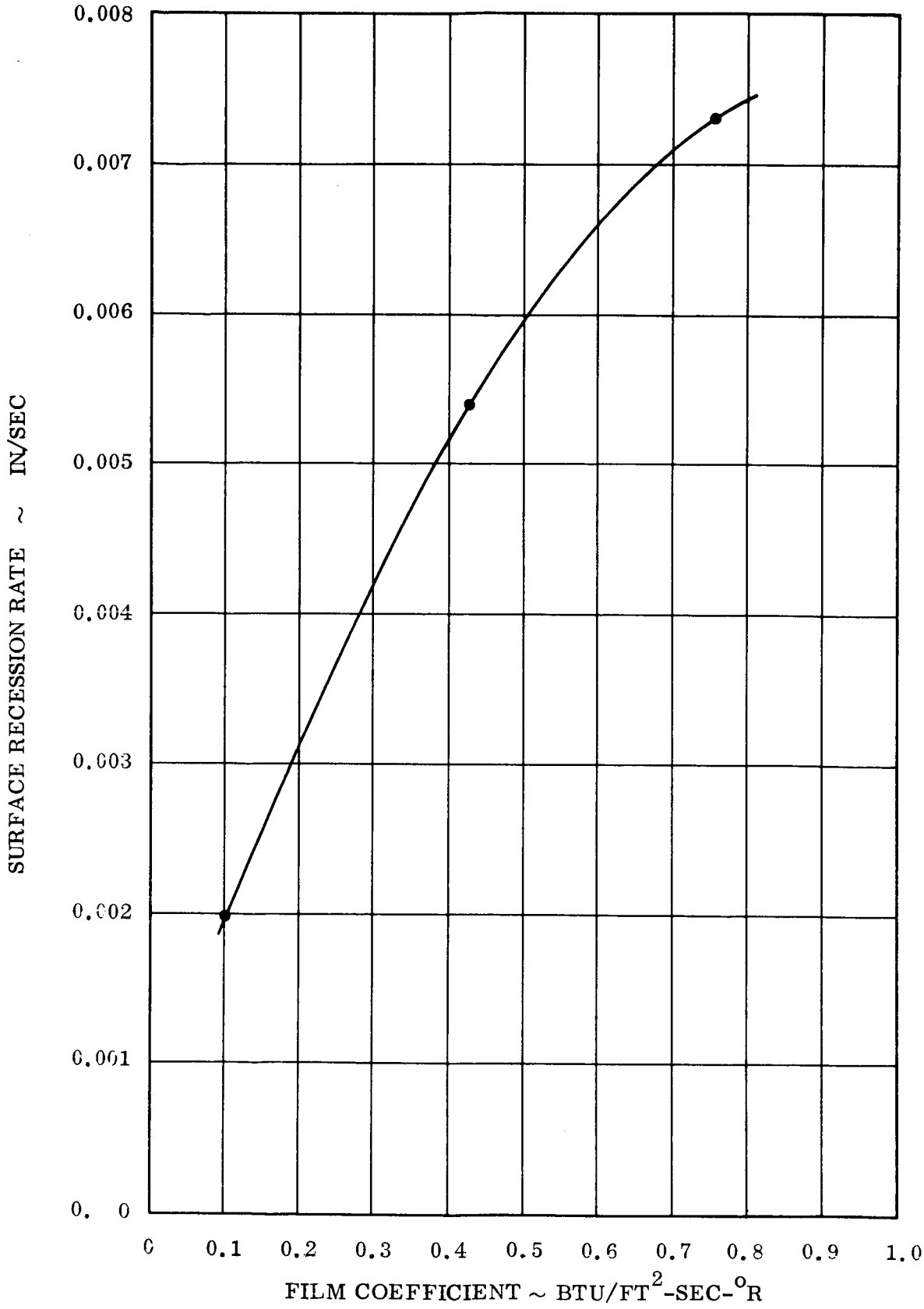

Figure 34. Surface Recession Rate Versus Film Coefficient Graphite Cloth/Epoxy Resin

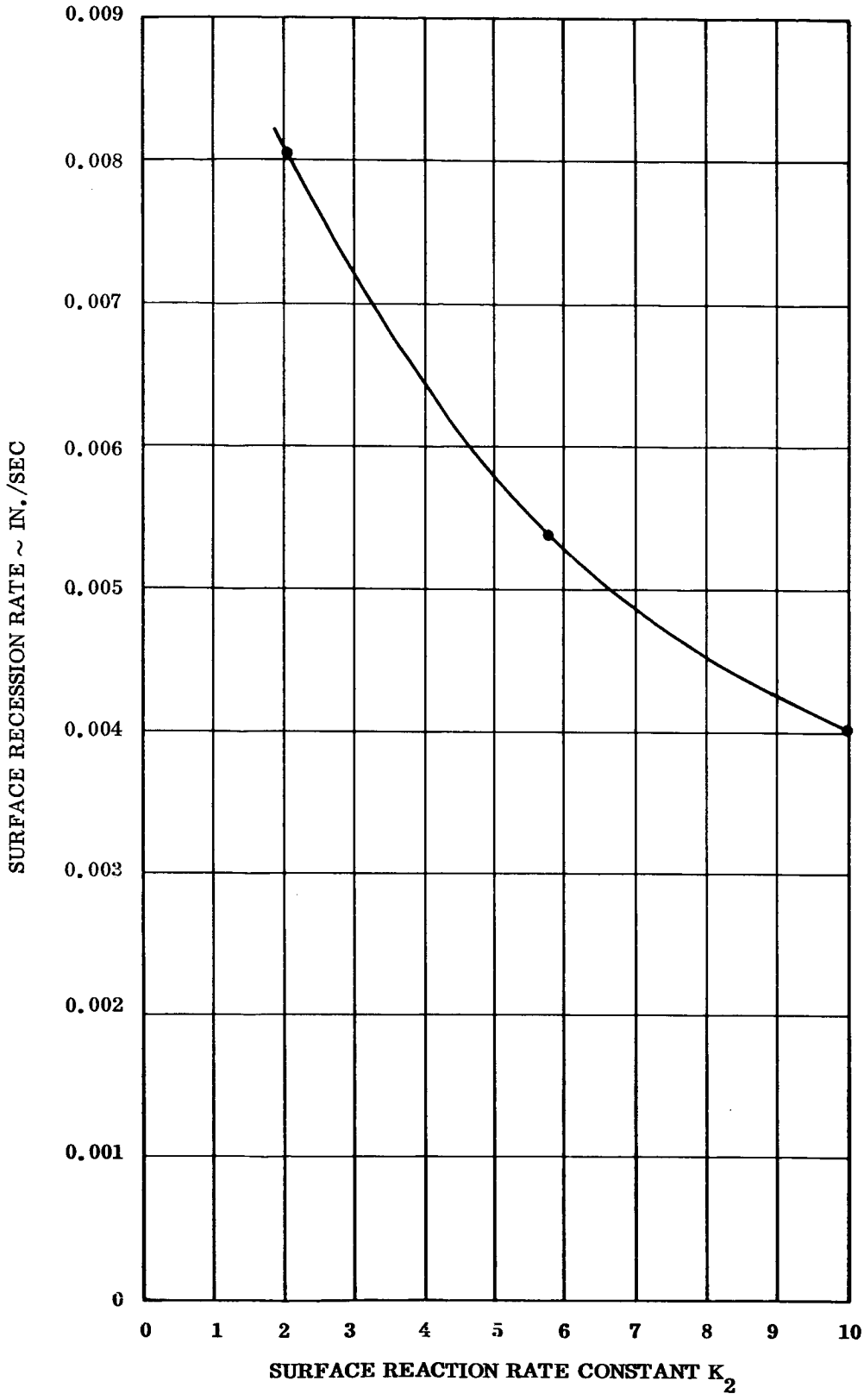

Figure 35. Surface Recession Rate Versus Surface Reaction Rate Constant K_2 Graphite Cloth/Epoxy Resin

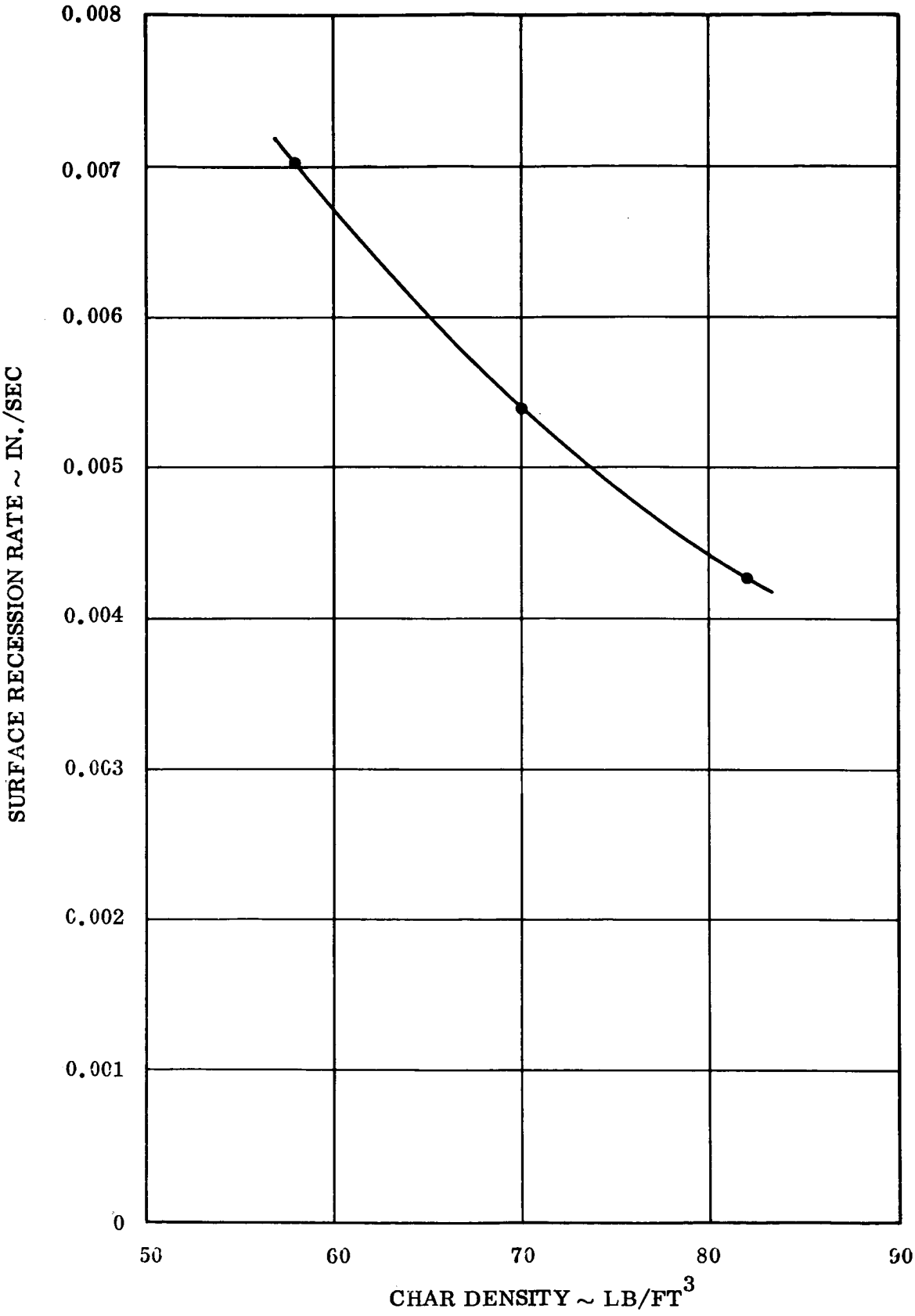

Figure 36. Surface Recession Rate Versus Char Density Graphite Cloth/Epoxy Resin

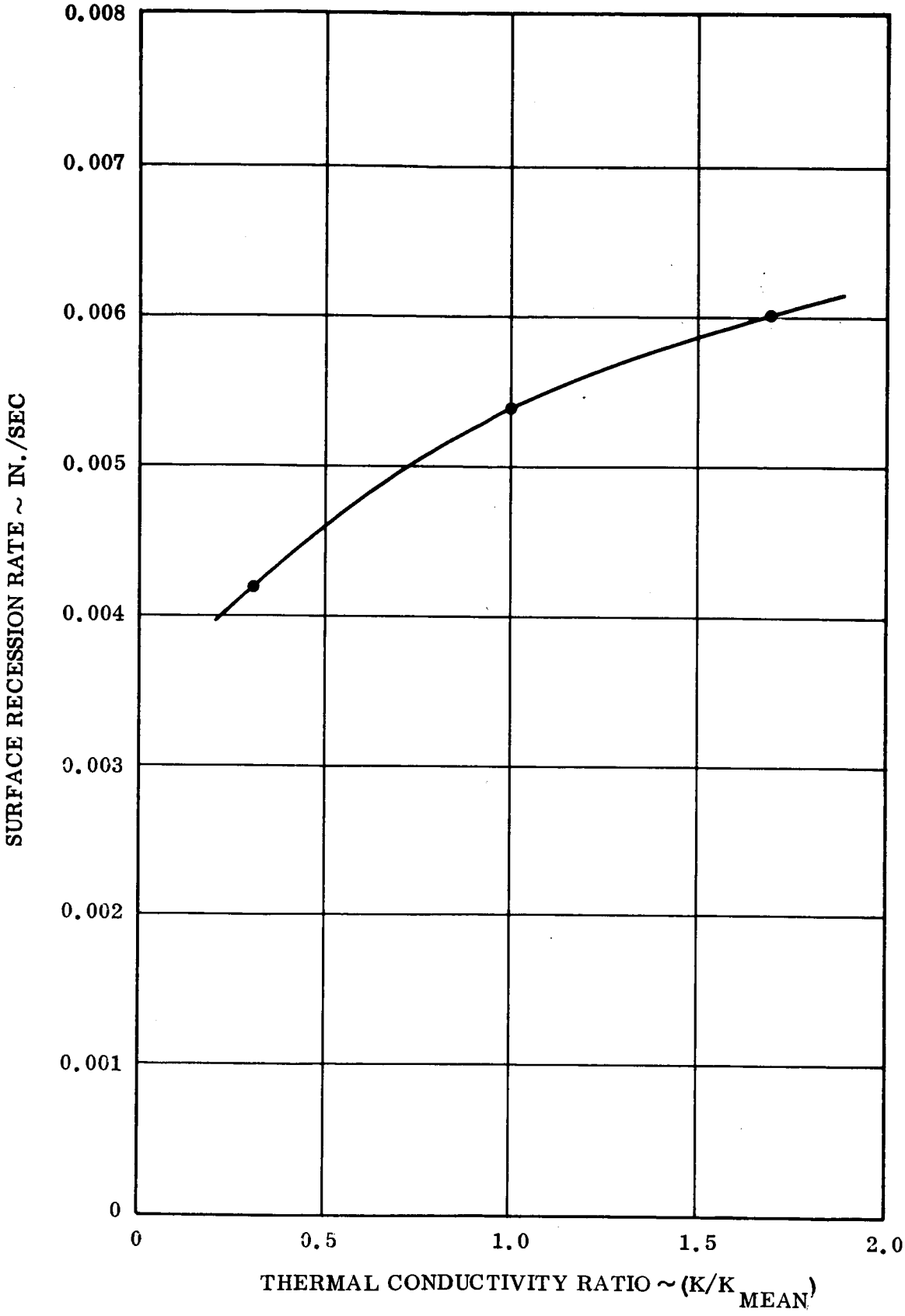

Figure 37. Surface Recession Rate Versus Thermal Conductivity Ratio Graphite Cloth/Epoxy Resin

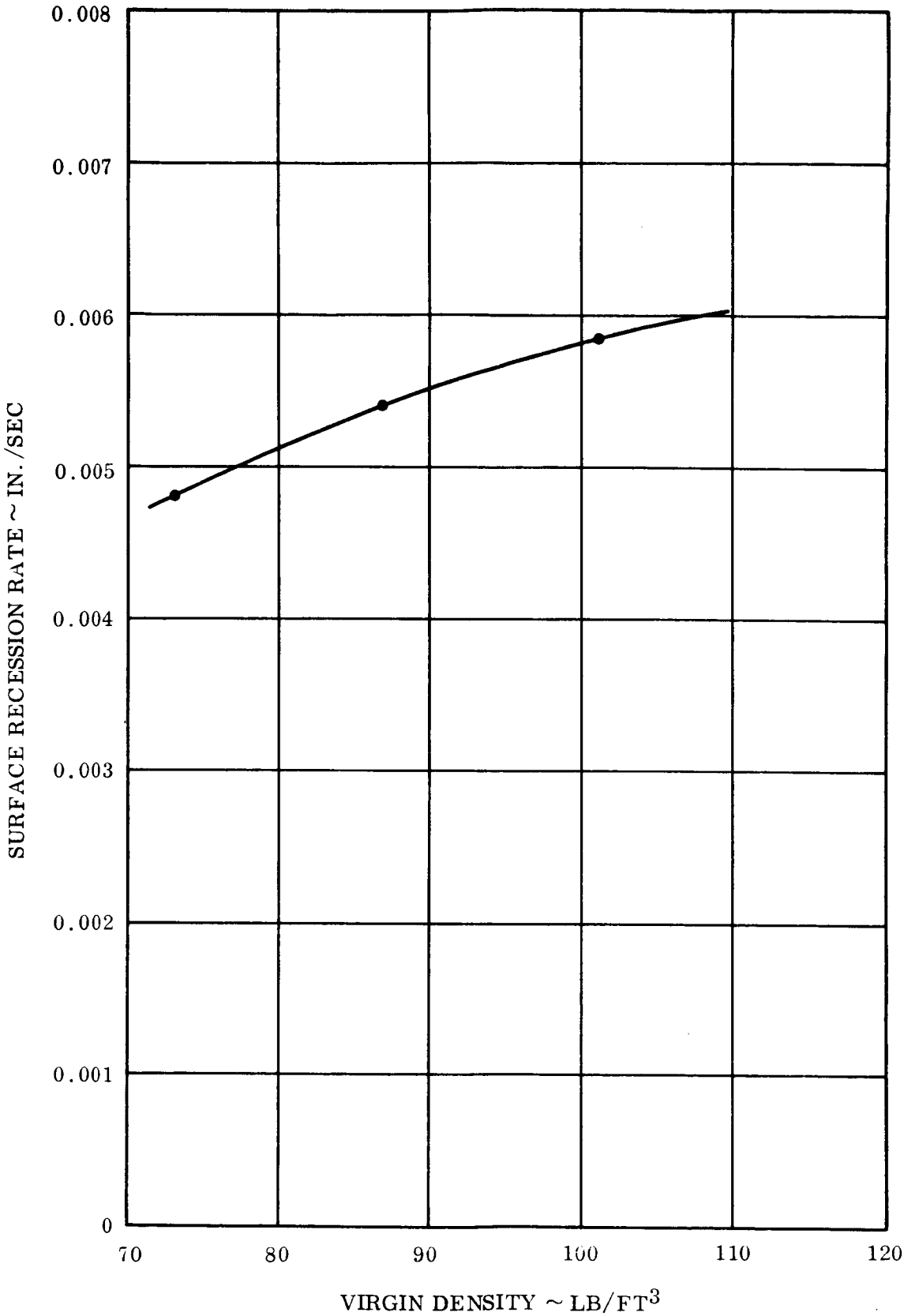

Figure 38. Surface Recession Rate Versus Virgin Density
Graphite Cloth/Epoxy Resin

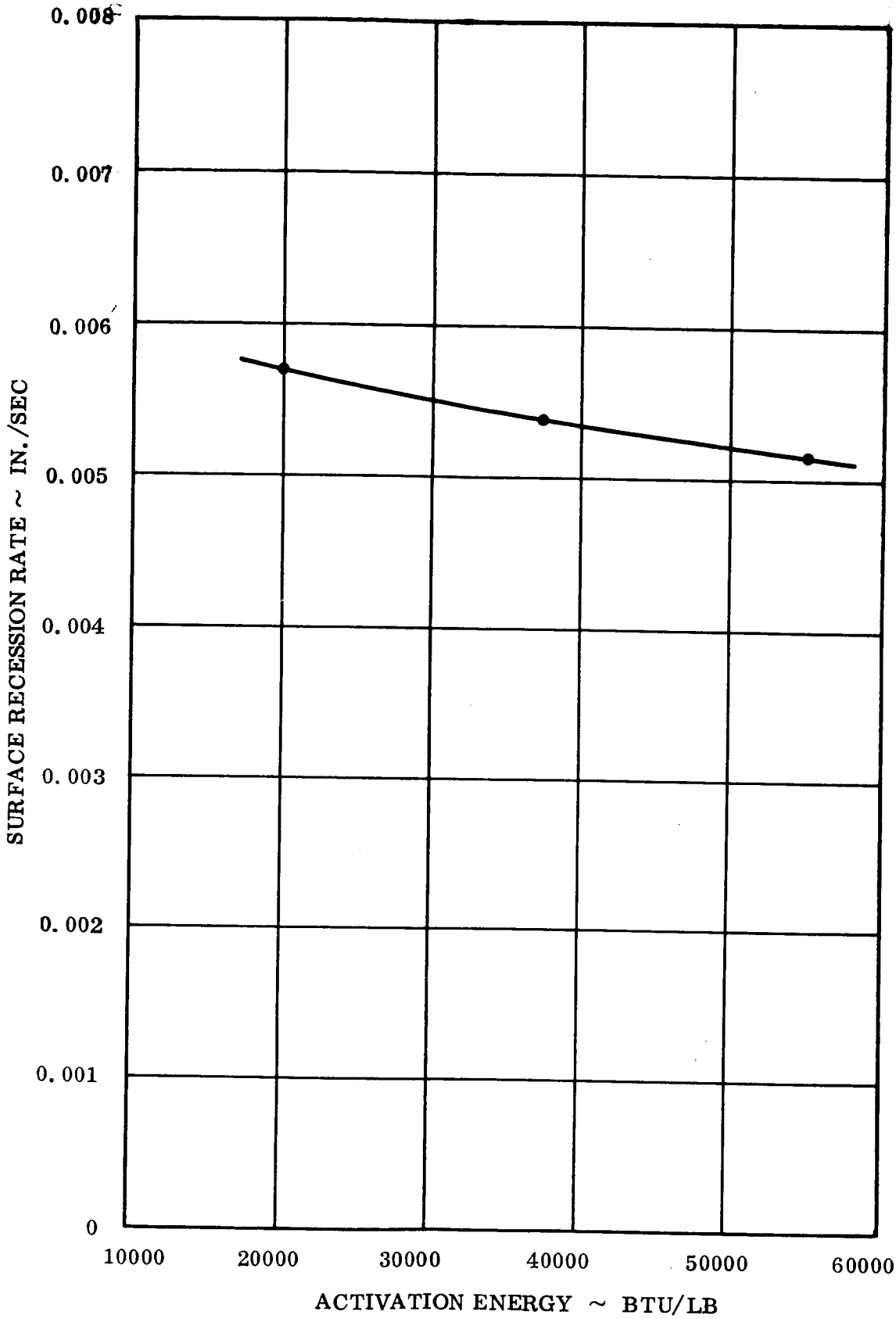

Figure 39. Surface Recession Rate Versus Activation Energy
Graphite Cloth/Epoxy Resin

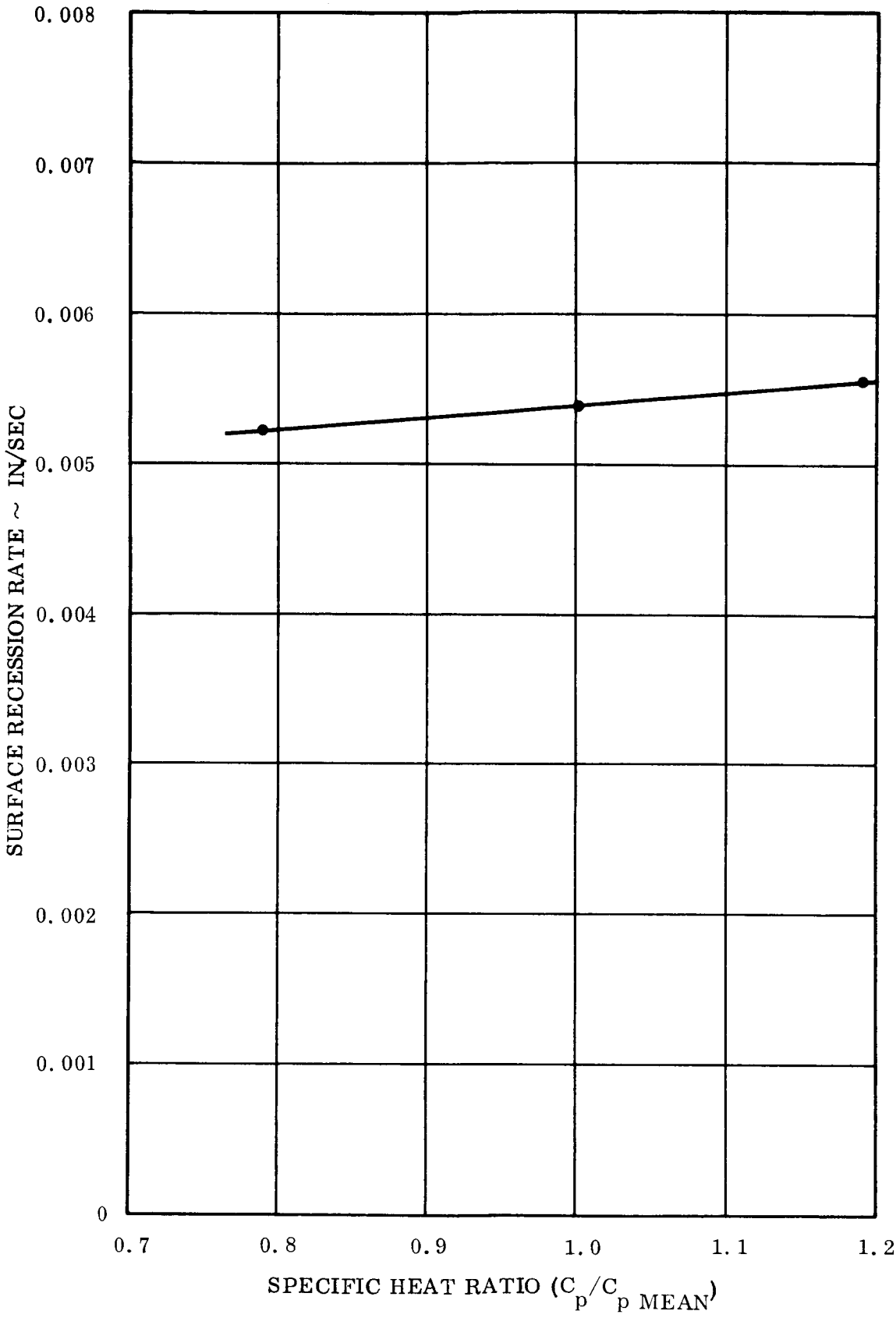

Figure 40. Surface Recession Rate Versus Specific Heat Ratio
Graphite Cloth/Epoxy Resin

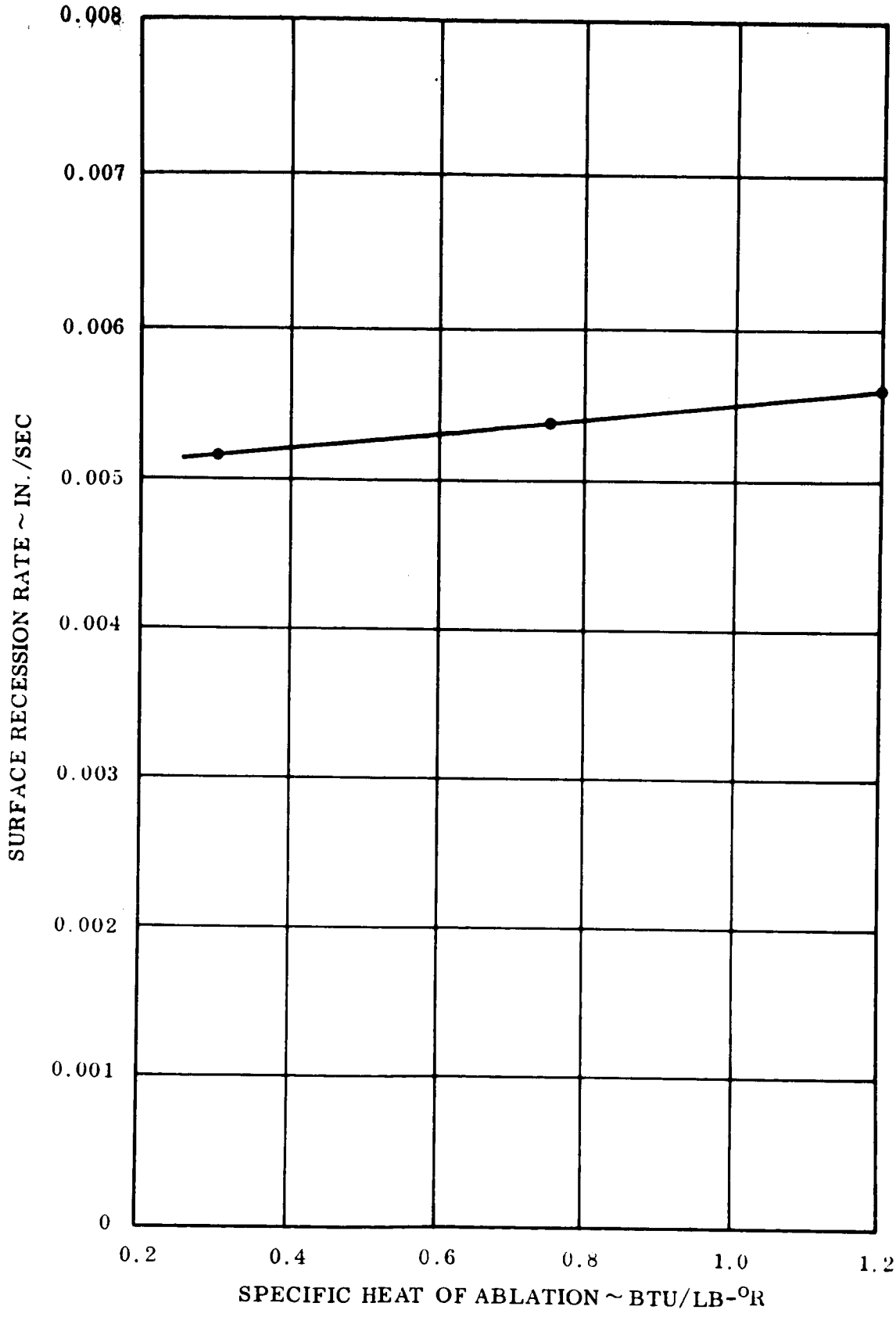

Figure 41. Surface Recession Rate Versus Specific Heat of Ablation Gases Graphite Cloth/Epoxy Resin

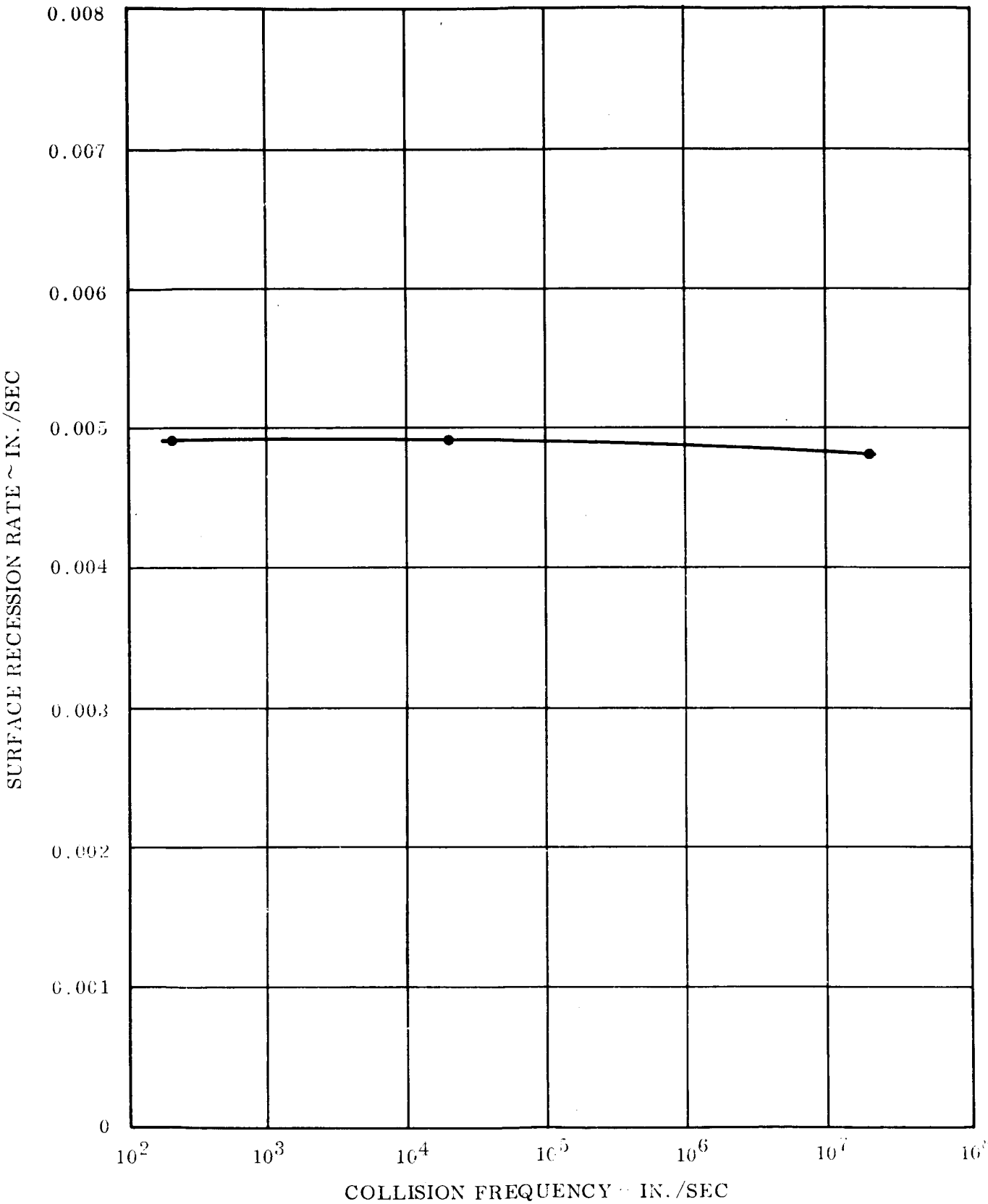

Figure 42. Surface Recession Rate Versus Collision Frequency Graphite Cloth/Epoxy Resin

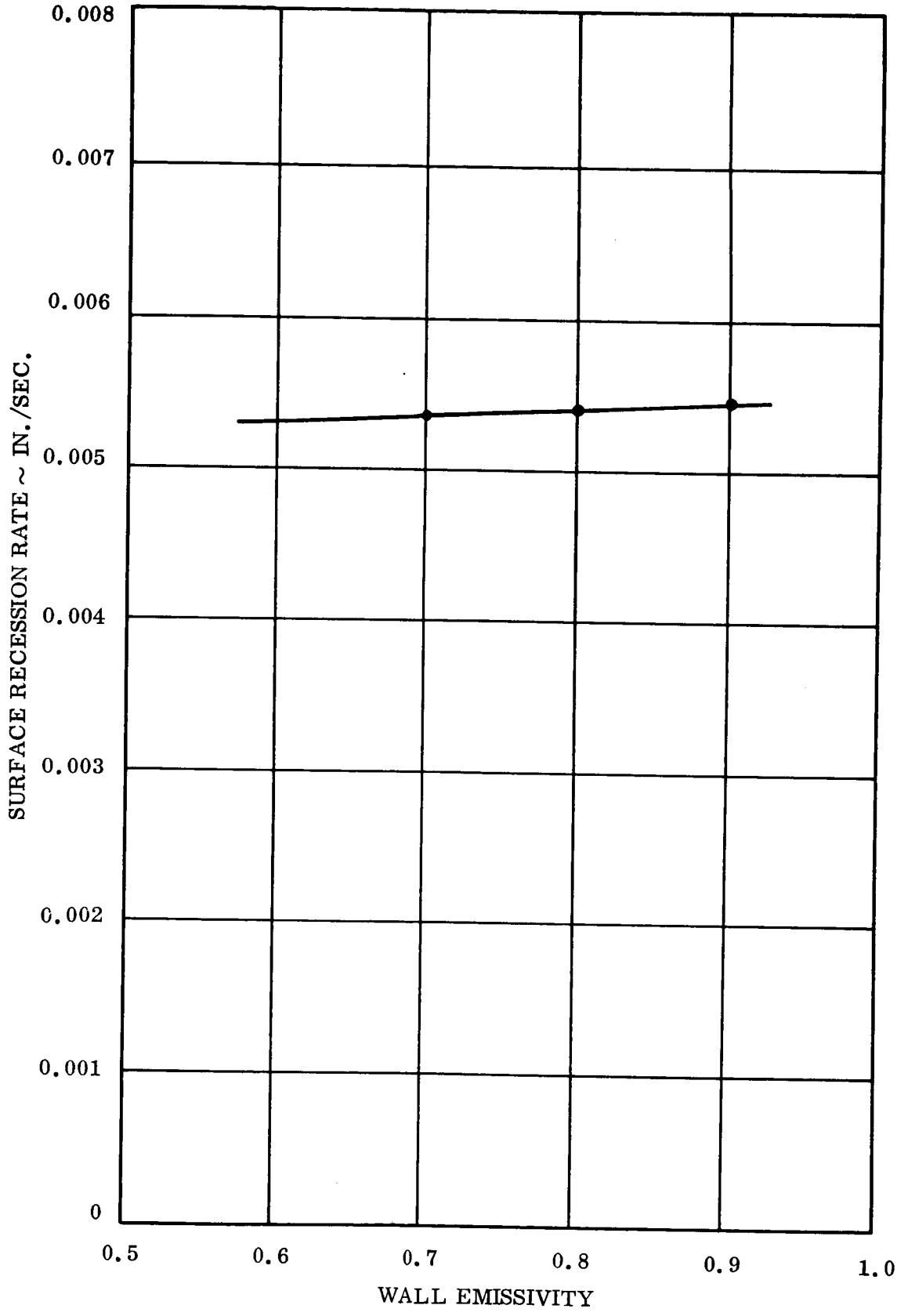

Figure 43. Surface Recession Rate Versus Wall Emissivity
Graphite Cloth/Epoxy Resin

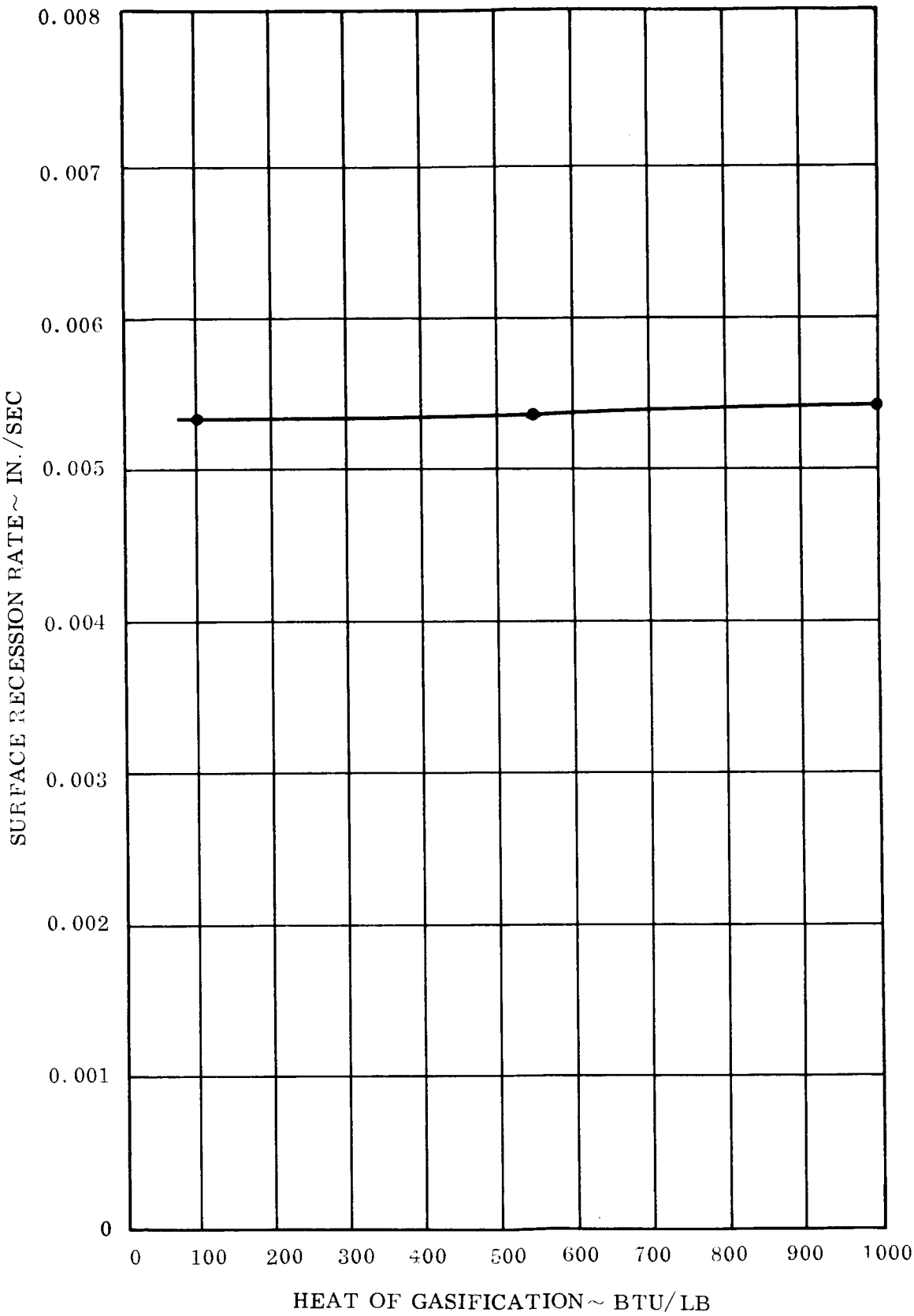

Figure 44. Surface Recession Rate Versus Heat of Gasification Graphite Cloth/Epoxy Resin

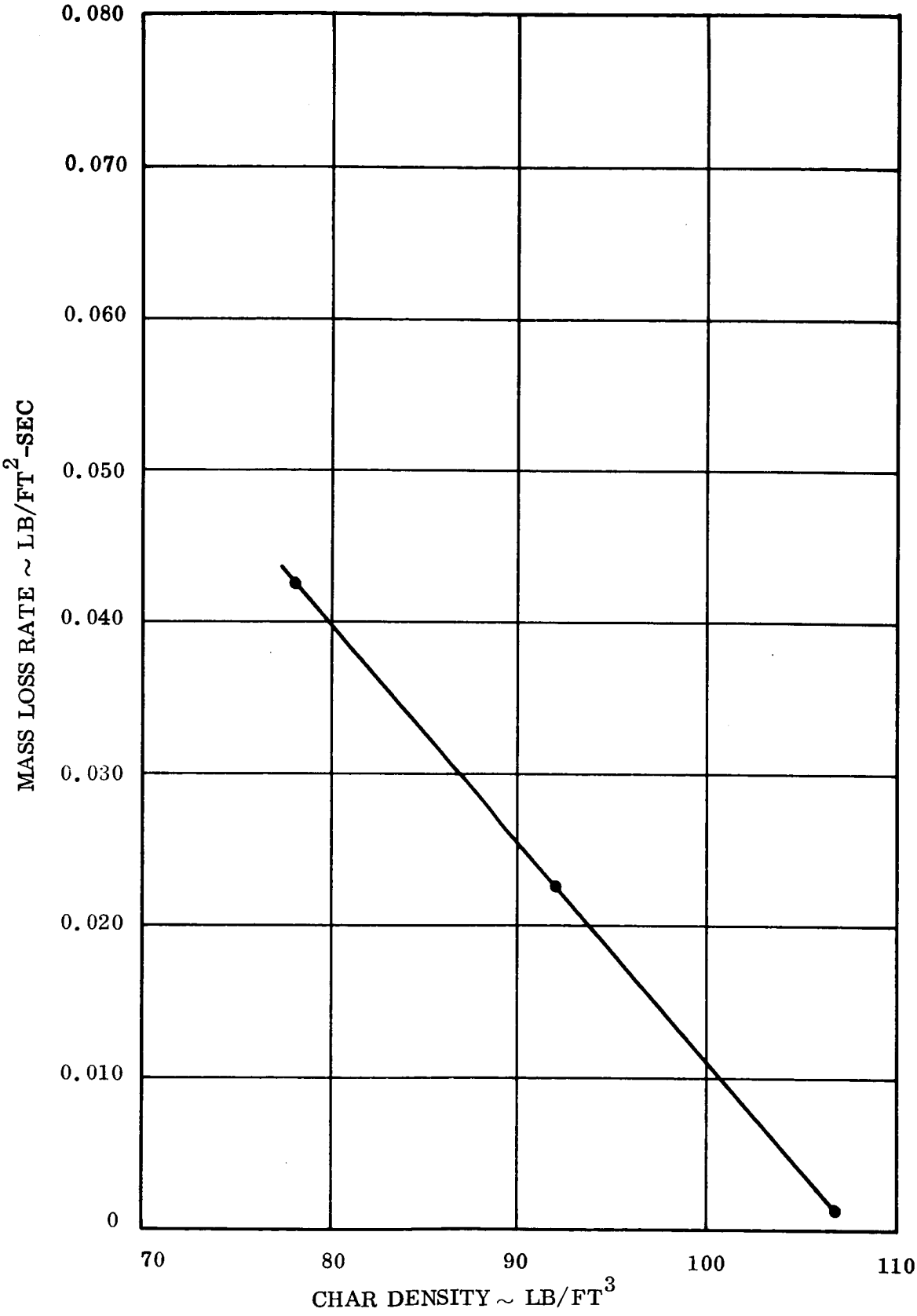

Figure 45. Mass Loss Rate Versus Char Density Silica Cloth/Phenolic Resin

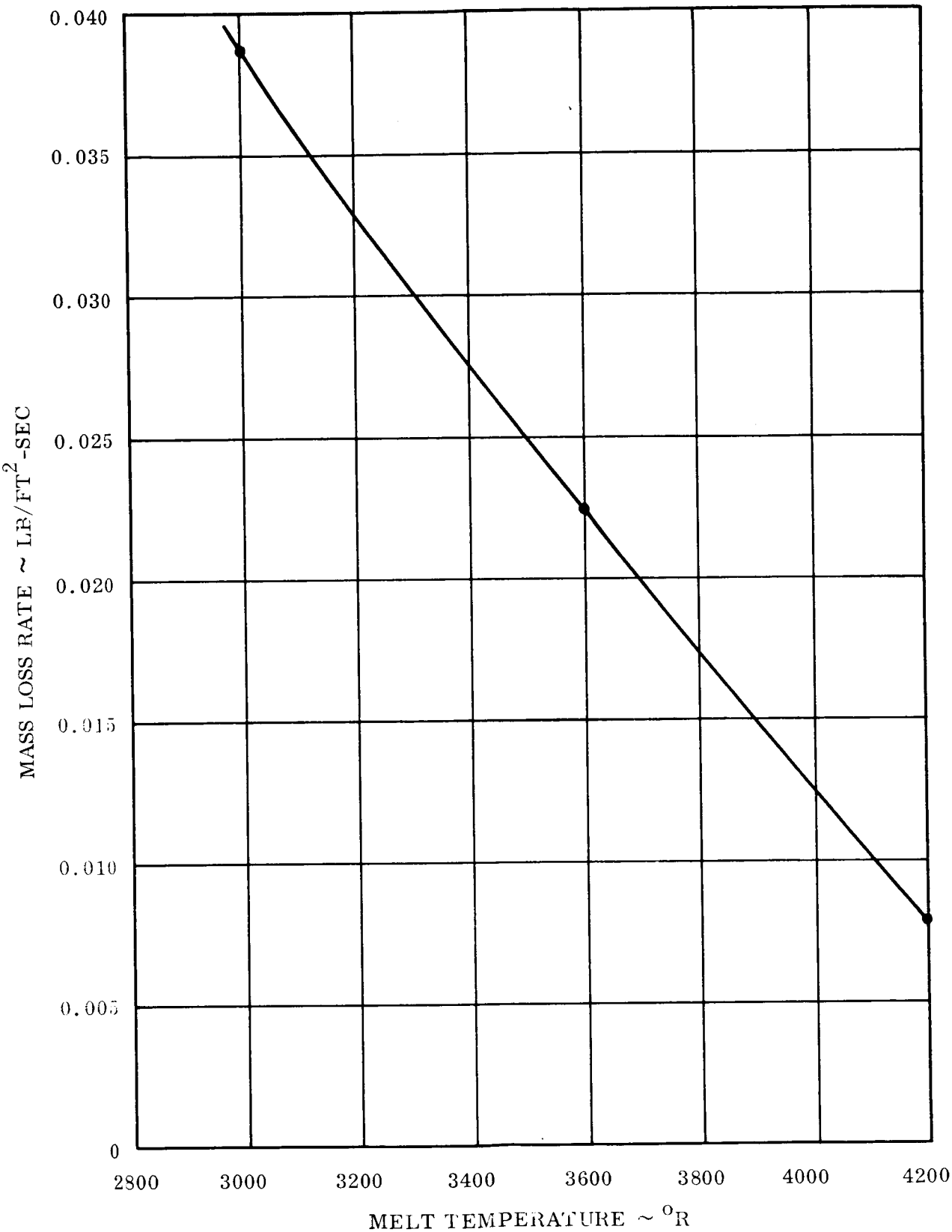

Figure 46. Mass Loss Rate Versus Melting Temperature of Reinforcing Fibers

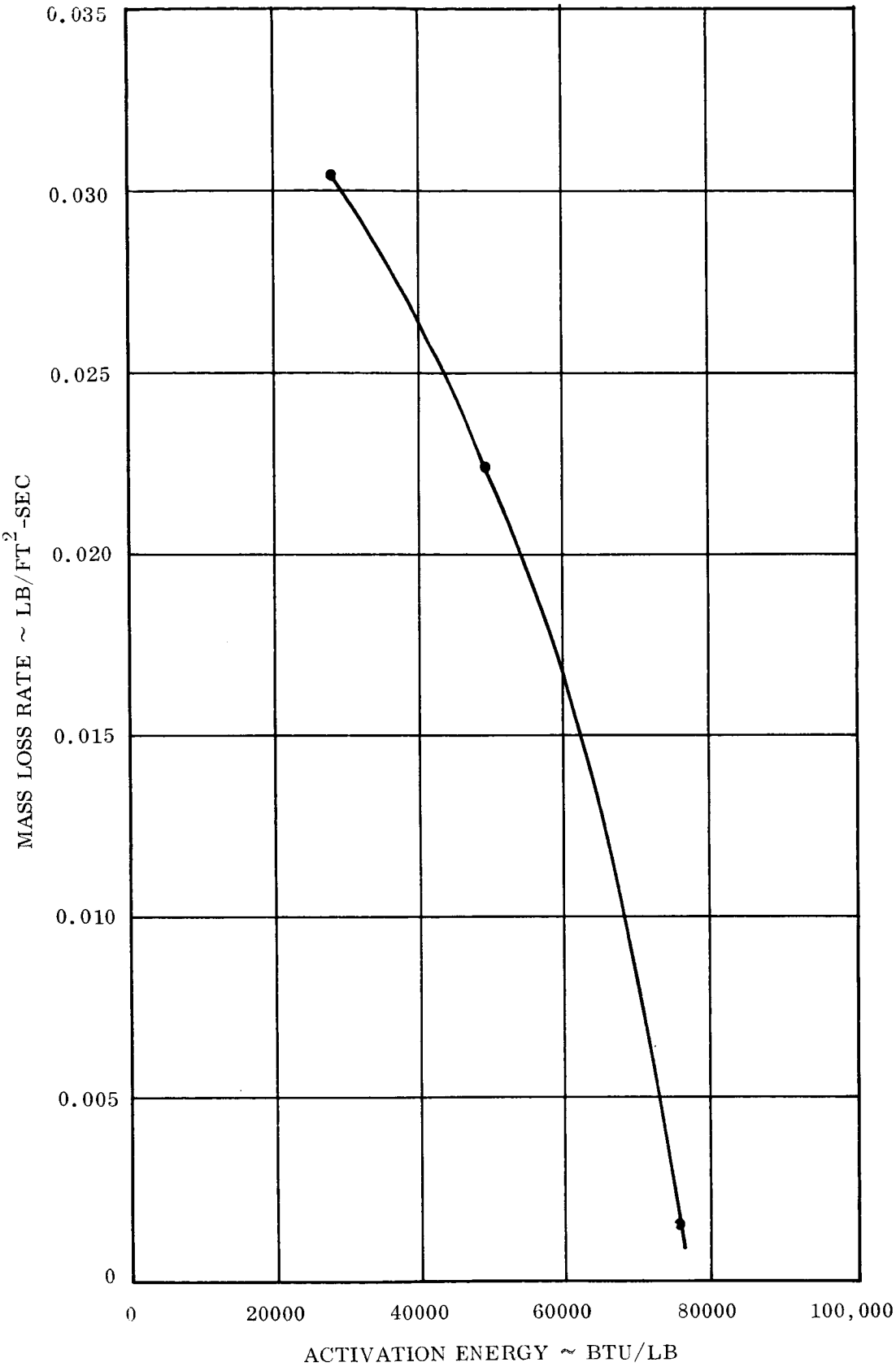

Figure 47. Mass Loss Rate Versus Activation Energy Silica Cloth/Phenolic Resin

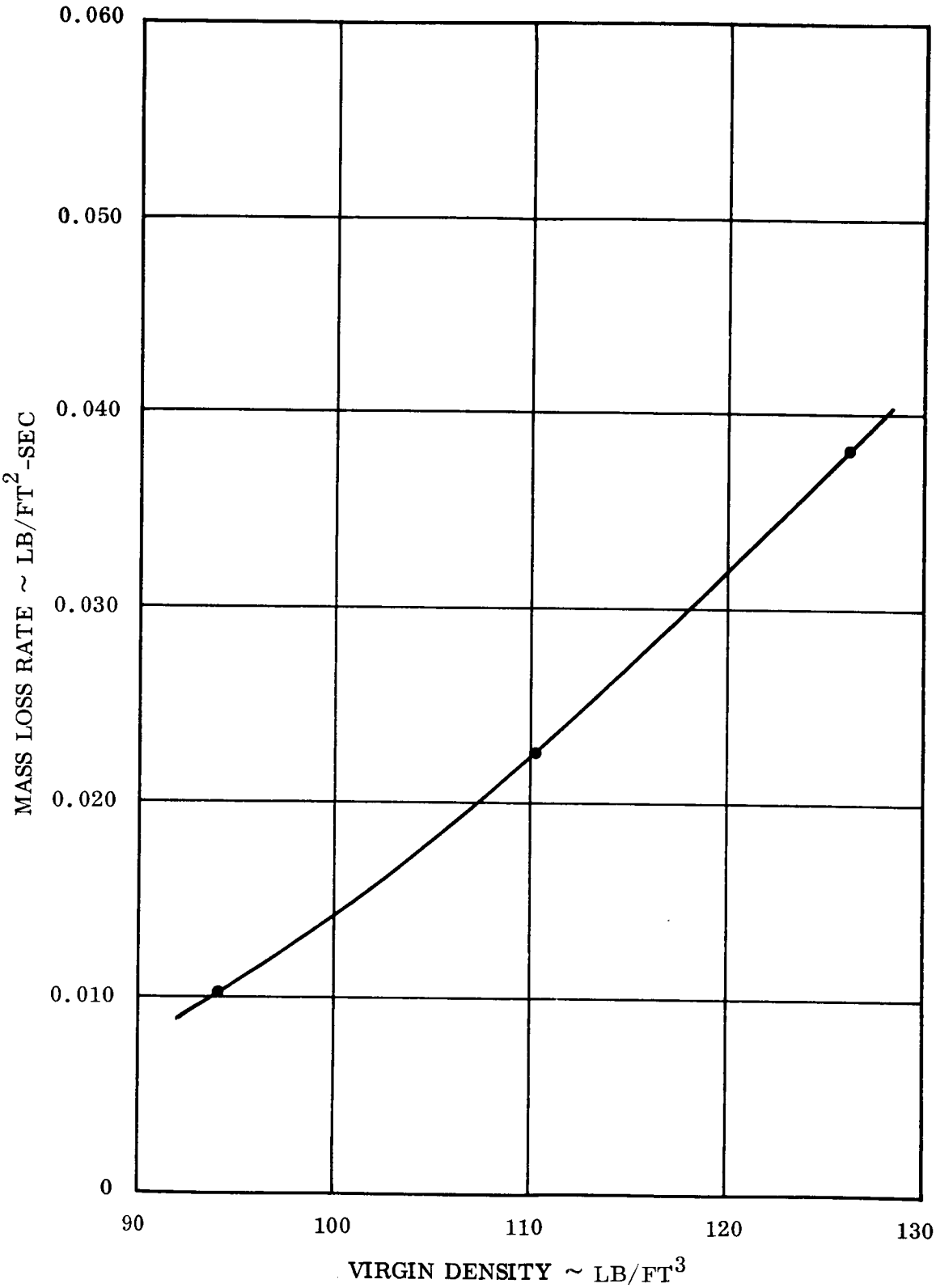

Figure 48. Mass Loss Rate Versus Virgin Density Silica Cloth/Phenolic Resin

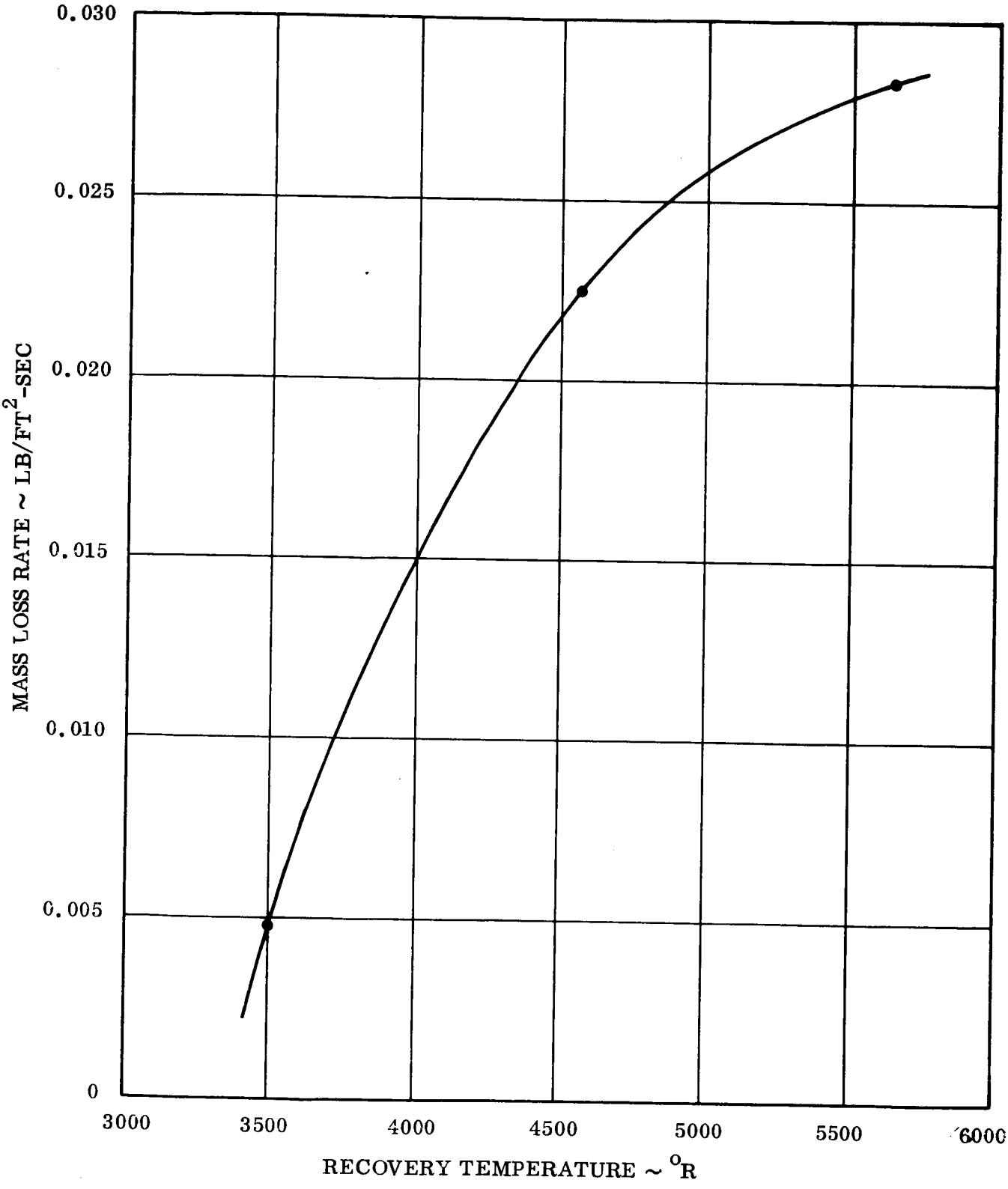

Figure 49. Mass Loss Rate Versus Recovery Temperature
Silica Cloth/Phenolic Resin

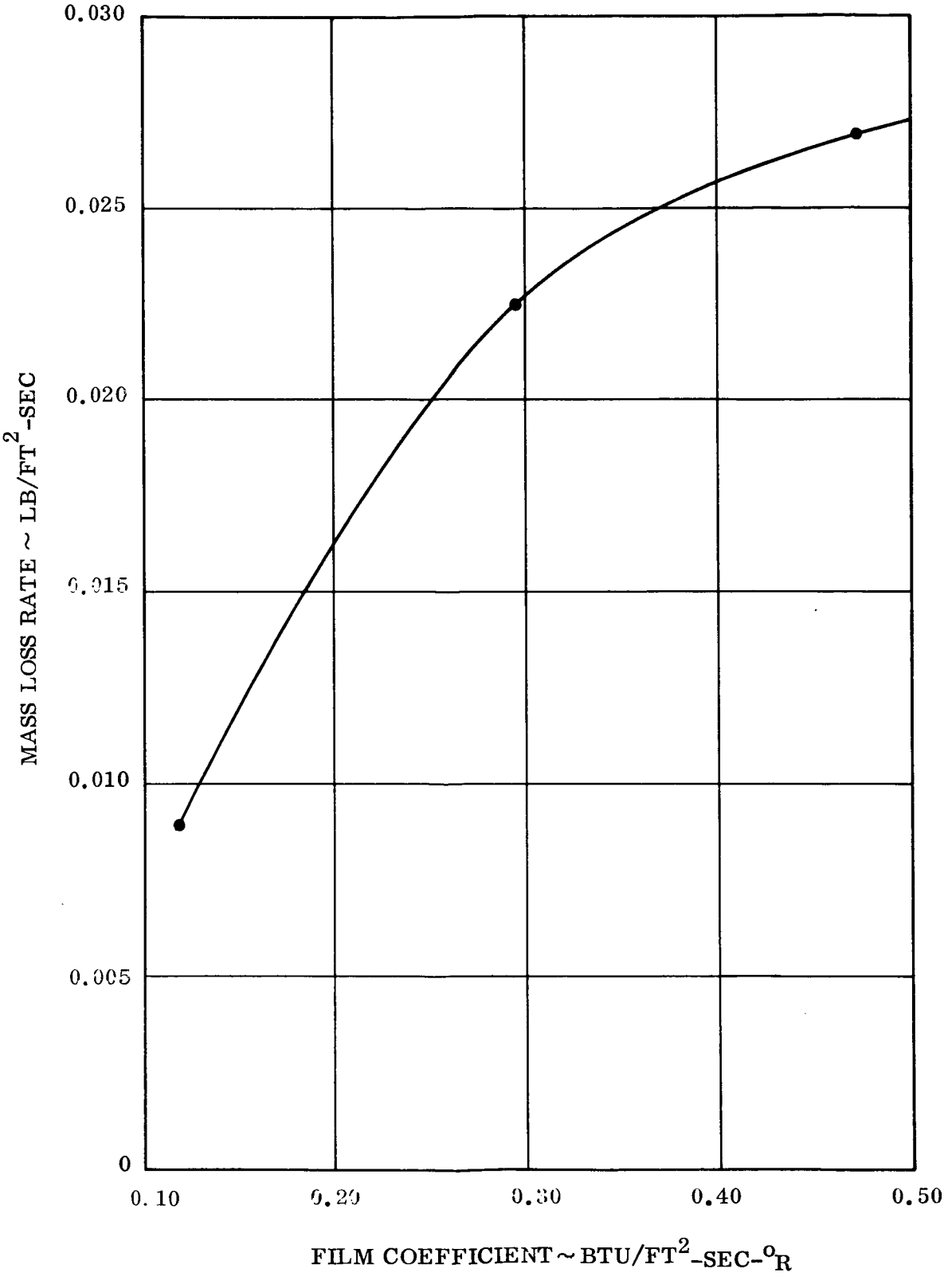

Figure 50. Mass Loss Rate Versus Film Coefficient
Silica Cloth/Phenolic Resin

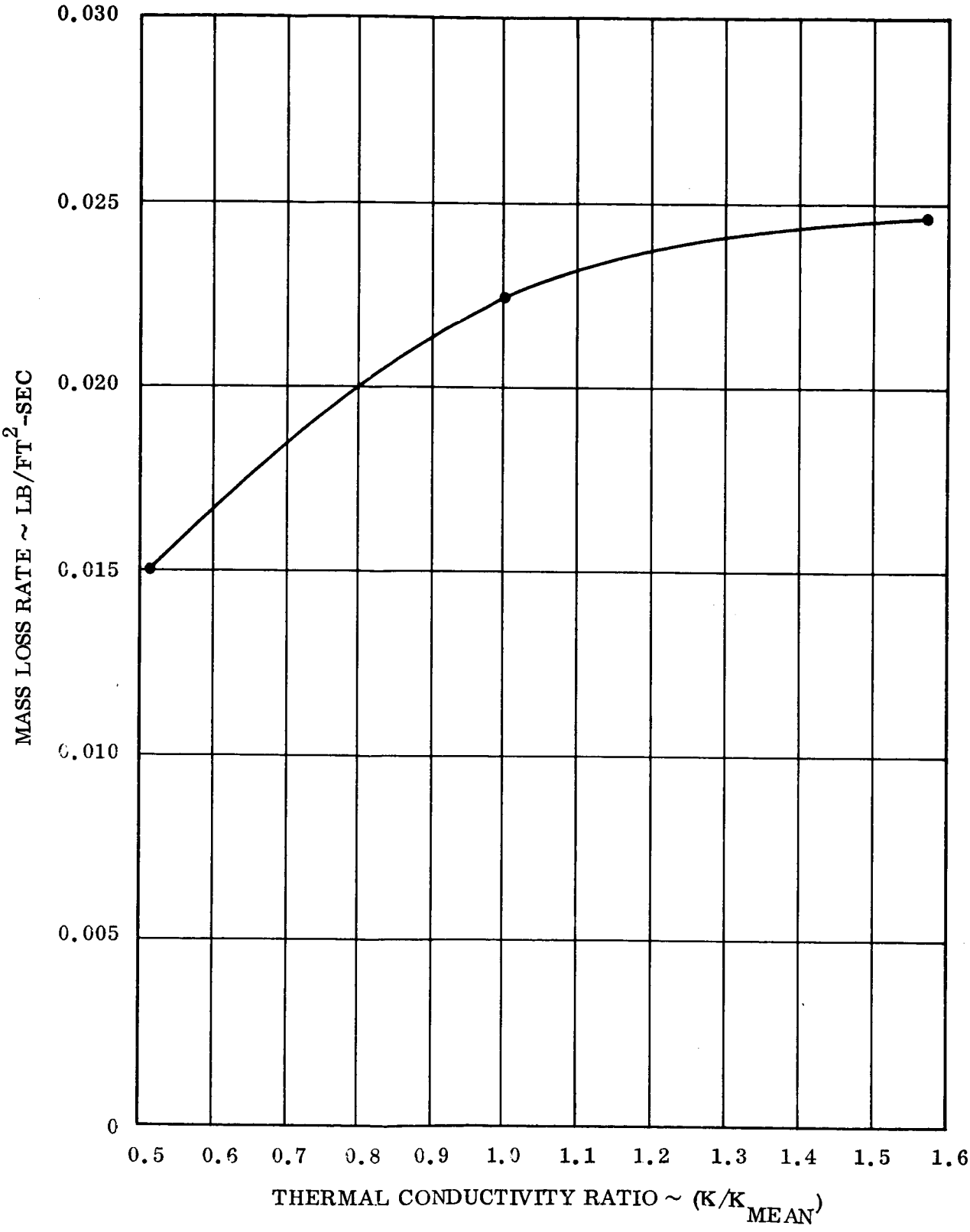

Figure 51. Mass Loss Rate Versus Thermal Conductivity Ratio
Silica Cloth/Phenolic Resin

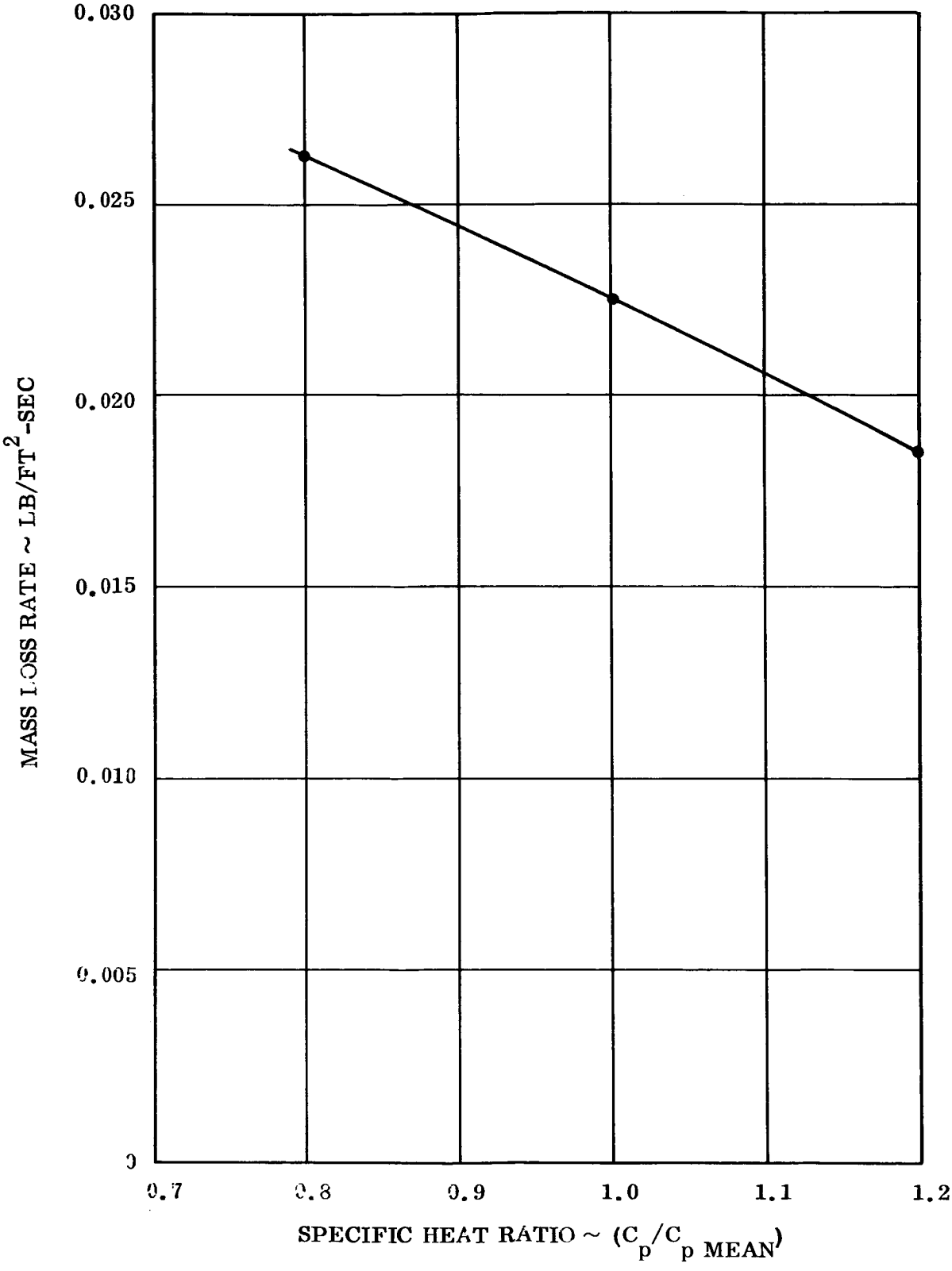

Figure 52. Mass Loss Rate Versus Specific Heat Ratio
Silica Cloth/Phenolic Resin

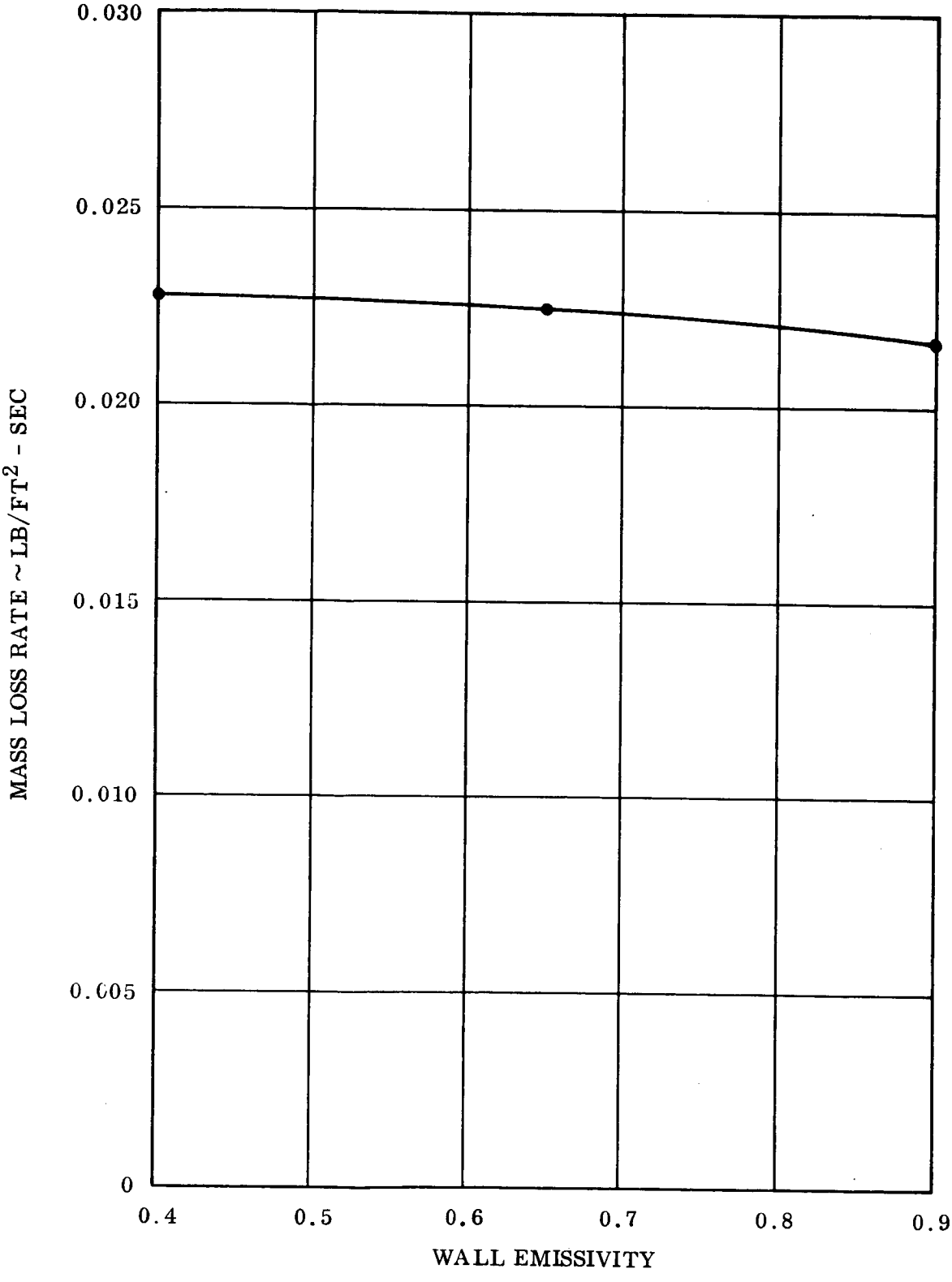

Figure 53. Mass Loss Rate Versus Wall Emissivity
Silica Cloth/Phenolic Resin

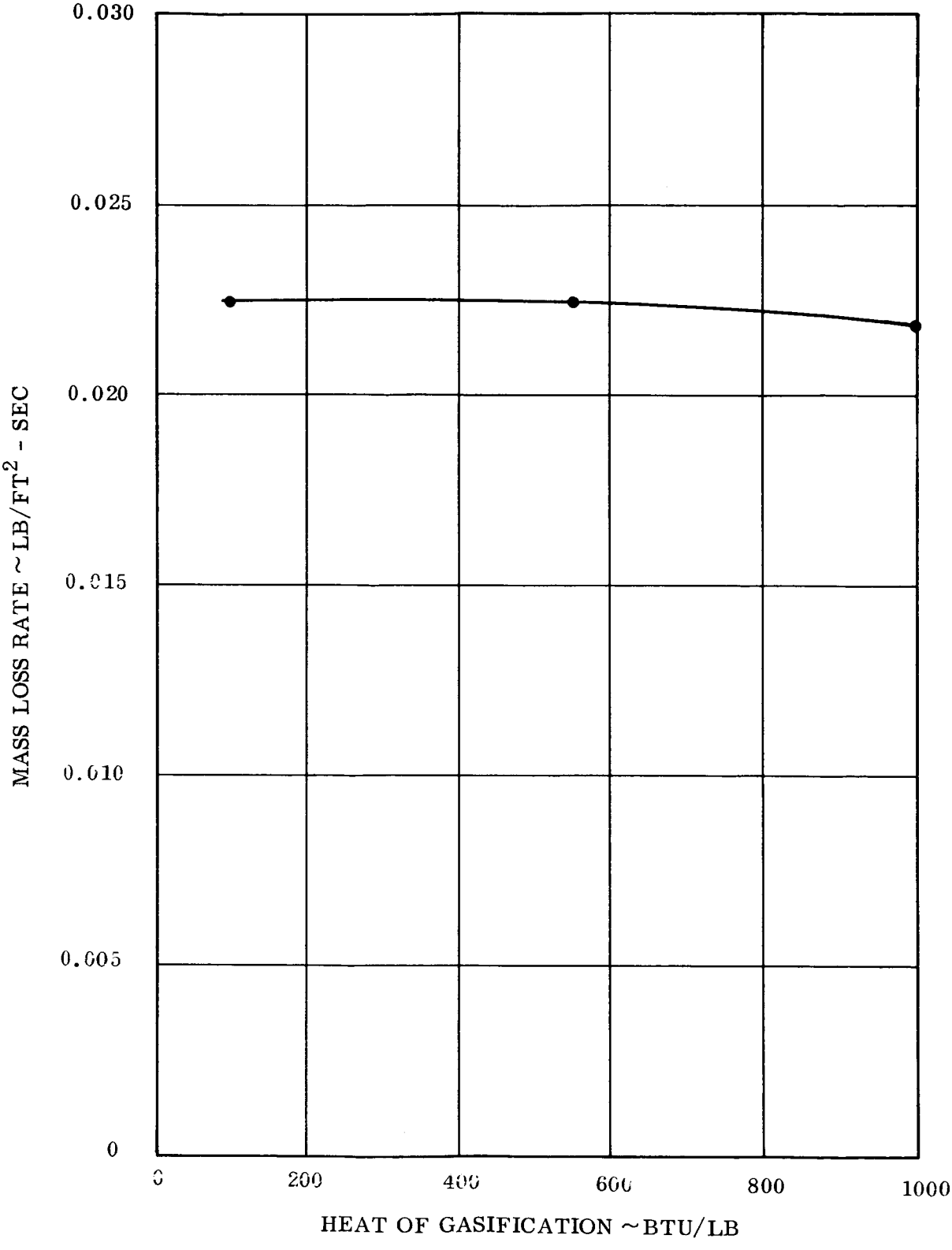

Figure 54. Mass Loss Rate Versus Heat of Gasification
Silica Cloth/Phenolic Resin

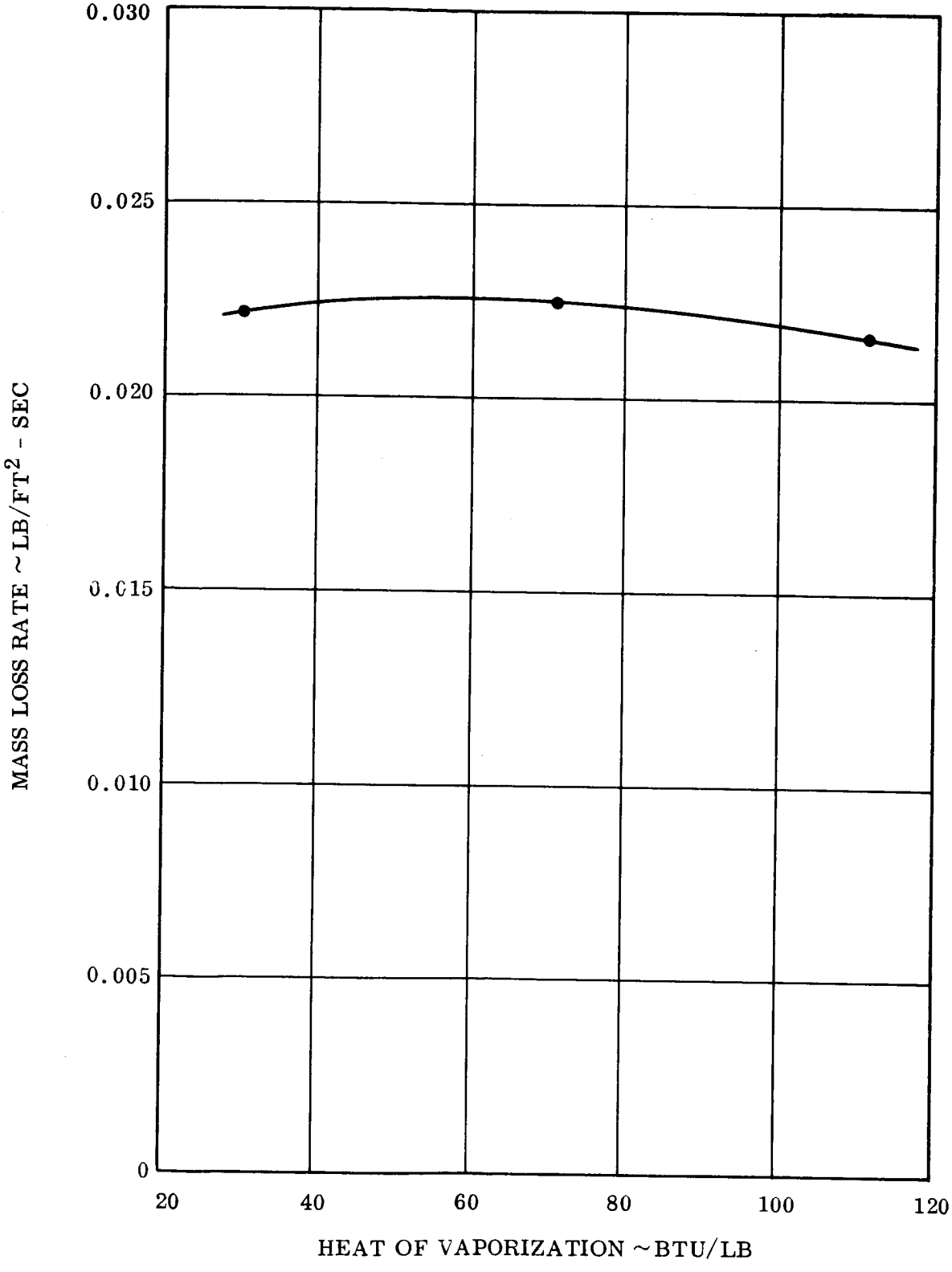

Figure 55. Mass Loss Rate Versus Heat of Vaporization
Silica Cloth/Phenolic Resin

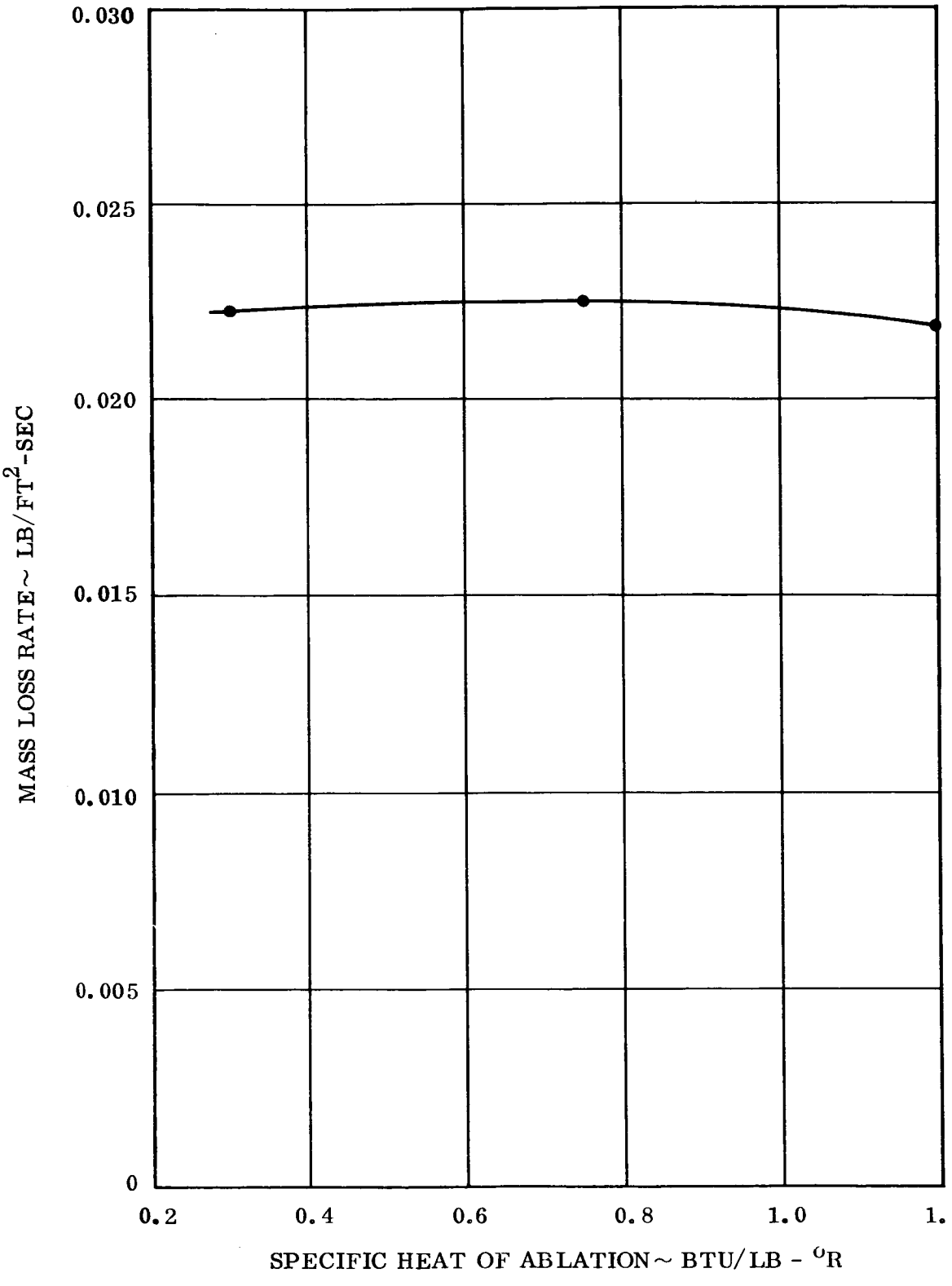

Figure 56. Melt Loss Rate Versus Specific Heat of Ablation Gases Silica Cloth/Phenolic Resin

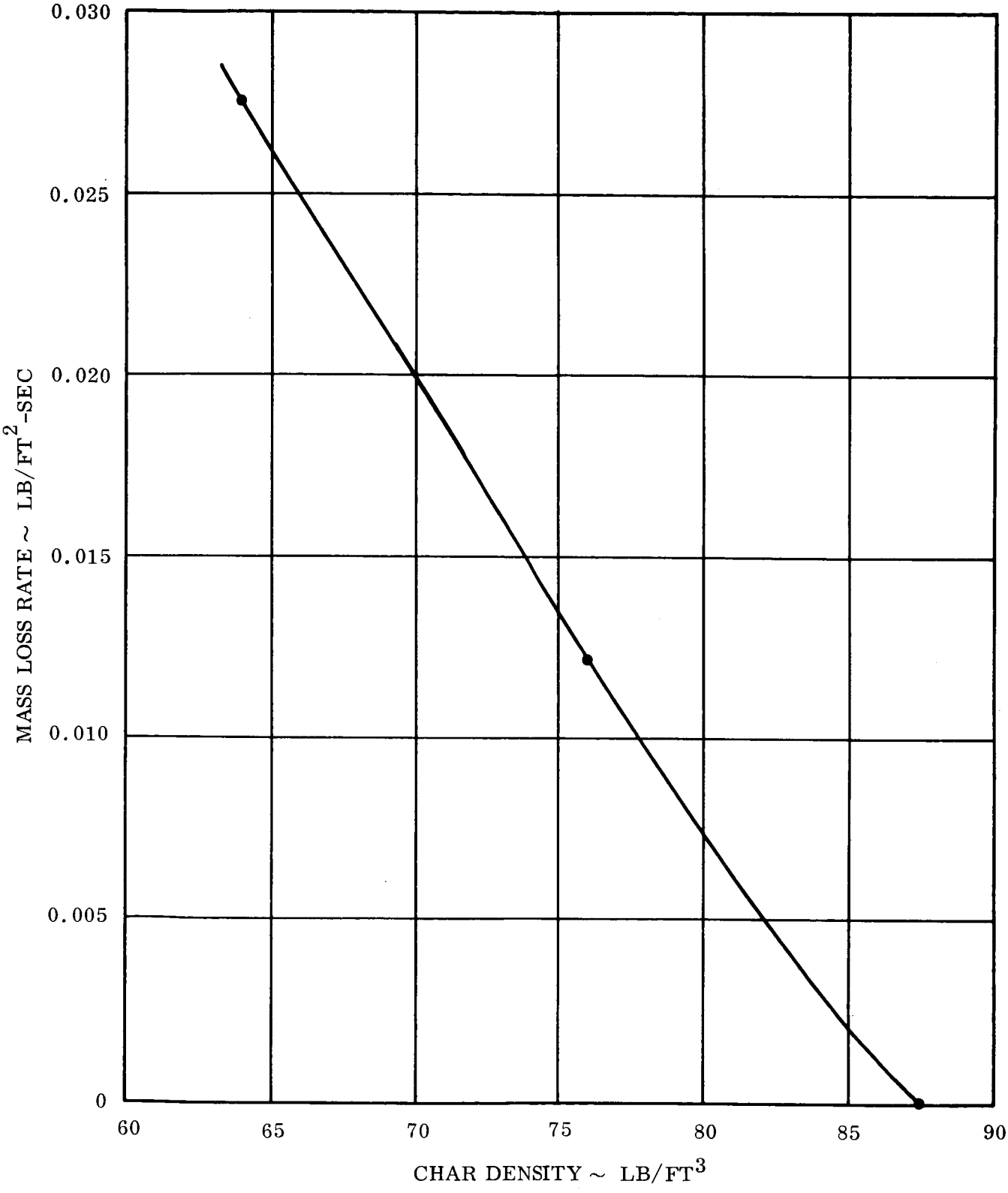

Figure 57. Mass Loss Rate Versus Char Density
Graphite Cloth/Phenolic Resin

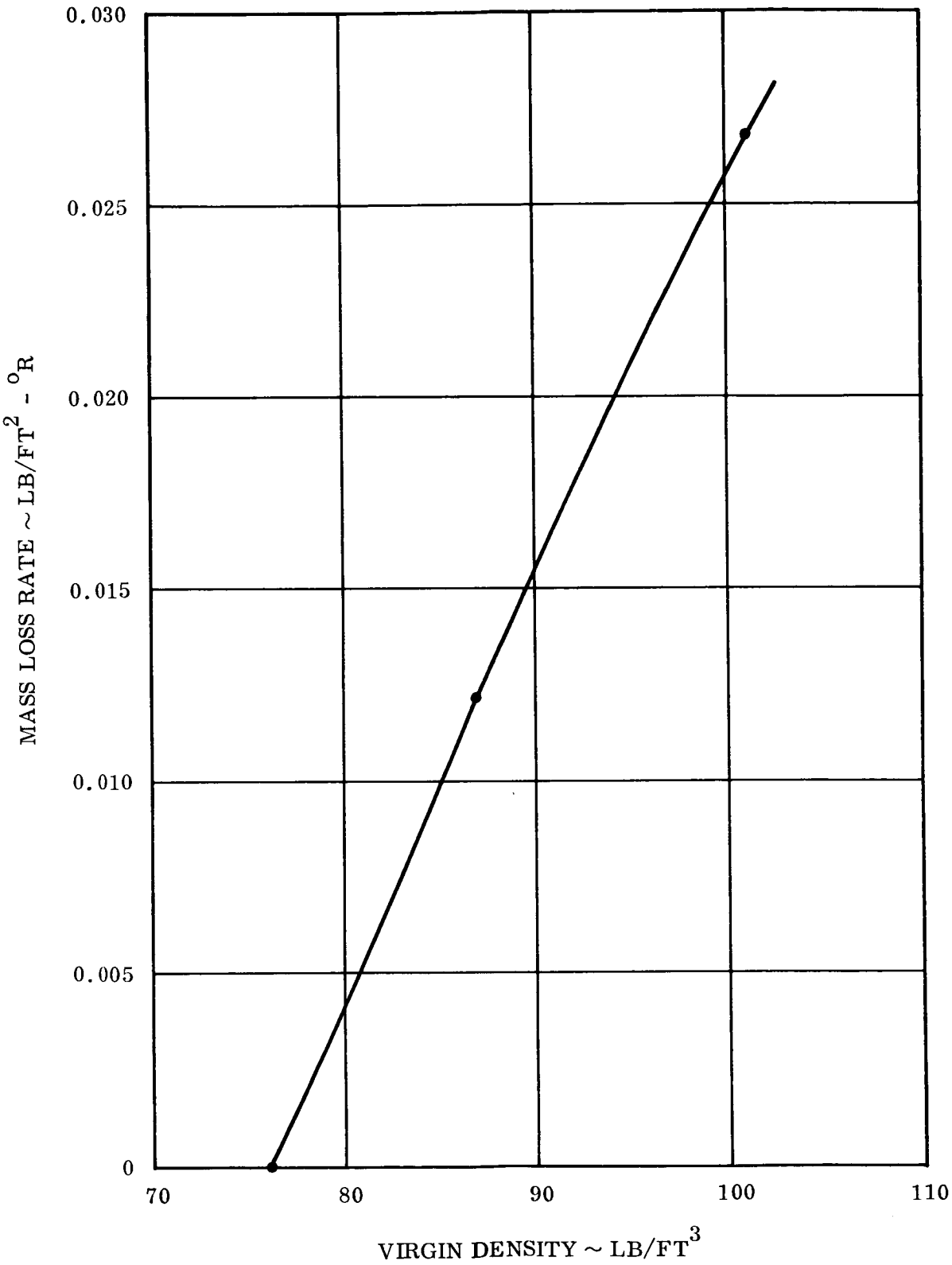

Figure 58. Mass Loss Rate Versus Virgin Density
Graphite Cloth/Phenolic Resin

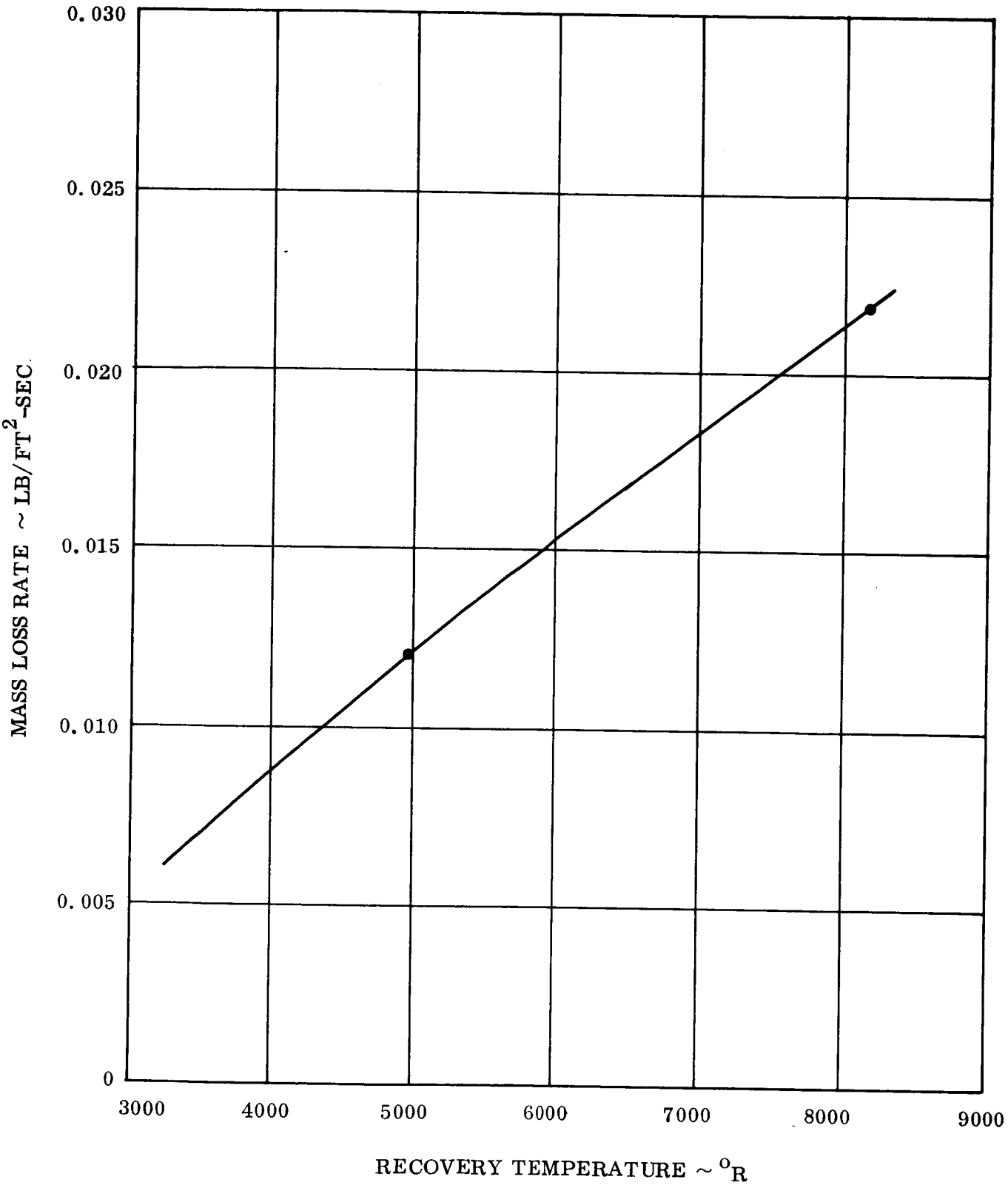

Figure 59. Mass Loss Rate Versus Recovery Temperature
Graphite Cloth/Phenolic Resin

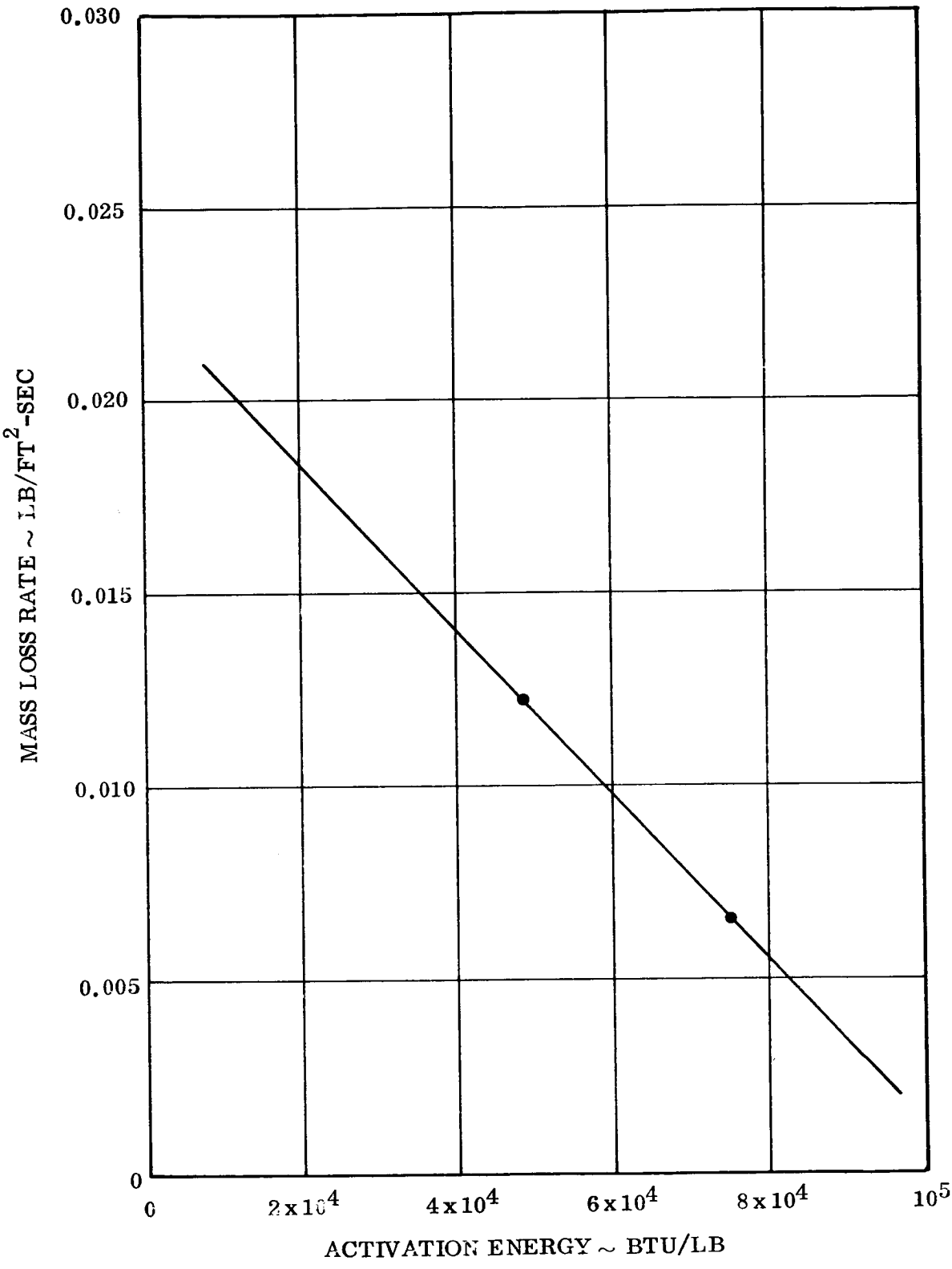

Figure 60. Mass Loss Rate Versus Activation Energy
Graphite Cloth/Phenolic Resin

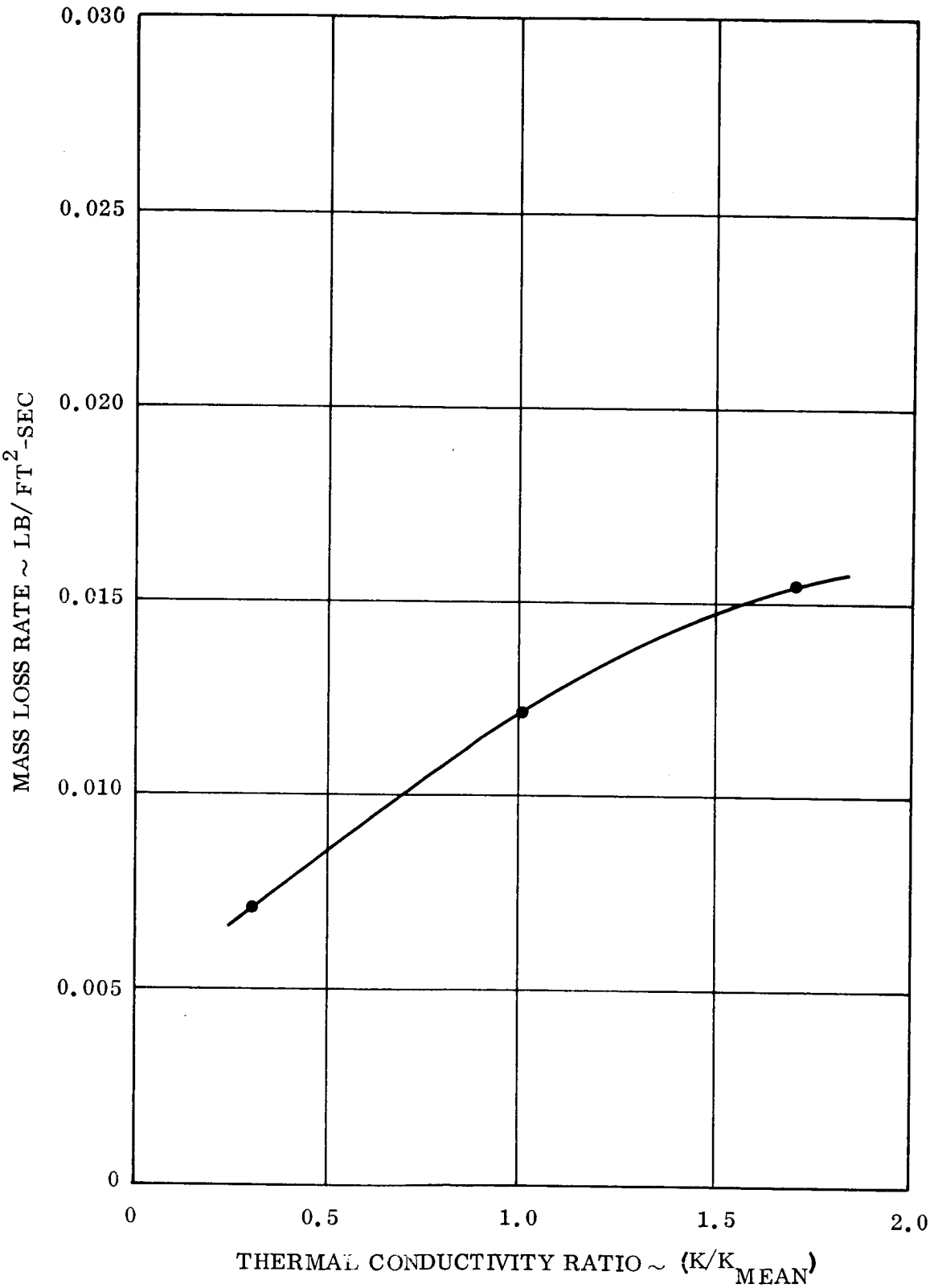

Figure 61. Mass Loss Rate Versus Thermal Conductivity Ratio
Graphite Cloth/Phenolic Resin

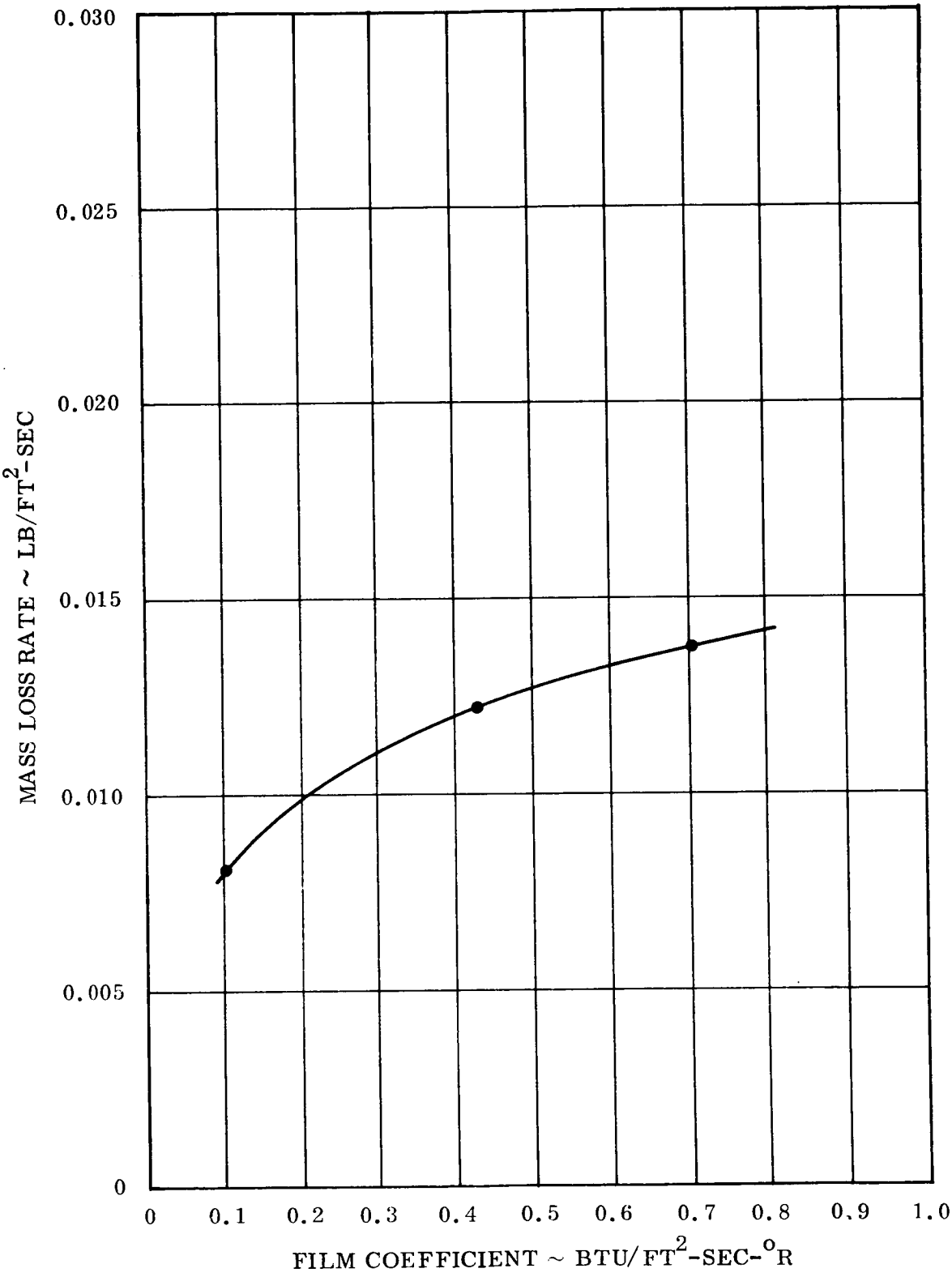

Figure 62. Mass Loss Rate Versus Film Coefficient
Graphite Cloth/Phenolic Resin

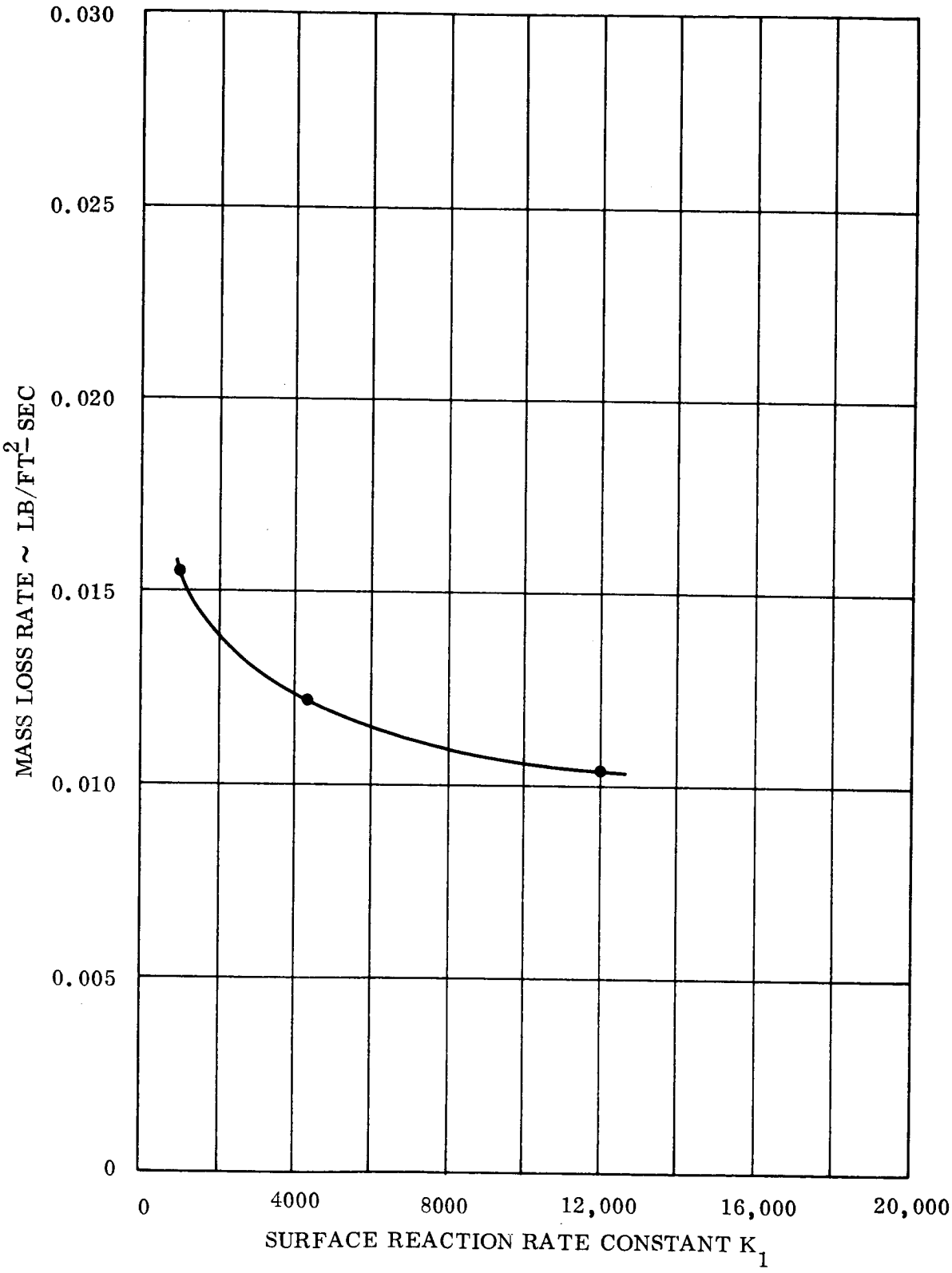

Figure 63. Mass Loss Rate Versus Surface Reaction Rate
Graphite Cloth/Phenolic Resin

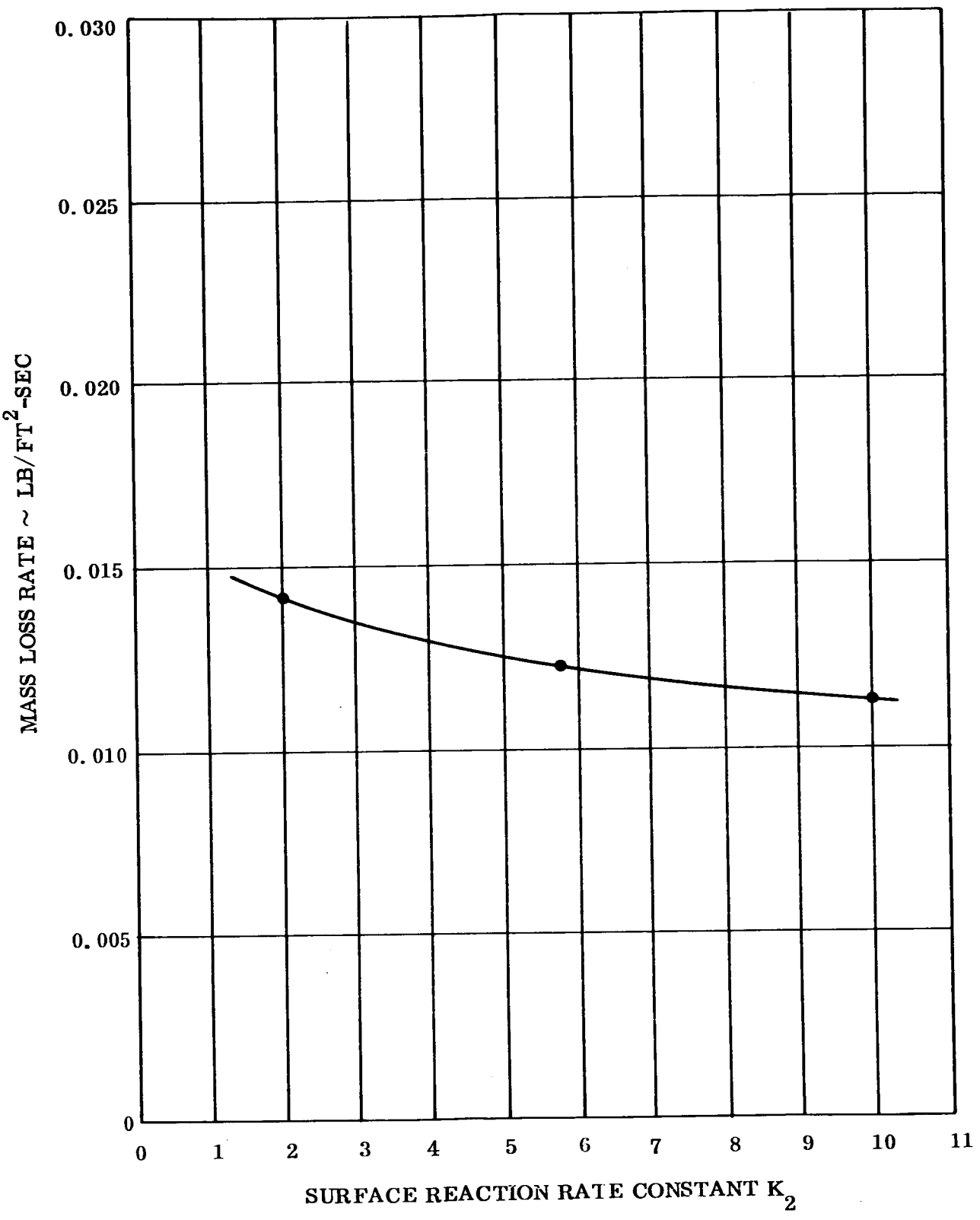

Figure 64. Mass Loss Rate Versus Surface Reaction Rail Constant K Graphite Cloth/Phenolic Resin

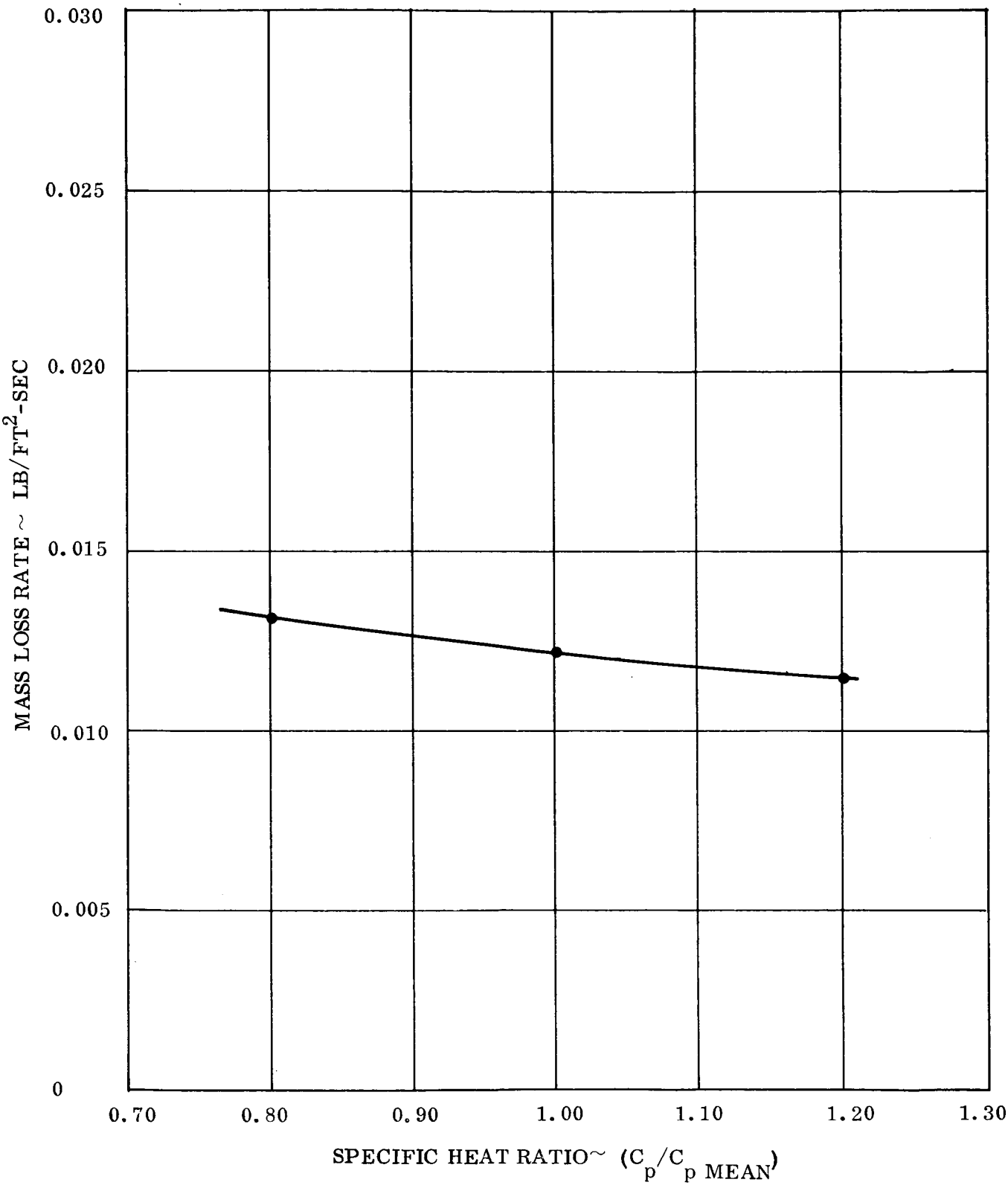

Figure 65. Mass Loss Rate Versus Specific Heat Ratio
Graphite Cloth/Phenolic Resin

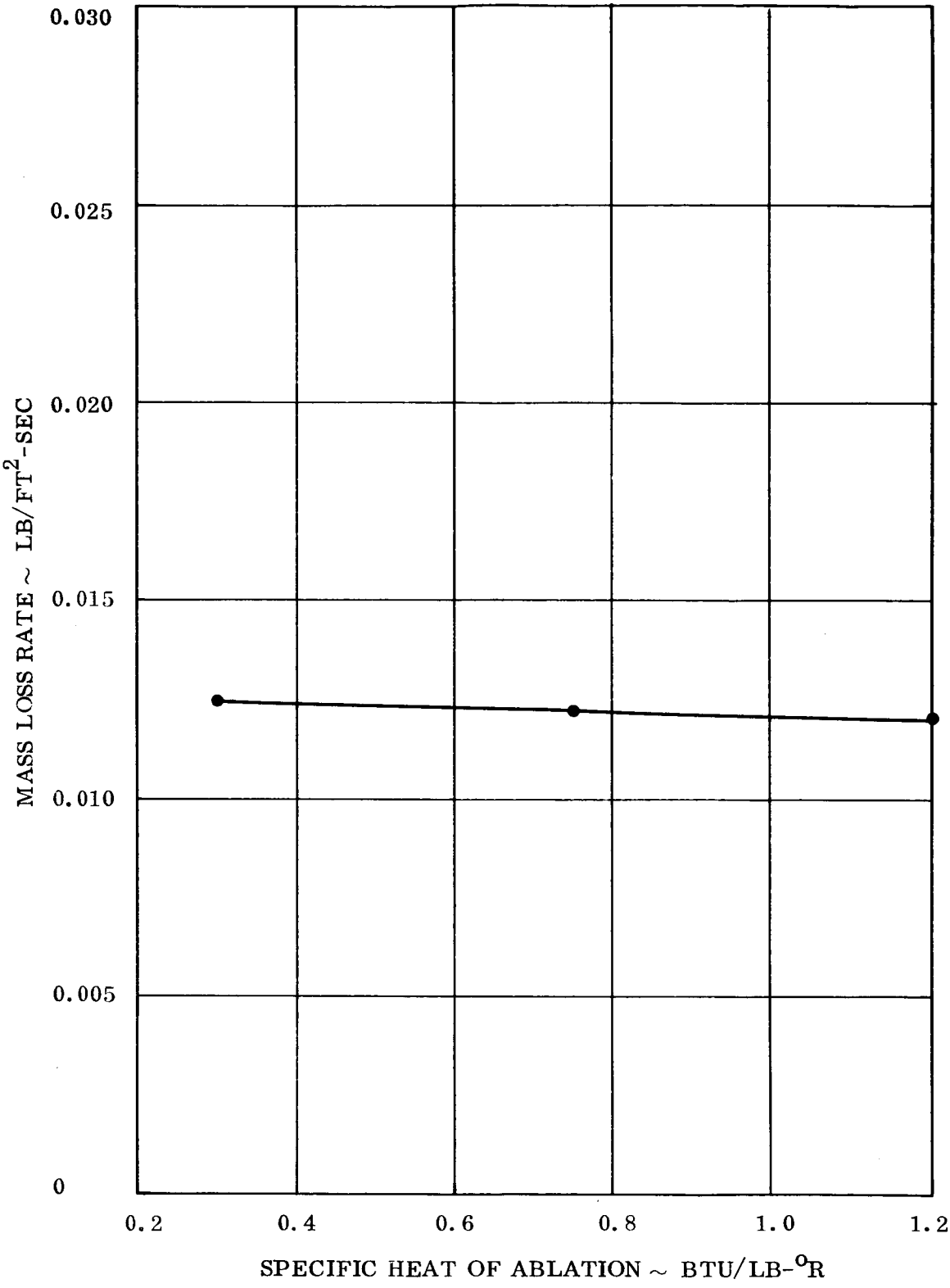

Figure 66. Mass Loss Rate Versus Specific Heat of Ablation Gases
Graphite Cloth/Phenolic Resin

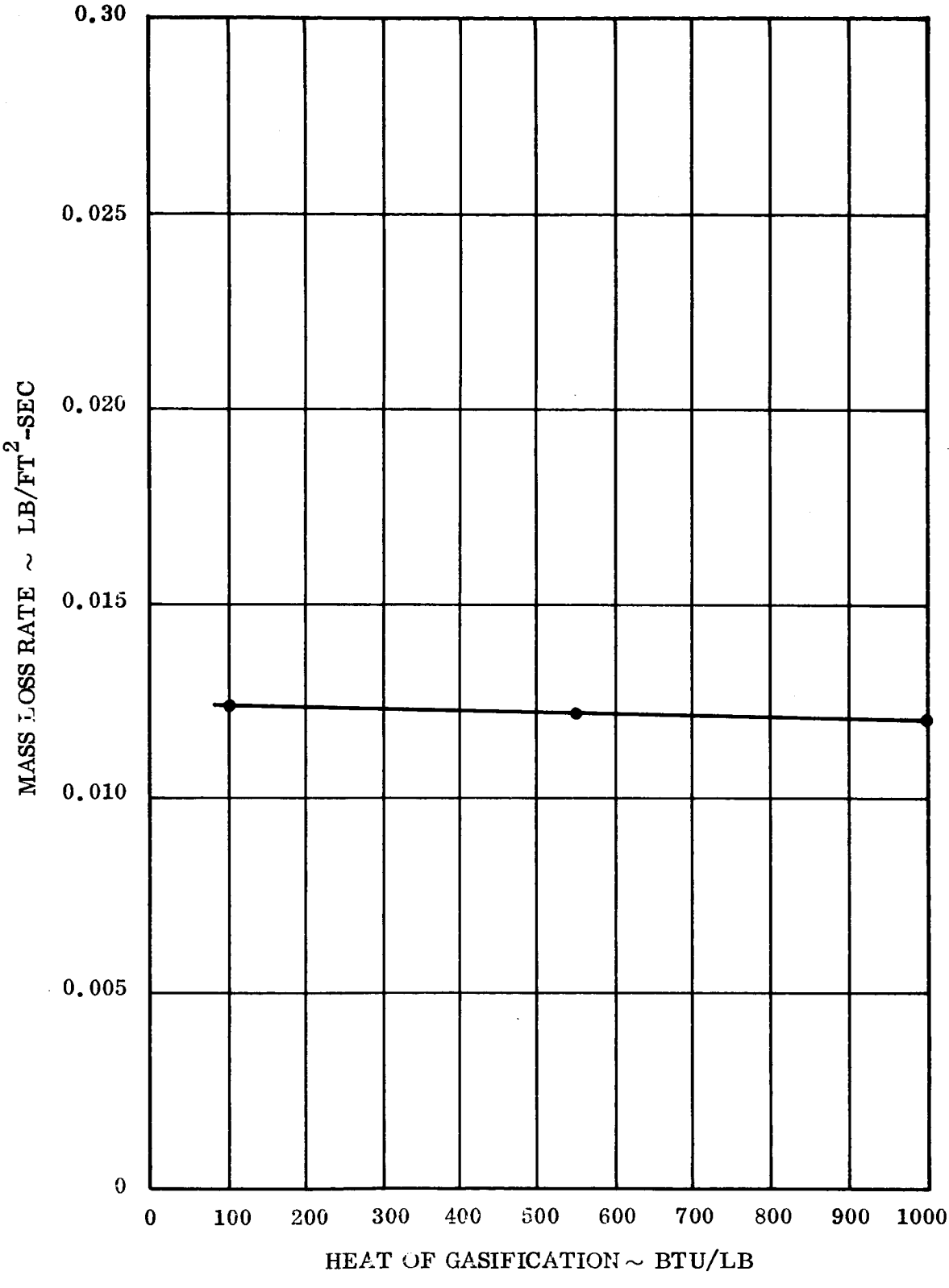

Figure 67. Mass Loss Rate Versus Heat of Gasification
Graphite Cloth/Phenolic Resin

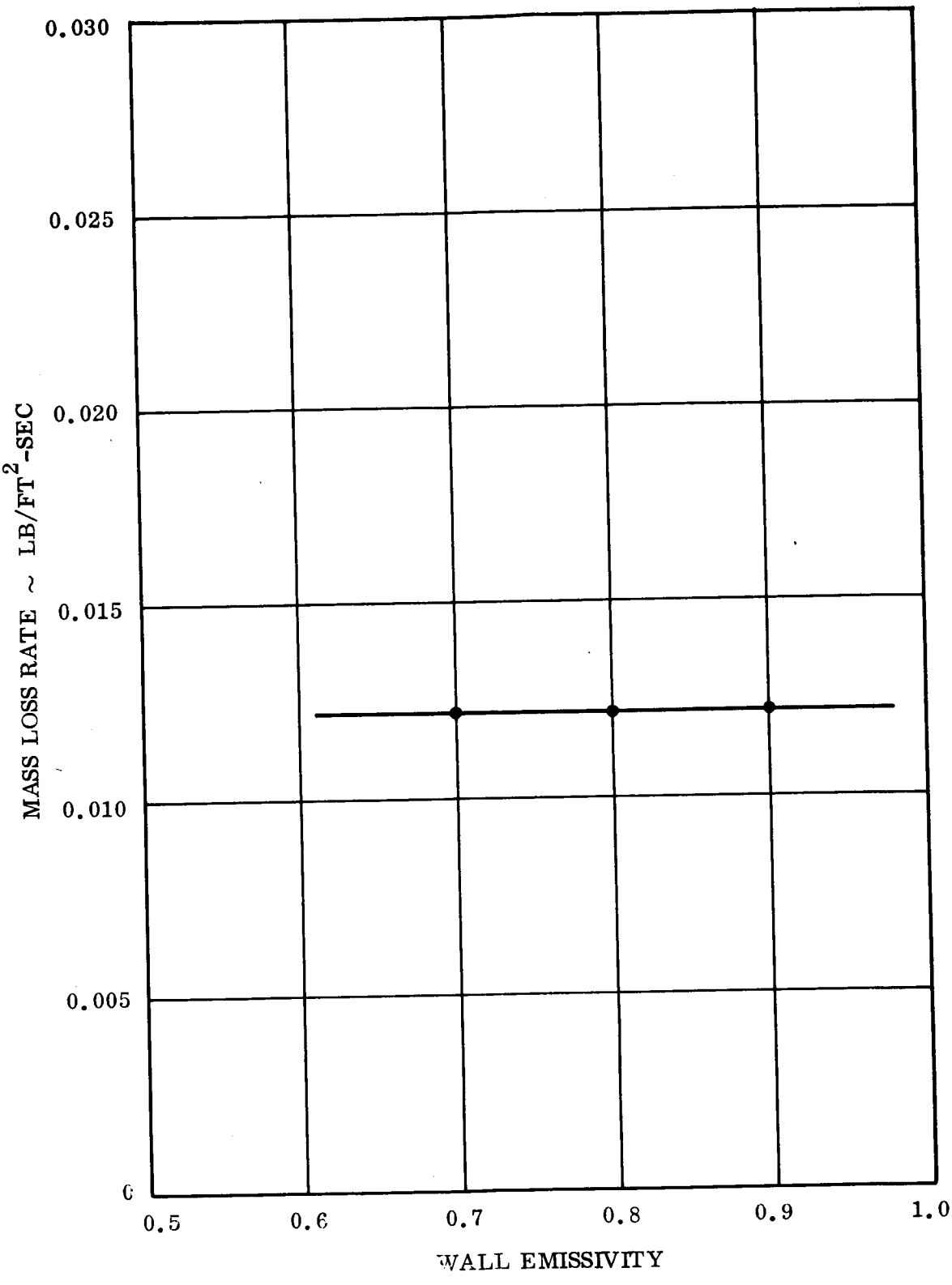

Figure 68. Mass Loss Rate Versus Wall Emissivity
Graphite Cloth/Phenolic Resin

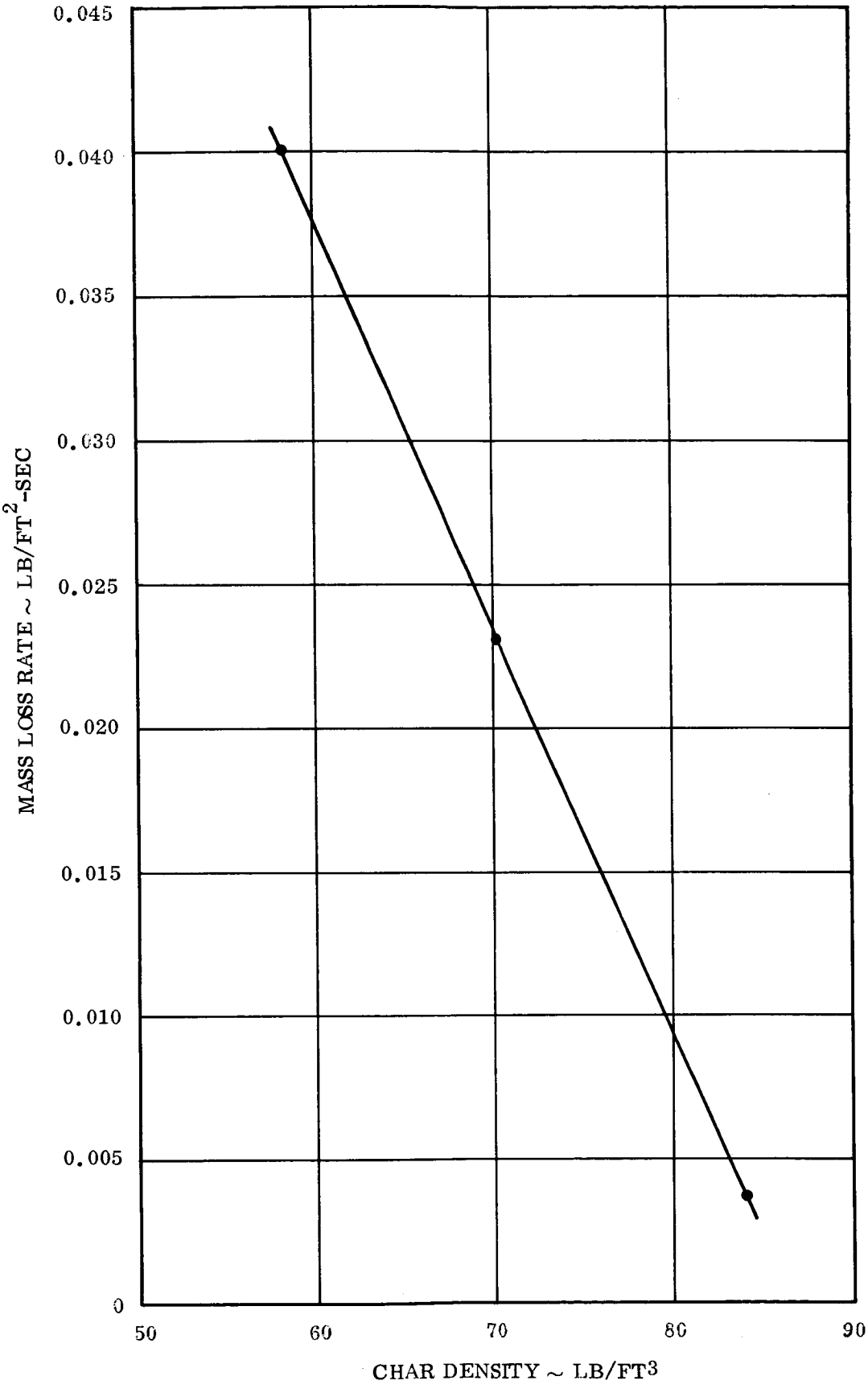

Figure 69. Mass Loss Rate Versus Char Density
Graphite Cloth/Epoxy Resin

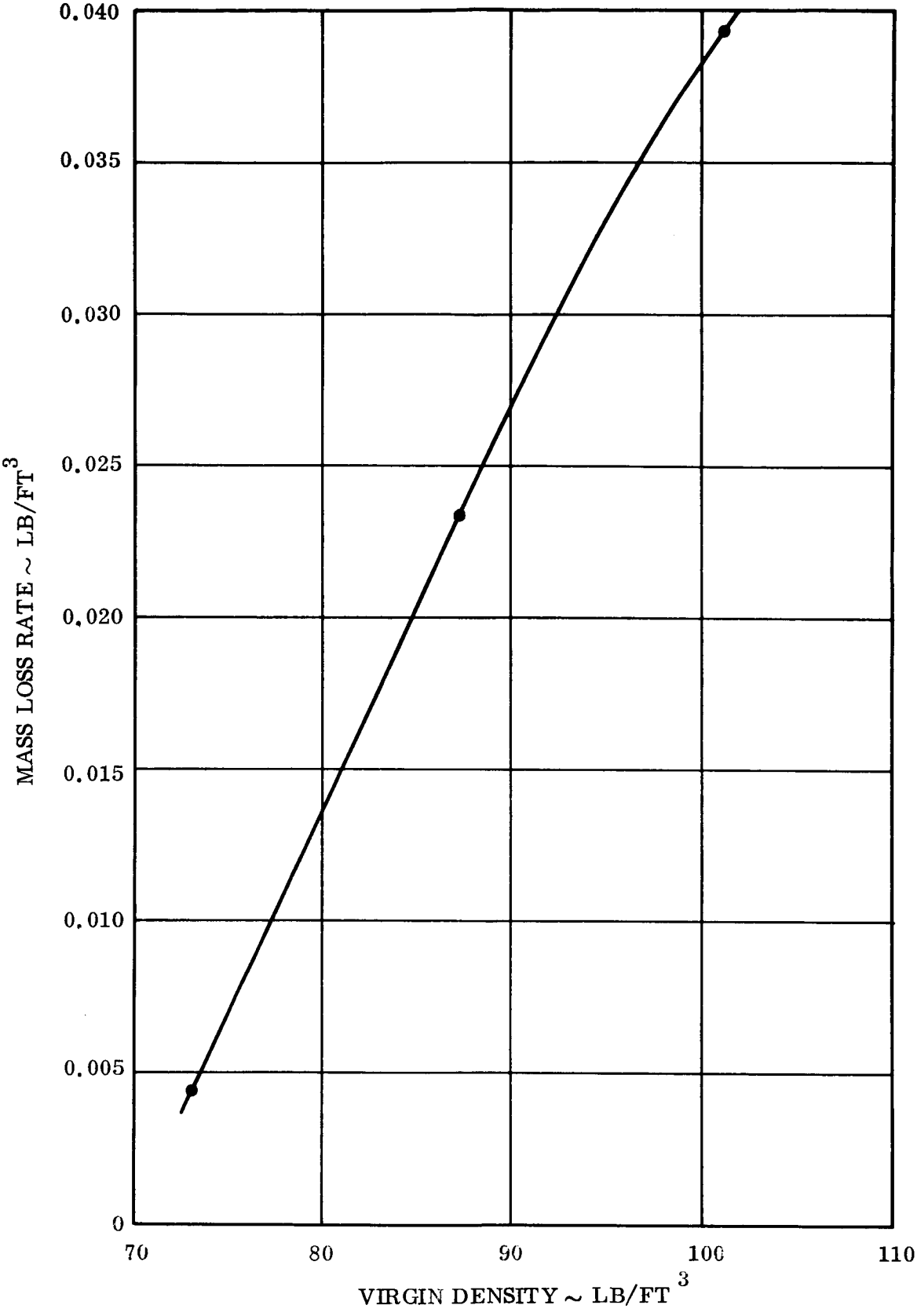

Figure 70. Mass Loss Rate Versus Virgin Density
Graphite Cloth/Epoxy Resin

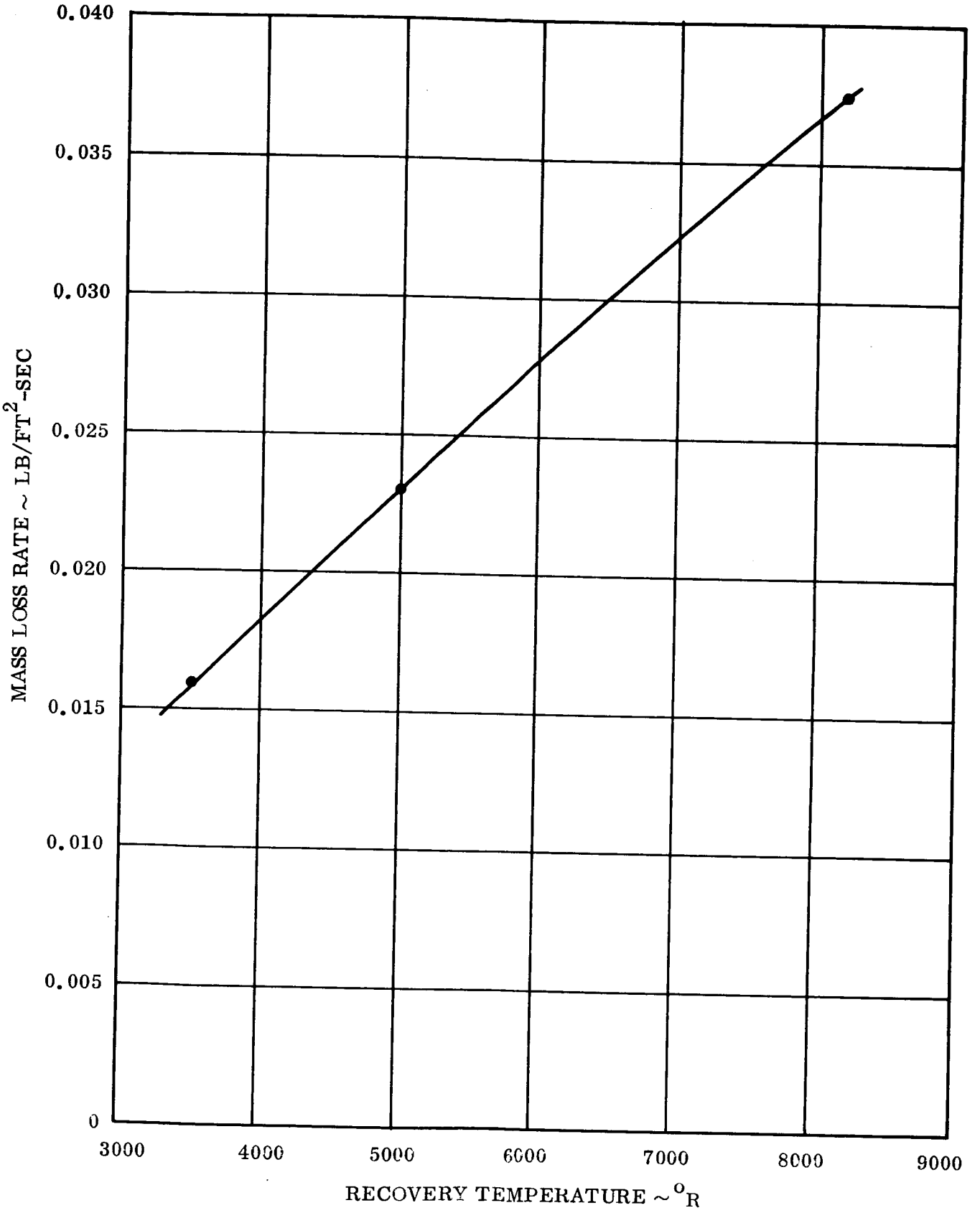

Figure 71. Mass Loss Rate Versus Recovery Temperature Graphite Cloth/Epoxy Resin

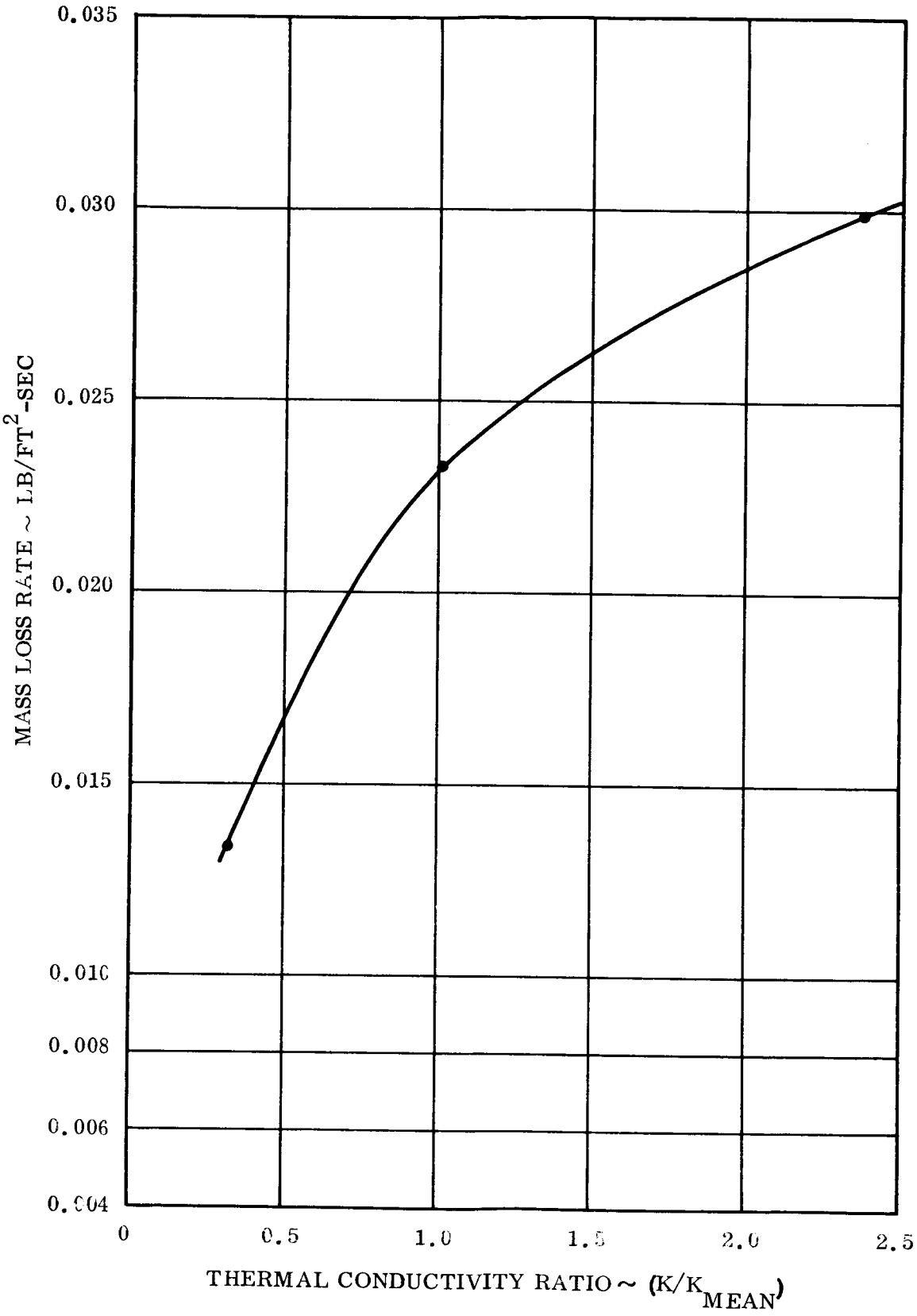

Figure 72. Mass Loss Rate Versus Thermal Conductivity Ratio Graphite Cloth/Epoxy Resin

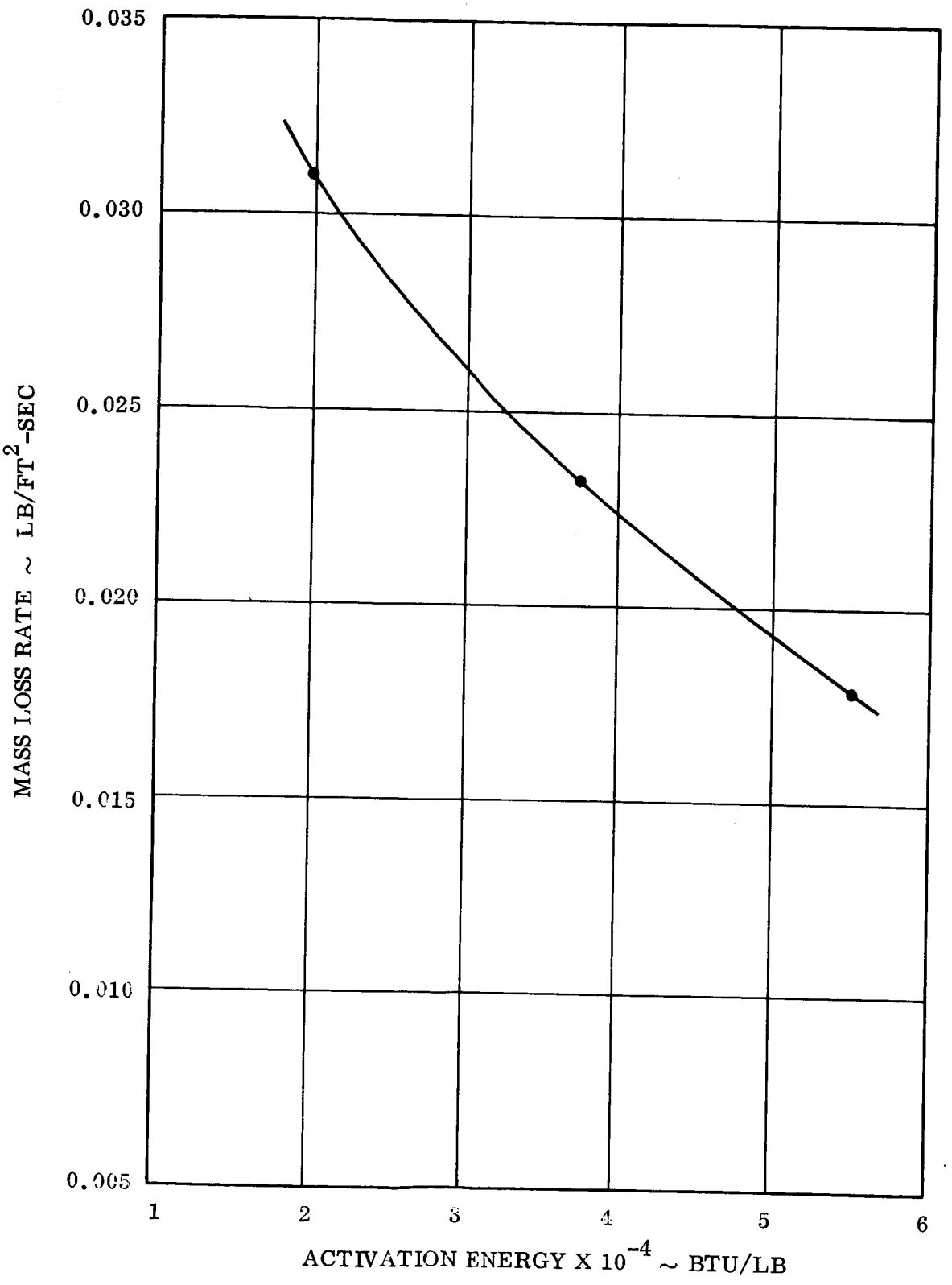

Figure 73. Mass Loss Rate Versus Activation Energy Graphite Cloth/Epoxy Resin

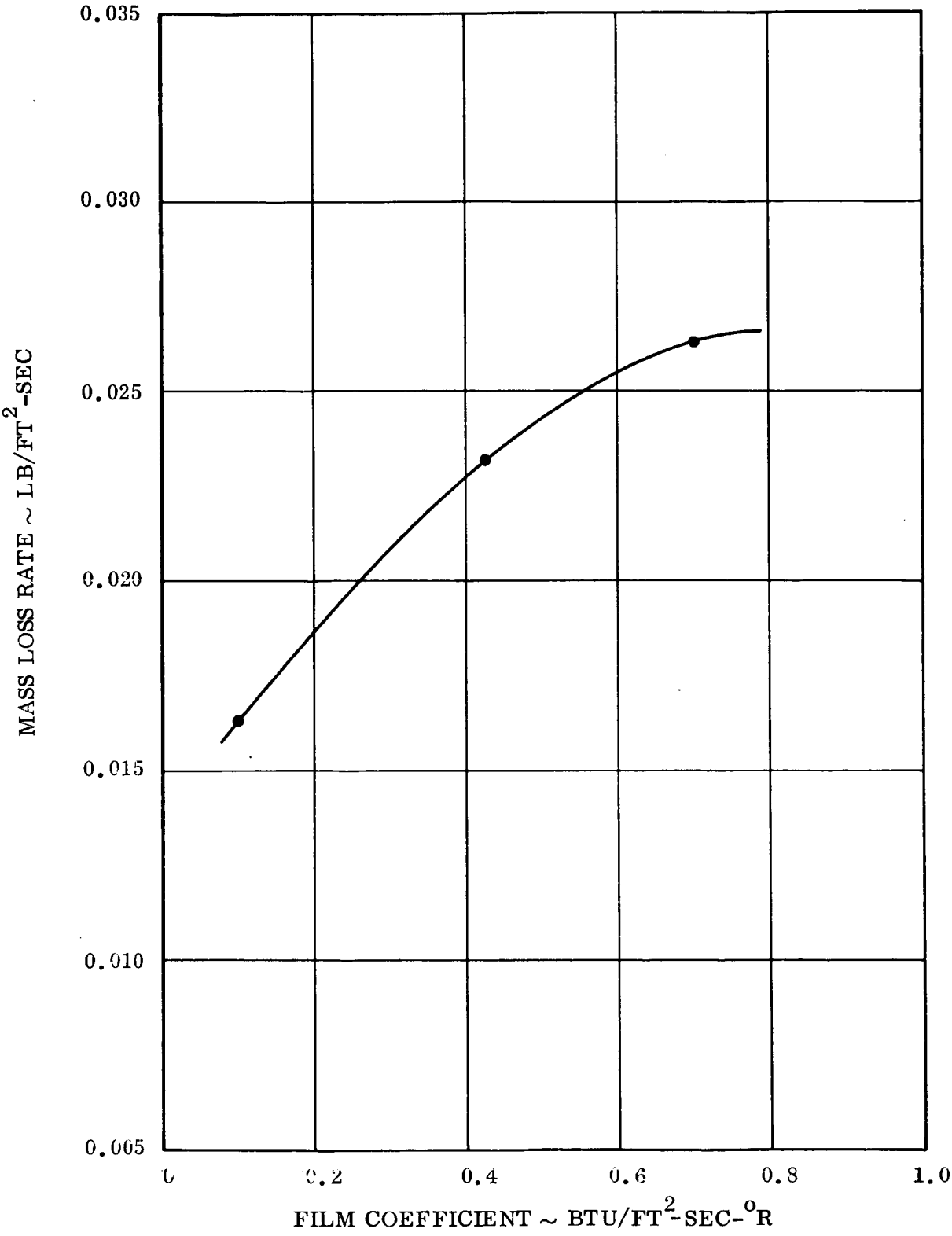

Figure 74. Mass Loss Rate Versus Film Coefficient Graphite Cloth/Epoxy Resin

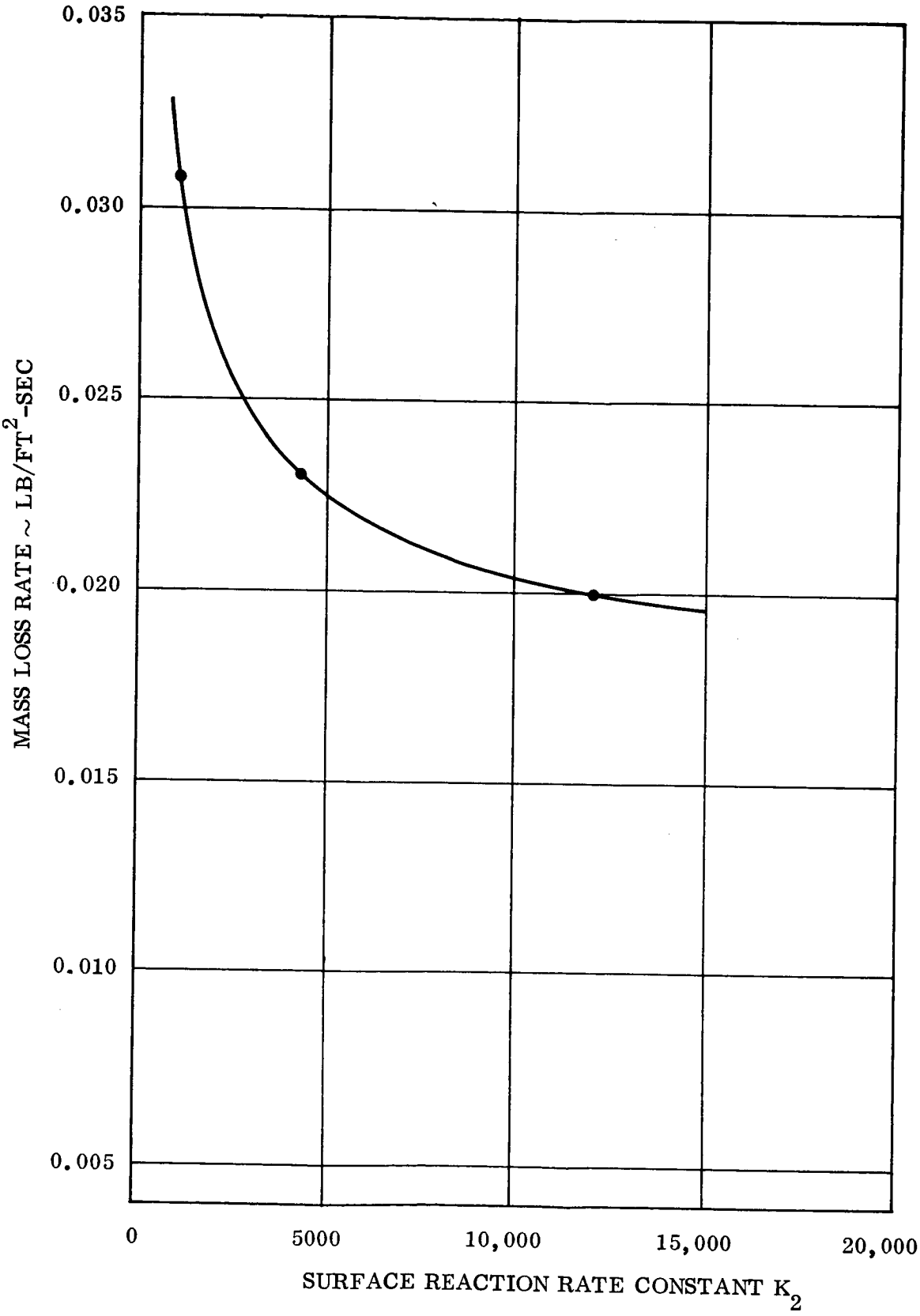

Figure 75. Mass Loss Rate Versus Surface Reaction Rate Constant K. Graphite Cloth/Epoxy Resin

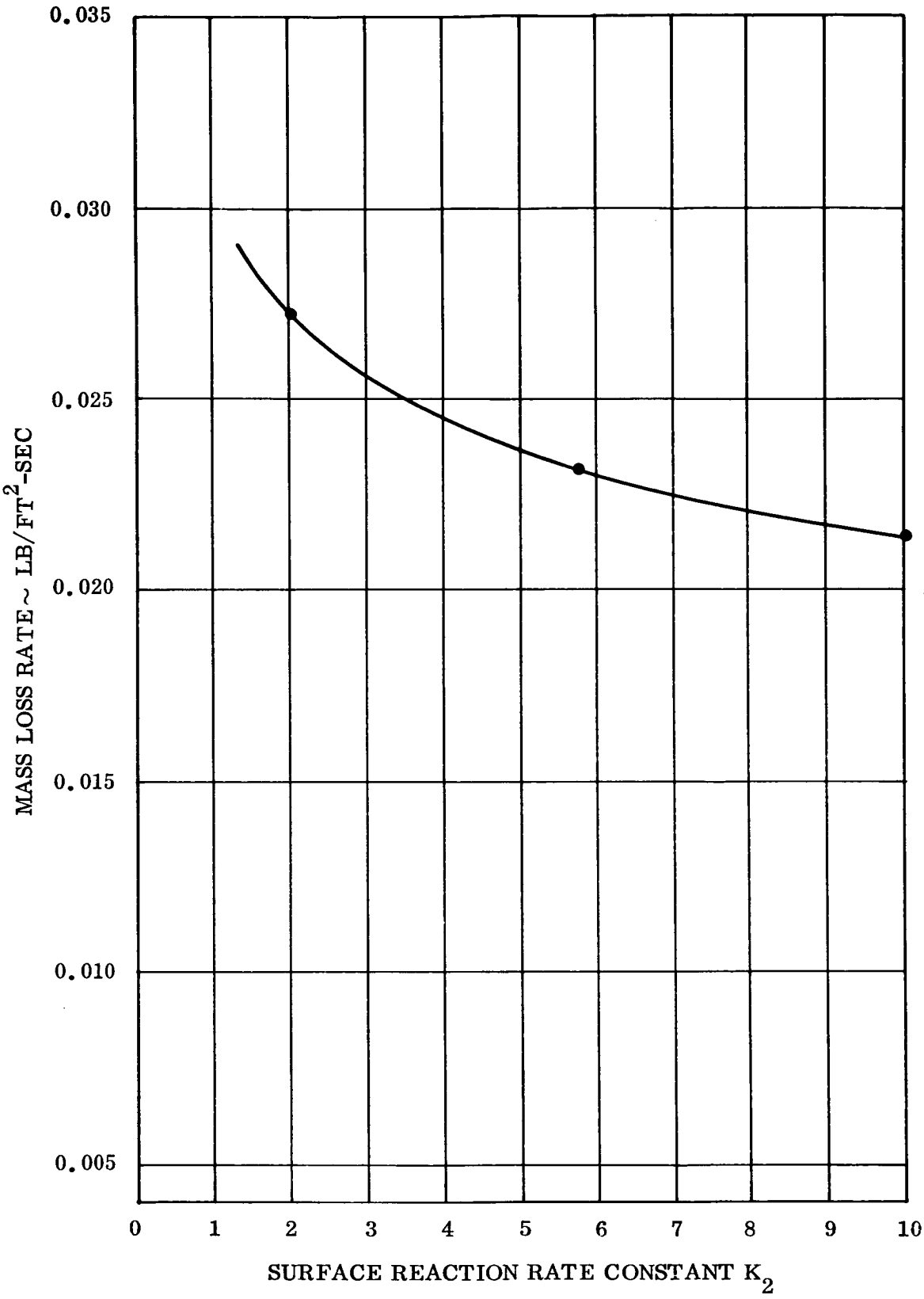

Figure 76. Mass Loss Rate Versus Surface Reaction Rate Constant K. Graphite Cloth/Epoxy Resin

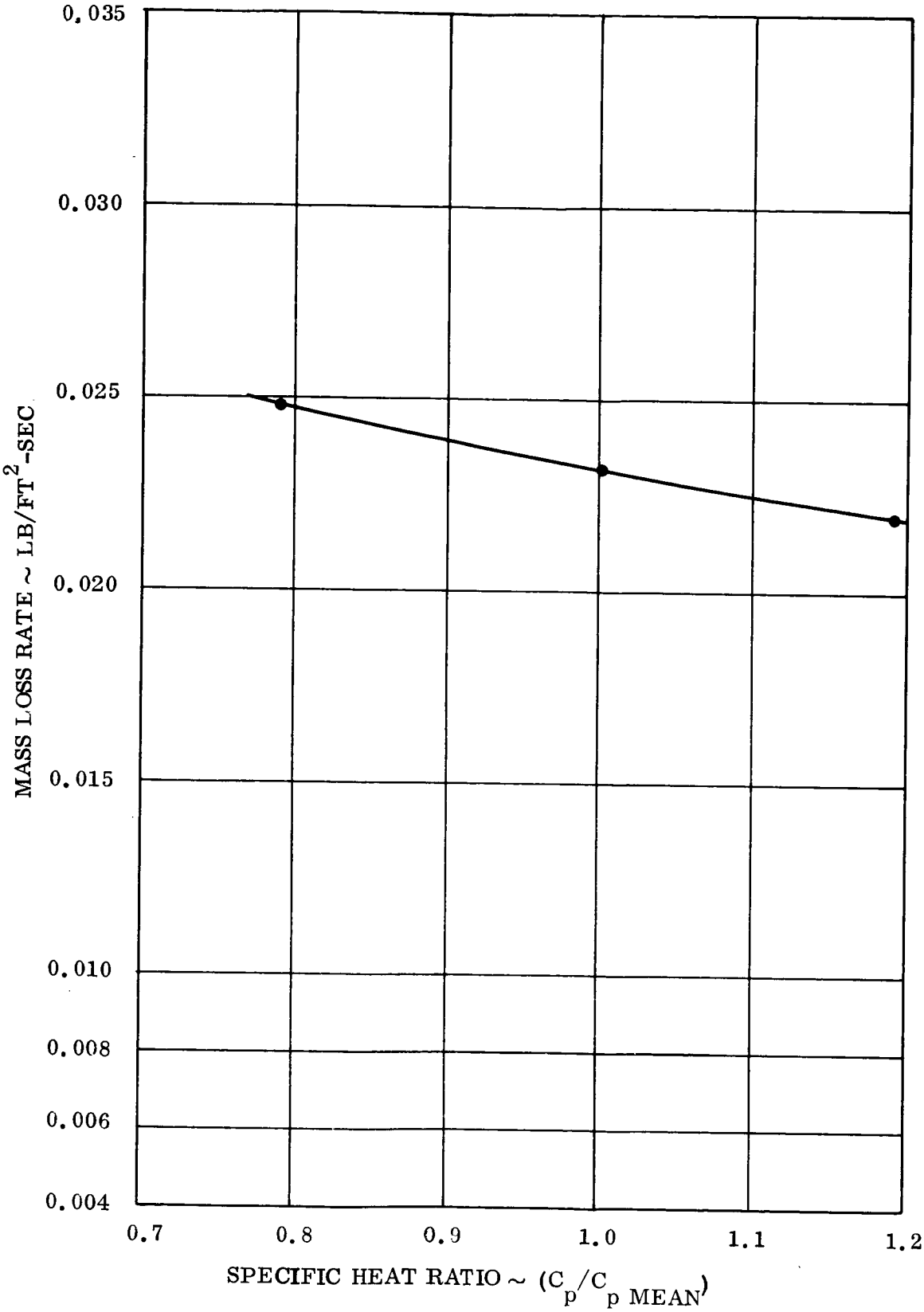

Figure 77. Mass Loss Rate Versus Specific Heat Ratio Graphite Cloth/Epoxy Resin

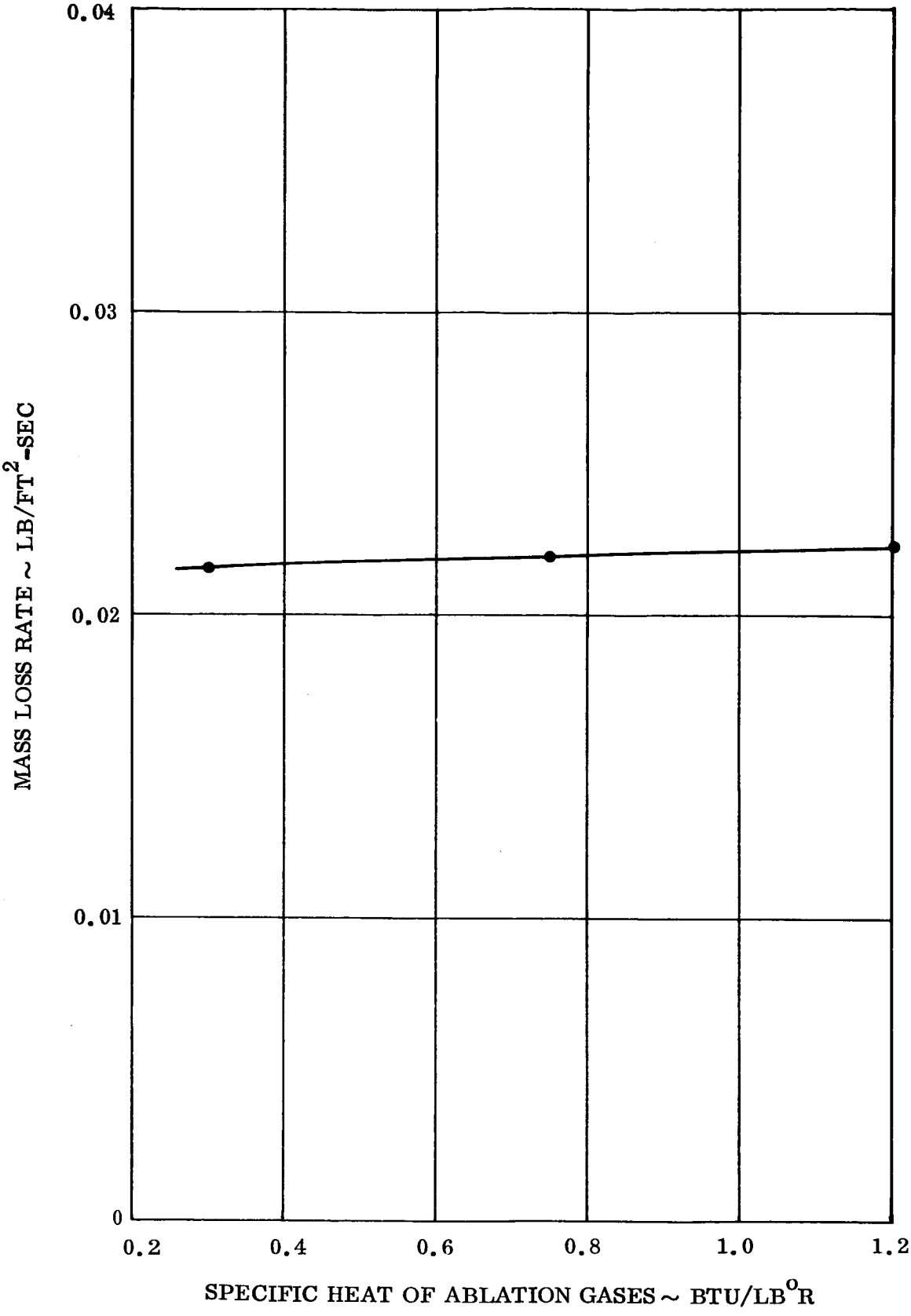

Figure 78. Mass Loss Rate Versus Specific Heat of Ablation Gases Graphite Cloth/Epoxy Resin

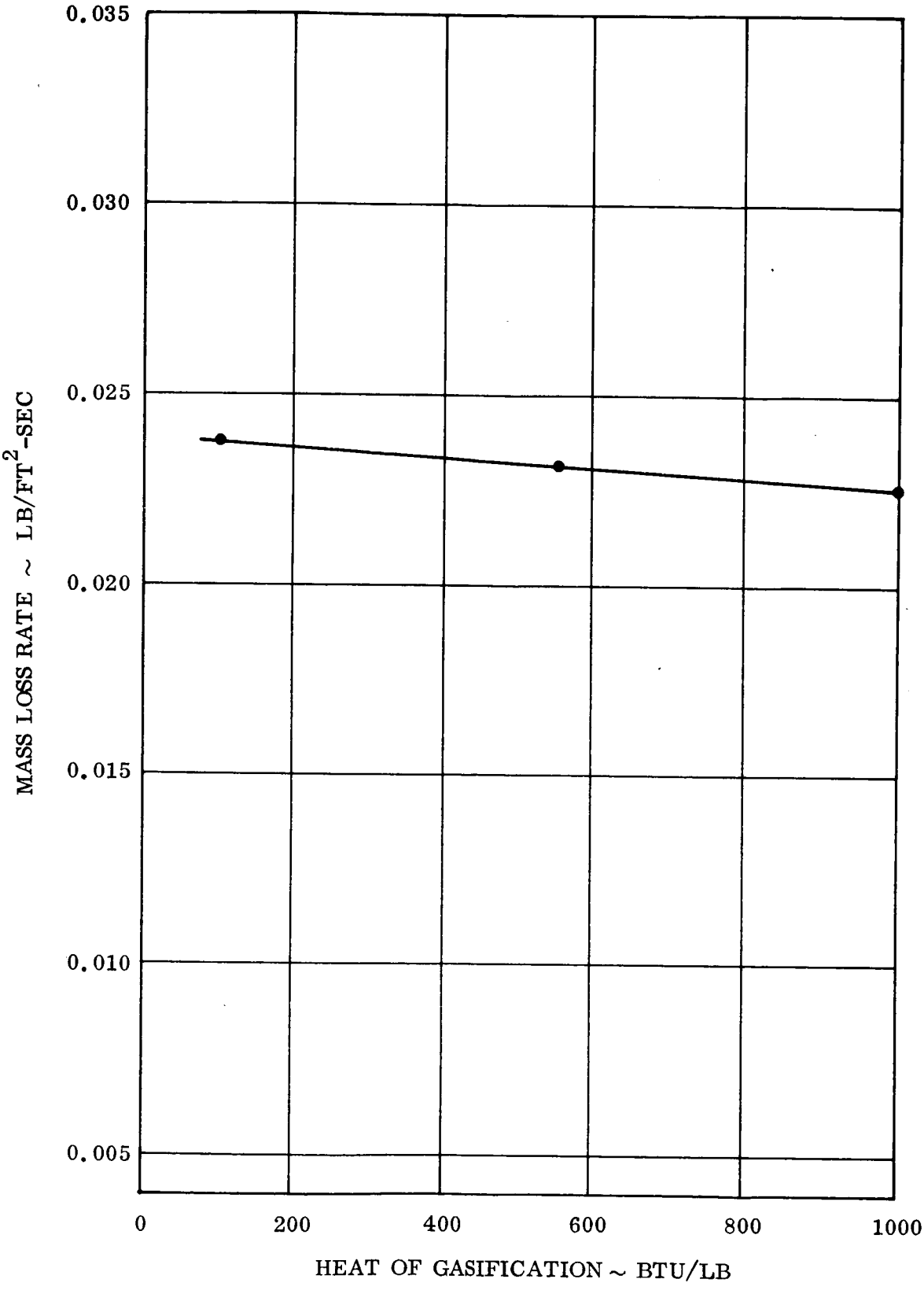

Figure 79. Mass Loss Rate Versus Heat of Gasification Graphite Cloth/Epoxy Resin

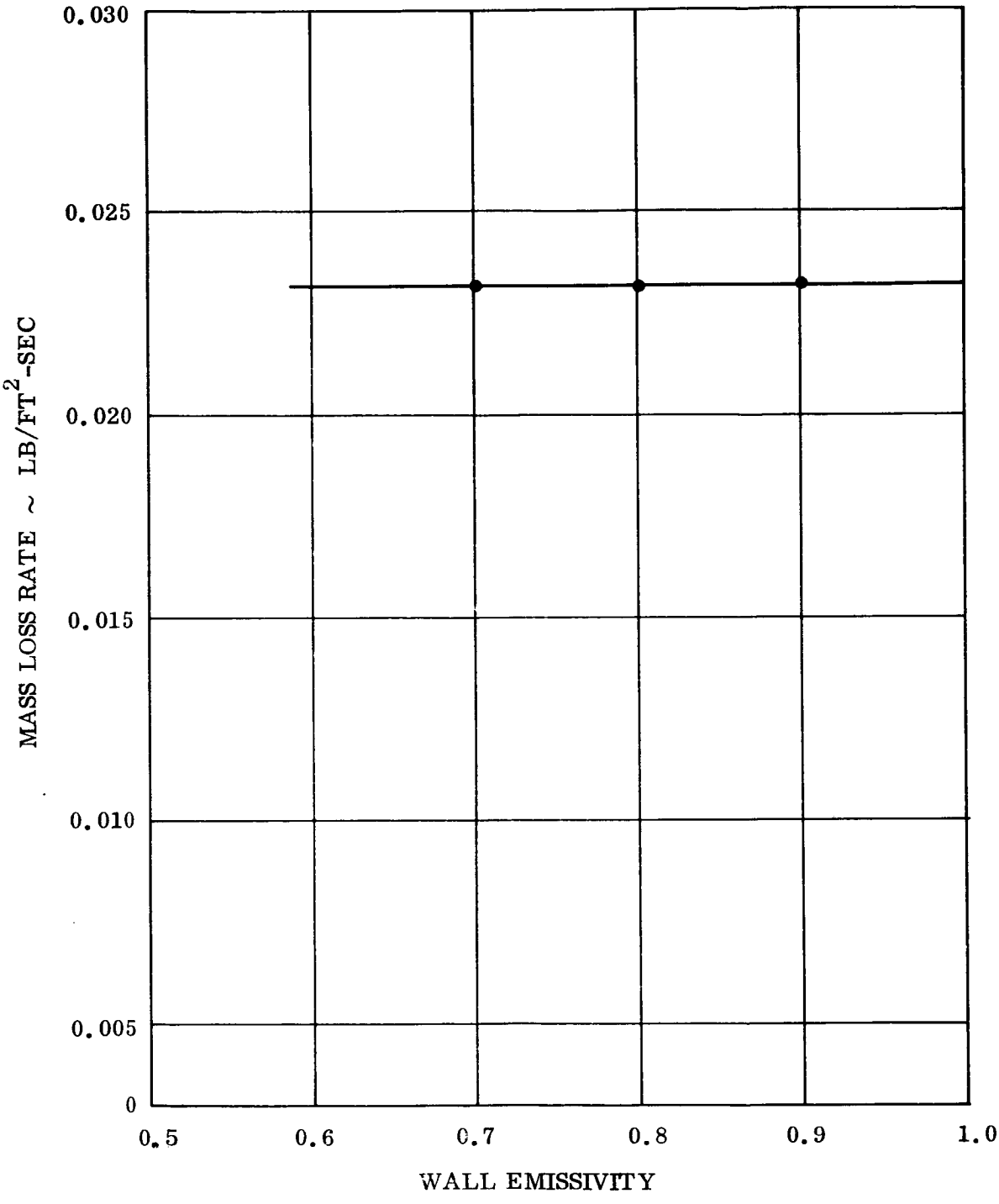

Figure 80. Mass Loss Rate Versus Wall Emissivity Graphite Cloth/Epoxy Resin

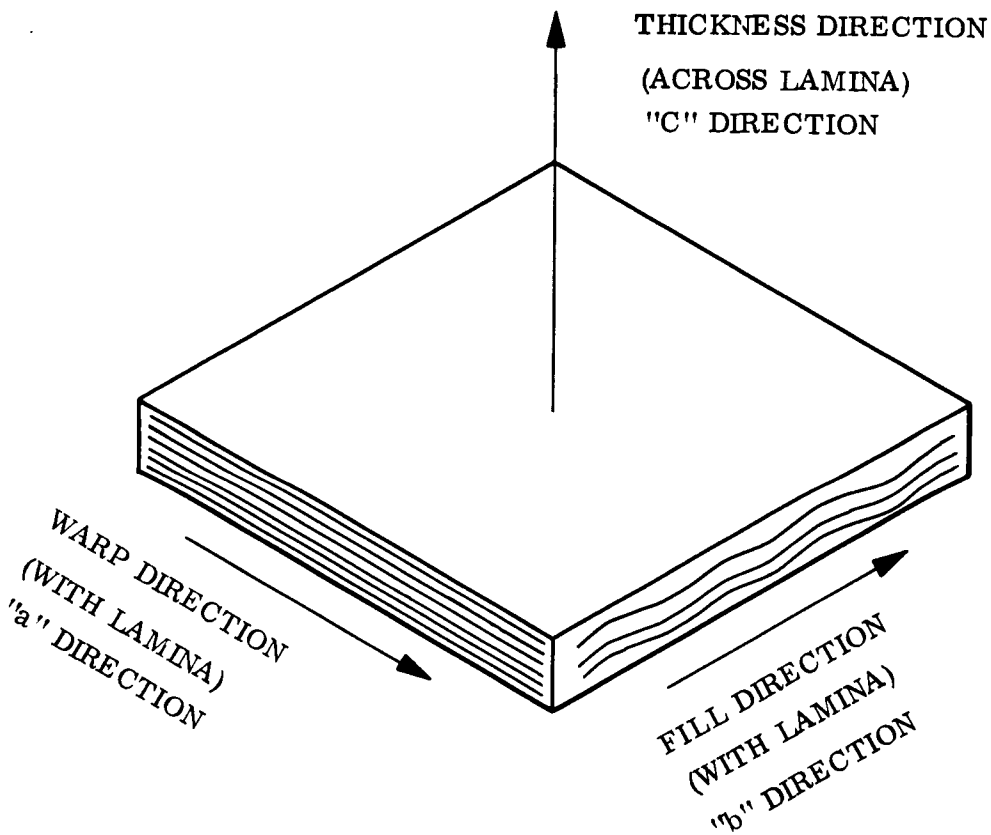

Figure 81. Sketch of Directions of Heat Flow

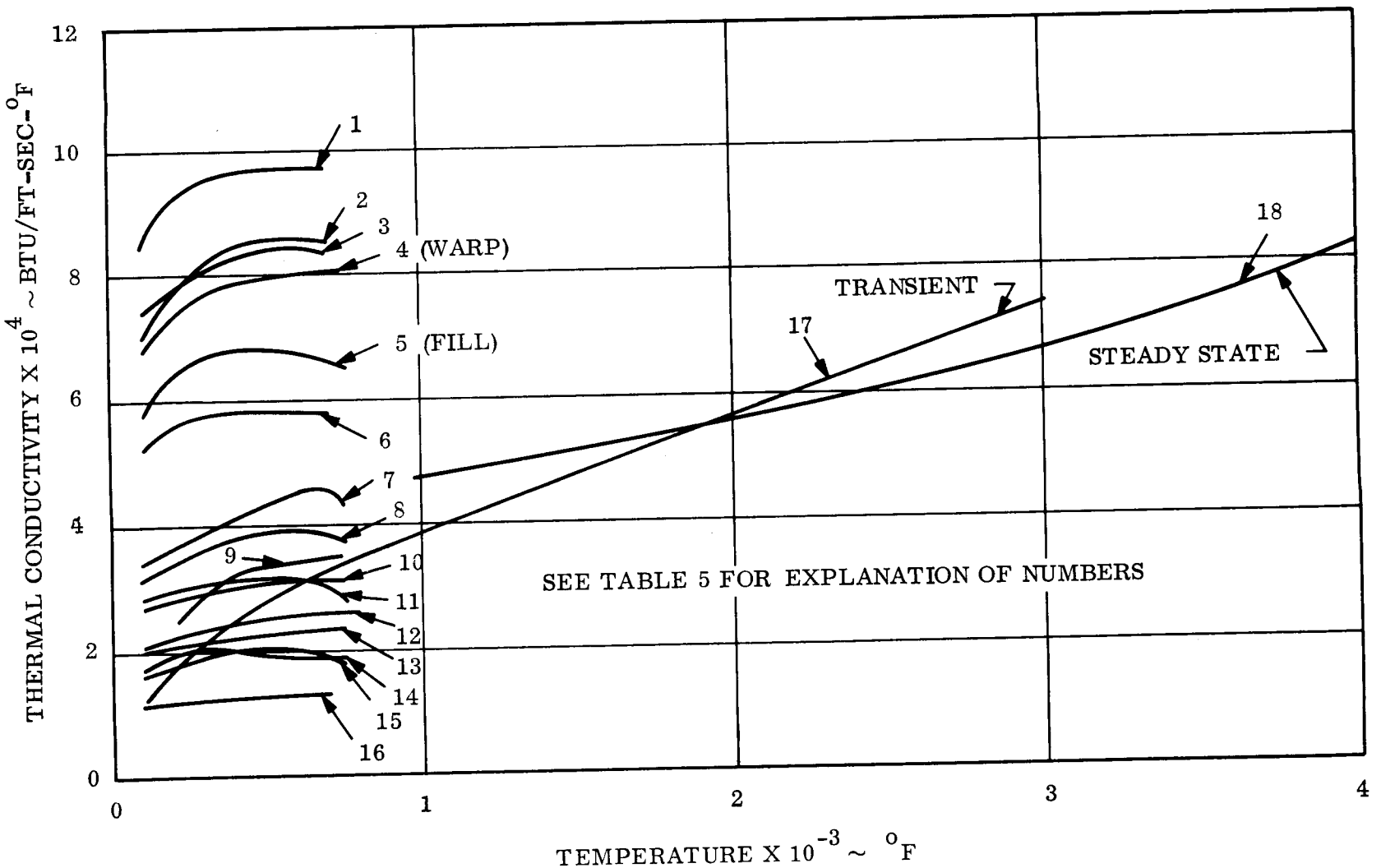

Figure 82. Variations in Thermal Conductivity Due to Changes in Lamination Angle, Resin Content, and Lot-to-Lot Variation of Graphite Cloth/Phenolic Resin (Literature Survey)

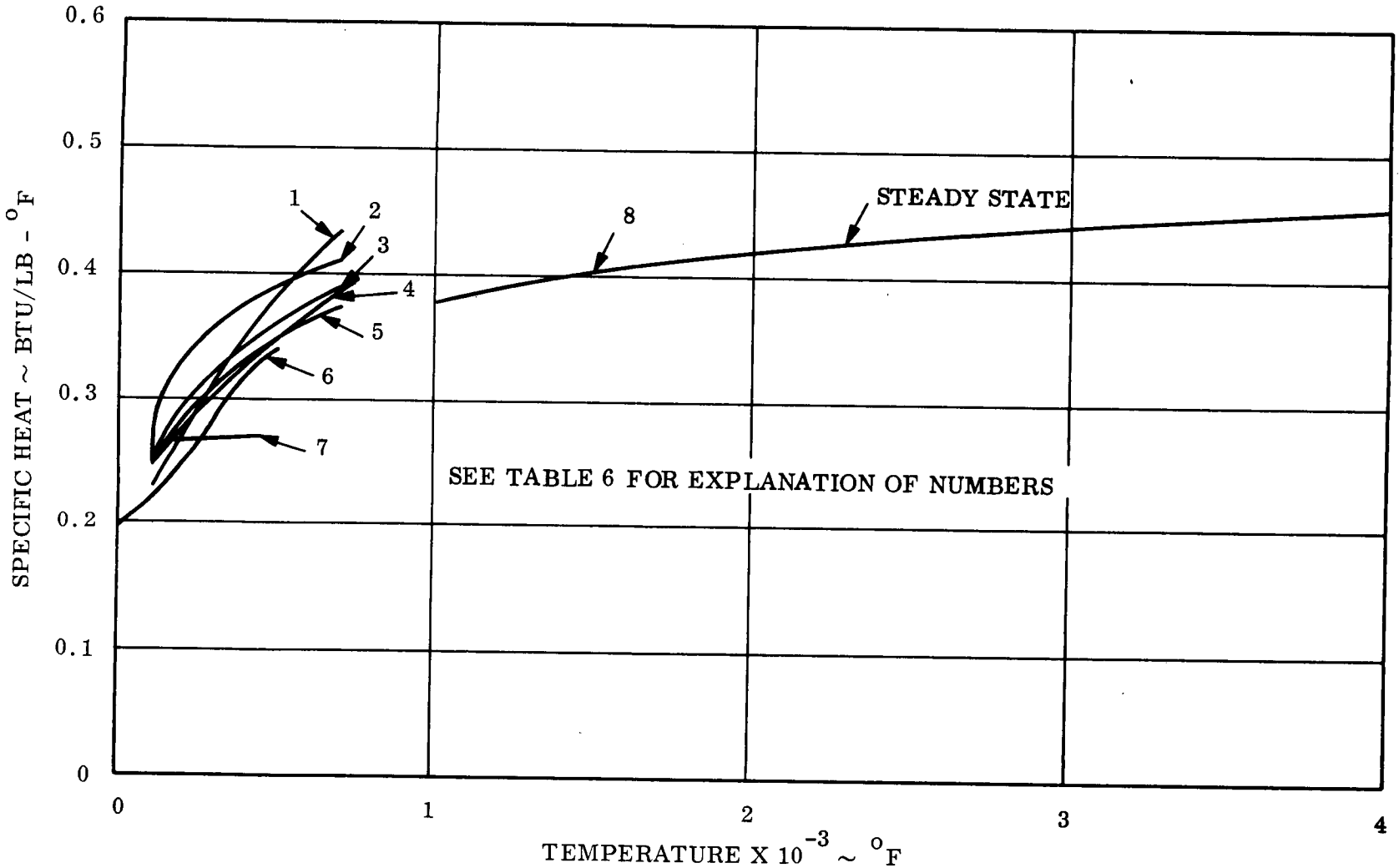

Figure 83. Variations in Specific Heat Due to Changes in Lamination Angle, Resin Content, and Lot-to-Lot Variation of Graphite Cloth/Phenolic Resin (Literature Survey)

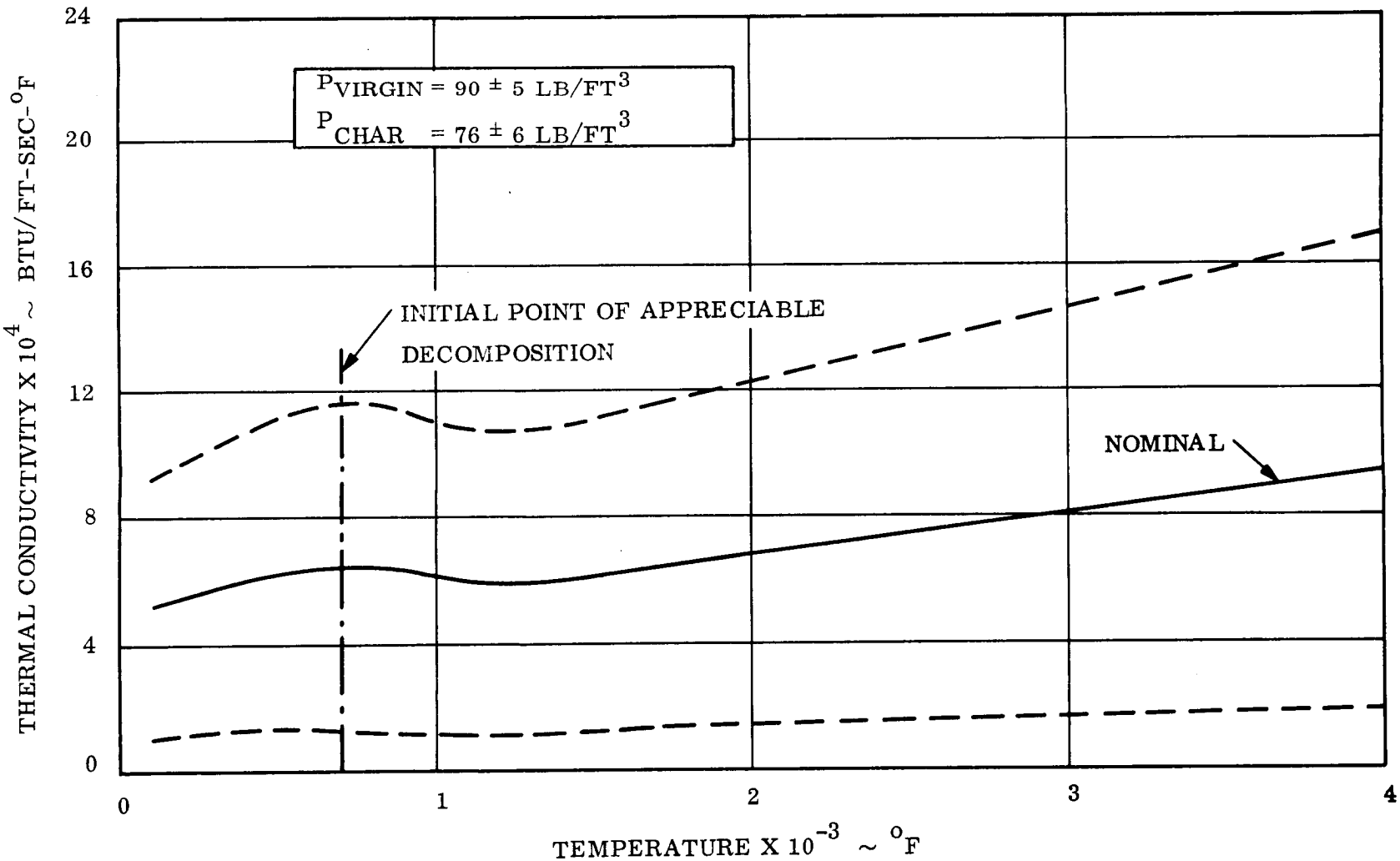

Figure 84. Thermal Conductivity of Graphite Cloth/Phenolic Resin (Literature Survey)

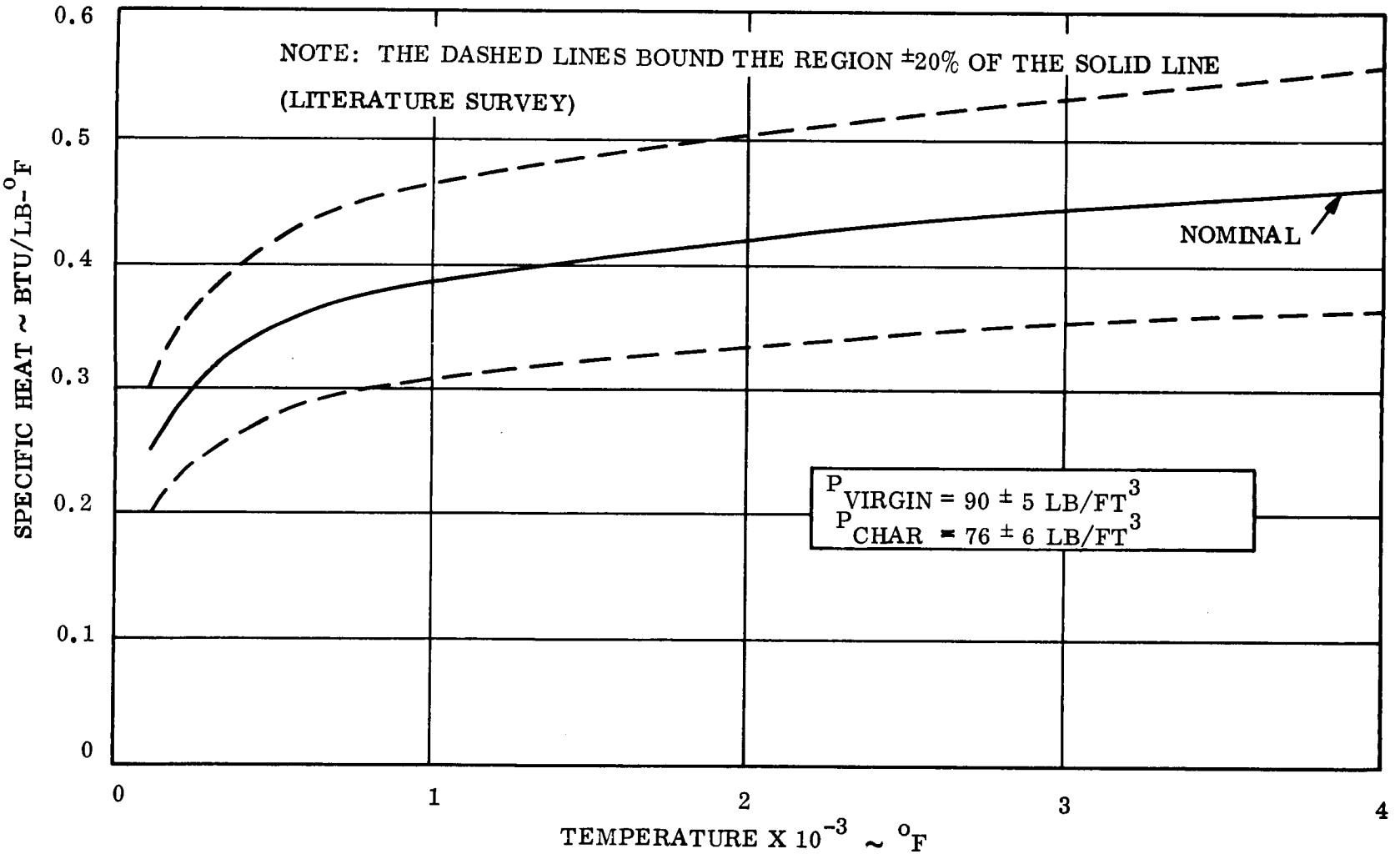

Figure 85. Specific Heat of Graphite Cloth/Phenolic Resin and Graphite Cloth/Epoxy Resin (Literature Survey)

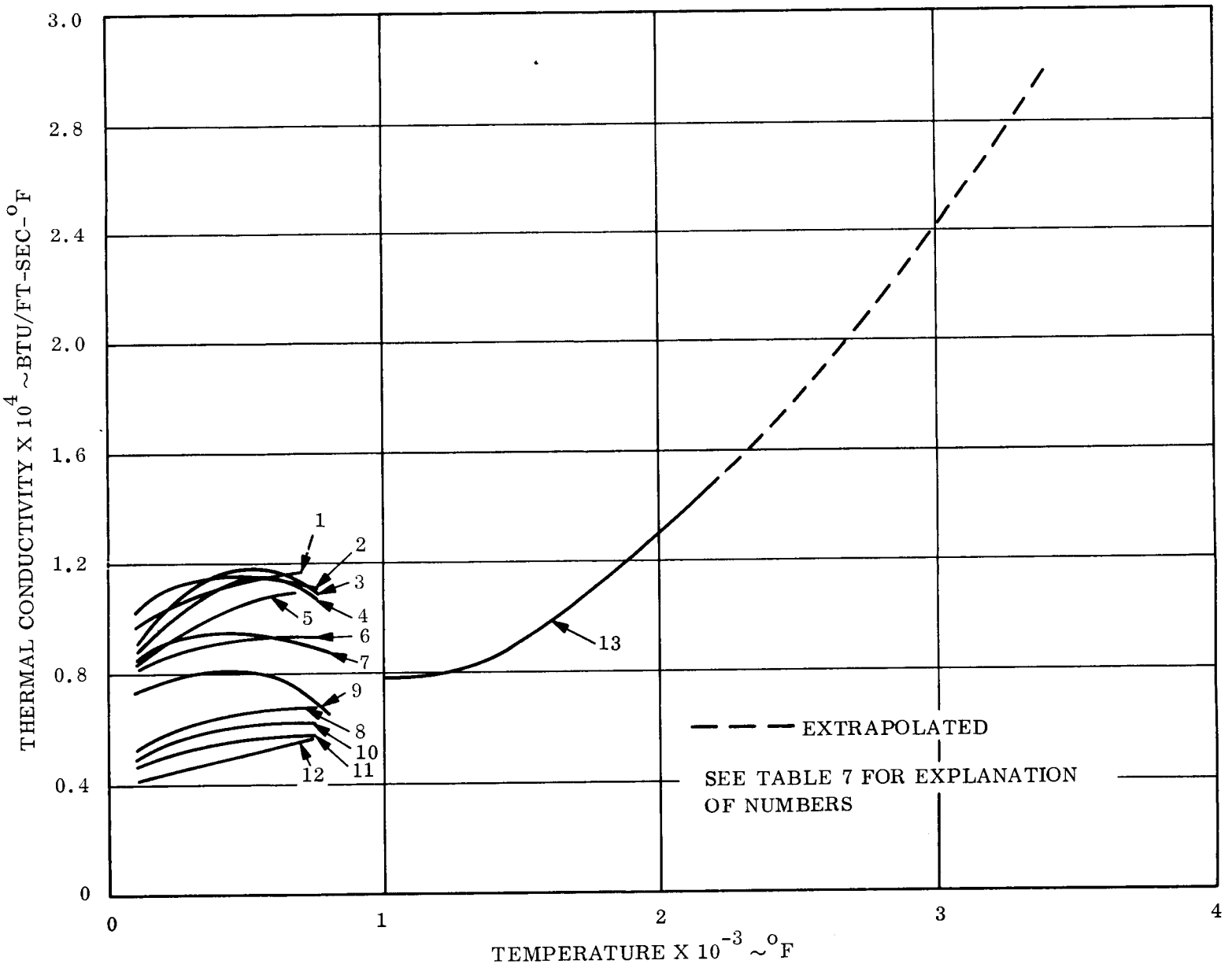

Figure 86. Variations in Thermal Conductivity Due to Changes in Lamination Angle, Resin Content, and Lot-to-Lot Variation of Silica Cloth/Phenolic Resin (Literature Survey)

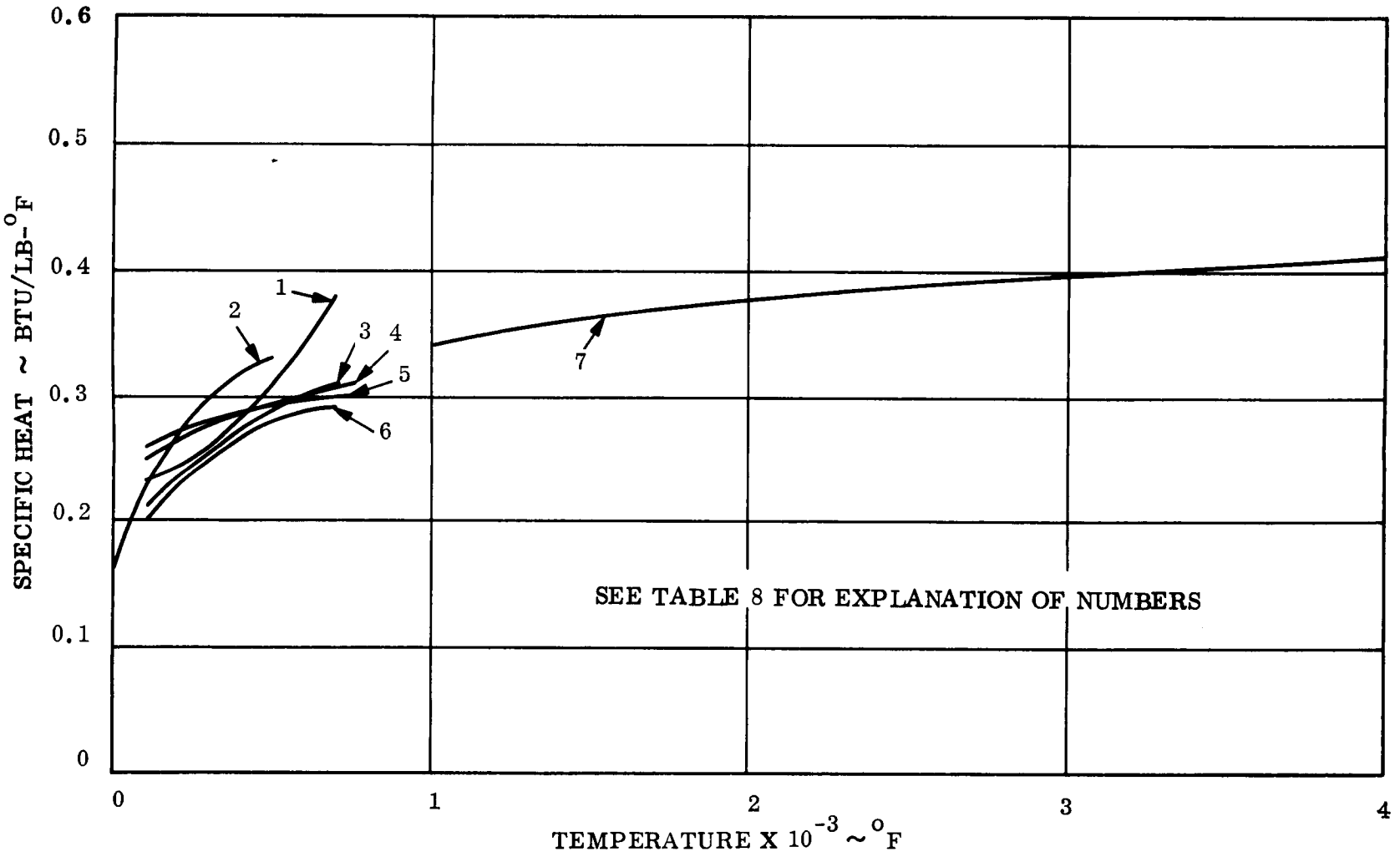

Figure 87. Variations in Specific Heat Due to Changes in Lamination Angle, Resin Content, and Lot-to-Lot Variation of Silica Cloth/Phenolic Resin (Literature Survey)

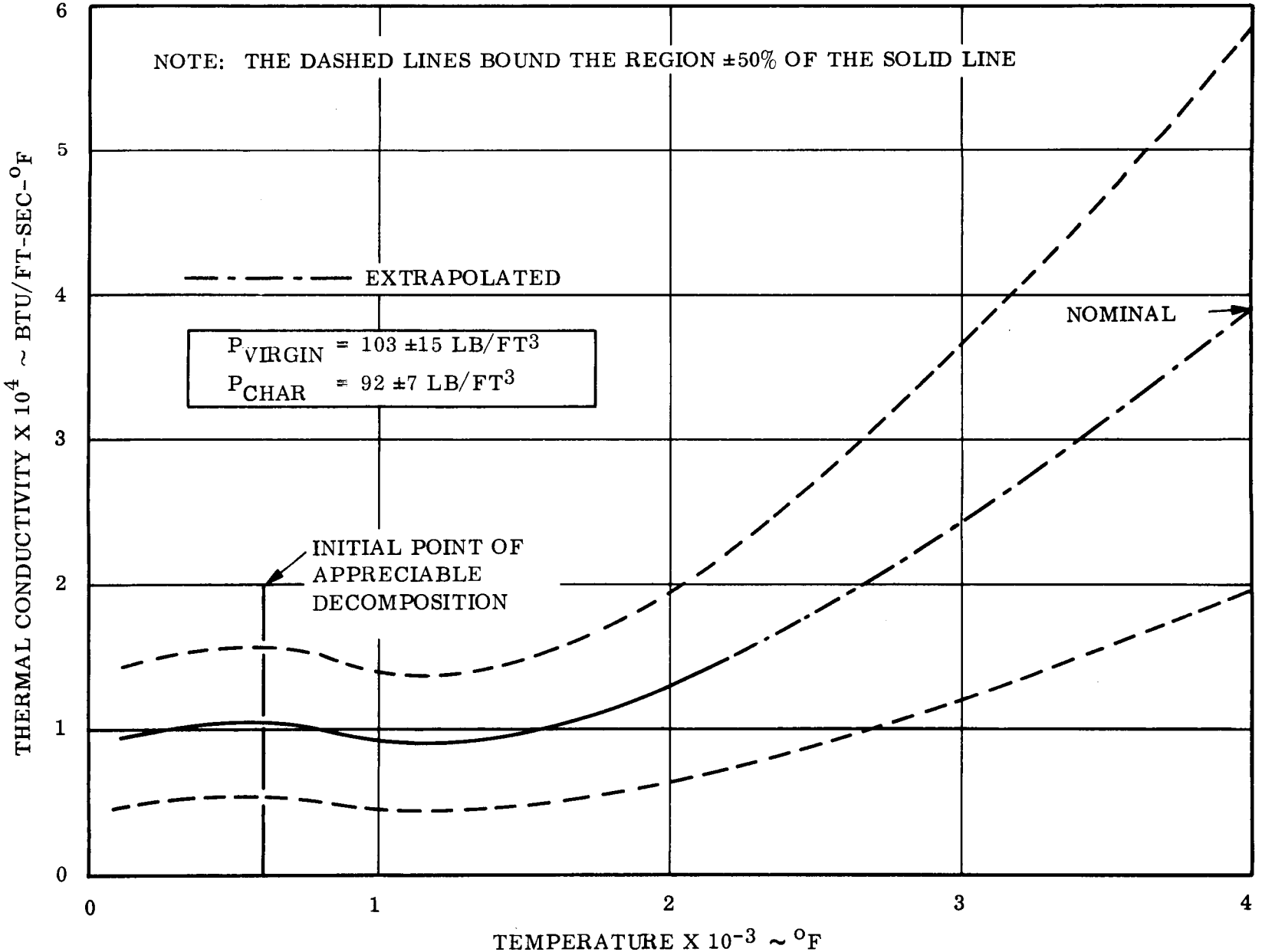

Figure 88. Thermal Conductivity of Silica Cloth/Phenolic Resin (Literature Survey)

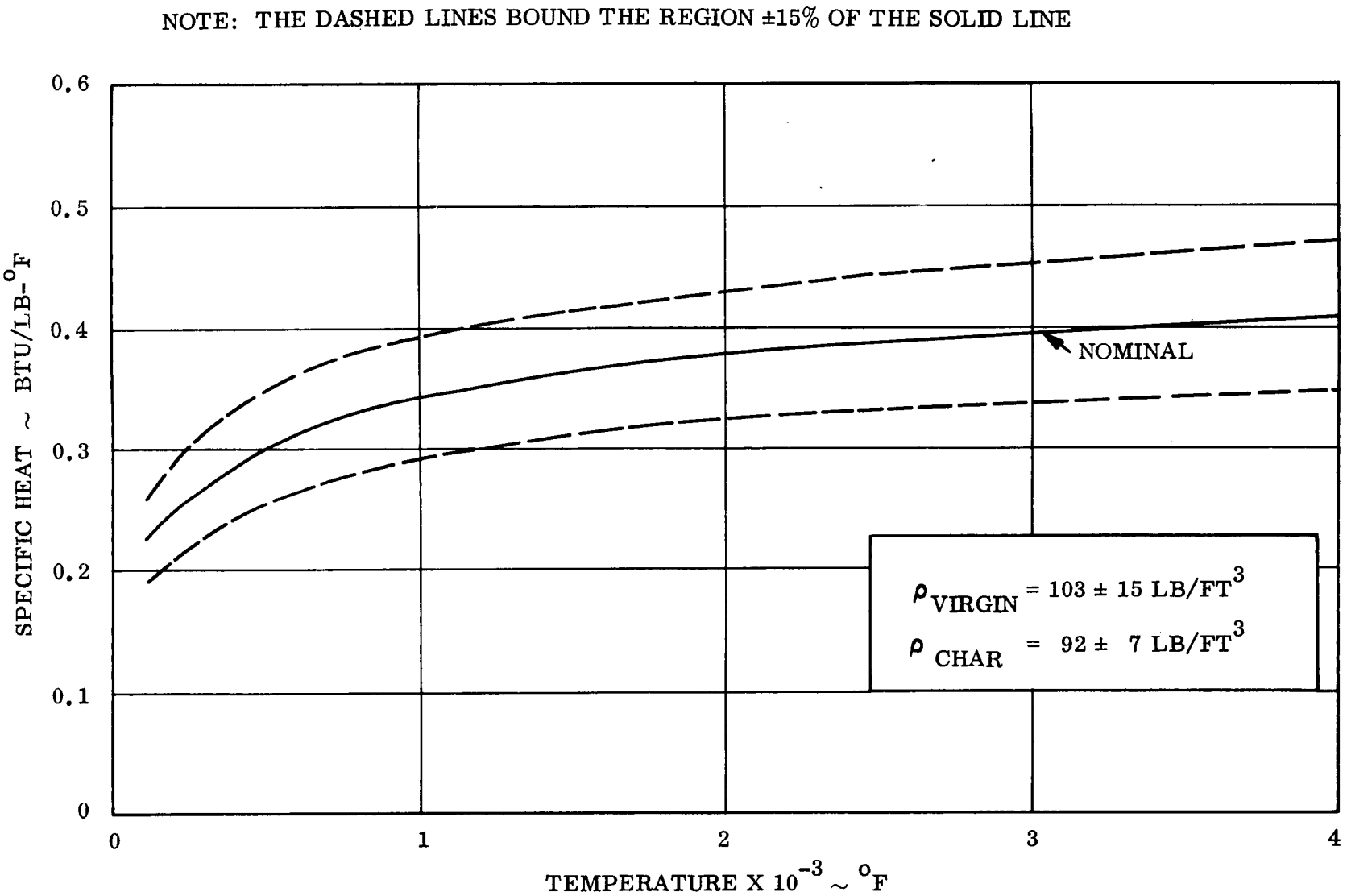

Figure 89. Specific Heat of Silica Cloth/Phenolic Resin (Literature Survey)

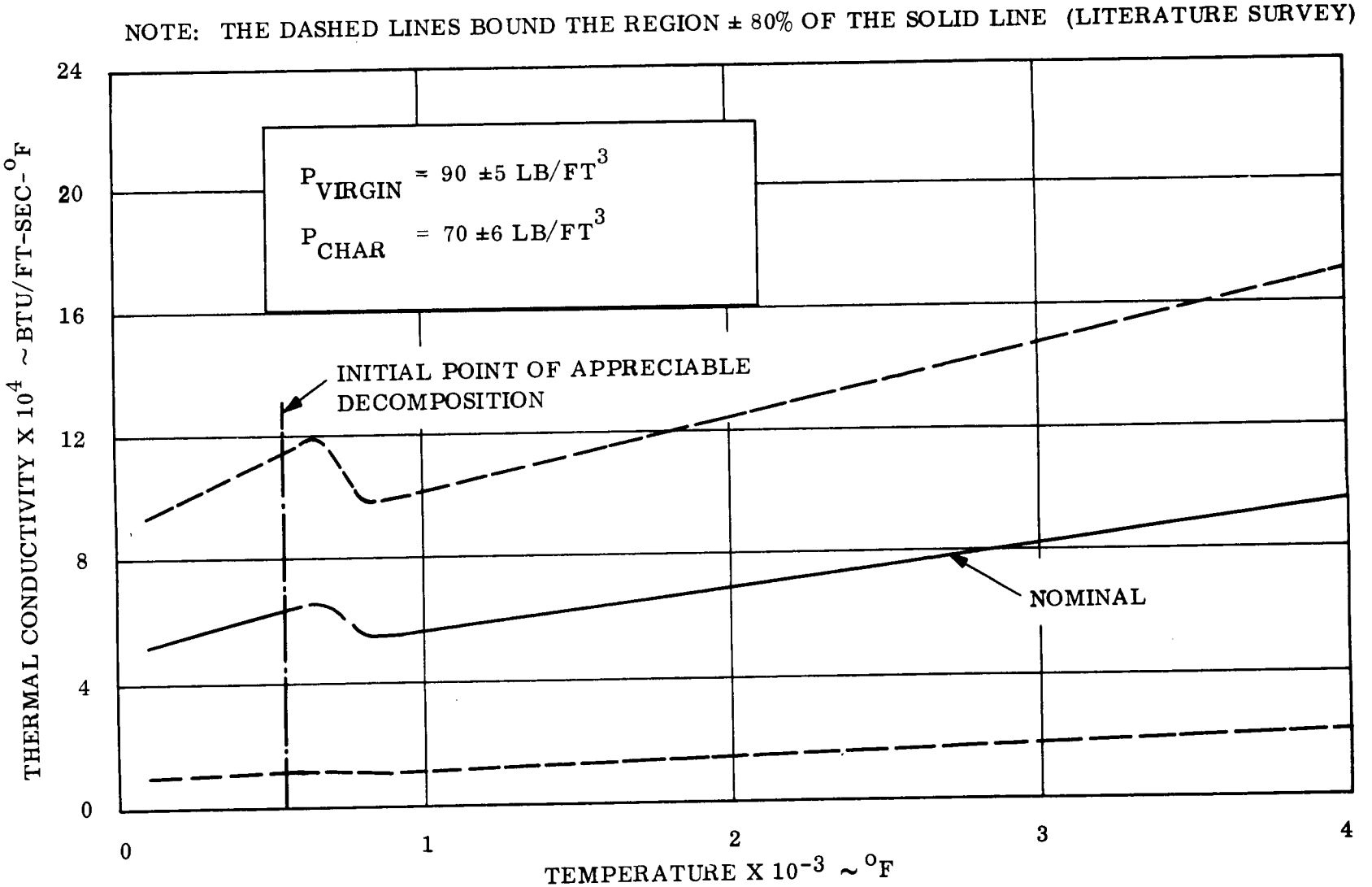

Figure 90. Thermal Conductivity of Graphite Cloth/Epoxy Resin (Literature Survey)

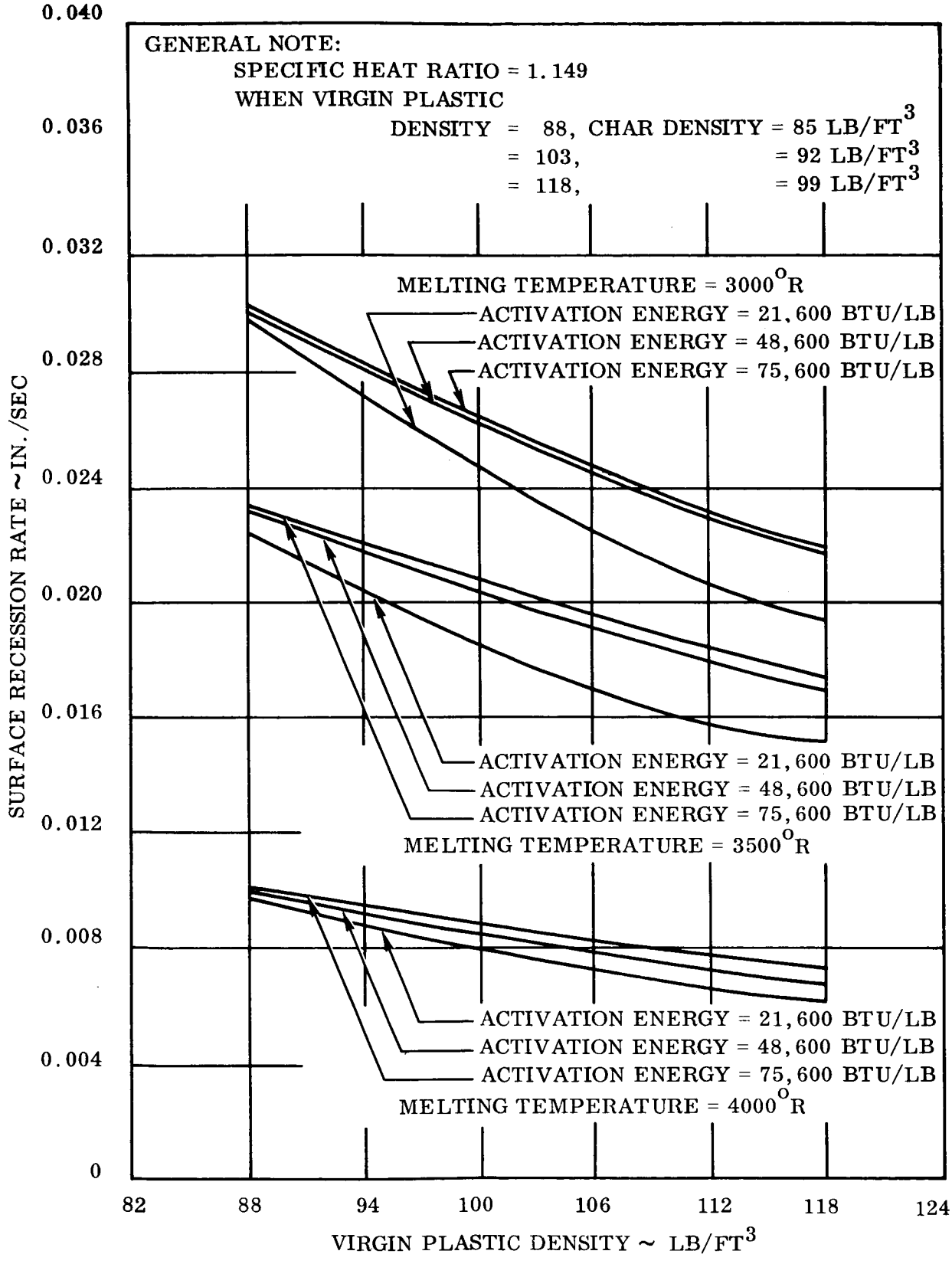

Figure 91. Surface Recession Rate Versus Virgin Plastic Density Silica Cloth/Phenolic Resin A (1.2 Inch Diameter Throat)

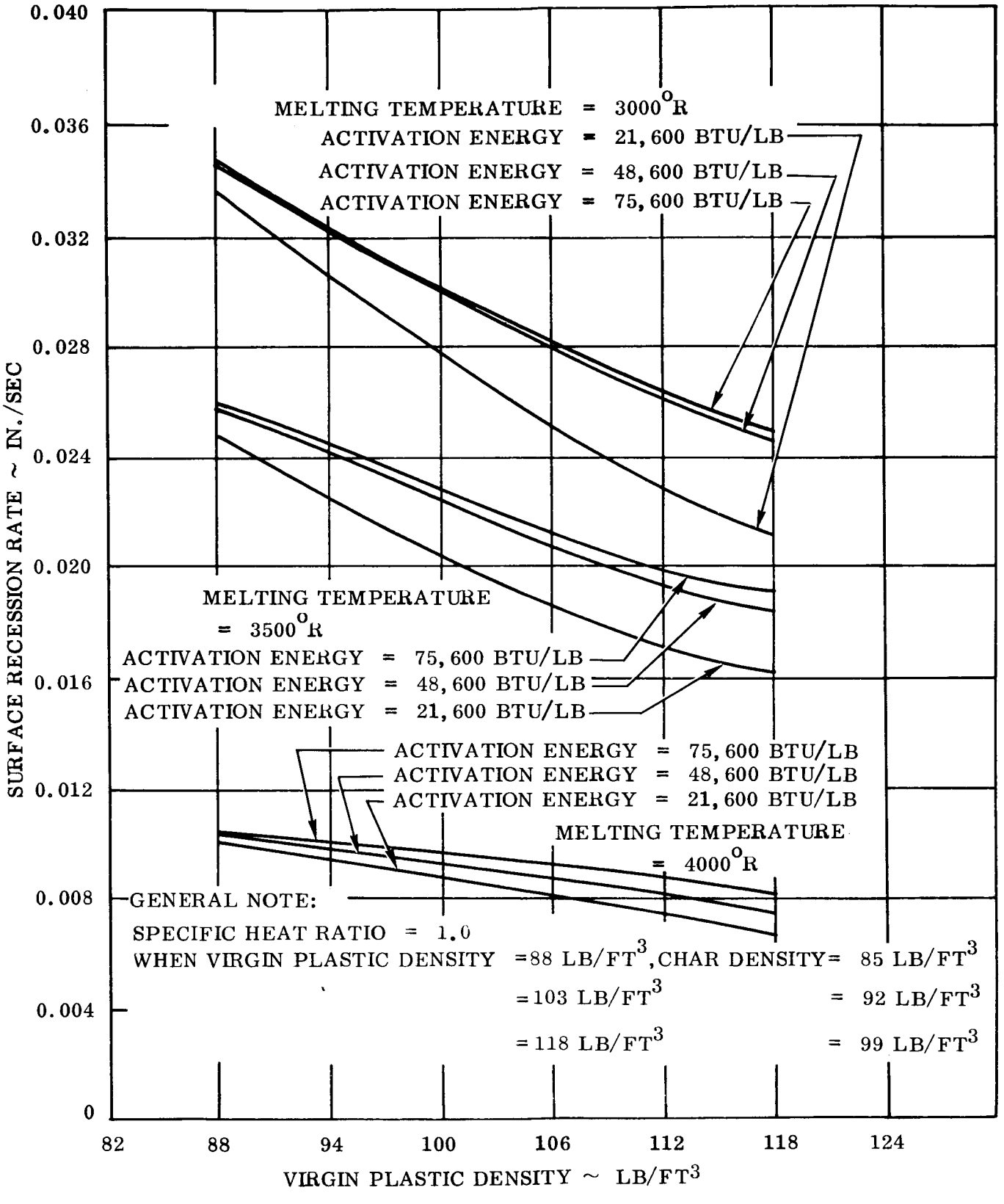

Figure 92. Surface Recession Rate Versus Virgin Plastic Density Silica Cloth/Phenolic Resin A (1.2 Inch Diameter Throat)

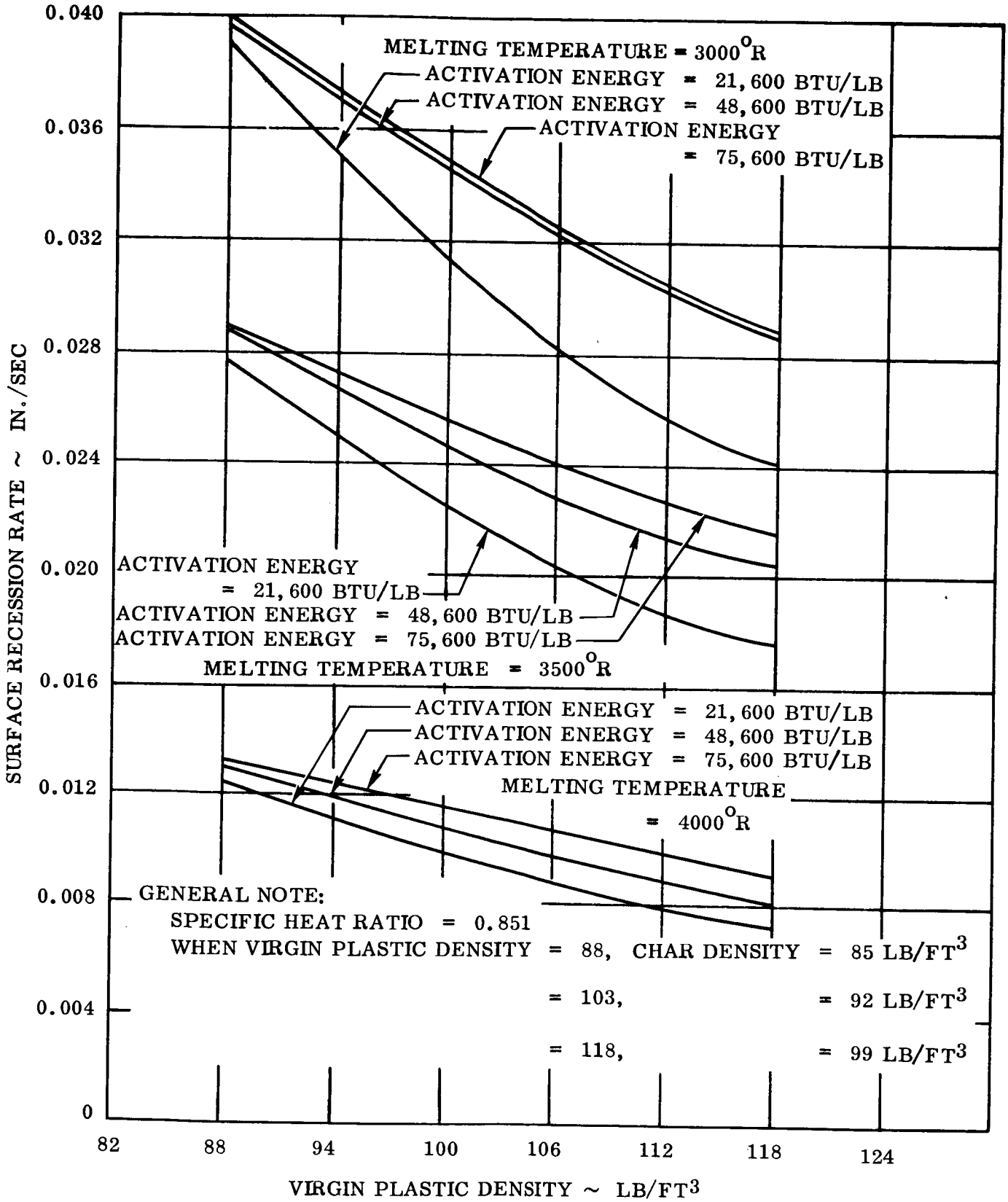

Figure 93. Surface Recession Rate Versus Virgin Plastic Density Silica Cloth/Phenolic Resin A (1.2 Inch Diameter Throat)

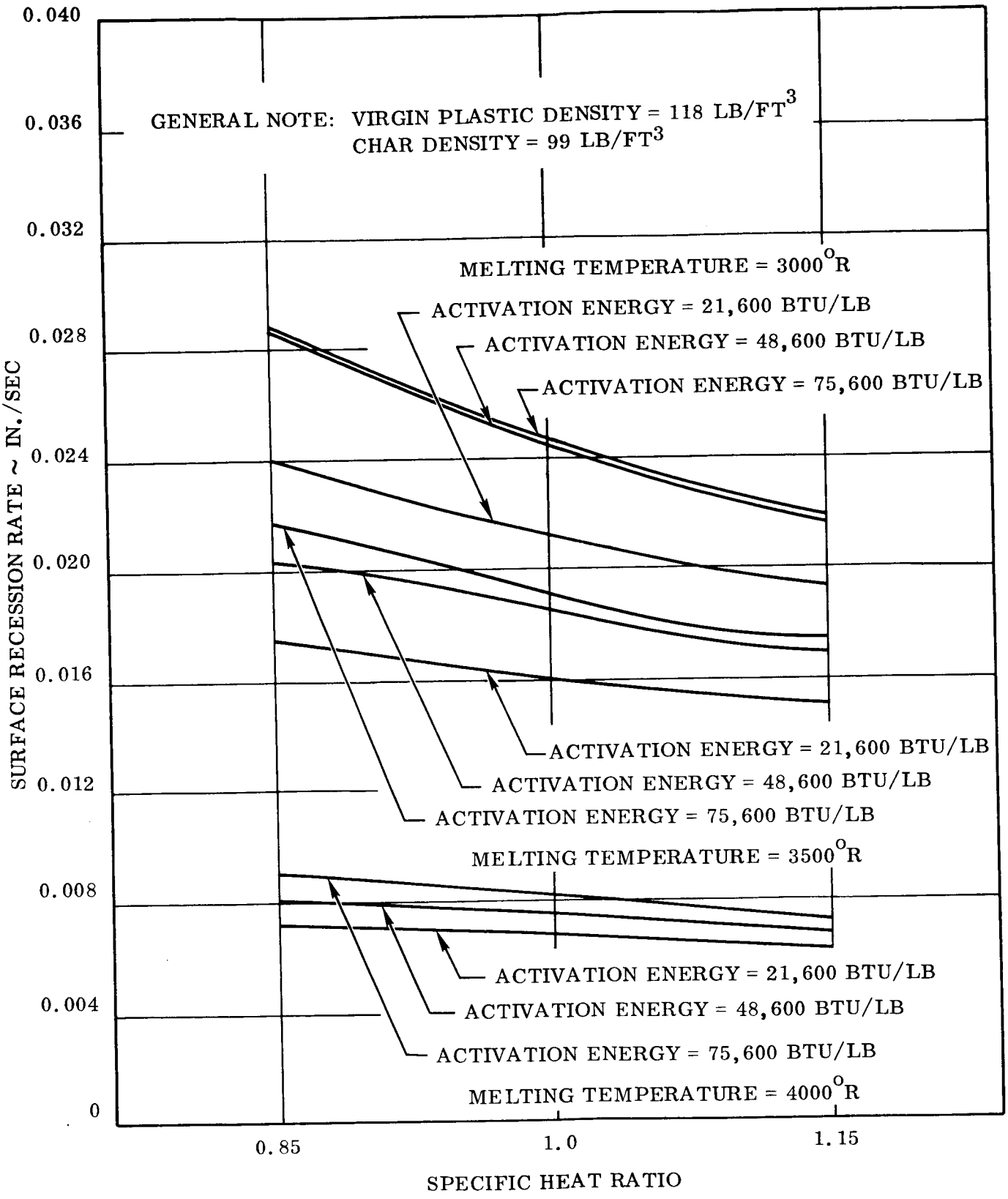

Figure 94. Surface Recession Rate Versus Specific Heat Ratio Silica Cloth/ Phenolic Resin A (1.2 Inch Diameter Throat)

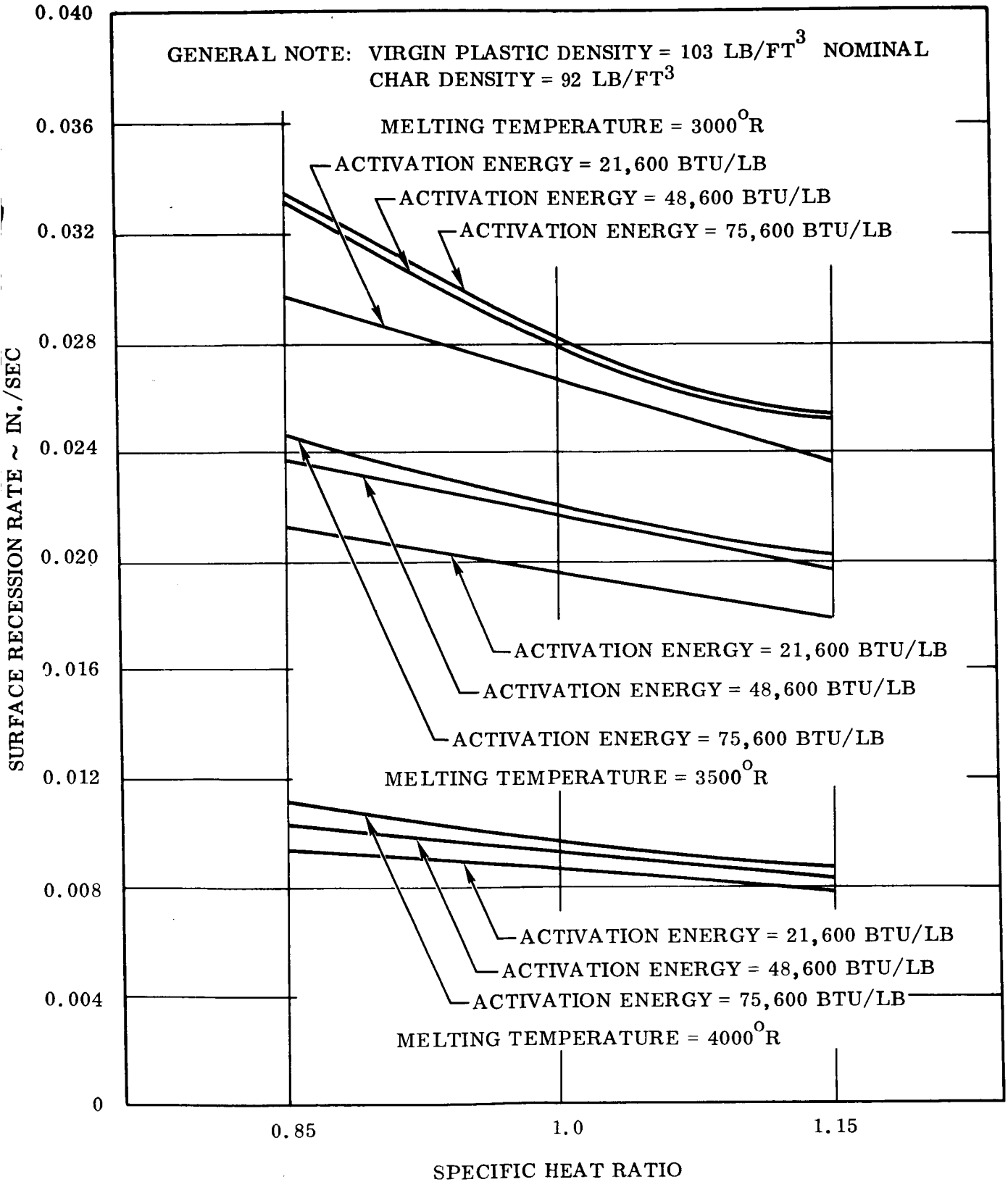

Figure 95. Surface Recession Rate Versus Specific Heat Ratio Silica Cloth/ Phenolic Resin A (1.2 Inch Diameter Throat)

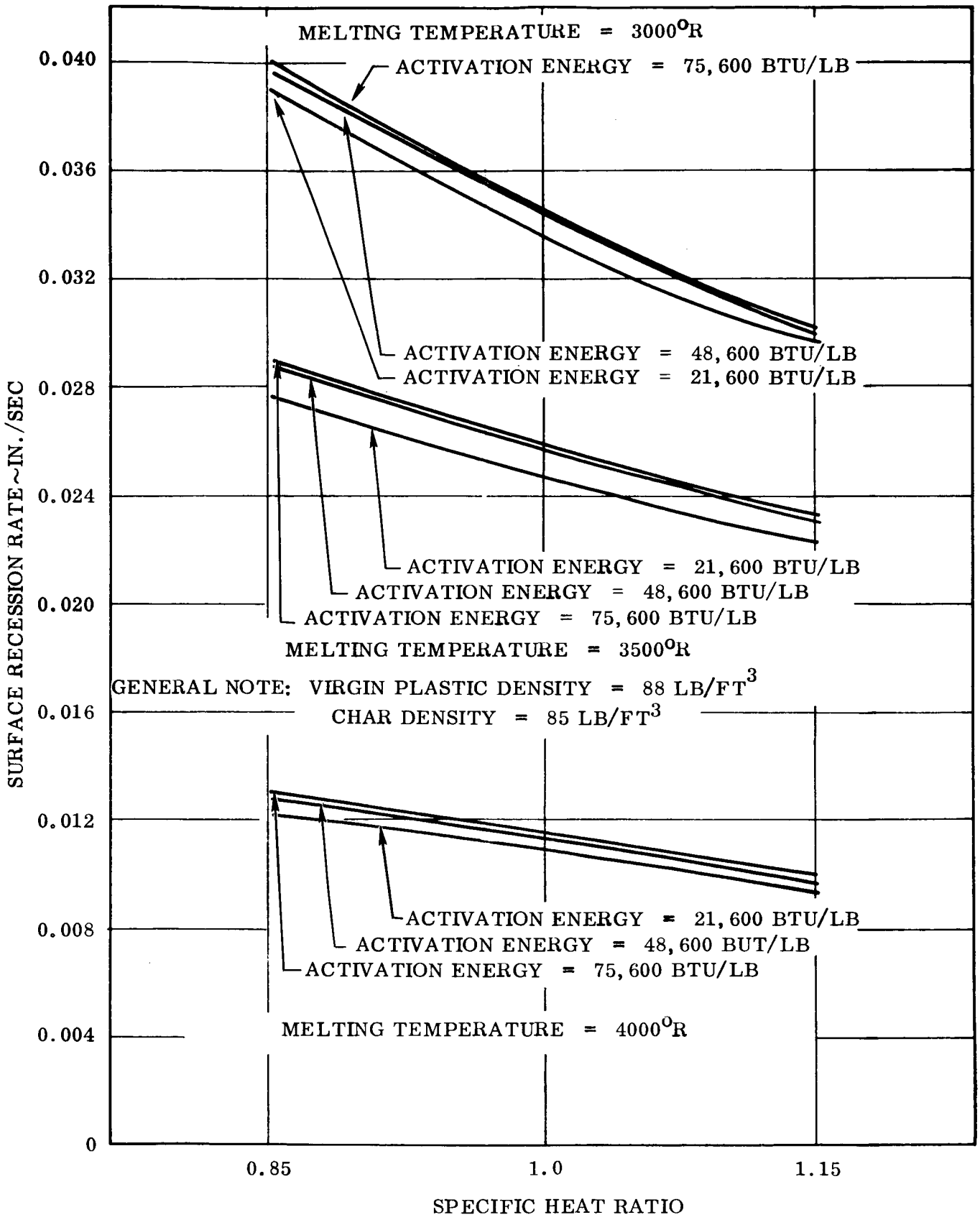

Figure 96. Surface Recession Rate Versus Specific Heat Ratio Silica Cloth/ Phenolic Resin A (1.2 Inch Diameter Throat)

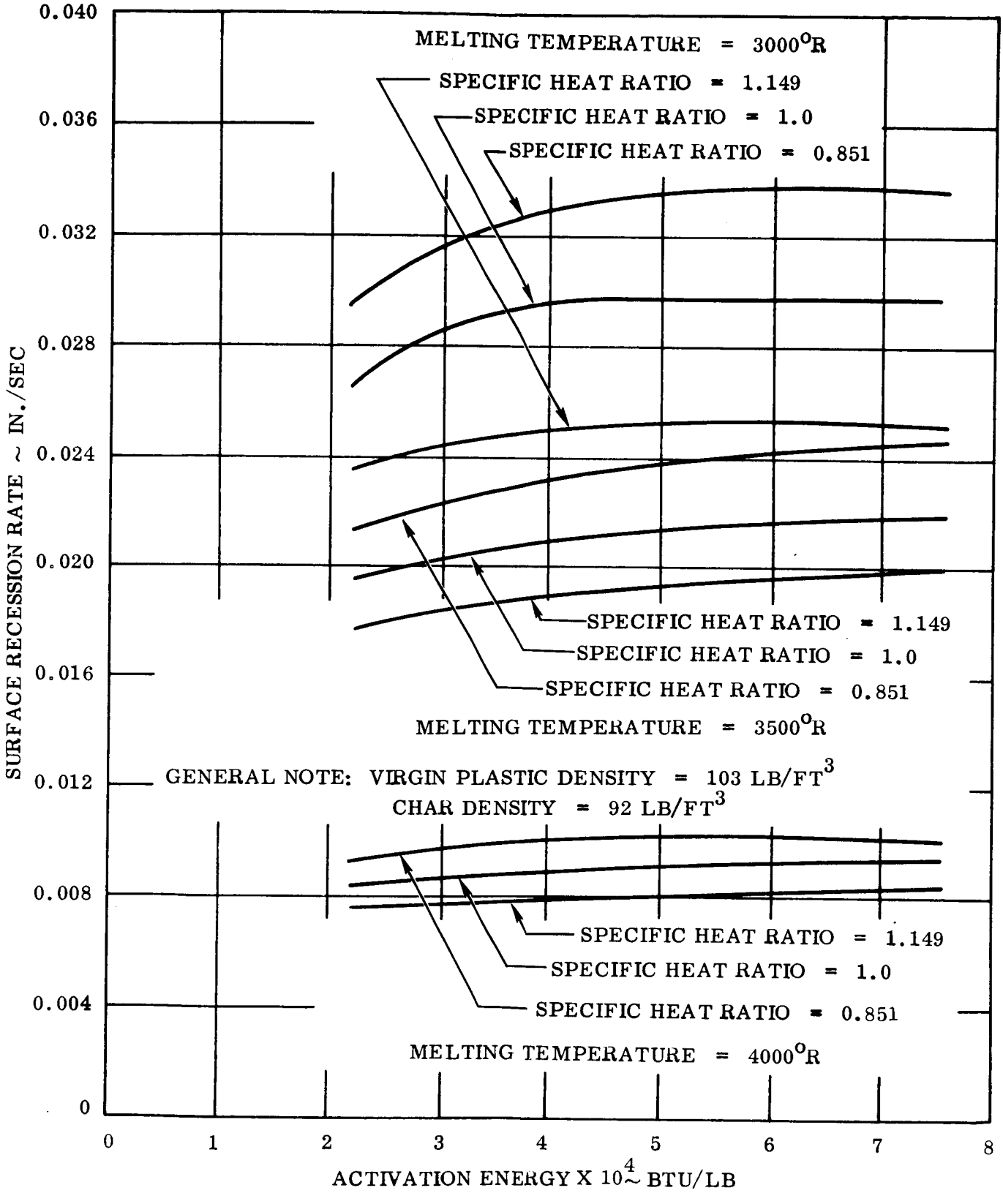

Figure 97. Surface Recession Rate Versus Activation Energy Silica Cloth/Phenolic Resin A (1.2 Inch Diameter Throat)

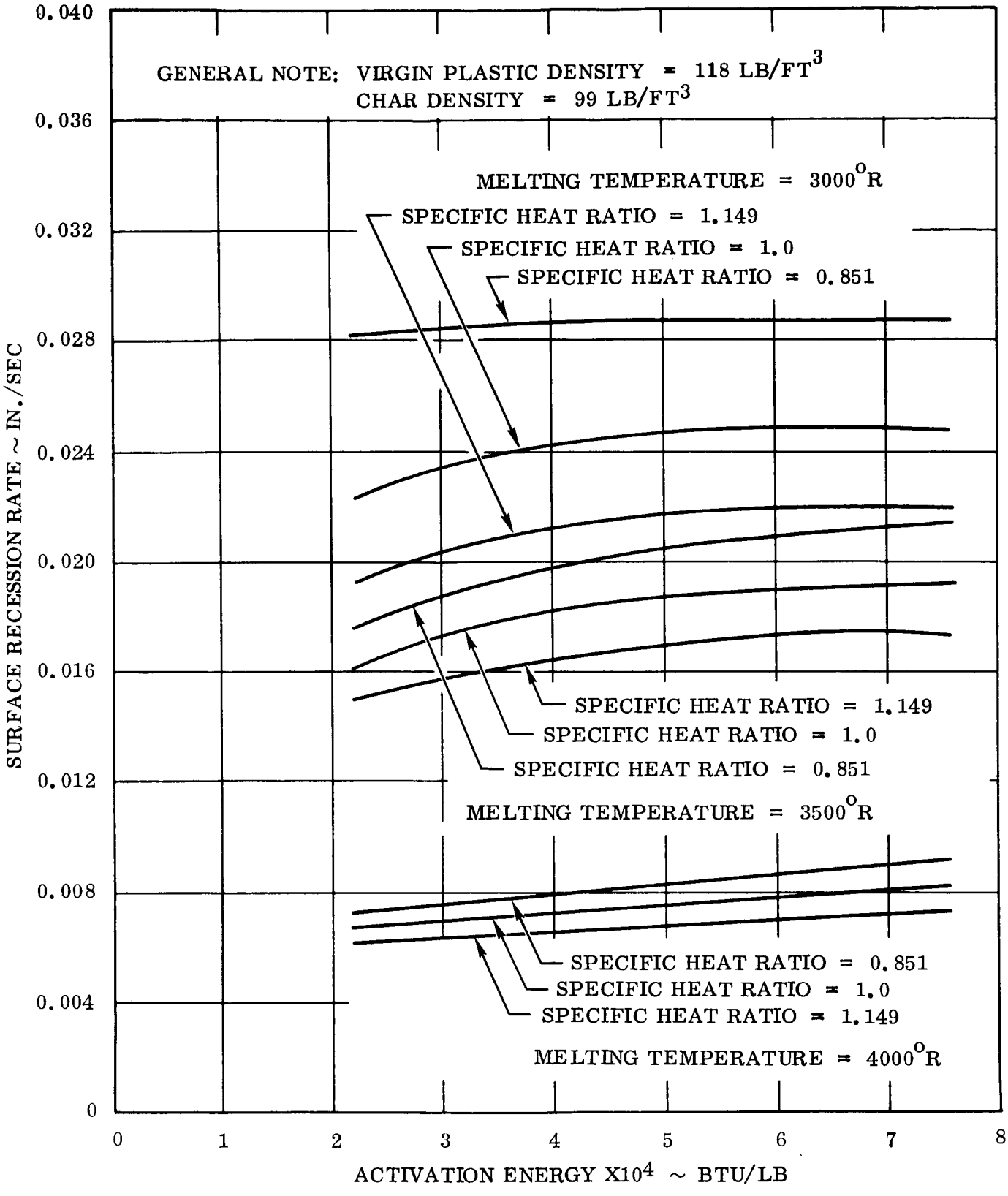

Figure 98. Surface Recession Rate Versus Activation Energy Silica Cloth/Phenolic Resin A (1.2 Inch Diameter Throat)

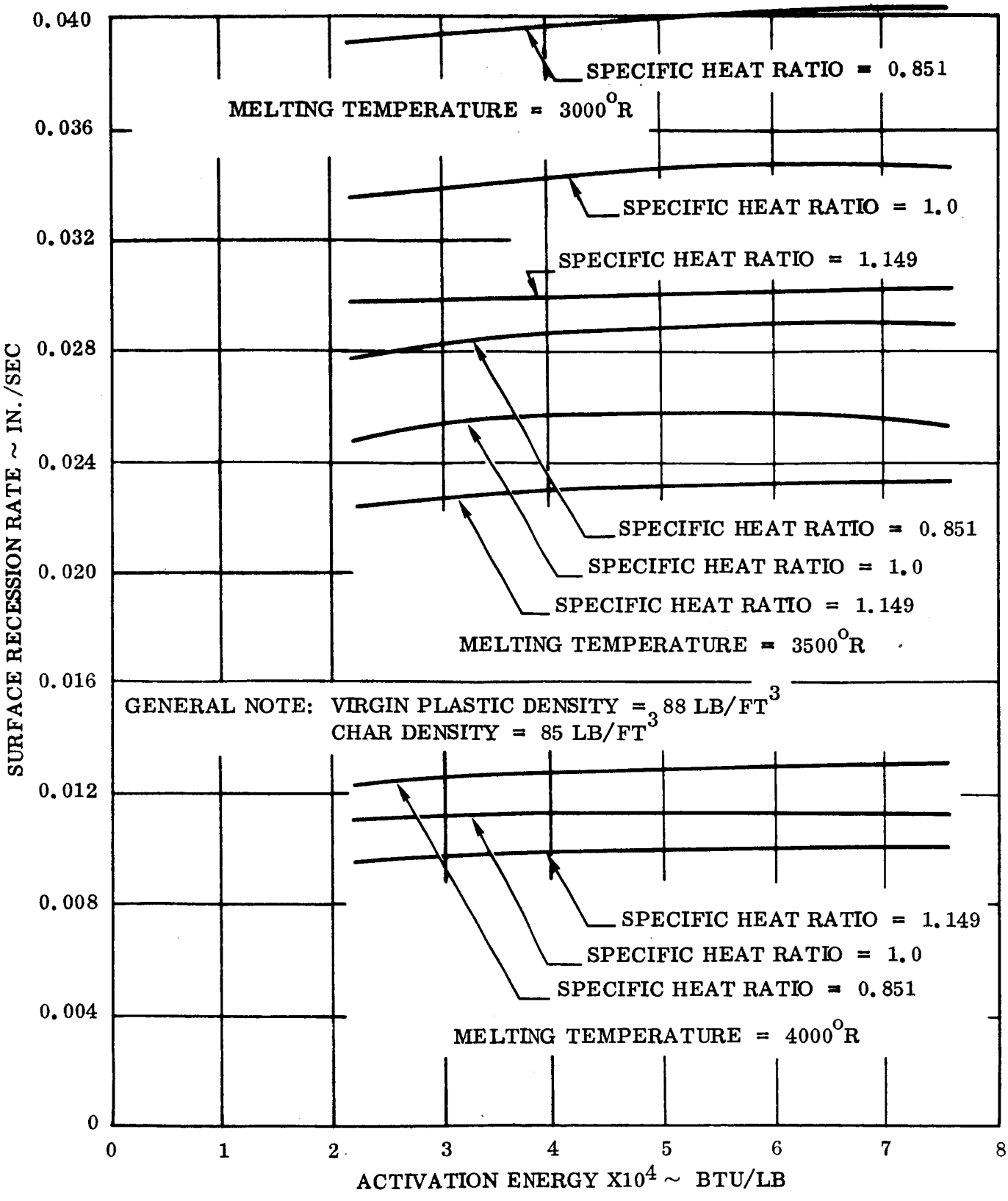

Figure 99. Surface Recession Rate Versus Activation Energy Silica Cloth/Phenolic Resin A (1.2 Inch Diameter Throat)

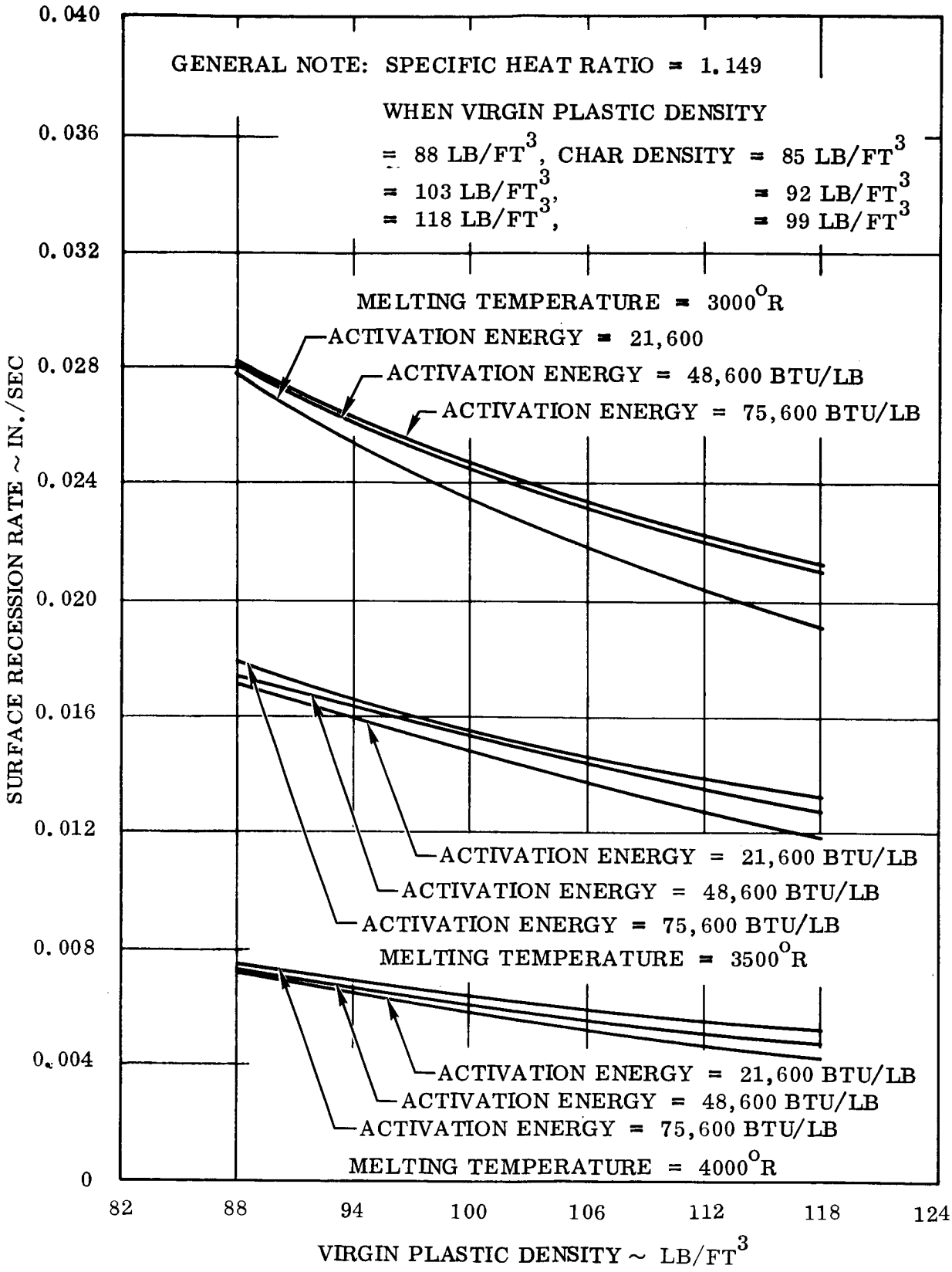

Figure 100. Surface Recession Rate Versus Virgin Plastic Density Silica Cloth/ Phenolic Resin B (7.82 Inch Diameter Throat)

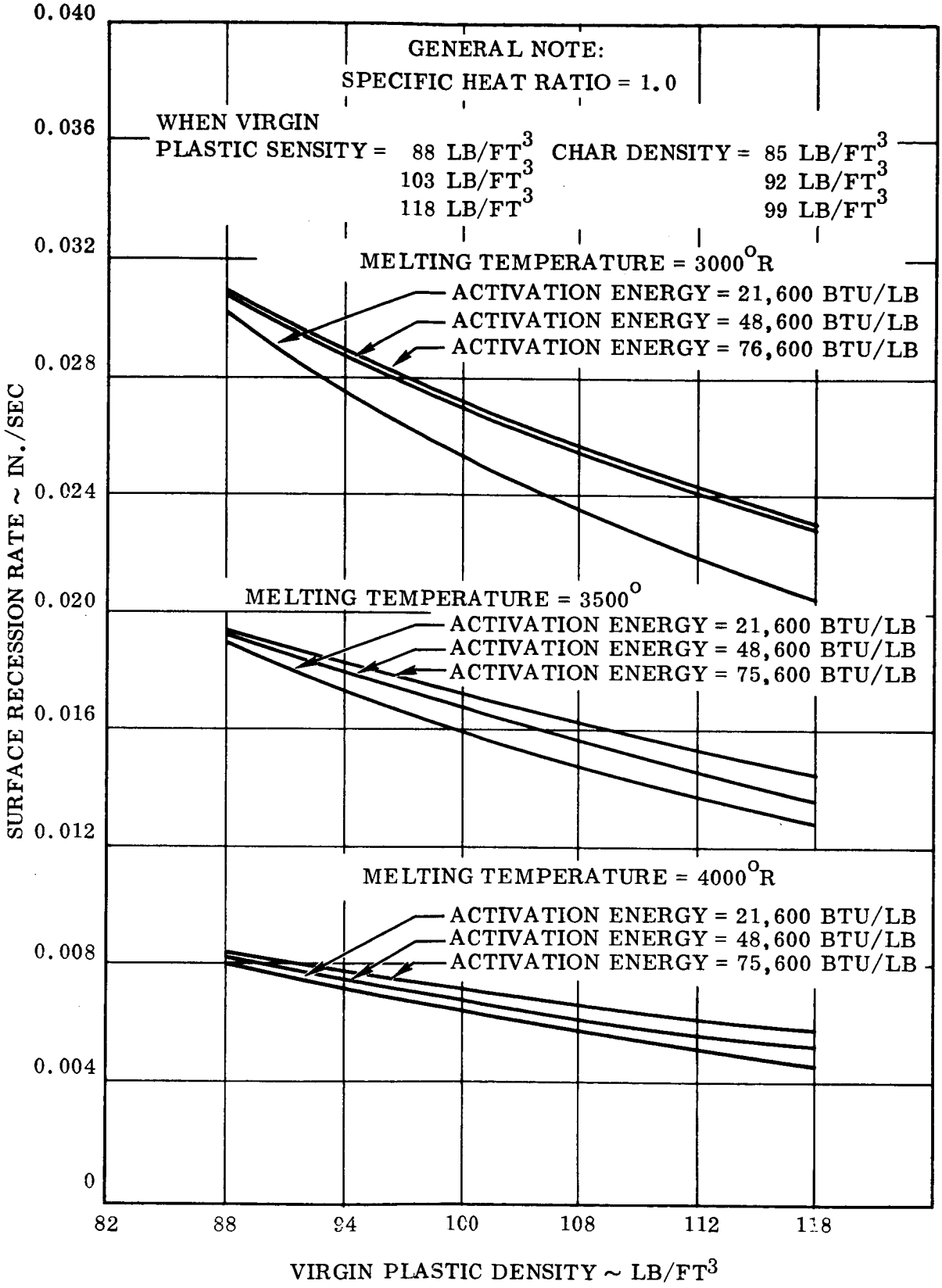

Figure 101. Surface Recession Rate Versus Virgin Plastic Density Silica Cloth/ Phenolic Resin B (7.82 Inch Diameter Throat)

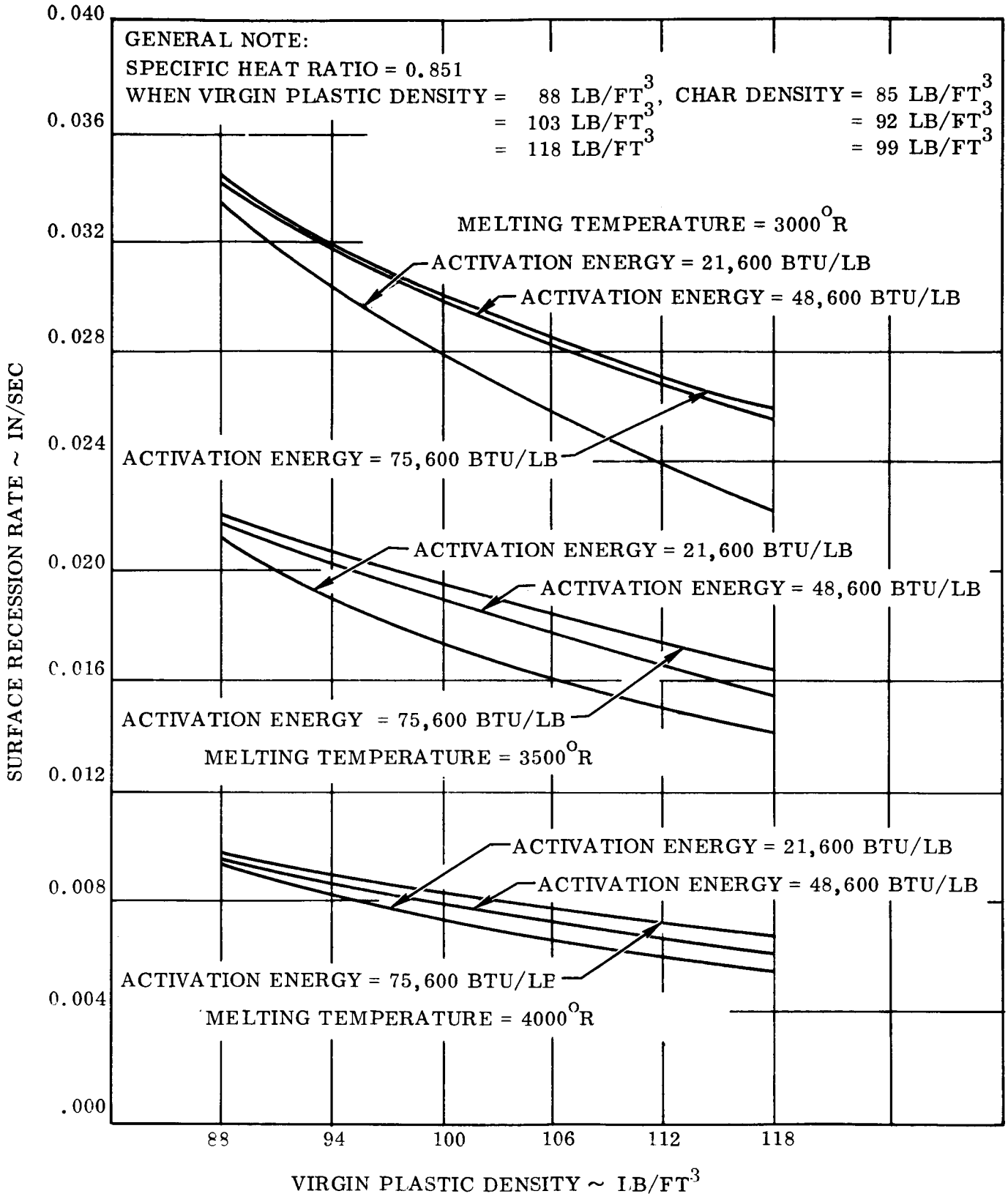

Figure 102. Surface Recession Rate Versus Virgin Plastic Density Silica Cloth/ Phenolic Resin B (7.82 Inch Diameter Throat)

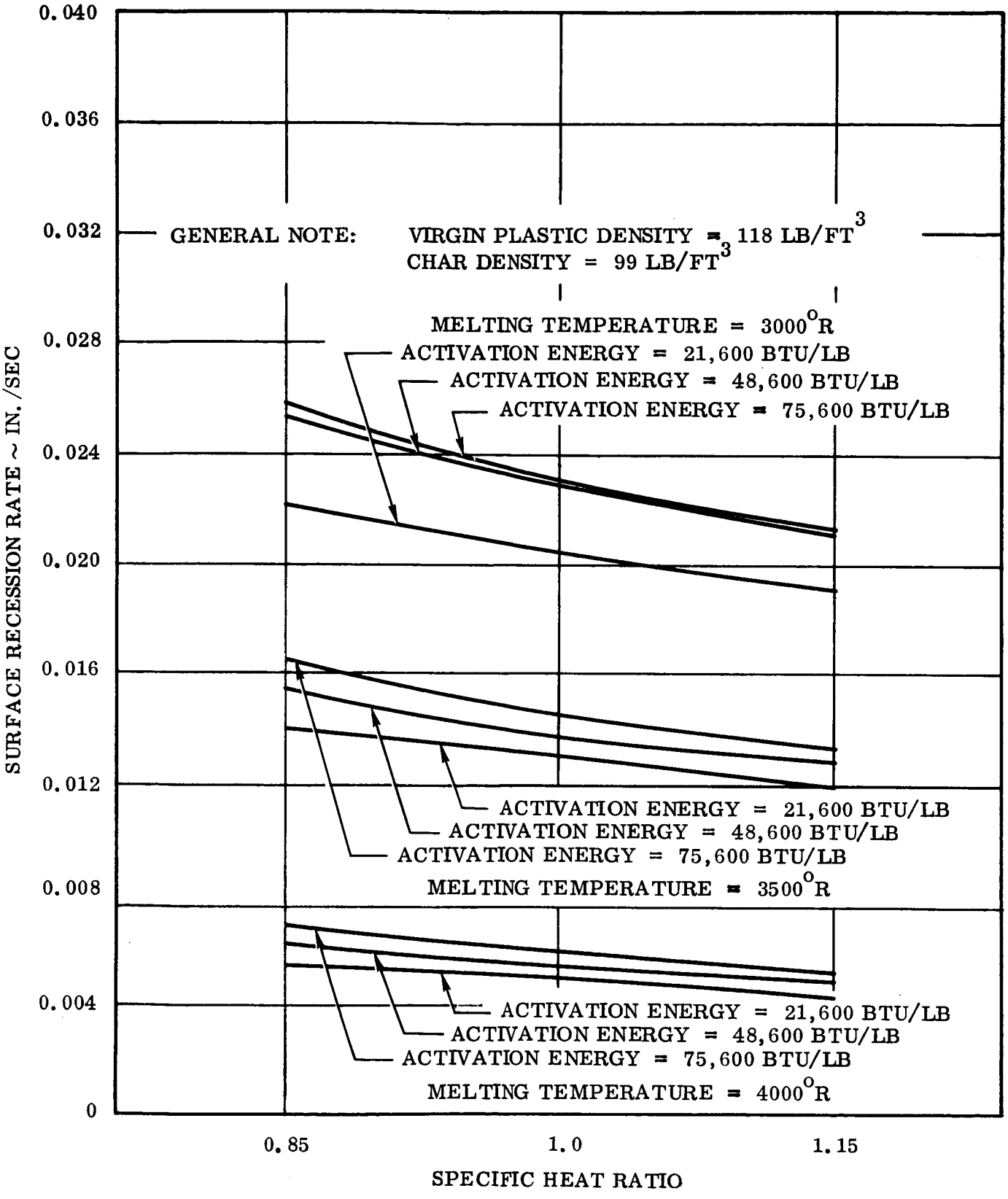

Figure 103. Surface Recession Rate Versus Specific Heat Ratio
Silica Cloth/Phenolic Resin B
(7.82 Inch Diameter Throat)

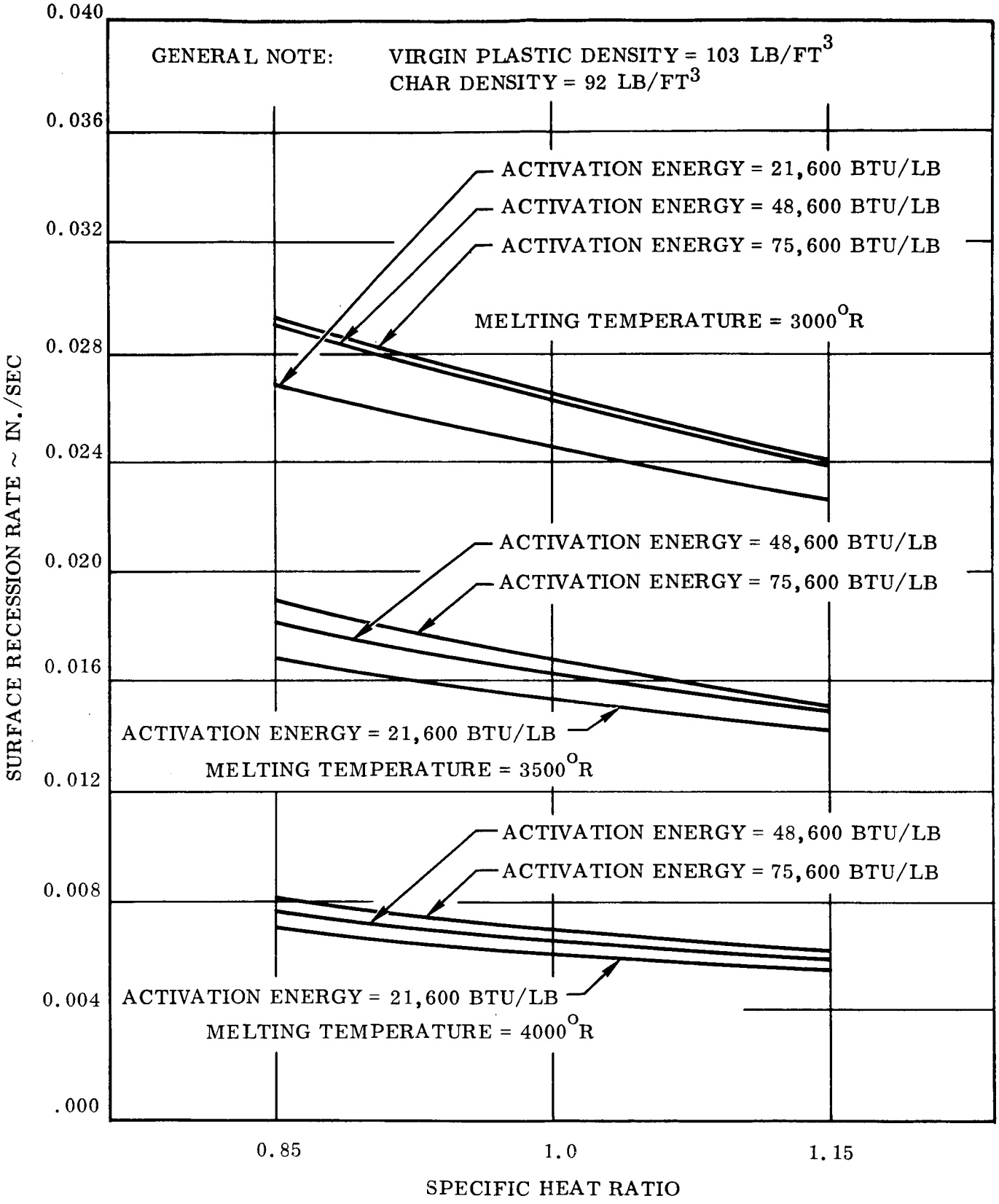

Figure 104. Surface Recession Rate Versus Specific Heat Ratio
Silica Cloth/Phenolic Resin B
(7.82 Inch Diameter Throat)

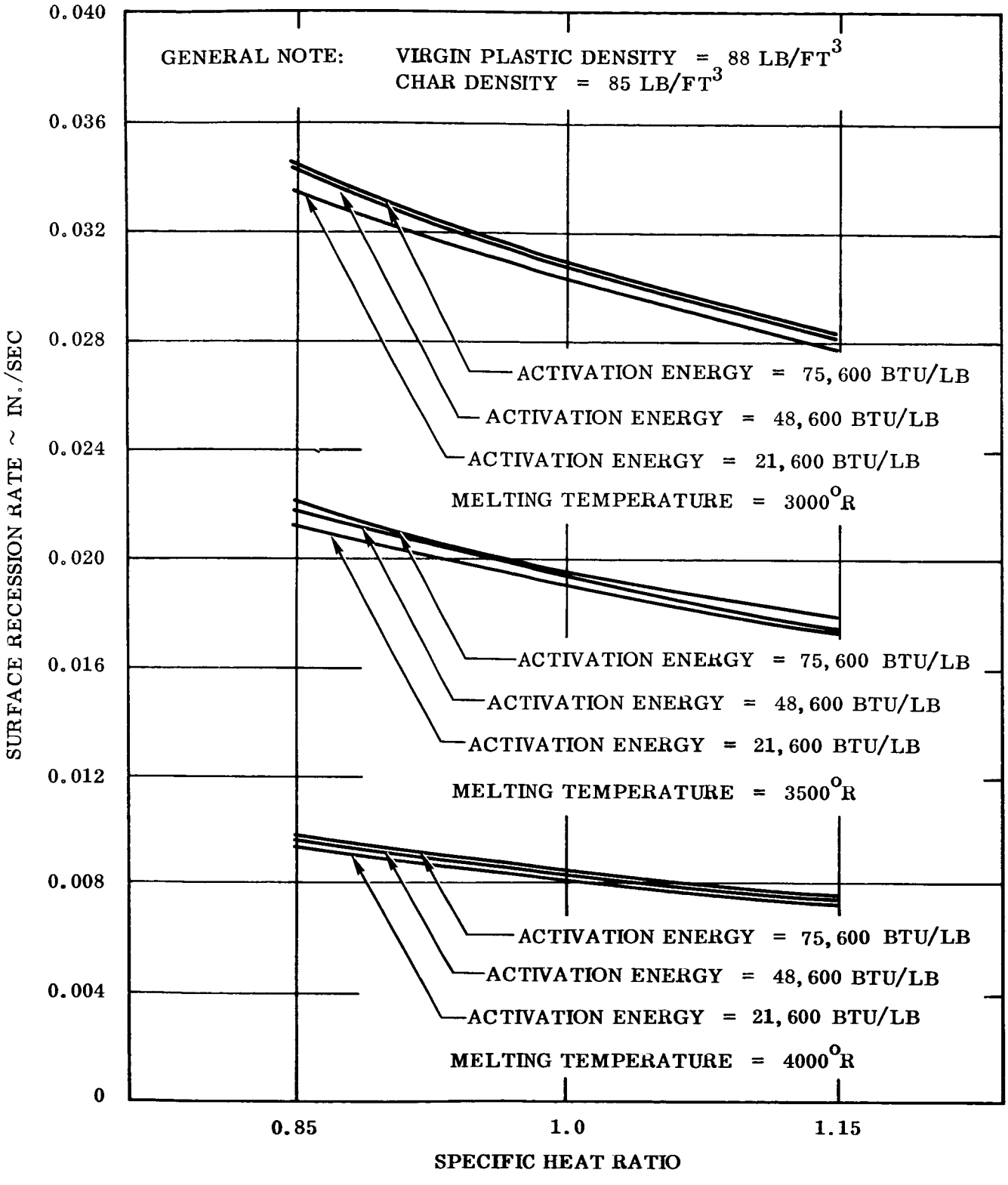

Figure 105. Surface Recession Rate Versus Specific Heat Ratio Silica Cloth/Phenolic Resin B (7.82 Inch Diameter Throat)

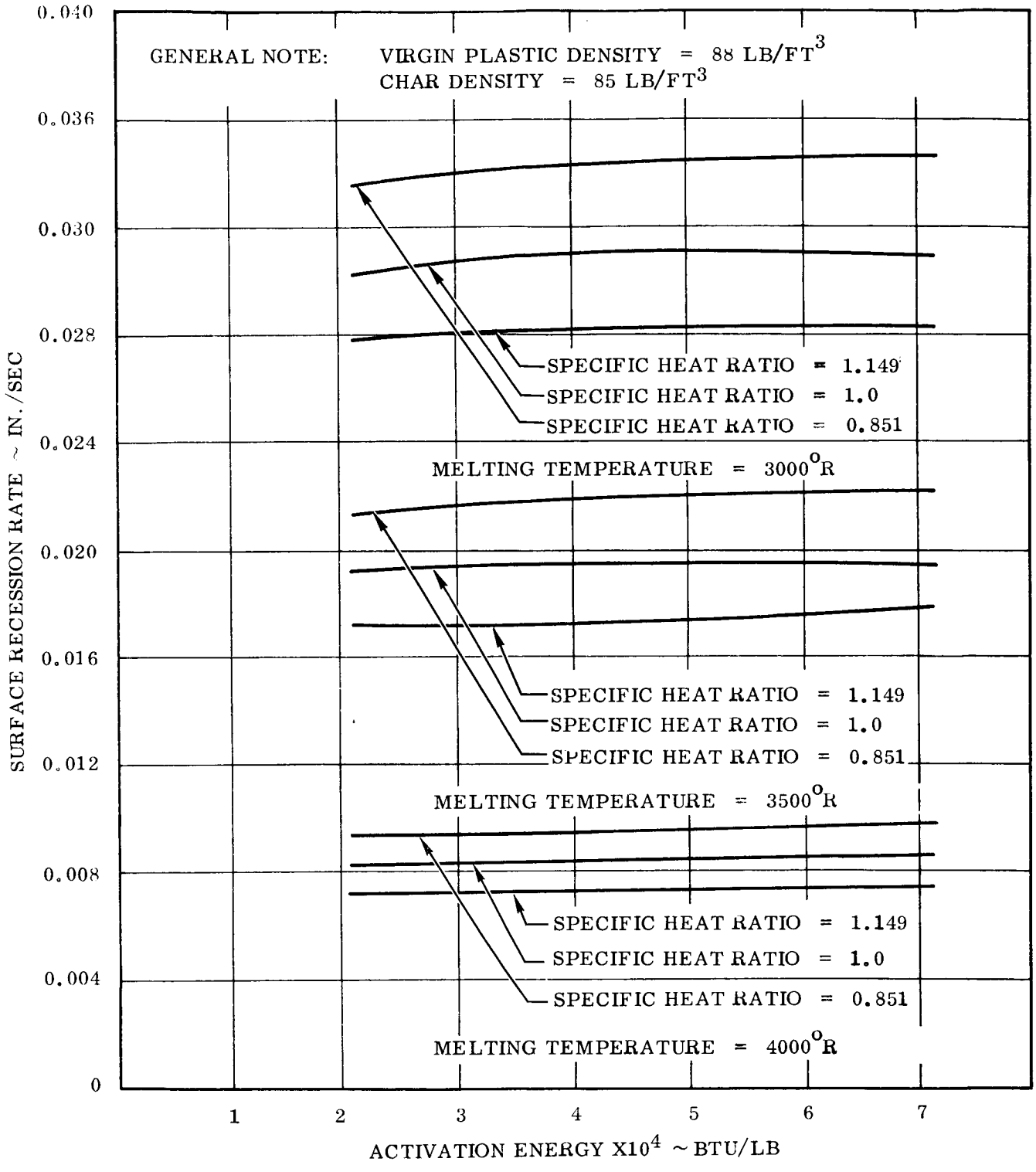

Figure 106. Surface Recession Rate Versus Activation Energy
Silica Cloth/Phenolic Resin B
(7.82 Inch Diameter Throat)

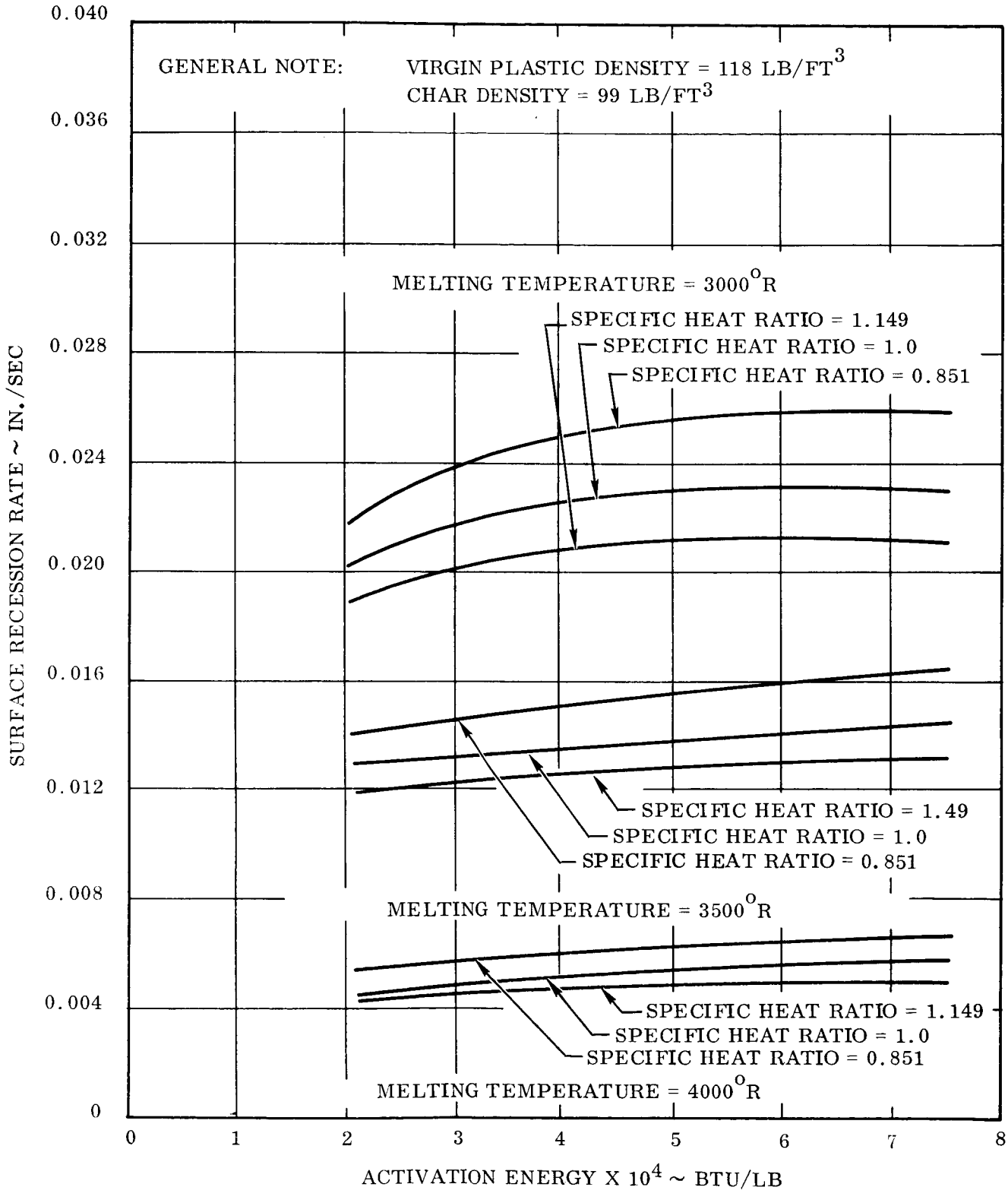

Figure 108. Surface Recession Rate Versus Activation Energy
Silica Cloth/Phenolic Resin B
(7.82 Inch Diameter Throat)

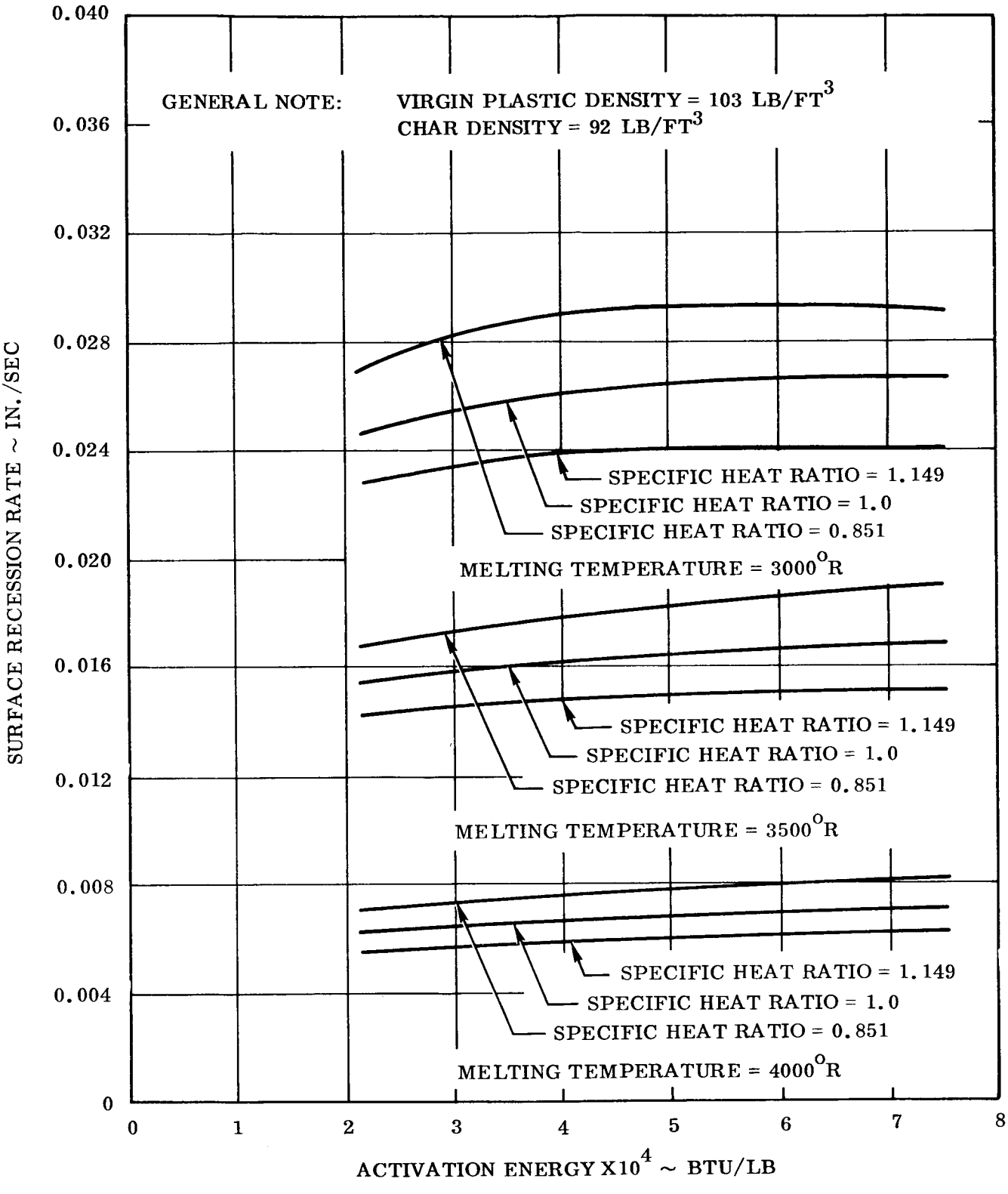

Figure 107. Surface Recession Rate Versus Activation Energy Silica Cloth/Phenolic Resin B (7.82 Inch Diameter Throat)

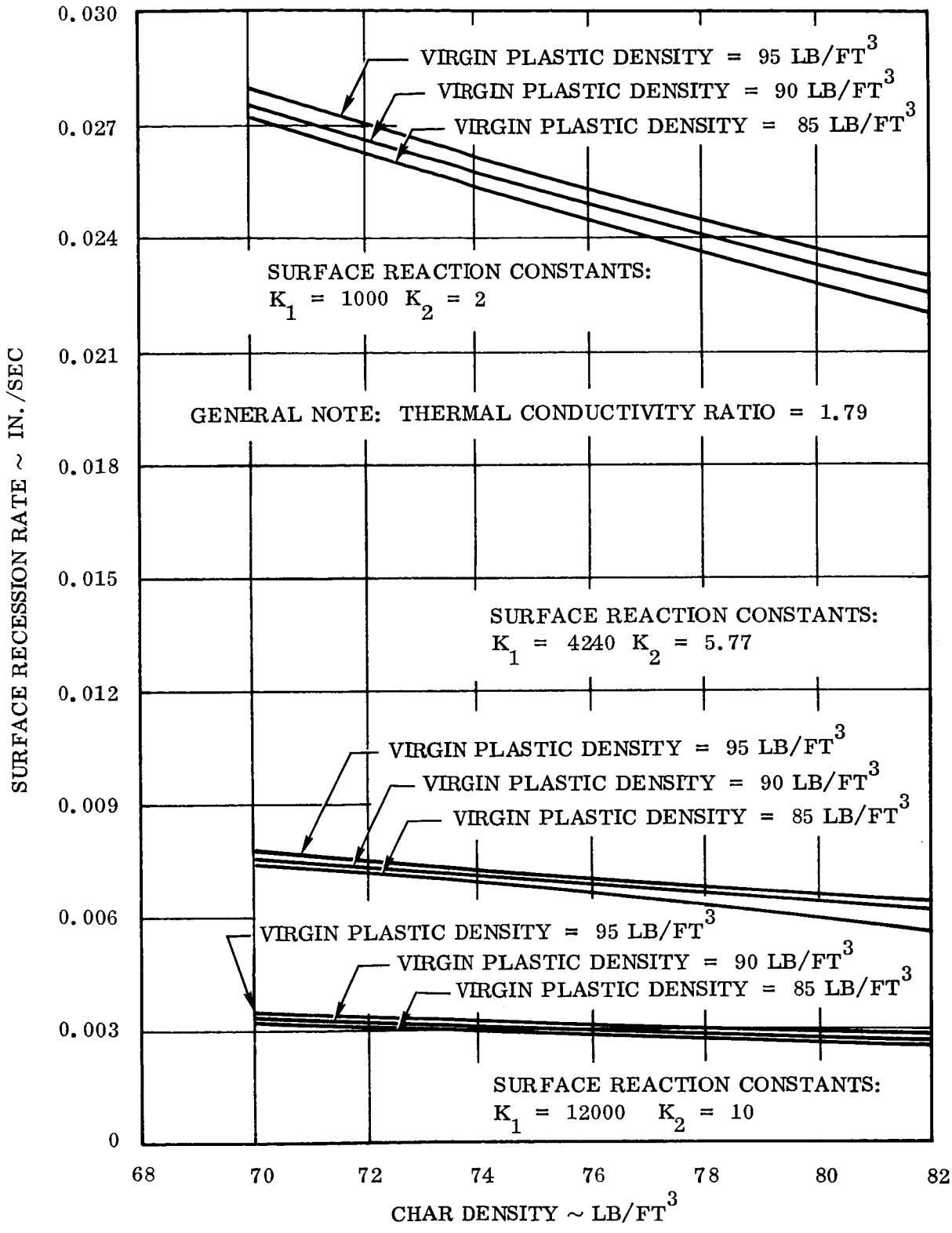

Figure 109. Surface Recession Rate Versus Char Density
Graphite Cloth/Phenolic Resin

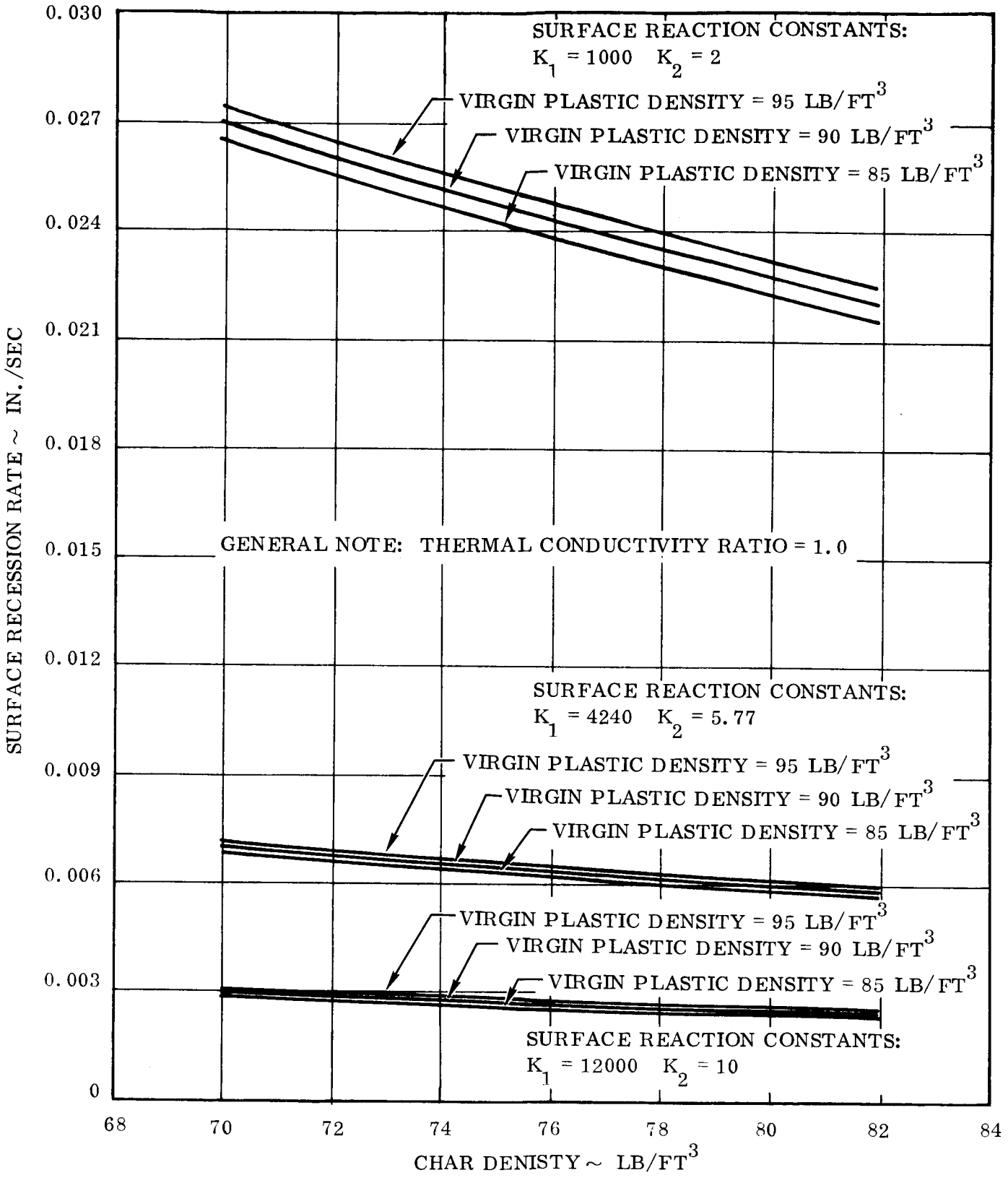

Figure 110. Surface Recession Rate Versus Char Density
Graphite Cloth/Phenolic Resin

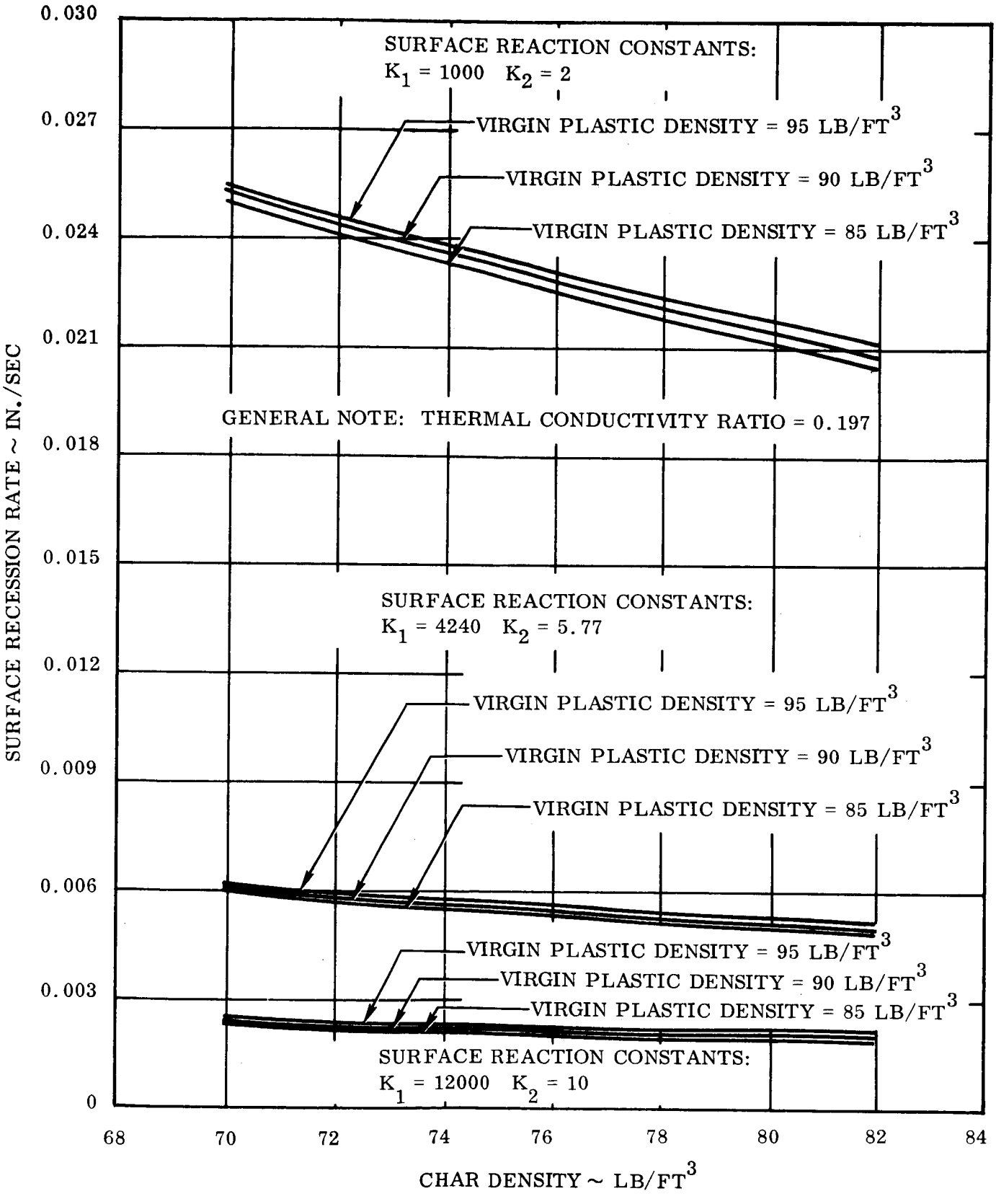

Figure 111. Surface Recession Rate Versus Char Density
Graphite Cloth/Phenolic Resin

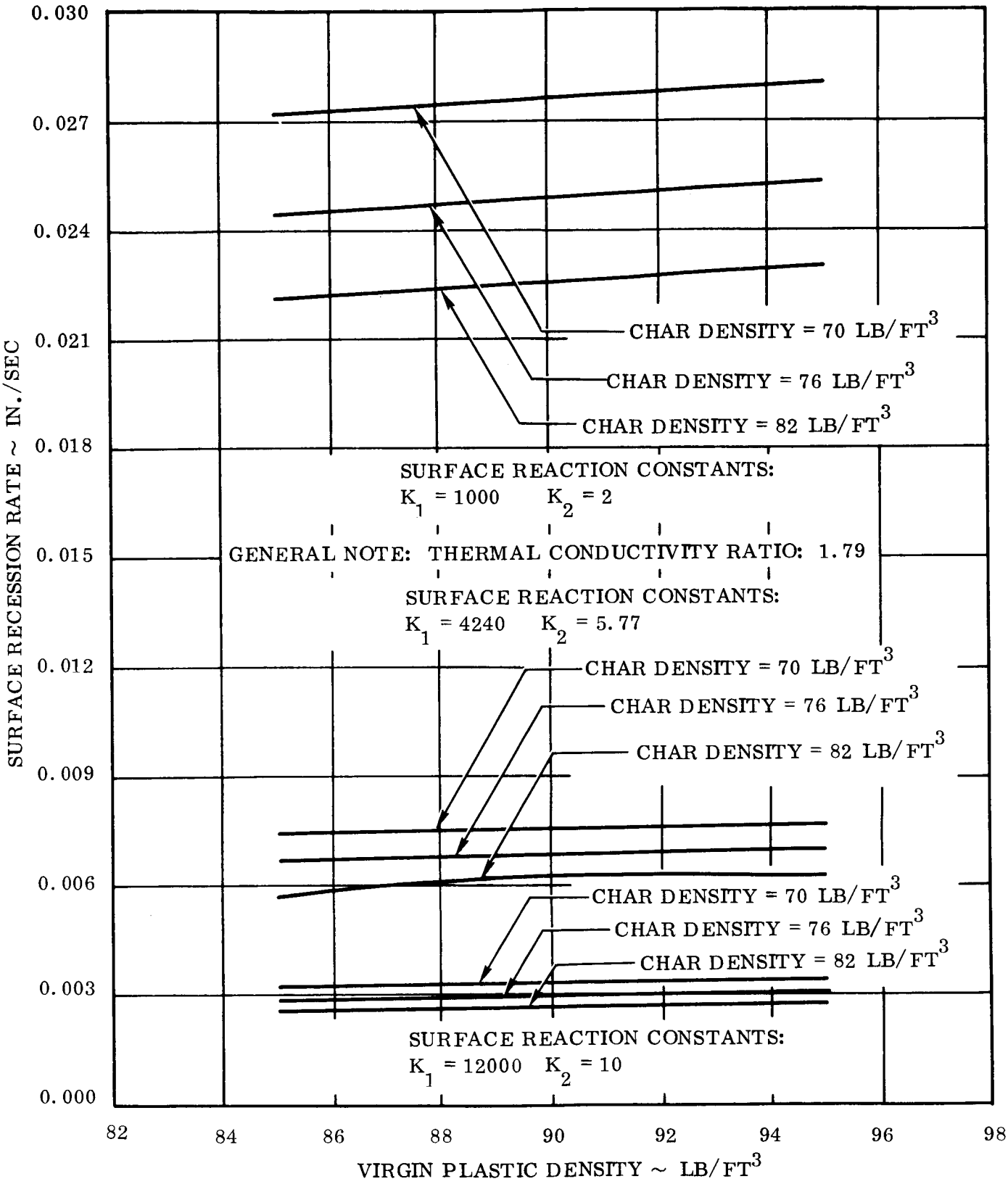

Figure 112. Surface Recession Rate Versus Virgin Plastic Density
Graphite Cloth/Phenolic Resin

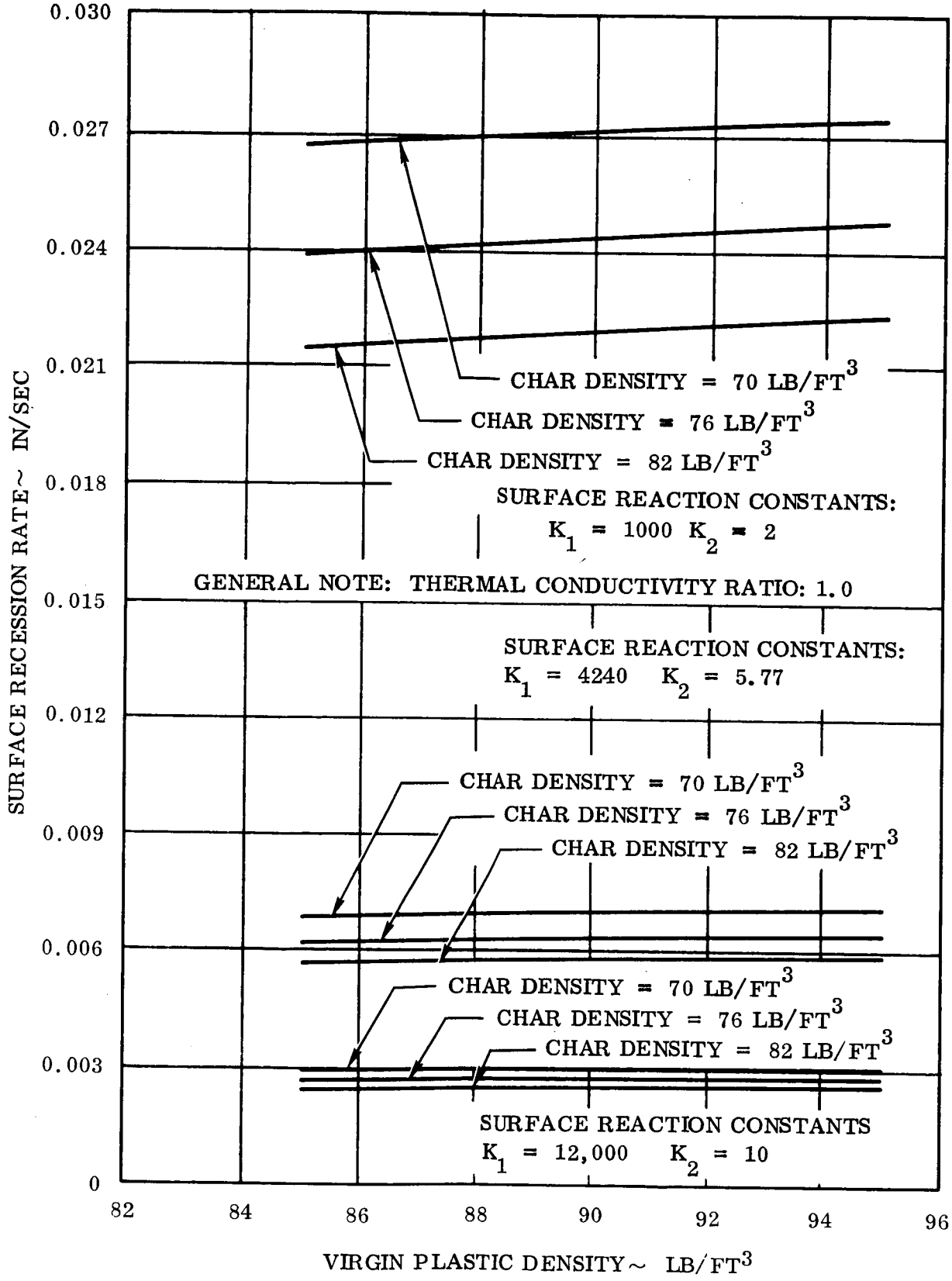

Figure 113. Surface Recession Rate Versus Virgin Plastic Density Graphite Cloth/Phenolic Resin

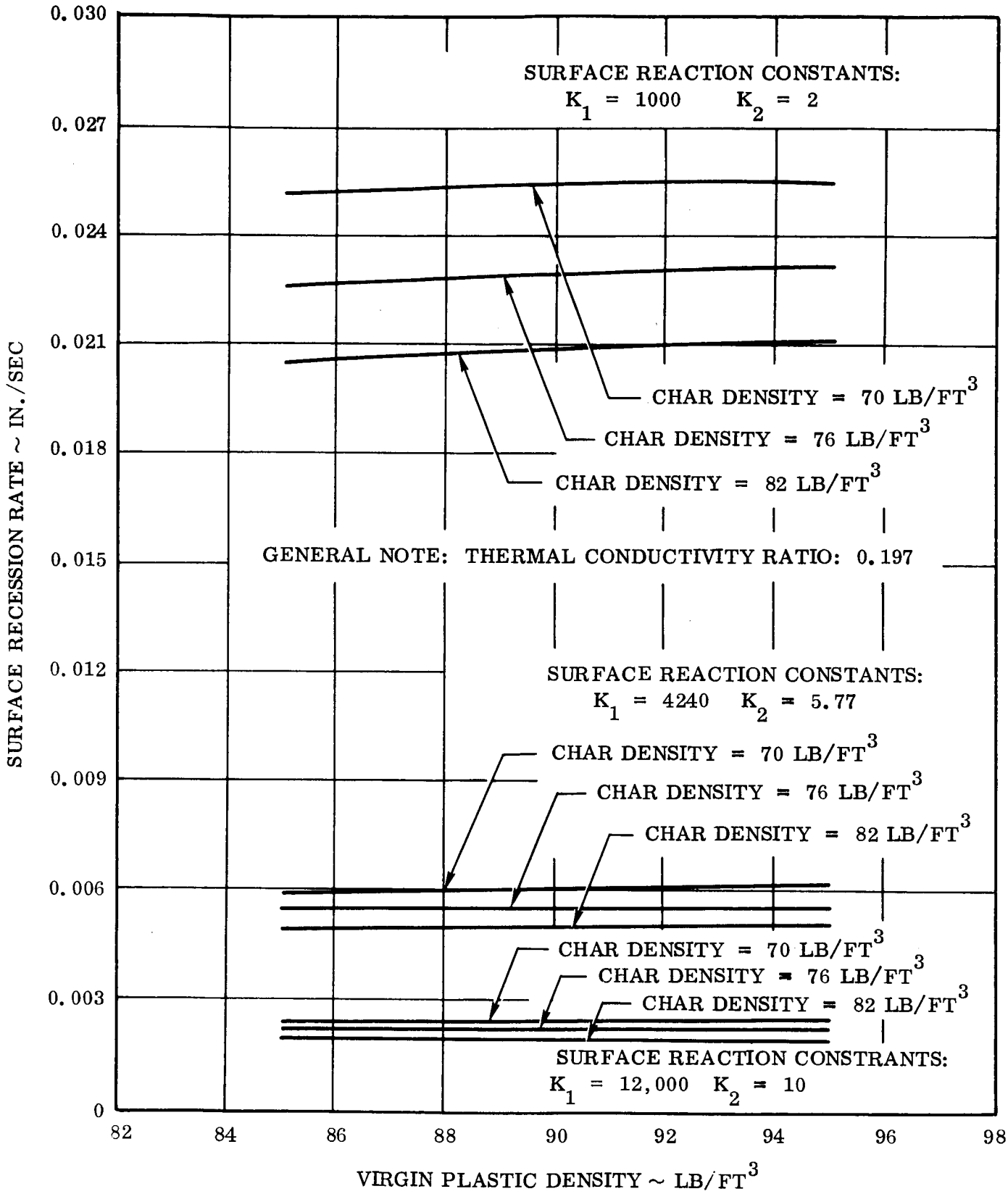

Figure 114. Surface Recession Rate Versus Virgin Plastic Density
Graphite Cloth/Phenolic Resin

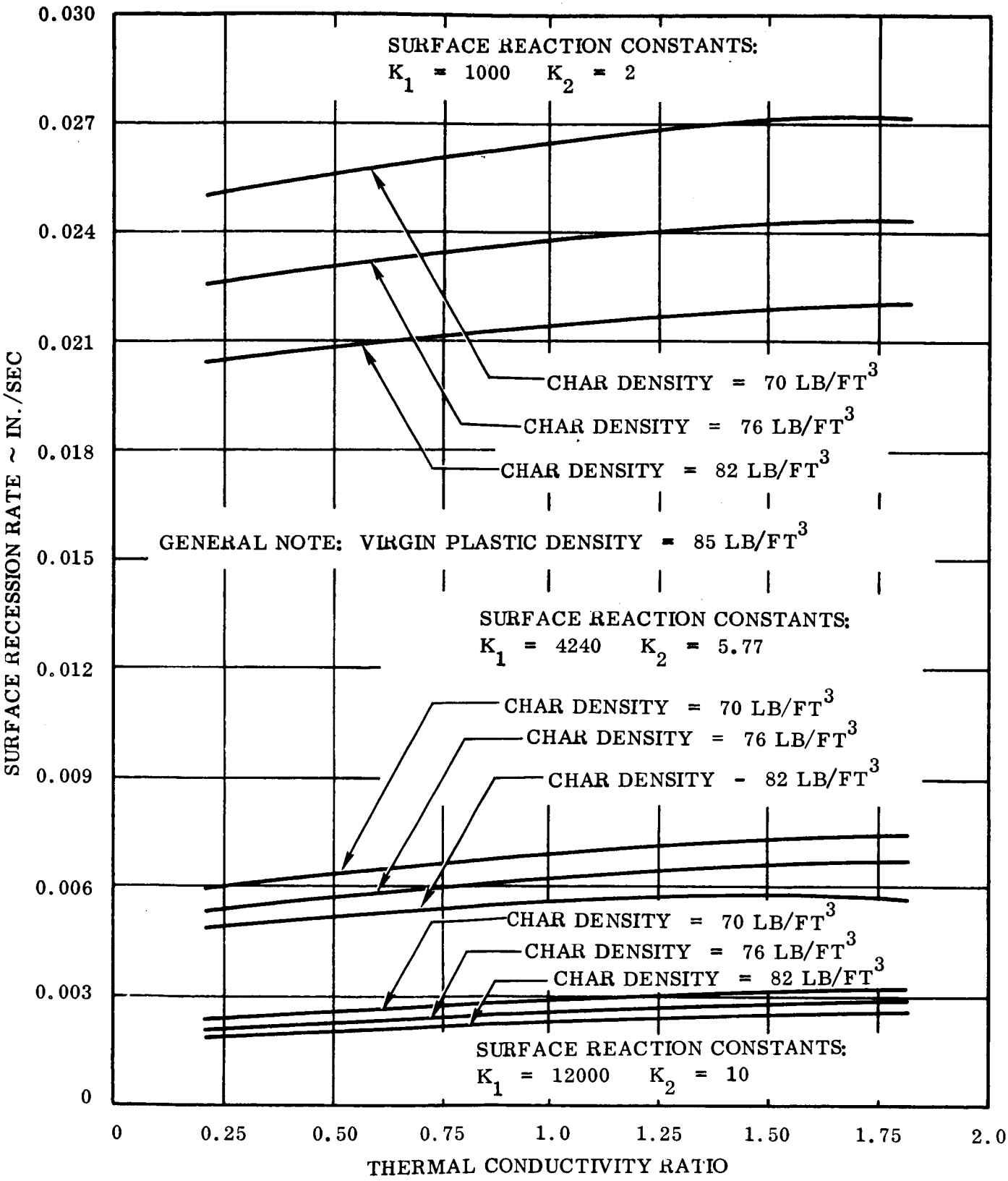

Figure 115. Surface Recession Rate Versus Thermal Conductivity Ratio Graphite Cloth/Phenolic Resin

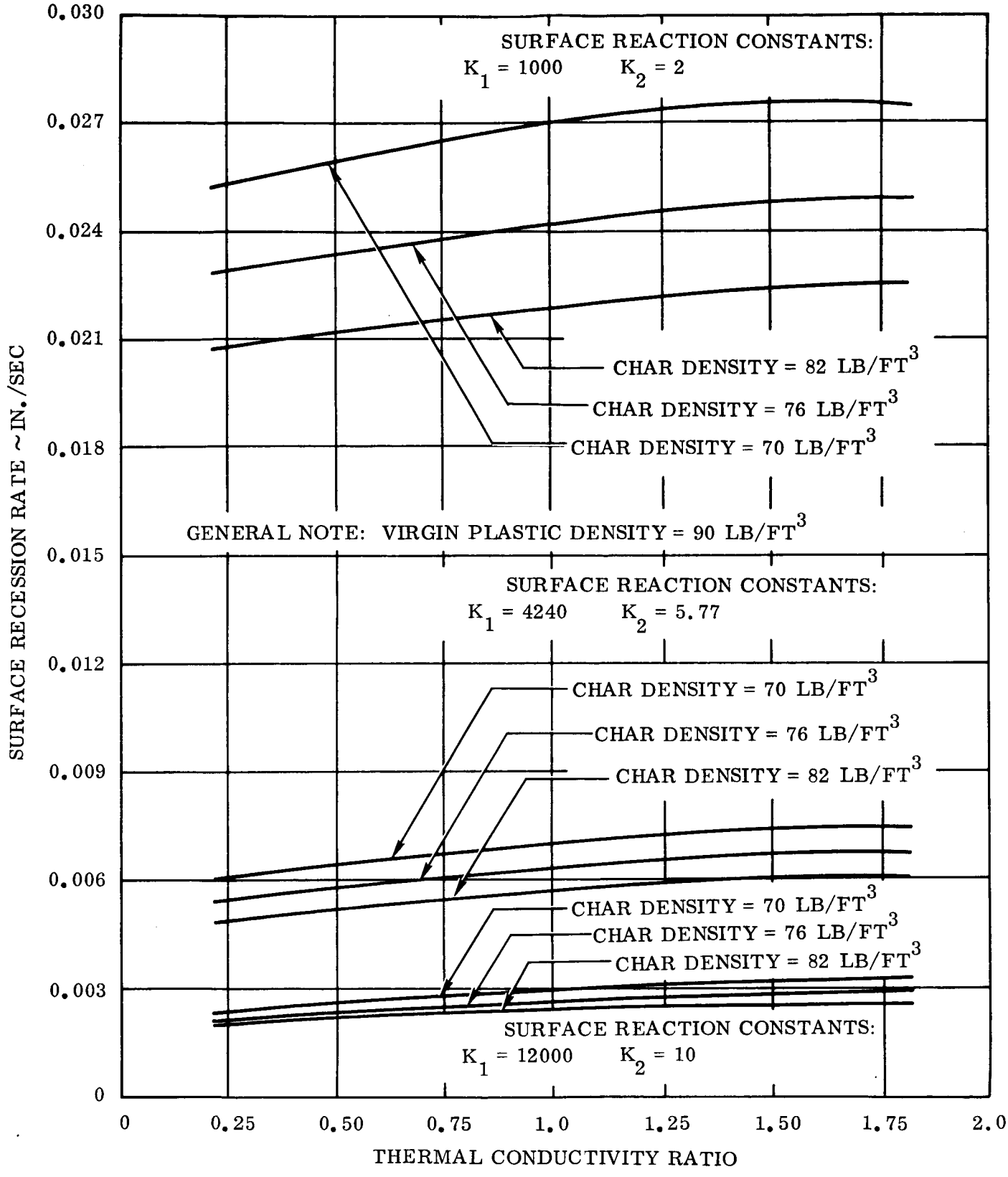

Figure 116. Surface Recession Rate Versus Thermal Conductivity Ratio Graphite Cloth/Phenolic Resin

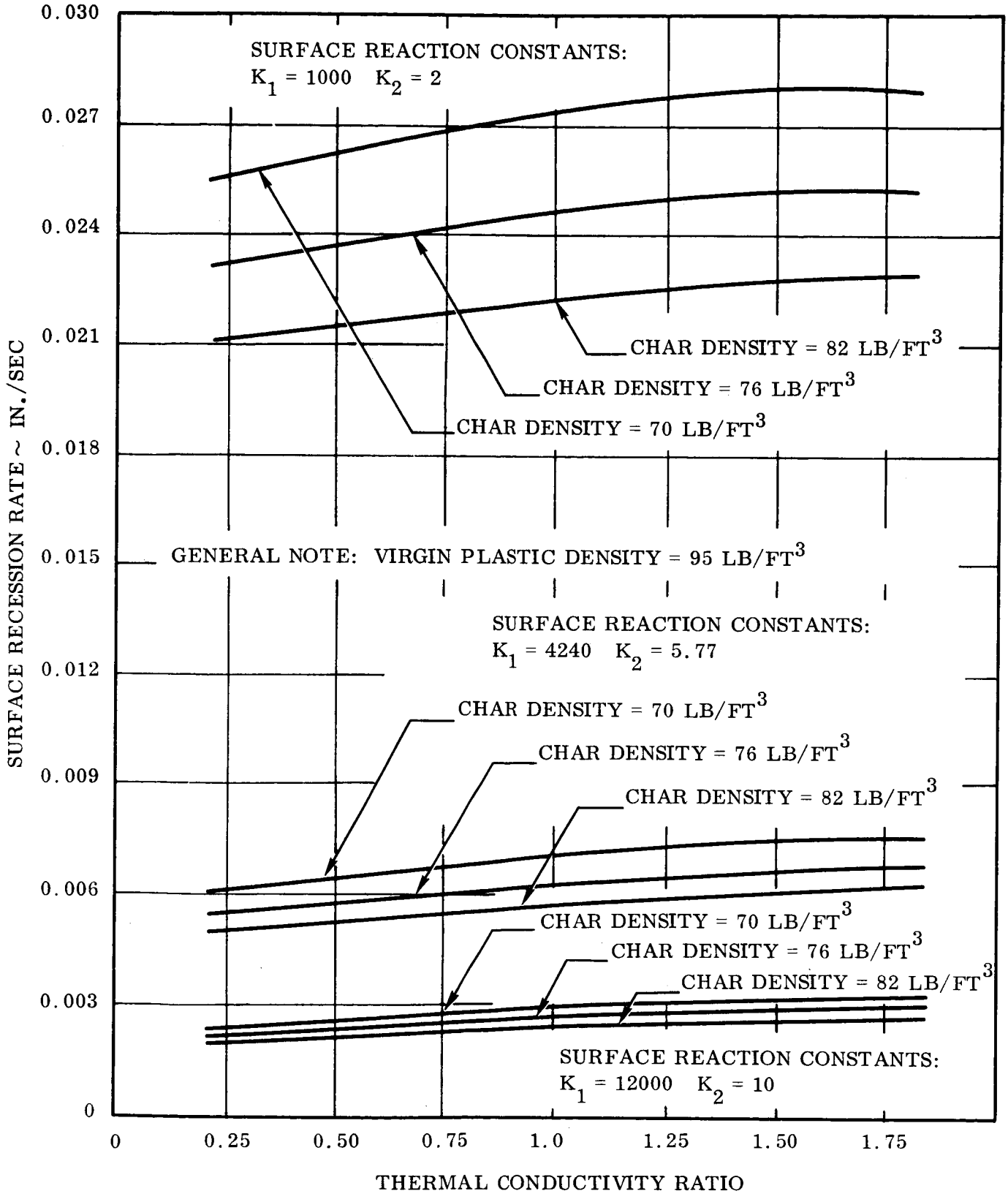

Figure 117. Surface Recession Rate Versus Thermal Conductivity Ratio Graphite Cloth/Phenolic Resin

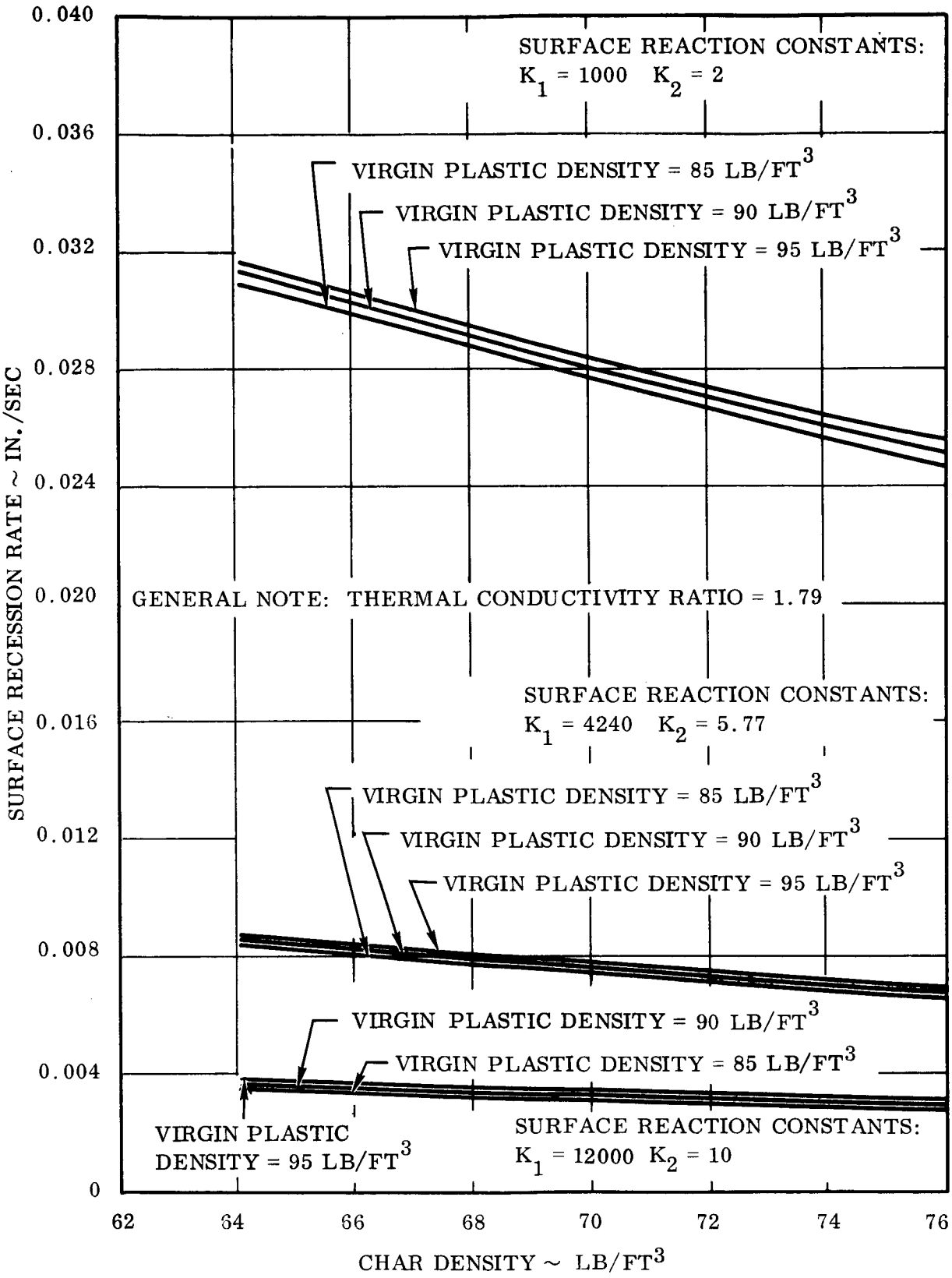

Figure 118. Surface Recession Rate Versus Char Density
Graphite Cloth/Epoxy Resin

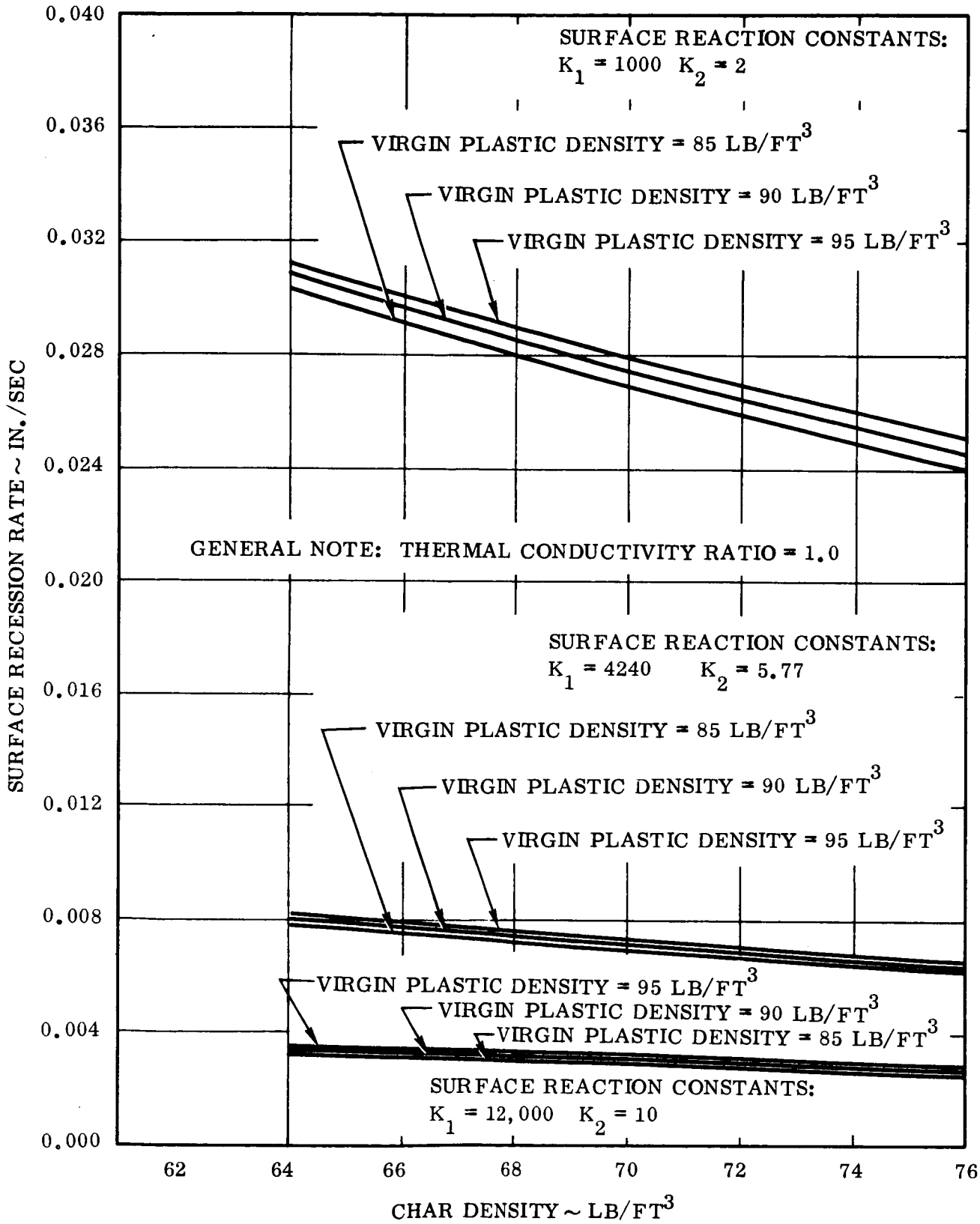

Figure 119. Surface Recession Rate Versus Char Density
Graphite Cloth/Epoxy Resin

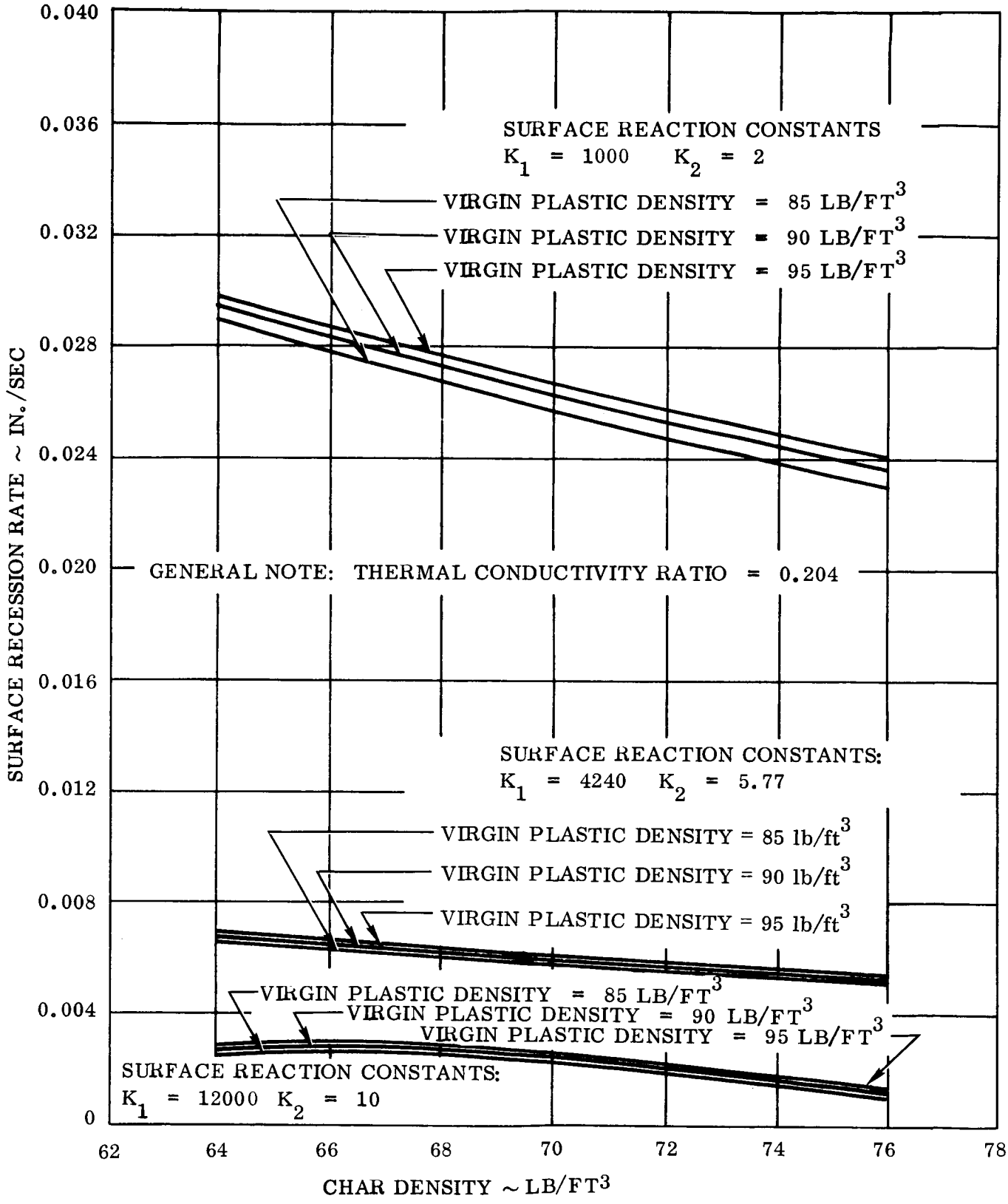

Figure 120. Surface Recession Rate Versus Char Density
Graphite Cloth/Epoxy Resin

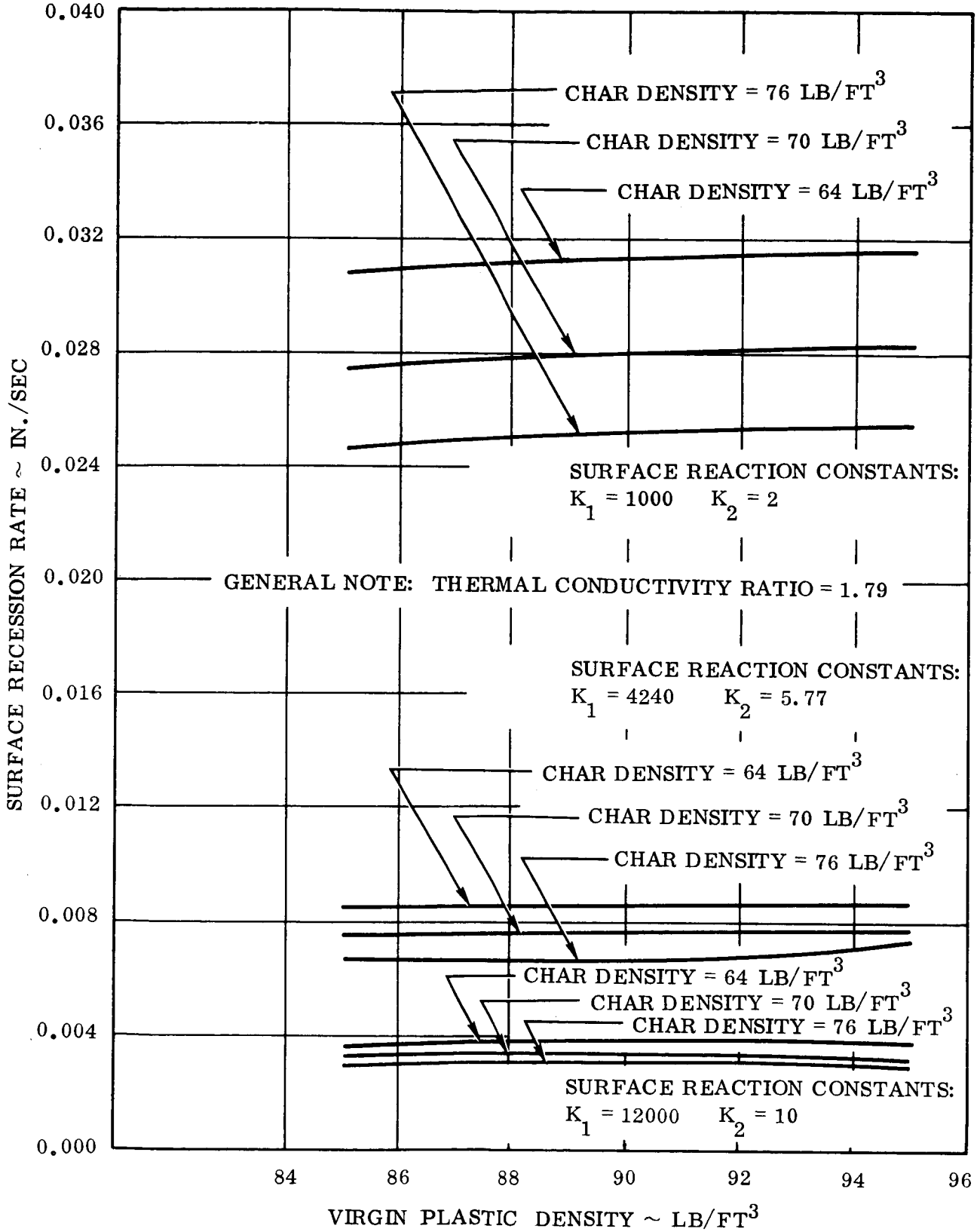

Figure 121. Surface Recession Rate Versus Virgin Plastic Density
Graphite Cloth/Epoxy Resin

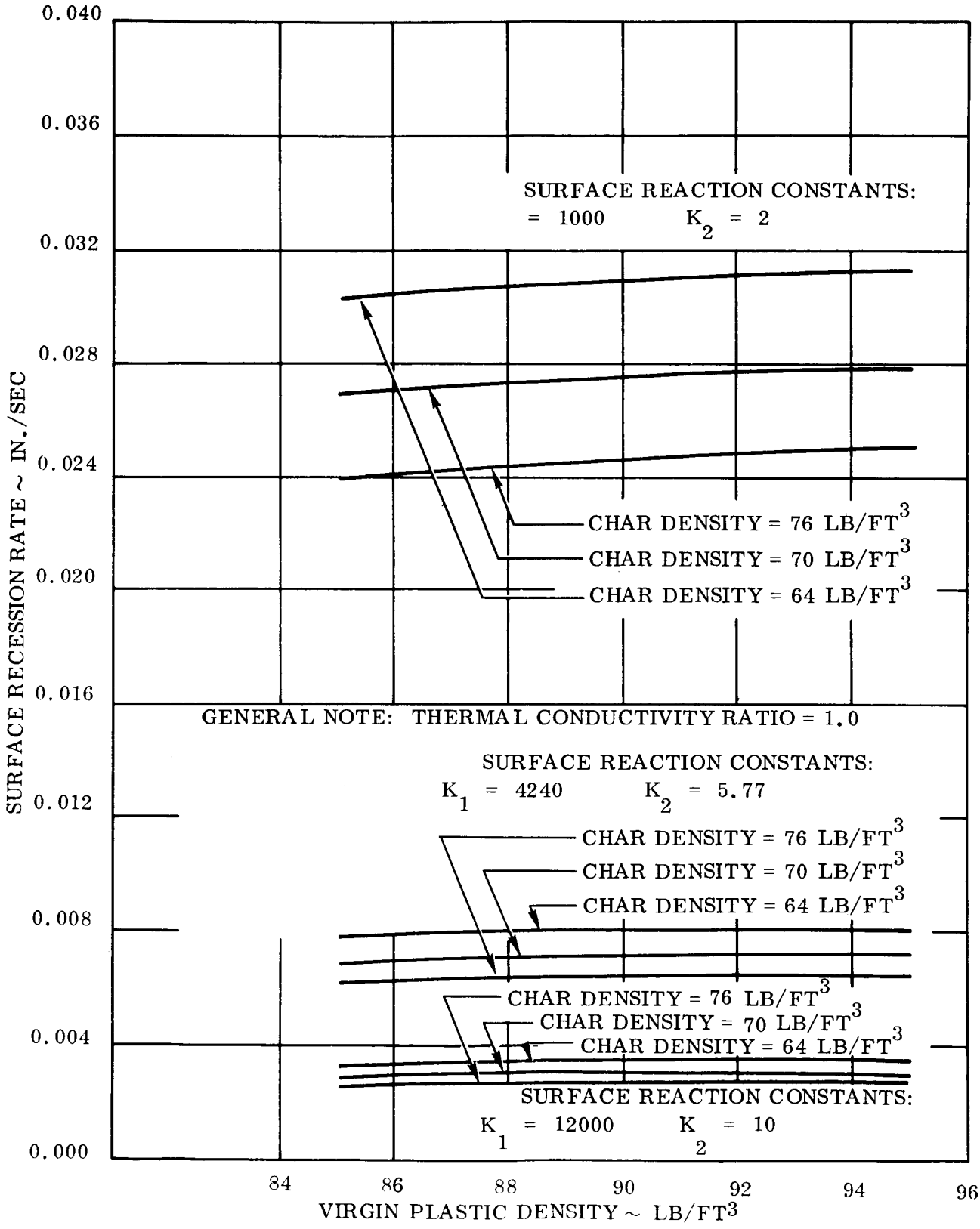

Figure 122. Surface Recession Rate Versus Virgin Plastic Density
Graphite Cloth/Epoxy Resin

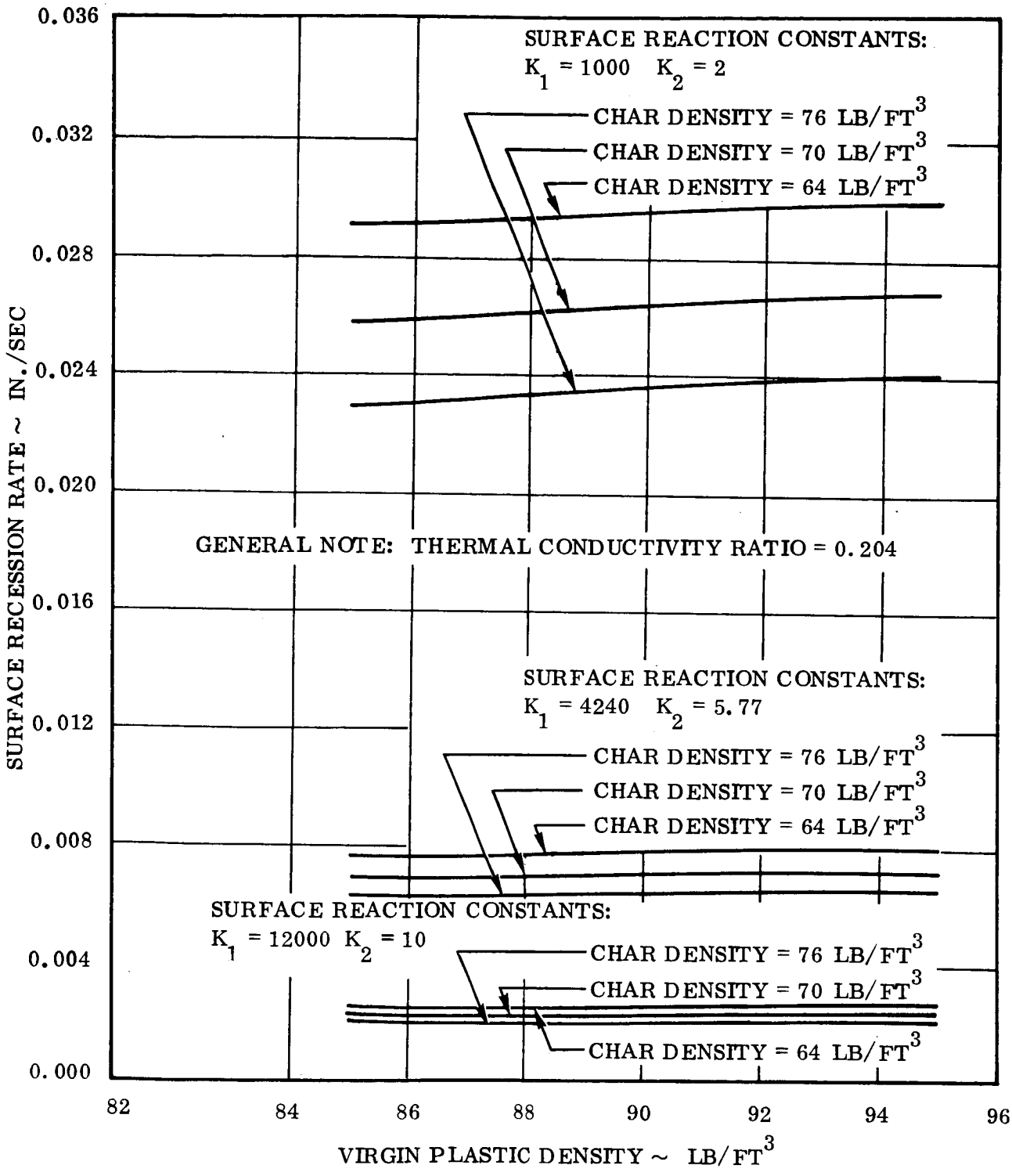

Figure 123. Surface Recession Rate Versus Virgin Plastic Density
Graphite Cloth/Epoxy Resin

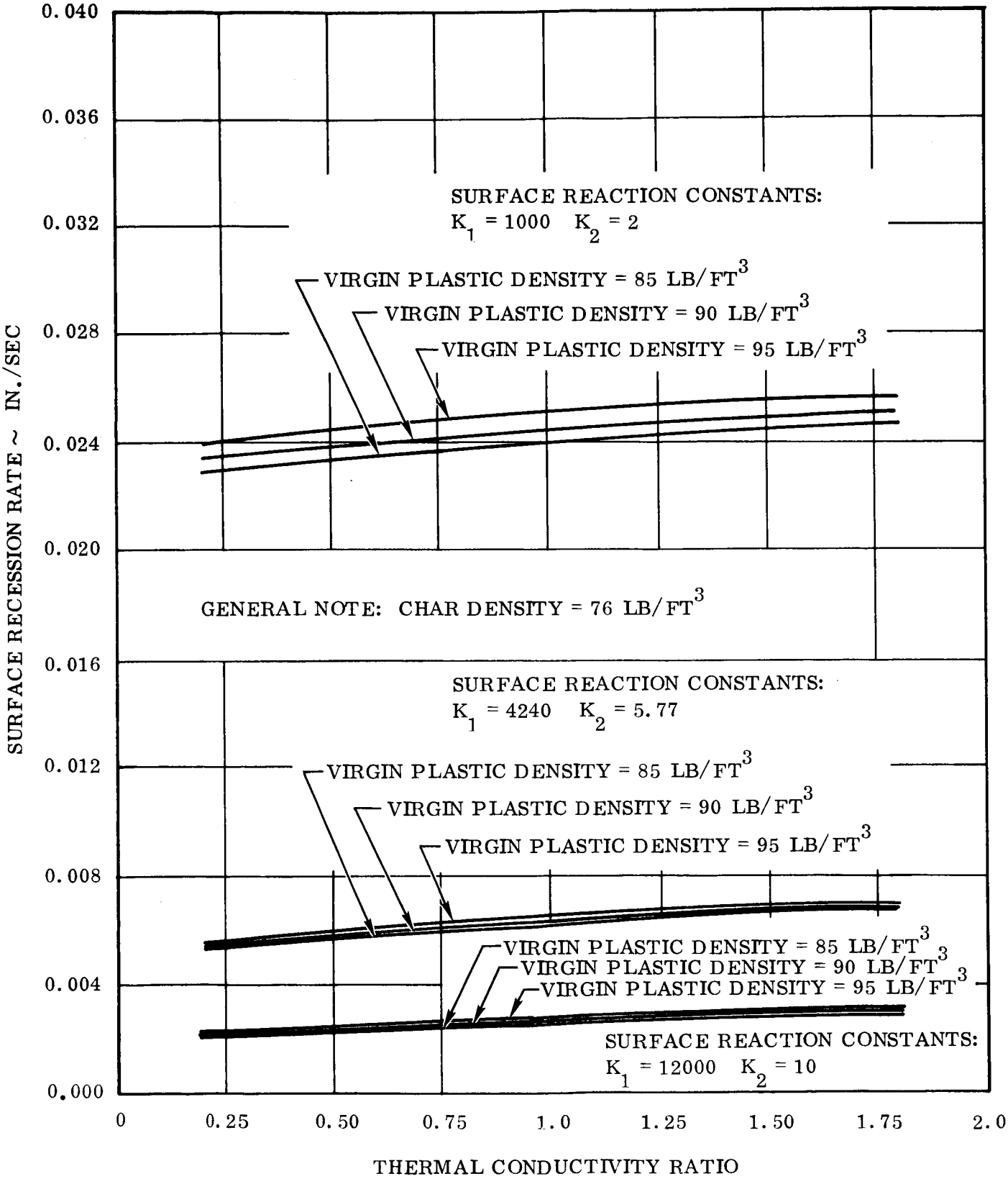

Figure 124. Surface Recession Rate Versus Thermal Conductivity Ratio Graphite Cloth/Epoxy Resin

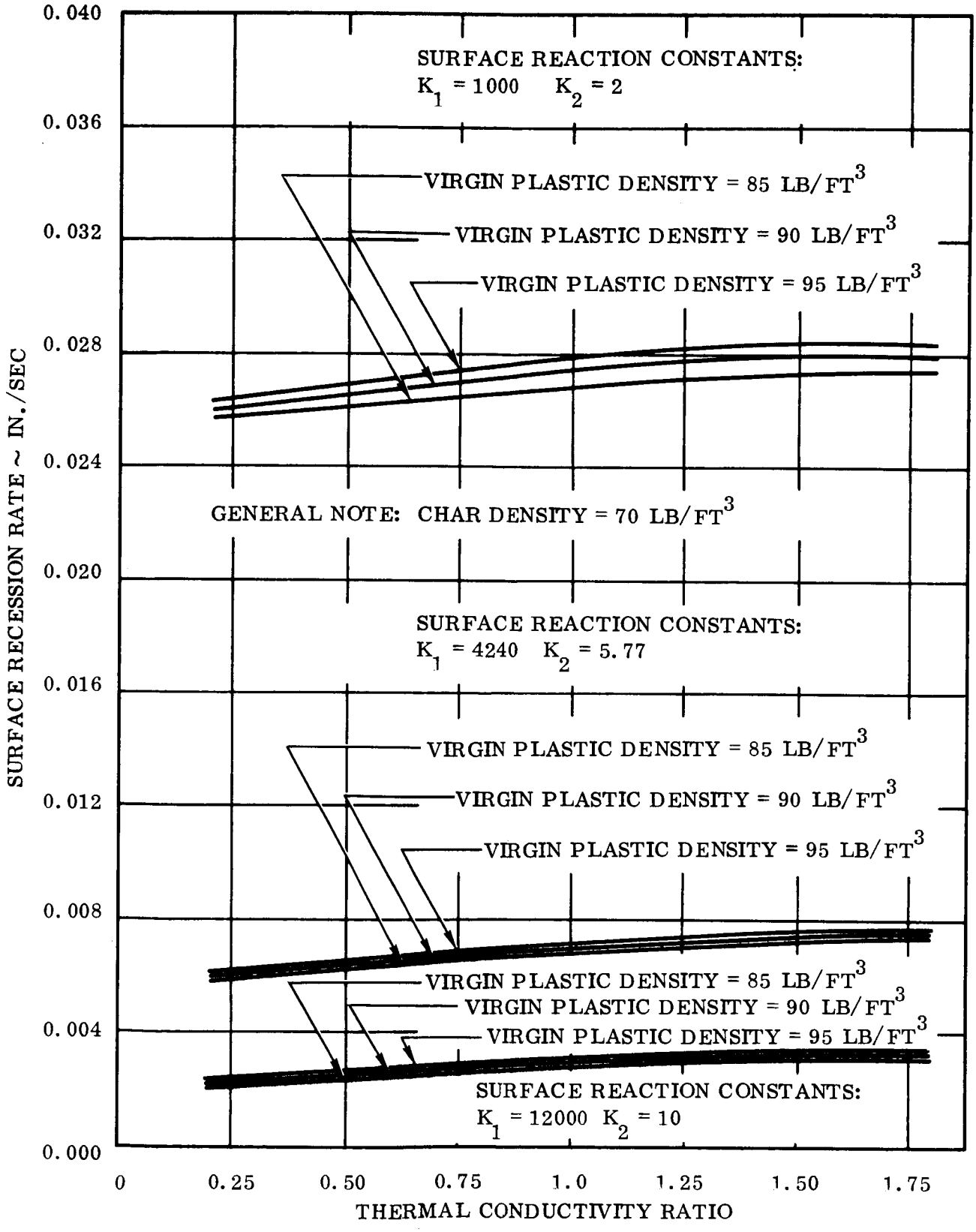

Figure 125. Surface Recession Rate Versus Thermal Conductivity Ratio Graphite Cloth/Epoxy Resin

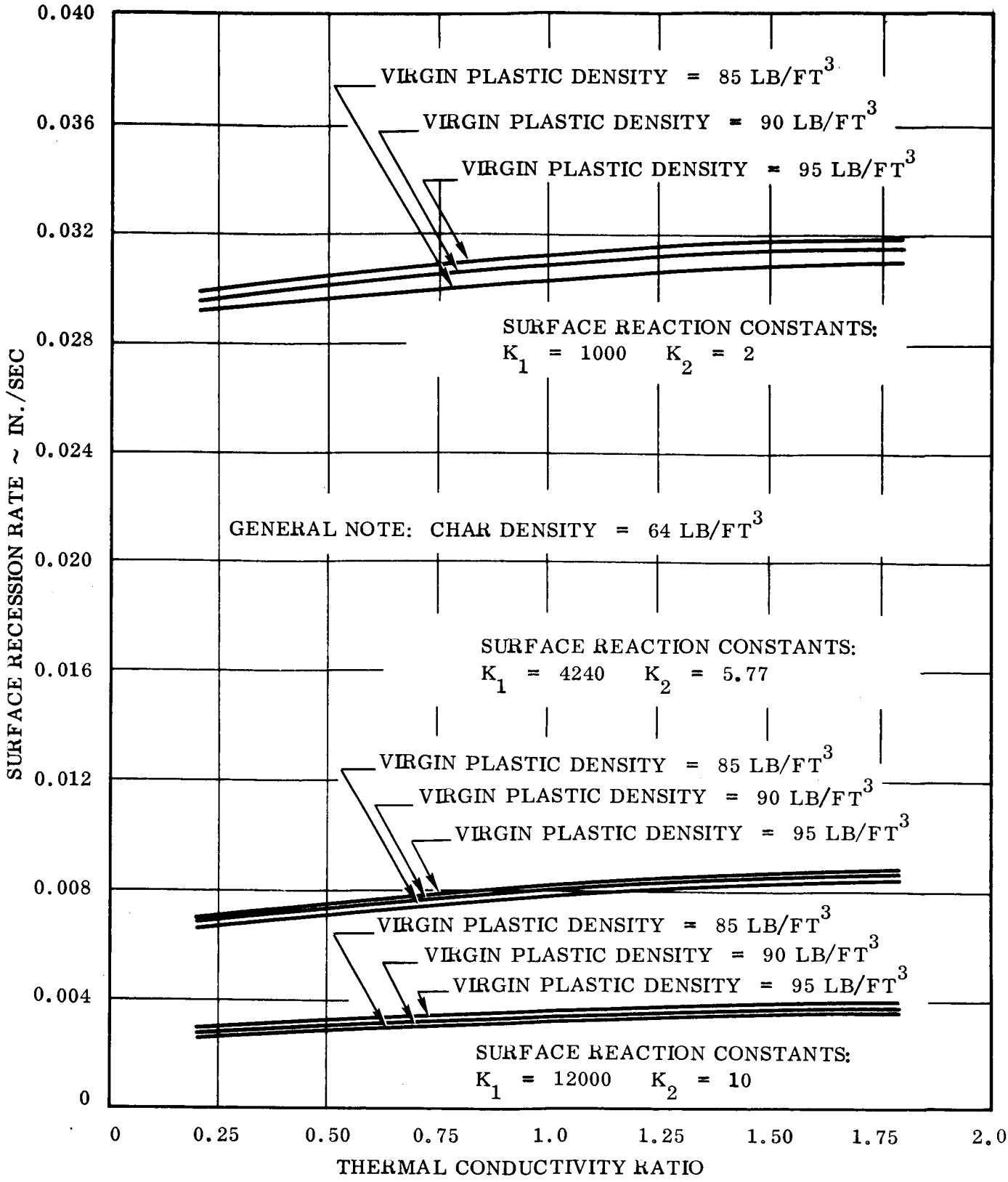

Figure 126. Surface Recession Rate Versus Thermal Conductivity Ratio
Graphite Cloth/Epoxy Resin

APPENDIX A

MATHEMATICAL DESCRIPTION OF THE REACTION KINETICS ABLATION PROGRAM

INTRODUCTION

In this appendix, a thermal ablation model is derived for a thermosetting plastic. Consideration is given first to the general three-dimensional case. Simplifications are then introduced to obtain an equation which reasonably satisfies the physical model.

The philosophy of this derivation is to start from fundamental physical principles and to utilize the concepts of continuum mechanics to proceed in a step-by-step fashion, listing all assumptions.

Figure A1 shows a cross-section of the ablation model. Initially, the outer boundary coincides with the broken line as indicated. The ambient temperature is low enough so that no chemical reactions occur within the plastic. Furthermore, the outer boundary temperature is the same as its surroundings and, therefore, radiation to or from the front face is zero.

Convective and radiative heat fluxes (arbitrary with time) are impressed on the outer boundary. As a consequence of thermal conduction, laminates of the plastic near the outer boundary increase in temperature and the front face begins to radiate heat. In time, the hotter laminates undergo a chemical reaction which converts the virgin plastic into hydrocarbon gas and a porous char residue.

The gas pressure within the porous char increases as the virgin material undergoes chemical reaction. As a consequence, a pressure profile is established throughout the porous region causing the gas to flow to adjacent pores of lower pressure. In general, the gas flow will be to the outer boundary and result in thermal energy being introduced due to friction. Heat transfer will occur between char and gas if their respective temperatures are different. Varying temperature or pressure changes, or any combination of these two conditions, can result in chemical changes in the gas (cracking or recombination), which will absorb or generate thermal energy. As the gas passes the outer boundary, a portion of the convective heat flux is blocked. As more and more heat enters the front face, reacting laminates will completely de-gas, thus forming a char layer while moving the reaction zone deeper into the body. And, of course, the outer boundary moves as a result of structural failure, oxidation, or both. If the outer boundary temperature becomes high enough, the char layer will either melt as in the case of the material having silica fibers, or undergo surface reaction with the boundary layer gases as for the graphite materials.

Physical Model

The physical model is that of a multicomponent flow of chemically reacting gases through a porous media which is itself undergoing chemical reactions. The ablation material consists of unreacted solid (denoted by subscript p), which decomposes to a porous solid (subscript C) and gaseous products of reaction (subscript g). The decomposition process can be schematically represented as:

$$P(S) \rightarrow C(S) + G(g)$$

Before decomposition begins, the ablation material consists solely of unreacted solid. After the process has gone to completion, only solid and gaseous products of reaction exist.

All densities are based on the same unit reference volume of the mixture (solid and gas). Consequently, as the decomposition proceeds at a given location, ρ_p decreases from some initial value to zero while ρ_c is simultaneously increasing from zero to some final value.

The gaseous ablation products are formed by the decomposition of the unreacted solid material. They are a mixture of many different chemical species which flow and diffuse through the porous solid. The various species may react with one another in the gas phase resulting in the familiar "cracking" effect. They may also react with the surrounding solid material, causing a reduction (or increase) in solid density.

In order to validly apply continuum theory to a porous media, all quantities are presumed to be suitably averaged over a small area - small with respect to the macroscopic dimensions of the material but large with respect to pore size. It is assumed that the ratio of pore area to total area is the same as that of pore volume to total volume, the latter quantity being the definition of porosity.

The solid species remain stationary as the displacements due to thermal expansion, a stress field and/or changes in molecular structure are generally negligible. All species are considered to be pure substances. External body forces (e.g. gravity) have been neglected as they are small for all practical applications.

Equations of State

The caloric equation of state for each solid specie is assumed to be of the form:

$$e_p = e_p(T) \qquad e_c = e_c(T)$$

Thus, for any process:

$$e_p = \int_{T_R}^{T} C_{vp}\, dT + \left(e_{F_p}\right)_{T_R} \tag{1}$$

$$e_c = \int_{T_R}^{T} C_{v_c}\, dT \left(e_{F_c}\right)_{T_R} \tag{2}$$

The internal energy accounts for thermal and chemical energy. The solid species do not have a thermal equation of state as their densities are determined by the application of non-equilibrium reaction kinetics.

The gaseous products are assumed to be a mixture of chemical reacting perfect gases. Thus, the thermal and caloric equations of state for each specie are:

$$P_i = \rho_i \frac{R}{M_i} T \tag{3}$$

$$e_i = \int_{T_R}^{T} C_{v_i} \, dT + \left(e_{F_i} \right)_{T_R} \tag{4}$$

$$h_i = \int_{T_R}^{T} C_{p_i} \, dT + \left(e_{F_i} \right)_{T_R} \tag{5}$$

Note that P_i and ρ_i are partial quantities which are based on a reference volume of the entire mixture (solid plus gas).

For the gaseous mixture as a whole, we have (assuming Dalton's Law of Partial Pressures is valid):

$$P = \rho \frac{R}{\bar{M}_g} T \tag{6}$$

$$M_g = \frac{1}{\sum_i \frac{K_i}{M_i}} \qquad K_i = \frac{\rho_i}{\rho} \tag{7}$$

$$e_g = \sum_i K_i e_i \tag{8}$$

$$h_g = \sum_i K_i h_i \tag{9}$$

Note that these assumptions imply that pressure, stress, chemical reactions, etc. have a negligible effect on the specific internal energy of each species. Obviously, they do affect the amount of each species present at a given location and thus they do effect the total energy.

Diffusion Velocities

In the flow of multicomponent gases, diffusion currents are generated by gradients in concentration, pressure and temperature. For the present problem, pressure and thermal diffusion effects should be small and so they are neglected. The velocity of the ith species relative to a fixed coordinate system is defined as $\vec{V}_i$. The mass-averaged or observable velocity of the total gas flow is defined as:

$$\vec{V} = \frac{1}{\rho_g} \sum_i \rho_i \vec{V}_i$$

The diffusional velocity of the ith species ($\vec{V}_{d_i}$) is defined as the velocity of the ith specie relative to the mass-averaged velocity.

$$\vec{V}_{d_i} = \vec{V}_i - \vec{V}$$

Note that:

$$\sum_i \rho_i \vec{V}_{d_i} = \sum_i \rho_i \vec{V}_i - \sum_i \rho_i \vec{V}$$

$$\therefore \sum_i \rho_i \vec{V}_{d_i} = \rho_g \vec{V} - \rho_g \vec{V} = 0$$

To summarize, the absolute velocity of the ith species is given by the vector sum of the mean flow velocity and the diffusional velocity of the ith species, and the mass-averaged diffusional velocity is zero.

$$\vec{V}_i = \vec{V} + \vec{V}_{d_i}$$

$$\sum_i \rho \vec{V}_{d_i} = 0 \qquad (10)$$

For ordinary concentration diffusion in a multicomponent gas, a first order approximation for $\vec{V}_{d_i}$ is that it depends linearly upon the concentration gradients of all species. For a mixture of perfect gases (p. 569, Reference 4):

$$\rho_i \vec{V}_{d_i} = \frac{n^2}{\rho_g} \sum_{i \neq j} M_i M_j P_{i_j} \nabla X_j$$

Use of this equation results in a formidable mathematical problem to determine the composition of the mixture. Also, since we are dealing with transport phenomena in a porous media, its accuracy is not assured. It has been noted by Von Karman (Ref. 1) that ". . . the process in a multicomponent mixture is so complicated that one mostly uses an approximation by considering the diffusion between one appropriately chosen component and the mixture of the rest replaced by a homogeneous gas of average characteristics," i.e., an effective binary mixture insofar as diffusion is concerned.

With this approximation, the diffusion velocity is related to the mass concentration by Fick's Law:

$$\rho_i \vec{V}_{d_i} = -\rho_g D_{12} \nabla K_i \tag{11}$$

The concept of an effective binary mixture would be a useful starting point in accounting for the effects of diffusion. Probably the largest error in this approximation is that the diffusion coefficient for each specie is the same.

Momentum Equation

Experimental evidence for the flow of a gas through a porous media indicates that the usual momentum equation of fluid mechanics does not apply (e.g. Reference 9). Consequently, it must be replaced by an empirical relationship between velocity and pressure. For the flow of a homogeneous gas through a porous media at low velocities, Darcy's Law is reasonably accurate (Reference 9). Very little is known about the present case of chemically reacting flow through a media of variable porosity. It will be assumed that Darcy's Law gives an adequate representation for the present problem, although other forms could be used if desired. Thus:

$$\vec{V} = -\nabla \frac{k}{\mu} P \tag{12}$$

where k is the permeability of the charring material and μ is the viscosity of the ablation gases. These quantities are normally determined by experiments.

Continuity Equations

The principal of conservation of mass as applied to the ith gaseous specie within a stationary control volume says that the rate at which mass is accumulated within the volume equals the rate at which mass is transported out by convection and diffusion plus the net rate of production due to chemical reaction. The mathematical statement of this is:

$$\frac{d}{dt} \int_V \rho_i \, dV = - \int_A \rho_i \left(\vec{V} + \vec{V}_{d_i} \right) \cdot \vec{\eta} \, dA + \int_V \dot{W}_i \, dV \tag{13}$$

REPORT DISTRIBUTION LIST FOR
CONTRACT NO. NAS 3-6291

National Aeronautics and Space Administration
Lewis Research Center
21000 Brookpark Road
Cleveland, Ohio 44135
Attention: Contracting Officer, MS 500-210 (1)
Liquid Rocket Technology Branch, MS 500-209 (8)

Technical Report Control Office, MS 5-5 (1)

Technology Utilization Office, MS 3-16 (1)

AFSC Liaison Office, MS 4-1 (2)

Library (2)

Office of Reliability & Quality Assurance, MS 500-203 (1)

E. W. Conrad, MS 100-1 (1)

National Aeronautics and Space Administration
Washington, D. C. 20546
Attn: Code MT (1)
RPX (2)
RPL (2)
SV (1)

Scientific and Technical Information Facility
P. O. Box 33
College Park, Maryland 20740
Attn: NASA Representative
Code CPT (6)

National Aeronautics and Space Administration
Ames Research Center
Moffett Field, California 94035
Attn: Library (1)

National Aeronautics and Space Administration
Flight Research Center
P. O. Box 273
Edwards, California 93523
Attention: Library (1)

National Aeronautics and Space Administration
Goddard Space Flight Center
Greenbelt, Maryland 20771
Attention: Library (1)

National Aeronautics and Space Administration
John F. Kennedy Space Center
Cocoa Beach, Florida 32931
Attention: Library (1)

National Aeronautics and Space Administration
Langley Research Center
Langley Station
Hampton, Virginia 23365
Attention: Library (1)

National Aeronautics and Space Administration
Manned Spacecraft Center
Houston, Texas 77001
Attention: Library (1)

National Aeronautics and Space Administration
George C. Marshall Space Flight Center
Huntsville, Alabama 35812
Attention: Library (1)
Kieth Chandler, R-P&VE-PA (1)

National Aeronautics and Space Administration
Western Operations Office
150 Pico Boulevard
Santa Monica, California 90406
Attention: Library (1)

Jet Propulsion Laboratory
4800 Oak Grove Drive
Pasadena, California 91103
Attention: Library (1)

Office of the Director of Defense Research & Engineering
Washington, D. C. 20301
Attention Dr. H. W. Schulz, Office of Asst. Dir.
(Chem. Technology) (1)

Defense Documentation Center
Cameron Station
Alexandria, Virginia 22314 (1)

RTD(RTNP)
Bolling Air Force Base
Washington, D. C. 20332 (1)

Arnold Engineering Development Center
Air Force Systems Command
Tullahoma, Tennessee 37389
Attention: AEOIM (1)

Advanced Research Projects Agency
Washington, D. C. 20525
Attention: D. E. Mock (1)

Aeronautical Systems Division
Air Force Systems Command
Wright-Patterson Air Force Base,
Dayton, Ohio
Attention: D. L. Schmidt
Code ASRCNC-2 (1)

Air Force Systems Command
(SCLT/Capt. S. W. Bowen)
Andrews Air Force Base
Washington, D. C. 20332 (1)

Air Force Rocket Propulsion Laboratory
(RPR)
Edwards, California 93523 (1)

Air Force FTC (FTAT-2)
Edwards Air Force Base, California 93523
Attention: Col J. M. Silk (1)

Air Force Office of Scientific Research
Washington, D. C. 20333
Attention: SREP, Dr. J. F. Masi (1)

Office of Research Analyses (OAR)
Holloman Air Force Base, New Mexico 88330
Attention: RRRT (1)
Maj. R. E. Brocken, Code MDGRT (1)

U. S. Air Force
Washington 25, D. C.
Attention: Col. C. K. Stambaugh, Code AFRST (1)

Commanding Officer
U. S. Army Research Office (Durham)
Box CM, Duke Station
Durham, North Carolina 27706 (1)

U. S. Army Missile Command
Redstone Scientific Information Center
Redstone Arsenal, Alabama 35808
Attention: Chief, Document Section (1)

Bureau of Naval Weapons
Department of the Navy
Washington, D. C.
Attention: J. Kay, Code RTMS-41 (1)

Commander
U. S. Naval Missile Center
Point Mugu, California 93041
Attention: Technical Library (1)

Commander
U. S. Naval Ordnance Test Station
China Lake, California 93557
Attention: Code 45 (1)

Commanding Officer
Office of Naval Research
1030 E. Green Street
Pasadena, California 91101 (1)

Director (Code 6180)
U. S. Naval Research Laboratory
Washington, D. C. 20390
Attention: H. W. Carhart (1)

Aerotherm Corp.
460 California Avenue
Palo Alto, California 94306
Attention: R. A. Rindal (1)

AVCO Corp.
Space Systems Division
Industrial Park
Lowell, Massachusetts 01851
Attention: Dr. M. DeSesa (1)

Aerojet-General Corporation
P. O. Box 296
Azusa, California 91703
Attention: Librarian (1)

Aerojet-General Corporation
11711 Sourth Woodruff Avenue
Downey, California 90241
Attention: F. M. West, Chief Librarian (1)

Aerojet-General Corporation
P. O. Box 1947
Sacramento, California 95809
Attention: Technical Library 2484-2015A (1)
R. D. Glauz (1)

Aeronutronic Division of Philco Corp.
Ford Road
Newport Beach, California 92600
Attention: Technical Information
Department (1)

Aerospace Corporation
P. O. Box 95085
Los Angeles, California 90045
Attention: W. P. Herbig (1)
Library-Documents (1)

Arthur D. Little, Inc.
Acorn Park
Cambridge 40, Massachusetts
Attention: A. C. Tobey (1)

Astropower, Incorporated
Subs. of Douglas Aircraft Company
2968 Randolph Avenue
Costa Mesa, California
Attention: Dr. George Moc
Director, Research (1)

Astrosystems, Incorporated
1275 Bloomfield Avenue
Caldwell Township, New Jersey
Attention: A. Mendenhall (1)

ARO, Incorporated
Arnold Engineering Development Center
Arnold AF Station, Tennessee 37389
Attention: Dr. B. H. Goethert
Chief Scientist (1)

Atlantic Research Corporation
Shirley Highway & Edsall Road
Alexandria, Virginia 22314
Attention: Security Office for Library (1)

Battelle Memorial Institute
505 King Avenue
Columbus, Ohio 43201
Attention: Report Library, Room 6A (1)

Bell Aerosystems, Inc.
Box 1
Buffalo, New York 14205
Attention: T. Reinhardt (1)

Bendix Systems Division
Bendix Corporation
Ann Arbor, Michigan
Attention: John M. Bureger (1)

The Boeing Company
Aero Space Division
P. O. Box 3707
Seattle, Washington 98124
Attention: Ruth E. Peerenboom (1190) (1)

Chemical Propulsion Information Agency
Applied Physics Laboratory
8621 Georgia Avenue
Silver Spring, Maryland 20910 (1)

Chrysler Corporation
Space Division
New Orleans, Louisiani
Attention: Librarian (1)

Curtiss-Wright Corporation
Wright Aeronautical Division
Woodridge, New Jersey
Attention: G. Kelley (1)

University of Denver
Denver Research Institute
P. O. Box 10127
Denver, Colarado 80210
Attention: Security Office (1)

Douglas Aircraft Company, Inc.
Santa Monica Division
3000 Ocean Park Blvd.,
Santa Monica, California 90405
Attention: J. L. Waisman

Fairchild Stratos Corporation
Aircraft Missiles Division
Hagerstown, Maryland
Attention: J. S. Kerr

General Dynamics/ Astronautics
P. O. Box 1128
San Diego, California 92112
Attention: Library & Information
Services (128-00) (1)

Convair Division
General Dynamics Corporation
P. O. Box 1128
San Diego, California 92112
Attention: Mr. W. Fenning
Centaur Resident Project Office (1)

Grumman Aircraft Engineering Corp.
Bethpage, Long Island
New York
Attention: Joseph Gavin (1)

Houston Research Institute
6001 Gulf Freeway
Houston, Texas 77023
Attention: E. B. Miller (1)

Hercules Powder Company
Allegheny Ballistics Laboratory
P. O. Box 210
Cumberland, Maryland 21501
Attention: Library (1)

11T Research Institute
Technology Center
Chicago, Illinois 60616
Attention: C. K. Hersh, Chem. Div. (1)

Kidde Aero-Space Division
Walter Kidde & Company, Inc
675 Main Street
Belleville 9, New Jersey
Attention: R. J. Hanville, (1)
Director of Research Engineering

Lockheed Missiles & Space Company
P. O. Box 504
Sunnyvale, California
Attention: Power Systems R&D
Technical Information Center (1)

Kaman Nuclear
Garden of The Gods Road
Colorado Springs, Colorado 80907
Attention: A. P. Bridges (1)

Lockheed-California Company
10445 Glen Oaks Blvd.,
Pacoima, California
Attention: G. D. Brewer (1)

Lockheed Propulsion Company
P. O. Box 111
Redlands, California 92374
Attention: Miss Belle Berlad, Librarian (1)
G. R. Malsepeace (1)

Lockheed Missiles & Space Company
Propulsion Engineering Division (D. 55-11)
1111 Lockheed Way
Sunnyvale, California 94087 (1)

Marquardt Corporation
16555 Staicoy Street
Box 2013 - South Annex
Van Nuys, California 91404
Attention: Librarian (1)

Martin-Marietta Corporation
Martin Division
Baltimore 3, Maryland
Attention: John Calathes (3214) (1)

McDonnell Aircraft Corporation
P. O. Box 6106
Lambert Field, Missouri
Attention: R. A. Herzmark (1)

North American Aviation, Inc.
Space & Information Systems Division
12214 Lakewood Boulevard
Downey, California 90242
Attention: Technical Information Center,
D/096-722(AJ01) (1)

Northrop Space Laboratories
1001 East Broadway
Hawthorne, California
Attention: Dr. William Howard (1)

Purdue University
Lafayette, Indiana 47907
Attention: Technical Librarian (1)

Republic Aviation Corporation
Farmingdale, Long Island
New York
Attention: Dr. William O'Donnell (1)

Rocket Research Corporation
520 South Portland Street
Seattle, Washington 98108 (1)

Rocketdyne Division of
North American Aviation, Inc.
6633 Canoga Avenue
Canoga Park, California 91304
Attention: Library, Department 596-306 (1)

Rohm and Haas Company
Redstone Arsenal Research Division
Huntsville, Alabama 35808
Attention: Librarian (1)

Space-General Corporation
777 Flower Street
Glendale, California
Attention: C. E. Roth (1)

Stanford Research Institute
333 Ravenswood Avenue
Menlo Park, California 94025
Attention: Thor Smith (1)

Texaco Experiment, Incorporated
P. O. Box 1-T
Richmond, Virginia 23202
Attention: Librarian (1)

Thiokol Chemical Corporation
Alpha Division, Huntsville Plant
Huntsville, Alabama 35800
Attention: Technical Director: (1)

Thiokol Chemical Corporation
Reaction Motors Division
Denville, New Jersey 07834
Attention: Librarian (1)

Thiokol Chemical Corporation
Redstone Division
Huntsville, Alabama
Attention: John Goodloe (1)

TRW Systems, Incorporated
1 Space Park
Redondo Beach, California 90200
Attention: STL Tech. Lib. Doc.
Acquisitions (1)

TRW, Incorporated
TAPCO Division
23555 Euclid Avenue
Cleveland, Ohio 44117
Attention: P. T. Angell (1)

United Aircraft Corporation
Corporation Library
400 Main Street
East Hartford, Connecticut 06118
Attention: Dr. David Rix (1)

United Aircraft Corporation
Pratt & Whitney Division
Florida Research & Development Center
P. O. Box 2691
West Palm Beach, Florida 33402
Attention: Library (1)

United Aircraft Corporation
United Technology Center
P. O. Box 358
Sunnyvale, California 94088
Attention: Librarian

Vought Astronautics
Box 5907
Dallas 22, Texas
Attention: Warren C. Trent (1)